THE BELL SYSTEM
TECHNICAL JOURNAL

VOLUME XXXV JANUARY 1956 NUMBER 1

Diffused Emitter and Base Silicon Transistors*

By M. TANENBAUM and D. E. THOMAS

(Manuscript received October 21, 1955)

Silicon n-p-n transistors have been made in which the base and emitter regions were produced by diffusing impurities from the vapor phase. Transistors with base layers 3.8 × 10^{-4}-cm thick have been made. The diffusion techniques and the processes for making electrical contact to the structures are described.

The electrical characteristics of a transistor with a maximum alpha of 0.97 and an alpha-cutoff of 120 mc/sec are presented. The manner in which some of the electrical parameters are determined by the distribution of the doping impurities is discussed. Design data for the diffused emitter, diffused base structure is calculated and compared with the measured characteristics.

INTRODUCTION

The necessity of thin base layers for high-frequency operation of transistors has long been apparent. One of the most appealing techniques for controlling the distribution of impurities in a semiconductor is the diffusion of the impurity into the solid semiconductor. The diffusion coefficients of Group III acceptors and Group V donors into germanium and silicon are sufficiently low at judiciously selected temperatures so

* A portion of the material of this paper was presented at the Semiconductor Device Conference of the Institute of Radio Engineers, Philadelphia, Pa., June, 1955.

that it is possible to envision transistors with base layer thicknesses of a micron and frequency response of several thousand megacycles per second.

A major deterent to the application of diffusion to silicon transistor fabrication in the past was the drastic decrease in lifetime which generally occurs when silicon is heated to the high temperatures required for diffusion. There was also insufficient knowledge of the diffusion parameters to permit the preparation of structures with controlled layer thicknesses and desired dopings. Recently the investigations of C. S. Fuller and coworkers have produced detailed information concerning the diffusion of Group III and Group V elements in silicon. This information has made possible the controlled fabrication of transistors with base layers sufficiently thin that high alphas are obtained even though the lifetime has been reduced to a fraction of a microsecond. In a cooperative program with Fuller, diffusion structures were produced which have permitted the fabrication of transistors whose electrical behavior closely approximates the behavior anticipated from the design. This paper describes these techniques which have resulted in high alpha silicon transistors with alpha-cutoff of over 100 mc/sec.

1.0 FABRICATION OF THE TRANSISTORS

Fuller's work[1] has shown that in silicon the diffusion coefficient of a Group III acceptor is usually 10 to 100 times larger than that of the Group V donor in the same row in the periodic table at the same temperatures. These experiments were performed in evacuated silica tubes using the Group III and Group V elements as the source of diffusant. Under these conditions a particular steady state surface concentration of the diffusant is produced and the depth of diffusion is sensitive to this concentration as well as to the diffusion coefficient. The experiments show that the effective steady state surface concentration of the donor impurities produced under these conditions is ten to one hundred times greater than that of the acceptor impurities. Thus, by the simultaneous diffusion of selected donor and acceptor impurities into n-type silicon an n-p-n structure will result. The first n-layer forms because the surface concentration of the donor is greater than that of the acceptor. The p-layer is produced because the acceptor diffuses faster than the donor and gets ahead of it. The final n-region is simply the original background doping of the n-type silicon sample. It has been possible to produce n-p-n structures by the simultaneous diffusion of several combinations of donors and acceptors. Often, however, the diffusion coefficients and surface concentrations of the donors and acceptors are such that opti-

[1] C. S. Fuller, private communication.

mum layer thicknesses (see Sections 3 and 4) are not produced by simultaneous diffusion. In this case, one of the impurities is started ahead of the other in a prior diffusion, and then the other impurity is diffused in a second operation.

With the proper choice of diffusion temperatures and times it has been possible to make n-p-n structures with base layer thicknesses of 2×10^{-4} cm. The uniformity of the layers in a given specimen is better than ten per cent of the layer thickness. Fig. 1 illustrates the uniformity of the layers. This figure is an enlarged photograph of a view perpendicular to the surface of the specimen. A bevel which makes an angle of five degrees with the original surface has been polished on the specimen. This angle magnifies the layer thickness by 11.5. The layer is defined by an etchant which preferentially stains p-type silicon[1] and the width of the layer is measured with a calibrated microscope.

After diffusion the entire surface of the silicon wafer is covered with the diffused n- and p-type layers, see Fig. 2(a). Electrical contact must now be made to the three regions of the device. The base contact can be made by polishing a bevel on the specimen to expose and magnify the base layer and then alloying a lead to this region by the same tech-

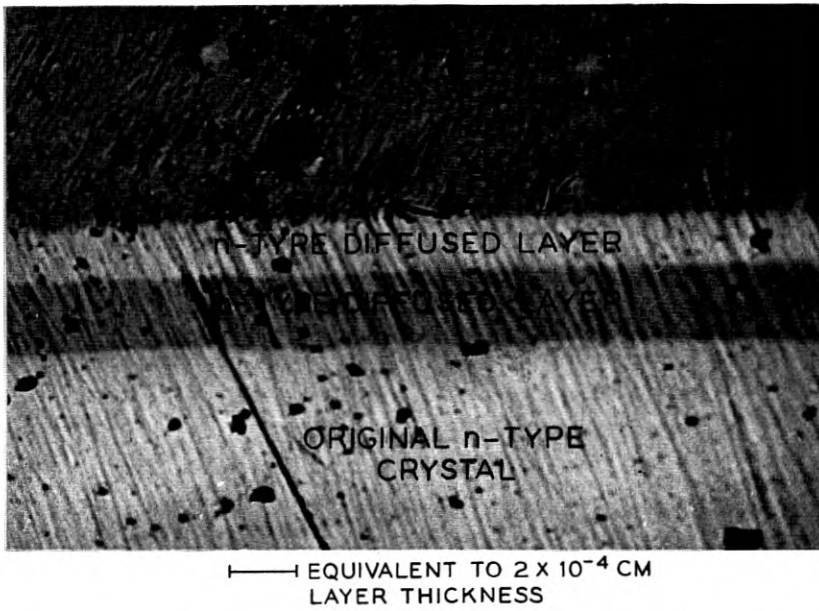

Fig. 1 — Angle section of a double diffused silicon wafer. The p-type center layer is approximately 2×10^{-4} cm thick.

niques employed in the fabrication of grown junction transistors, Fig. 2(b). However, a much simpler technique has been evolved. If the surface concentration of the donor diffusant is maintained below a certain critical value, it is possible to alloy an aluminum wire directly through the diffused n-type layer and thus make effective contact to the base layer, Fig. 2(c). Since the resistivity of the original silicon wafer is one to five ohm-cm, the aluminum will be rectifying to this region. It has been experimentally shown that if the surface concentration of the donor diffusant is less than the critical value mentioned above, the aluminum will also be rectifying to the diffused n-type region and the contact becomes merely an extension of the base layer. The n-layers produced by diffusing from elemental antimony are below the critical concentration and the direct aluminum alloying technique is feasible.

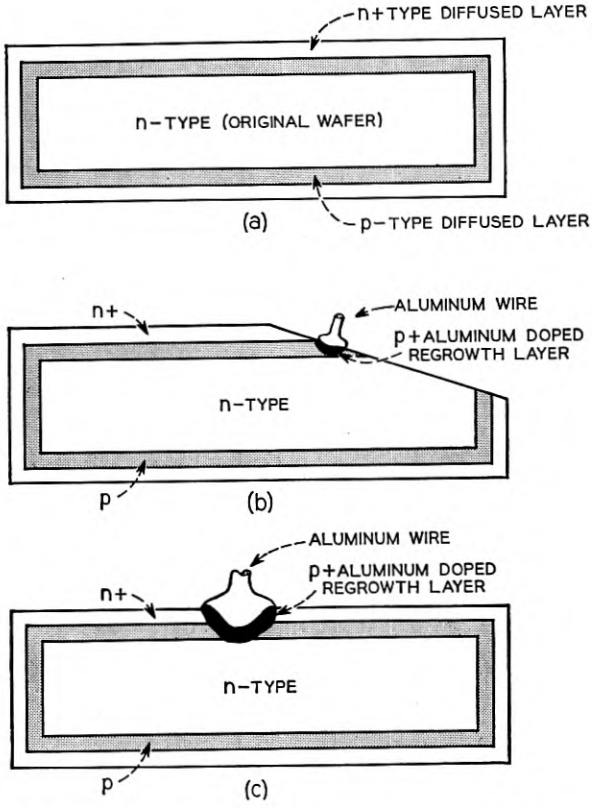

Fig. 2 — Schematic illustration of (a) double diffused n-p-n wafer, (b) angle section method of making base contact, and (c) direct alloying method of making base contact.

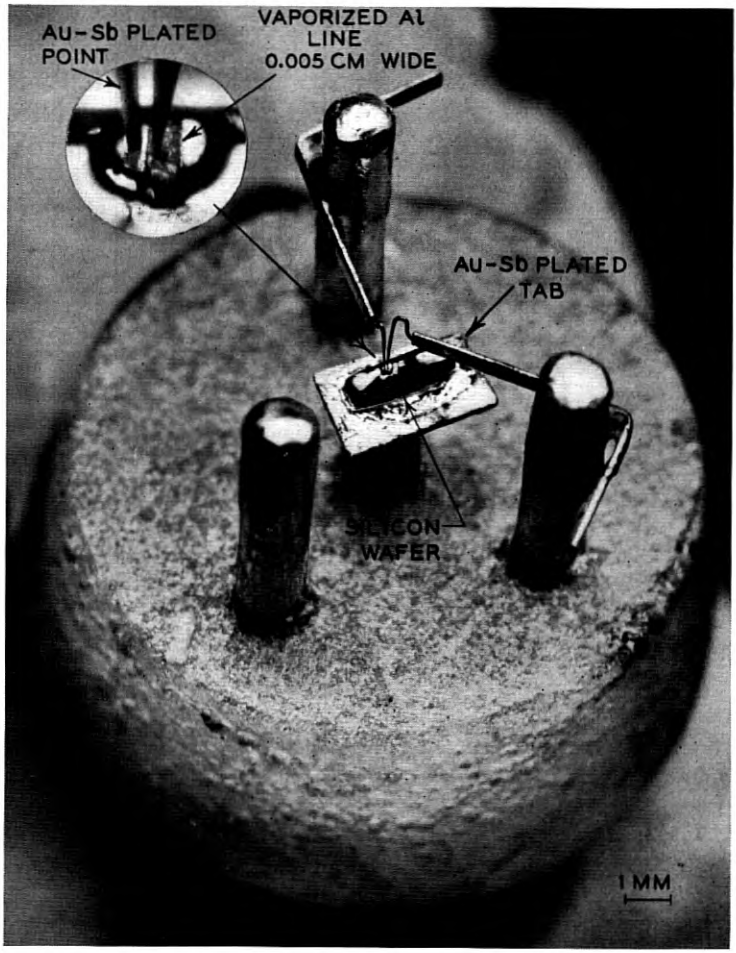

Fig. 3 — Mounted double diffused transistor.

Contact to the emitter layer is achieved by alloying a film of gold containing a small amount of antimony. Since this alloy will produce an n-type regrowth layer, it is only necessary to insure that the gold-antimony film does not alloy through the p-type base layer, thus shorting the emitter to the collector. This is controlled by limiting the amount of gold-antimony alloy which is available by using a thin evaporated film or by electroplating a thin film of gold-antimony alloy on an inert metal point and alloying this structure to the emitter layer.

Ohmic contact to the collector is produced by alloying the silicon wafer to an inert metal tab plated with a gold-antimony alloy.

The transistors whose characteristics are reported in this paper were prepared from 3 ohm-cm n-type silicon using antimony and aluminum as the diffusants. The base contact was produced by evaporating aluminum through a mask so that a line approximately 0.005 × 0.015 cm in lateral dimensions and 100,000 Å thick was formed on the surface. This aluminum line was alloyed through the emitter layer in a subsequent operation. The wafer was then alloyed onto the plated kovar tab. A small area approximately 0.015 cm in diameter was masked around the line and the wafer was etched to remove the unwanted layers. The unit was then mounted in a header. Electrical contact to the collector was made by soldering to the kovar tab. Contact to the base was made with a tungsten point pressure contact to the alloyed aluminum. Contact to the emitter was made by bringing a gold-antimony plated tungsten point into pressure contact with the emitter layer. The gold-antimony plate was then alloyed by passing a controlled electrical pulse between the plated point and the transistor collector lead. Fig. 3 is a photograph of a mounted unit.

2.0 ELECTRICAL CHARACTERISTICS

The frequency cutoffs of experimental double diffused silicon transistors fabricated as described above are an order of magnitude higher than the known cutoff frequencies of earlier silicon transistors. This is shown in Fig. 4 which gives the measured common base and common emitter current gains for one of these units as a function of frequency. The common base short-circuit current gain is seen to have a cutoff frequency of about 120 mc/sec.[2] The common emitter short-circuit current gain is shown on the same figure. The low-frequency current gain is better than thirty decibels and the cutoff frequency which is indicated by the frequency at which the gain is 3 db below its low-frequency value is 3 mc/sec. This is an exceptionally large common emitter bandwidth for a thirty db common emitter current gain and is of the same order of magnitude as that obtained with the highest frequency germanium transistors (e.g., p-n-i-p or tetrode) which had been made prior to the diffused base germanium transistor.[3]

[2] The increase in common base current gain above unity (indicated by current gain in decibels being positive) in the vicinity of 50 mc/sec is caused by a reactance gain error in the common base measurement. This error is caused by a combination of the emitter to ground parasitic capacitance and the positive reactance component of the transistor input impedance resulting from phase shift in the alpha current gain.

[3] C. A. Lee, A High-Frequency Diffused Base Germanium Transistor, see page 23.

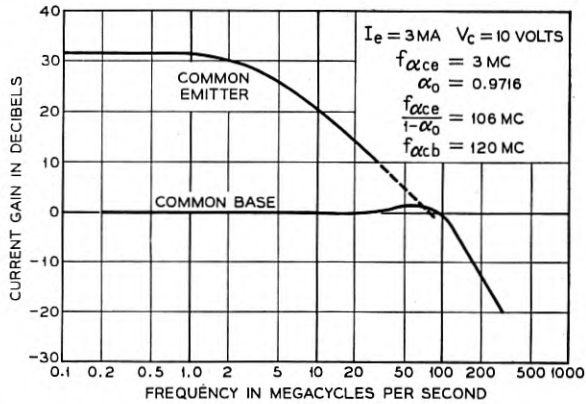

Fig. 4 — Short-circuit current gain of a double diffused silicon n-p-n transistor as a function of frequency in the common emitter and common base connections.

Fig. 5 shows a high-frequency lumped constant equivalent circuit for the double diffused silicon transistor whose current gain cutoff characteristic is shown in Fig. 4. External parasitic capacitances have been omitted from the circuit. The configuration is the conventional one for junction transistors with two exceptions. A series resistance r_e' has been added in the emitter circuit to account for contact resistance resulting from the fact that the present emitter point contacts are not perfectly ohmic. A second resistance r_c' has been added in the collector circuit to account for the ohmic resistance of the n-type silicon between the collector terminal and the effective collector junction. This resistance exists in all junction transistors but in larger area low frequency junction transistors its effect on alpha-cutoff is sufficiently small so that it has been ignored in equivalent circuits of these devices. The collector RC

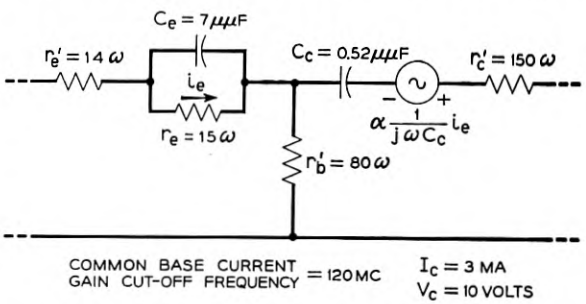

Fig. 5 — High-frequency lumped constant equivalent circuit for a double diffused silicon n-p-n transistor.

cutoff caused by the collector capacitance and the combined collector body resistance and base resistance is an order of magnitude higher than the measured alpha cutoff frequency and therefore is not too serious in impairing the very high-frequency performance of the transistor. This is due to the low capacitance of the collector junction which is seen to be approximately 0.5 mmf at 10 volts collector voltage. The base resistance of this transistor is less than 100 ohms which is quite low and compares very favorably with the best low frequency transistors reported previously.

The low-frequency characteristics of the double diffused silicon transistor are very similar to those of other junction transistors. This is illustrated in Fig. 6 where the static collector characteristics of one of these transistors are given. At zero emitter current the collector current is too small to be seen on the scale of this figure. The collector current

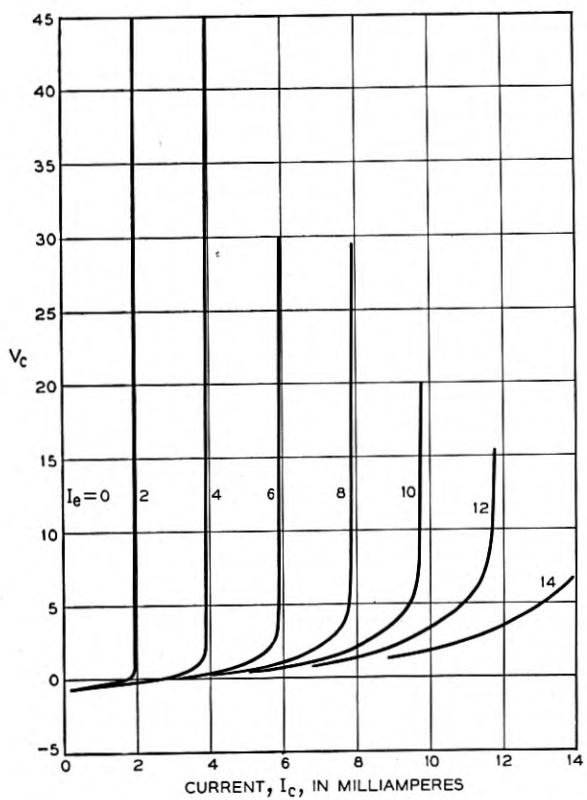

Fig. 6 — Collector characteristics of a double diffused silicon n-p-n transistor.

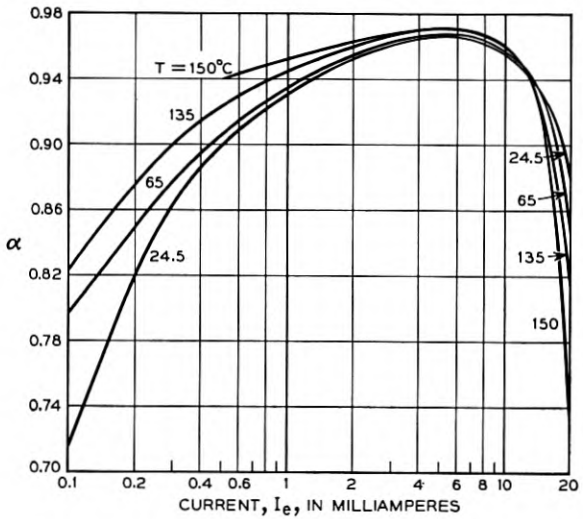

Fig. 7 — Alpha as a function of emitter current and temperature for a double diffused silicon n-p-n transistor.

under this condition does not truly saturate but collector junction resistance is very high. Collector junction resistances of 50 megohms at reverse biases of 50 volts are common.

The continuous power dissipation permissible with these units is also shown in Fig. 6. The figure shows dissipation of 200 milliwatts and the units have been operated at 400 milliwatts without damage. As illustrated in Fig. 3 no special provision has been made for power dissipation and it would appear from the performance obtained to date that powers of a few watts could be handled by these units with relatively minor provisions for heat dissipation. However, it can also be seen from Fig. 6 that at low collector voltages alpha decreases rapidly as the emitter current is increased. The transistor is, therefore, non-linear in this range of emitter currents and collector voltages. In many applications, this non-linearity may limit the operating range of the device to values below those which would be permissible from the point of view of continuous power dissipation.

Fig. 7 gives the magnitude of alpha as a function of emitter current for a fixed collector voltage of 10 volts and a number of ambient temperatures. These curves are presented to illustrate the stability of the parameters of the double diffused silicon transistor at increased ambient temperatures. Over the range from 1 to 15 milliamperes emitter current and 25°C to 150°C ambient temperature, alpha is seen to change only

by approximately 2 per cent. This amounts to only 150 parts per million change in alpha per degree centigrade change in ambient temperature.

The decrease in alpha at low emitter currents shown in Fig. 7 has been observed in every double diffused silicon transistor which has been made to date. Although this effect is not completely understood at present it could be caused by recombination centers in the base layer that can be saturated at high injection levels. Such saturation would result in an increase in effective lifetime and a corresponding increase in alpha. The large increase in alpha with temperature at low emitter currents is consistent with this proposal. It has also been observed that shining a strong light on the transistor will produce an appreciable increase in alpha at low emitter currents but has little effect at high emitter currents. A strong light would also be expected to saturate recombination centers which are active at low emitter currents and this behavior is also consistent with the above proposal.

3.0 DISCUSSION OF THE TRANSISTOR STRUCTURE

Although the low frequency electrical characteristics of the double diffused silicon transistor which are presented in Section 2 are quite similar to those usually obtained in junction transistors, the structure of the double diffused transistor is sufficiently different from that of the grown junction or alloy transistor that a discussion of some design principles is warranted. This section is devoted to a general discussion of the factors which determine the electrical characteristics of the transistors. In Section 4 the general ideas of Section 3 are applied in a more specialized fashion to the double diffused structure and a detailed calculation of electrical parameters is presented.

One essential difference between the double diffused transistor and grown junction or alloy transistors arises from the manner in which the impurities are distributed in the three active regions. In the ideal case of a double-doped grown junction transistor or an alloy transistor the concentration of impurities in a given region is essentially uniform and the transition from one conductivity type to another at the emitter and collector junctions is abrupt giving rise to step junctions. On the other hand in the double diffused structure the distribution of impurities is more closely described by the error function complement and the emitter and collector junctions are graded. These differences can have an appreciable influence on the electrical behavior of the transistors.

Fig. 8(a) shows the probable distribution of donor impurities, N_D, and acceptor impurities, N_A, in a double diffused n-p-n. Fig. 8(b) is a

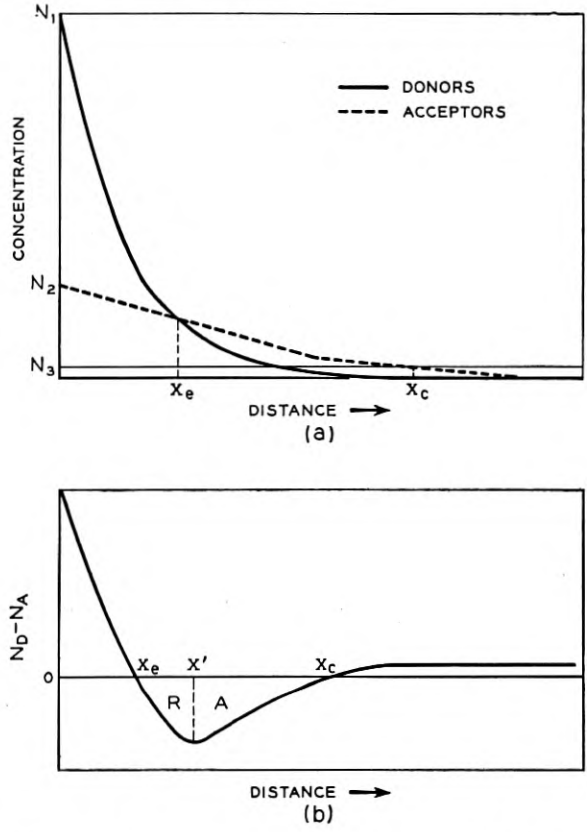

Fig. 8 — Diagrammatic representation of (a) donor and acceptor distributions and (b) uncompensated impurity distribution in a double diffused n-p-n transistor.

plot of $N_D - N_A$ which would result from the distribution in Fig. 8(a). Krömer[4] has shown that a nonuniform distribution of impurities in a semiconductor will produce electric fields which can influence the flow of electrons and holes. For example, in the base region the fields between the emitter junction, x_e, and the minimum in the $N_D - N_A$ curve, x', will retard the flow of electrons toward the collector while the fields between this minimum and the collector junction, x_c, will accelerate the flow of electrons toward the collector. These base layer fields will affect the transit time of minority carriers across the base and thus contribute

[4] H. Krömer, On Diffusion and Drift Transistor Theory I, II, III, Archiv. der Electr. Übertragung, **8**, pp. 223–228, pp. 363–369, pp. 499–504, 1954.

to the frequency response of the transistor. In addition the base resistance will be dependent on the distribution of both diffusants. These three factors are discussed in detail below.

Moll and Ross[5] have determined that the minority current, I_m, that will flow into the base region of a transistor if the base is doped in a non-uniform manner is given by

$$I_m = \frac{n_i^2 q D_m}{\int_b N(x)\, dx} e^{qV/kT} \tag{3.1}$$

where n_i is the carrier concentration in intrinsic material, q is the electronic charge, V is the applied voltage, D_m is the diffusion coefficient of the minority carriers, and the integral represents the total number of uncompensated impurities in the base. The primary assumptions in this derivation are (1) planar junctions, (2) no recombination in the base region, and (3) a boundary condition at the collector junction that the minority carrier density at this point equals zero. It is also assumed that the minority carrier concentration in the base region just adjacent to the emitter junction is equal to the equilibrium minority carrier density at this point multiplied by the Boltzman factor exp (qV/kT). It is of special interest to note that I_m depends only on the total number of uncompensated impurities in the base and not on the manner in which they are distributed.

In the double diffused transistor, it has been convenient from the point of ease of fabrication to make the emitter layer approximately the same thickness as the base layer. It has been observed that heating silicon to high temperatures degrades the lifetime of n- and p-type silicon in a similar manner.[6] Both base and emitter layers have experienced the same heat treatment and to a first approximation it can be assumed that the lifetime in the two regions will be essentially the same. Thus assumptions (1) and (2) should also apply to current flow from base to emitter. If we assume that the surface recombination velocity at the free surface of the emitter is infinite, then this imposes a boundary condition at this side of the emitter which under conditions of forward bias on the emitter is equivalent to assumption (3). Thus an equation of the form of (3.1) should also give the minority current flow from base to emitter. Since the emitter efficiency, γ, is given by

[5] J. L. Moll and I. M. Ross, The Dependence of Transistor Parameters on the Distribution of Base Layer Resistivity, Proc. I.R.E. in press.

[6] G. Bemski, private communication.

$$\gamma = \frac{I_m(\text{emitter to base})}{I_m(\text{emitter to base}) + I_m(\text{base to emitter})}$$

proper substitution of (3.1) will give the emitter efficiency of the double diffused n-p-n transistor,

$$\gamma = \frac{1}{1 + \dfrac{D_p}{D_n} \dfrac{\int_b (N_A - N_D)\, dx}{\int_e (N_D - N_A)\, dx}} \tag{3.2}$$

In (3.2), D_p is the diffusion coefficient of holes in the emitter, D_n is the diffusion coefficient of electrons in the base and the ratio of integrals is the ratio of total uncompensated doping in the base to that in the emitter.

A calculation of transit time is more difficult. Krömer[4] has studied the case of an aiding field which reduces transit time of minority carriers across the base region and thus increases frequency response. In the double diffused transistor the situation is more complex. Near the emitter side of the base region the field is retarding (Region R, see Fig. 8) and becomes aiding (Region A) only after the base region doping reaches a maximum. The case of retarding fields has been studied by Lee[3] and by Moll.[7] At present, the case for a base region containing both types of fields has not been solved. However, at the present state of knowledge some speculations about transit time can be made.

The two factors of primary importance are the magnitude of the built-in fields and the distance over which they extend. In the double diffused transistor, the widths of regions R and A are determined by the surface concentrations and diffusion coefficients of the diffusants. It can be shown by numerical computation[7] that if region R constitutes no more than 30–40 per cent of the entire base layer width, then the overall effect of the built-in fields will be to aid the transport of minority carriers and to produce a reduction in transit time. In addition the absolute magnitude of region R is important. If the point x' should occur within an effective Debye length from the emitter junction, i.e., if x' is located in the space charge region associated with the emitter junction, then the retarding fields can be neglected.

The base resistance can also be calculated from surface concentrations and diffusion coefficients of the impurities. This is done by considering the base layer as a conducting sheet and determining the sheet con-

[7] J. L. Moll, private communication.

ductivity from the total number of uncompensated impurities per square centimeter of sheet and the appropriate mobility weighted to account for impurity scattering.

4.0 CALCULATION OF DESIGN PARAMETERS

To calculate the parameters which determine emitter efficiency, transit time, and base resistance it is assumed that the distribution of uncompensated impurities is given by

$$N(x) = N_1 erfc \frac{x}{L_1} - N_2 erfc \frac{x}{L_2} + N_3 \tag{4.1}$$

where N_1 and N_2 are the surface concentrations of the emitter and base impurity diffusants respectively, L_1 and L_2 are their respective diffusion lengths, and N_3 is the original doping of the semiconductor into which the impurities are diffused. The impurity diffusion lengths are defined as

$$L_1 = 2\sqrt{D_1 t_1} \quad \text{and} \quad L_2 = 2\sqrt{D_2 t_2} \tag{4.2}$$

where the D's are the respective diffusion coefficients and the t's are the diffusion times.

Equation (4.1) can be reduced to

$$\Gamma(\xi) = \Gamma_1 \operatorname{erfc} \xi - \Gamma_2 \operatorname{erfc} \lambda\xi + 1 \tag{4.3}$$

where

$$\Gamma(\xi) = \frac{N(\xi)}{N_3}; \qquad \Gamma_1 = \frac{N_1}{N_3}; \qquad \Gamma_2 = \frac{N_2}{N_3}; \qquad \xi = \frac{x}{L_1}; \qquad \lambda = \frac{L_1}{L_2}$$

For cases of interest here, $\Gamma(\xi)$ will be zero at two points, α and β, and will have one minimum at ξ'. In the transistor structure the emitter junction occurs at $\xi = \alpha$ and the collector junction occurs at $\xi = \beta$. Thus the base width is determined by $\beta - \alpha$. The extent of aiding and retarding fields in the base is determined by ξ'. The integral of (4.3) from 0 to α, I_1, and from α to β, I_2, are the integrals of interest in (3.2) and thus determine emitter efficiency. In addition I_2 is the integral from which base resistance can be calculated.

The calculations which follow apply only for values of Γ_1/Γ_2 and Γ_2 greater than ten. Some of the simplifying assumptions which are made will not apply at lower values of these parameters where the distribution of both diffusants as well as the background doping affect the structure in all three regions of the device.

4.1 *Base Width*

From Fig. 8 and (4.3) it can be seen that for $\Gamma_2 \geqq 10$, α is essentially independent of Γ_2 and is primarily a function of Γ_1/Γ_2 and λ. Fig. 9 is a plot of α versus Γ_1/Γ_2 with λ as the parameter. The particular plot is for $\Gamma_2 = 10^4$. Although as stated α is essentially independent of Γ_2, at lower values of Γ_2, α may not exist for the larger values of λ, i.e., the p-layer does not form.

In the same manner, it can be seen that β is essentially independent of Γ_1/Γ_2 and is a function only of Γ_2 and λ. Fig. 10 is a plot of β versus Γ_2 with λ as a parameter. This plot is for $\Gamma_1/\Gamma_2 = 10$ and at larger Γ_1/Γ_2, β may not exist at large λ.

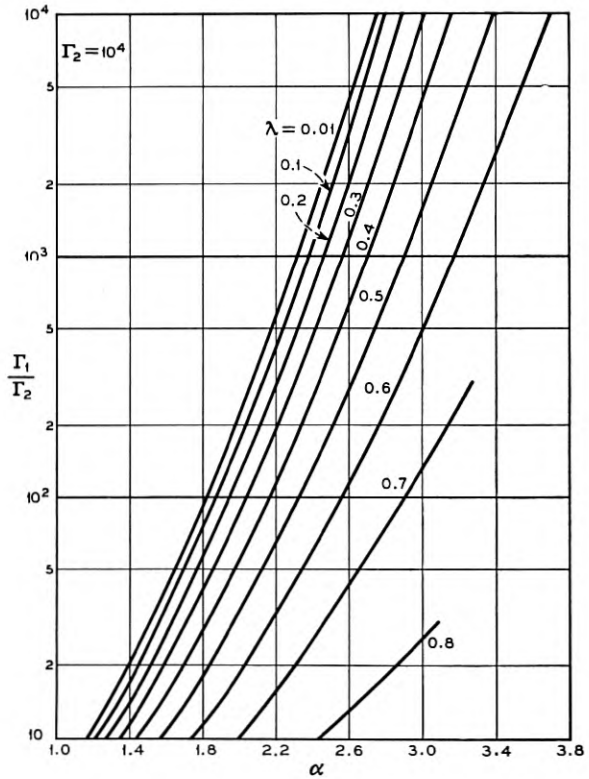

Fig. 9 — Emitter layer thickness (in reduced units) as a function of the ratio of the surface concentrations of the diffusing impurities (Γ_1/Γ_2) and the ratio of their diffusion lengths (λ).

The base width

$$w = \beta - \alpha$$

can be obtained from Figs. 9 and 10. α, β and w can be converted to centimeters by multiplying by the appropriate value of L_1.

4.2 *Emitter Efficiency*

With the limits α and β determined above, the integrals I_1 and I_2 can be calculated. Examination of the integrals shows that I_1 is closely proportional to Γ_1/Γ_2 and also to Γ_2. On the other hand I_2 is closely proportional to Γ_2 and essentially independent of Γ_1/Γ_2. Thus, the ratio of I_2/I_1 which determines γ depends primarily on Γ_1/Γ_2. Fig. 11 is a plot of the constant I_2/I_1 contours in the $\Gamma_1/\Gamma_2 - \lambda$ plane for I_2/I_1 in the range from -1.0 to -0.01. The graph is for $\Gamma_2 = 10^4$. Since from (3.2)

$$\gamma = \frac{1}{1 - \dfrac{D_p}{D_n}\dfrac{I_2}{I_1}} \tag{4.4}$$

for an n-p-n transistor, and assuming $D_p/D_n = \frac{1}{3}$ for silicon, then

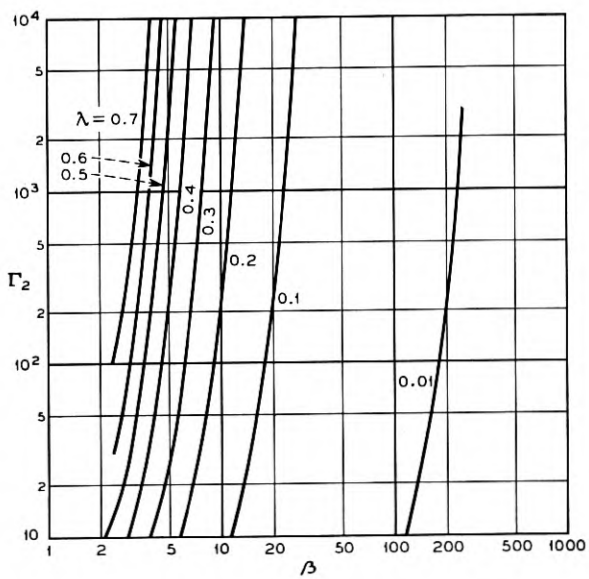

Fig. 10 — Collector junction depth (in reduced units) as a function of the surface concentration (in reduced units) of the diffusant which determines the conductivity type of the base layer (Γ_2) and the ratio of the diffusion lengths (λ) of the two diffusing impurities.

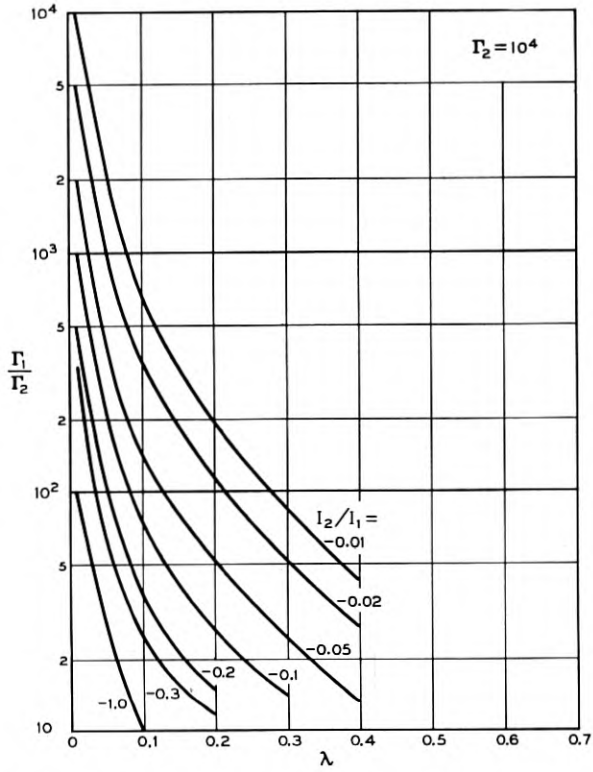

Fig. 11 — Dependence of emitter efficiency upon diffusant surface concentrations and diffusion lengths. The lines of constant I_2/I_1 are essentially lines of constant emitter efficiency. The ordinate is the ratio of surface concentrations of the two diffusants and the abscissa is the ratio of their diffusion lengths.

$I_2/I_1 = -1.0$ corresponds to a γ of 0.75 and $I_2/I_1 = -0.01$ corresponds to a γ of 0.997.

4.3 *Base Resistance*

It was indicated above that I_2 depends principally on Γ_2 and λ. Fig. 12 is a plot of the constant I_2 contours in the $\Gamma_2 - \lambda$ plane for I_2 in the range from -10^4 to -10. The graph is for $\Gamma_1/\Gamma_2 = 10$. The base layer sheet conductivity, g_b, can be calculated from these data as

$$g_b = -q\bar{\mu}I_2L_1N_3 \tag{4.5}$$

where q, L_1 and N_3 are as defined above and $\bar{\mu}$ is a mobility properly weighted to account for impurity scattering in the non-uniformly doped base region. The units of g_b are mhos per square.

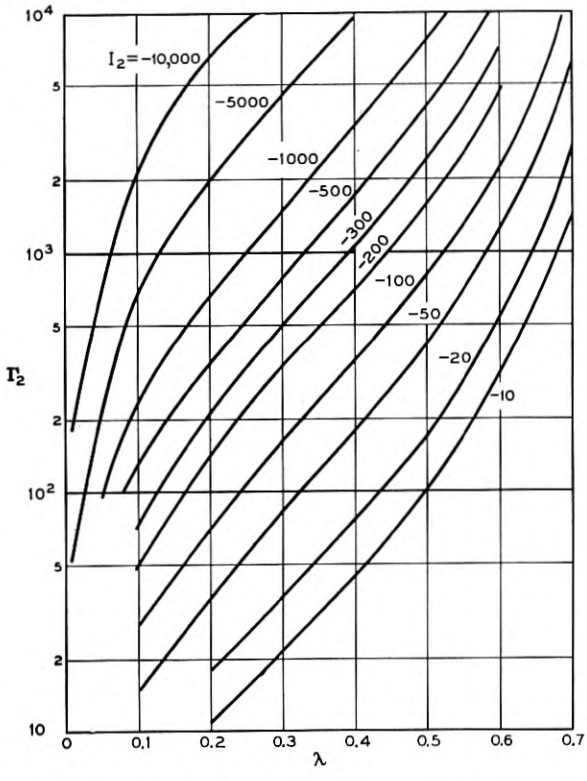

Fig. 12 — Dependence of base layer sheet conductivity on diffusant surface concentrations and diffusion lengths. The lines of constant I_2 are essentially lines of constant base sheet conductivity. The ordinate is the surface concentration (in reduced units) of the diffusant which determines the conductivity type of the base layer and the abscissa is the ratio of the diffusion lengths of the two diffusing impurities.

4.4 *Transit Time*

With a knowledge of where the minimum value, ξ', of (4.3) occurs, it is possible to calculate over what fraction of the base width the fields are retarding. The interesting quantity here is

$$\Delta R = \frac{\xi' - \alpha}{\beta - \alpha}$$

ξ' is a function of Γ_1/Γ_2 and λ and varies only very slowly with Γ_1/Γ_2. α is also a function of Γ_1/Γ_2 and λ and varies only slowly with Γ_1/Γ_2. The most rapidly changing part of ΔR is β which depends primarily on Γ_2 as noted above. Fig. 13 is a plot of the constant ΔR contours in the $\Gamma_2 - \lambda$ plane for values of ΔR in the range 0.1 to 0.3. This graph is

for data with $\Gamma_1/\Gamma_2 = 10$. As Γ_1/Γ_2 increases at constant Γ_2 and λ, ΔR decreases slightly. At $\Gamma_1/\Gamma_2 = 10^4$, the average change in ΔR is a decrease of about 25 per cent for constant Γ_2 and λ when $\Delta R \leqq 0.3$. The error is larger for values of ΔR greater than 0.3. It was noted above that when ΔR becomes greater than 0.3, the retarding fields become dominant. Therefore, this region is of slight interest in the design of a high frequency transistor.

4.5 *A Sample Design*

By superimposing Figs. 11, 12 and 13 the ranges of Γ_2, Γ_1/Γ_2 and λ which are consistent with desired values of γ, g_b and ΔR can be deter-

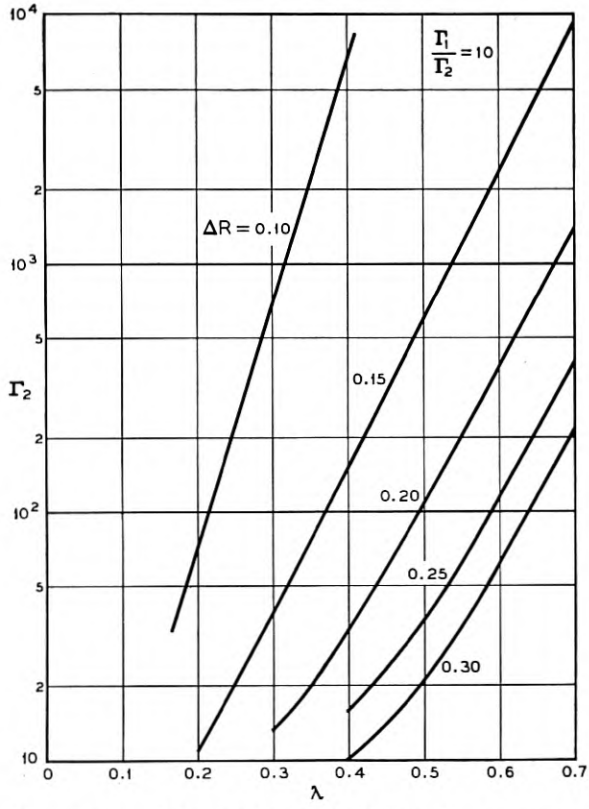

Fig. 13 — Dependence of the built-in field distribution on concentrations and diffusion lengths. The lines of constant ΔR indicate the fraction of the base layer thickness over which built-in fields are retarding. The ordinate is the surface concentration (in reduced units) of the diffusant which determines the conductivity type of the base layer and the abscissa is the ratio of the diffusion lengths of the two diffusing impurities.

mined by the area enclosed by the specified contour lines. It is also possible to compare the measured parameters of a specific device and observe how closely they agree with what is predicted from the estimated concentrations and diffusion coefficients. This is done below for the transistor described in Sections 1 and 2.

The comparison is complicated by the fact that the exact values of the surface concentrations and diffusion coefficients are not known precisely enough at present to permit an accurate evaluation of the design theory. However, the following values of concentrations and diffusion coefficients are thought to be realistic for this transistor.[1]

$$N_1 = 5 \times 10^{18} \qquad D_1 = 3 \times 10^{-12} \qquad t_1 = 5.7 \times 10^{3}$$

$$N_2 = 4 \times 10^{17} \qquad D_2 = 2.5 \times 10^{-11} \qquad t_2 = 1.2 \times 10^{3}$$

$$N_3 = 10^{15}$$

From these values it is seen that

$$\Gamma_1/\Gamma_2 = 12.5; \qquad \Gamma_2 = 400; \qquad \lambda = 0.6$$

From Fig. 9, $\alpha = 1.9$ and from Fig. 10, $\beta = 3.6$ and therefore $w = 1.7$. Measurement of the emitter and base layer dimensions showed that these layers were approximately the same thickness which was 3.8×10^{-4} cm. Thus the measured ratio of emitter width to base width of unity is in good agreement with the value of 1.1 predicted from the assumed concentrations and diffusion coefficients.

From Fig. 11, $I_2/I_1 \approx -0.01$. If this value is substituted into (4.4), $\gamma = 0.997$. This compares with a measured maximum alpha of 0.972.

From Fig. 12, $I_2 = -15$. Assuming an average hole mobility of 350 cm^2/volt. sec. and evaluating L_1 from the measured emitter thickness and the calculated α, (4.5) gives a value of $g_b = 1.7 \times 10^{-4}$ mhos per square. The geometry of the emitter and base contacts as shown in Fig. 3 makes it difficult to calculate the effective base resistance from the sheet conductivity even at very small emitter currents. In addition at the very high injection levels at which these transistors are operated the calculation of effective base resistance becomes very difficult. However, from the geometry it would be expected that the effective base resistance would be no greater than 0.1 of the sheet resistivity or 600 ohms. This is about seven times larger than the measured value of 80 ohms reported in Section 2.

From Fig. 13, ΔR is approximately 0.20. Thus there should be an overall aiding effect of the built-in fields. In addition the impurity gradient at the emitter junction is believed to be approximately 10^{21}/cm^4 and the

space charge associated with this gradient will extend approximately 2×10^{-5} cm into the base region. The base thickness over which retarding fields extend is ΔR times the base width or 7.6×10^{-5} cm. Thus the first quarter of region R will be space charge and can be neglected.

The frequency cutoff from pure diffusion transit is given by

$$f_\alpha = \frac{2.43D}{2\pi W^2} \tag{4.6}$$

where W is the measured base layer thickness. Assuming $D = 25$ cm^2/sec for electrons in the base region, $f_\alpha = 67$ mc/sec. Since the measured cutoff was 120 mc/sec, the predicted aiding effect of the built-in field is evidently present.

These computations illustrate how the measured electrical parameters can be used to check the values of the surface concentrations and diffusion coefficients. Conversely knowledge of the concentrations and diffusion coefficients aid in the design of devices which will have prescribed electrical parameters. The agreement in the case of the transistor described above is not perfect and indicates errors in the proposed values of the concentrations and diffusion coefficients. However, it is sufficiently close to be encouraging and indicate the value of the calculations.

The discussion of design has been limited to a very few of the important parameters. Junction capacitances, emitter and collector resistances are among the other important characteristics which have been omitted here. Presumably all of these quantities can be calculated if the detailed structure of the device is known and the structure should be susceptible to the type of analysis used above. Another fact, which has been ignored, is that these transistors were operated at high injection levels and a low level analysis of electrical parameters was used. All of these other factors must be considered for a detailed understanding of the device. The object of this last section has been to indicate one path which the more detailed analysis might take.

5.0 CONCLUSIONS

By means of multiple diffusion, it has been possible to produce silicon transistors with alpha-cutoff above 100 mc/sec. Refinements of the described techniques offer the possibility of even higher frequency performance. These transistors show the other advantages expected from silicon such as low saturation currents and satisfactory operation at high temperatures.

The structure of the double diffused transistor is susceptible to design

analysis in a fashion similar to that which has been applied to other junction transistors. The non-uniform distribution of impurities produces significant electrical effects which can be controlled to enhance appreciably the high-frequency behavior of the devices.

The extreme control inherent in the use of diffusion to distribute impurities in a semiconductor structure suggests that this technique will become one of the most valuable in the fabrication of semiconductor devices.

ACKNOWLEDGEMENT

The authors are indebted to several people who contributed to the work described in this paper. In particular, the double diffused silicon from which the transistors were prepared was supplied by C. S. Fuller and J. A. Ditzenberger. The data on diffusion coefficients and concentrations were also obtained by them.

P. W. Foy and G. Kaminsky assisted in the fabrication and mounting of the transistors and J. M. Klein aided in the electrical characterization. The computations of the various solutions of the diffusion equation, (4.3), were performed by Francis Maier. In addition many valuable discussions with C. A. Lee, G. Weinreich, J. L. Moll, and G. C. Dacey helped formulate many of the ideas presented herein.

A High-Frequency Diffused Base Germanium Transistor

By CHARLES A. LEE

(Manuscript received November 15, 1955)

Techniques of impurity diffusion and alloying have been developed which make possible the construction of p-n-p junction transistors utilizing a diffused surface layer as a base region. An important feature is the high degree of dimensional control obtainable. Diffusion has the advantages of being able to produce uniform large area junctions which may be utilized in high power devices, and very thin surface layers which may be utilized in high-frequency devices.

Transistors have been made in germanium which typically have alphas of 0.98 and alpha-cutoff frequencies of 500 mc/s. The fabrication, electrical characterization, and design considerations of these transistors are discussed.

INTRODUCTION

Recent work [1, 2] concerning diffusion of impurities into germanium and silicon prompted the suggestion[3] that the dimensional control inherent in these processes be utilized to make high-frequency transistors.

One of the critical dimensions of junction transistors, which in many cases seriously restricts their upper frequency limit of operation, is the thickness of the base region. A considerable advance in transistor properties can be accomplished if it is possible to reduce this dimension one or two orders of magnitude. The diffusion constants of ordinary donors and acceptors in germanium are such that, with n realizable temperatures and times, the depth of diffused surface layers may be as small as 10^{-6} cm. Already in the present works layers slightly less than 1 micron (10^{-4} cm) thick have been made and utilized in transistors. Moreover, the times and temperatures required to produce 1 micron surface layers permit good control of the depth of penetration and the concentration of the diffusant in the surface layer with techniques described below.

If one considers making a transistor whose base region consists of such

a diffused surface layer, several problems become immediately apparent:

(1) Control of body resistivity and lifetime during the diffusion heating cycle.

(2) Control of the surface concentration of the diffusant.

(3) Making an emitter on the surface of a thin diffused layer and controlling the depth of penetration.

(4) Making an ohmic base contact to the diffused surface layer.

One approach to the solution of these problems in germanium which has enabled us to make transistors with alpha-cutoff frequencies in excess of 500 mc/sec is described in the main body of the paper.

An important characteristic feature of the diffusion technique is that it produces an impurity gradient in the base region of the transistor. This impurity gradiant produces a "built-in" electric field in such a direction as to aid the transport of minority carriers from emitter to collector. Such a drift field may considerably enhance the frequency response of a transistor for given physical dimensions.[4]

The capabilities of these new techniques are only partially realized by their application to the making of high frequency transistors, and even in this field their potential has not been completely explored. For example, with these techniques applied to making a p-n-i-p structure the possibility of constructing transistor amplifiers with usable gain at frequencies in excess of 1,000 mc/sec now seems feasible.

DESCRIPTION OF TRANSISTOR FABRICATION AND PHYSICAL CHARACTERISTICS

As starting material for a p-n-p structure, p-type germanium of 0.8 ohm-cm resistivity was used. From the single crystal ingot rectangular bars were cut and then lapped and polished to the approximate dimensions: 200 × 60 × 15 mils. After a slight etch, the bars were washed in deionized water and placed in a vacuum oven for the diffusion of an n-type impurity into the surface. The vacuum oven consisted of a small molybdenum capsule heated by radiation from a tungsten coil and surrounded by suitable radiation shields made also of molybdenum. The capsule could be baked out at about 1,900°C in order that impurities detrimental to the electrical characteristics of the germanium be evaporated to sufficiently low levels.[5]

As a source of n-type impurity to be placed with the p-type bars in the molybdenum oven, arsenic doped germanium was used. The relatively high vapor pressure of the arsenic was reduced to a desirable range (about 10^{-4} mm of Hg) by diluting it in germanium. The use of germanium eliminated any additional problems of contamination by the

dilutant, and provided a convenient means of determining the degree of dilution by a measurement of the conductivity. The arsenic concentrations used in the source crystal were typically of the order of 10^{17}–10^{19}/cc. These concentrations were rather high compared to the concentrations desired in the diffused surface layers since compensation had to be made for losses of arsenic due to the imperfect fit of the cover on the capsule and due to some chemical reaction and adsorption which occurred on the internal surfaces of the capsule.

The layers obtained after diffusion were then evaluated for sheet conductivity and thickness. To measure the sheet conductivity a four-point probe method[6] was used. An island of the surface layer was formed by masking and etching to reveal the junction between the surface layer and the p-type body. The island was then biased in the reverse direction with respect to the body thus effectively isolating it electrically during the measurement of its sheet conductivity. The thickness of the surface layer was obtained by first lapping at a small angle to the original surface ($\frac{1}{2}°$–1°) and locating the junction on the beveled surface with a thermal probe; then multiplying the tangent of the angle between the two surfaces by the distance from the edge of the bevel to the junction gives the desired thickness. Another particularly convenient method of measuring the thickness[7] is to place a half silvered mirror parallel to the original surface and count fringes, of the sodium *D*-line for example, from the edge of the bevel to the junction. Typically the transistors described here were prepared from diffused layers with a sheet conductivity of about 200 ohms/square, and a layer thickness of $(1.5 \pm 0.3) \times 10^{-4}$ cm.

When the surface layer had been evaluated, the emitter and base contacts were made using techniques of vacuum evaporation and alloying. For the emitter, a film of aluminum approximately 1,000 Å thick was evaporated onto the surface through a mask which defined an emitter area of 1 × 2 mils. The bar with the evaporated aluminum was then placed on a strip heater in a hydrogen atmosphere and momentarily brought up to a temperature sufficient to alloy the aluminum. The emitter having been thus formed, the bar was again placed in the masking jig and a film of gold-antimony alloy from 3,000 to 4,000 Å thick was evaporated onto the surface. This film was identical in area to the emitter, and was placed parallel to and 0.5 to 1 mil away from the emitter. The bar was again placed on the heater strip and heated to the gold-germanium eutectic temperature, thus forming the ohmic base contact. The masking jig was constructed to permit the simultaneous evaporation of eight pairs of contacts on each bar. Thus, using a 3-mil diamond saw, a bar could be cut into eight units.

Each unit, with an alloyed emitter and base contact, was then soldered to a platinum tab with indium, a sufficient quantity of indium being used to alloy through the n-type surface layer on the back of the unit. One of the last steps was to mask the emitter and base contacts with a 6- to 8-mil diameter dot of wax and form a small area collector junction by etching the unit attached to the platinum tab, in CP4. After washing in solvents to remove the wax, the unit was mounted in a header designed to allow electrolytically pointed wire contacts to be made to the base and emitter areas of the transistor. These spring contacts were made of 1-mil phosphor bronze wire.

ELECTRICAL CHARACTERIZATION

Of the parameters that characterize the performance of a transistor, one of the most important is the short circuit current gain (alpha) versus frequency. The measured variation of α and $\alpha/(1-\alpha)$ (short-circuit current gain in the grounded emitter circuit) as a function of frequency for a typical unit is shown in Fig. 1. For comparison the same parameters for an exceptionally good unit are shown in Fig. 2.

In order that the alpha-cutoff frequency be a measure of the transit time of minority carriers through the active regions of the transistor, any resistance-capacity cutoffs, of the emitter and collector circuits, must lie considerably higher than the measured f_α. In the emitter circuit, an external contact resistance to the aluminum emitter of the order of 10

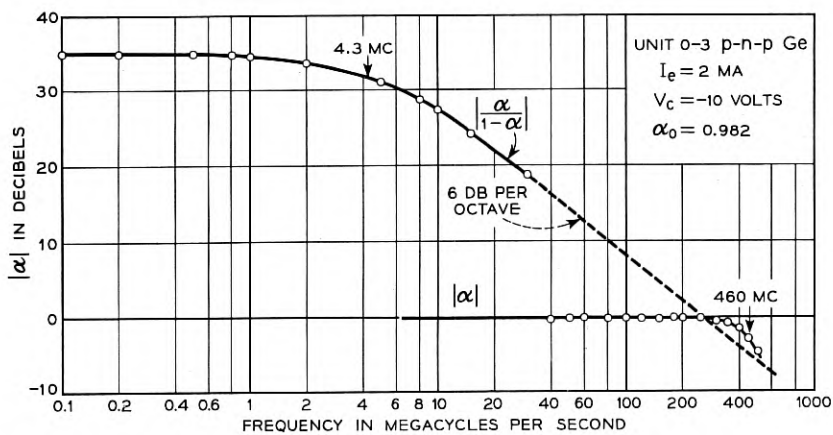

Fig. 1 — The grounded emitter and grounded base response versus frequency for a typical unit.

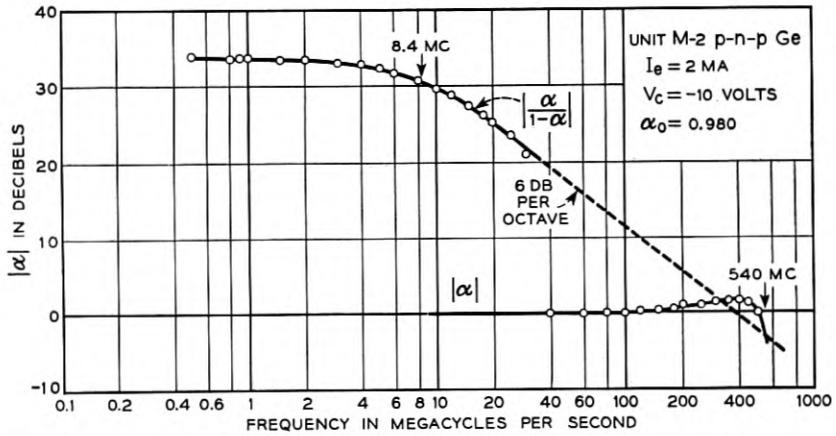

Fig. 2 — The grounded emitter and grounded base response versus frequency for an exceptionally good unit.

to 20 ohms and a junction transition capacity of 1 $\mu\mu$fd were measured. The displacement current which flows through this transition capacity reduces the emitter efficiency and must be kept small relative to the injected hole current. With 1 milliampere of current flowing through the emitter junction, and consequently an emitter resistance of 26 ohms, the emitter cutoff for this transistor was above 6,000 mc/sec. One can now see that the emitter area must be small and the current density high to attain a high emitter cutoff frequency. The fact that a low base resistance requires a high level of doping in the base region, and thus a high emitter transition capacity, restricts one to small areas and high current densities.

In the collector circuit capacities of 0.5 to 0.8 $\mu\mu$fd at a collector voltage of -10 volts were measured. There was a spreading resistance in the collector body of about 100 ohms which was the result of the small emitter area. The base resistance was approximately 100 ohms. If the phase shift and attenuation due to the transport of minority carriers through the base region were small at the collector cutoff frequency, the effective base resistance would be decreased by the factor $(1 - \alpha)$. The collector cutoff frequency is then given by

$$f_c = \frac{1}{2\pi C_c R_c}$$

where C_c = collector transition capacity

and R_c = collector body spreading resistance.

However, in the transistors described here the base region produces the major contribution to the observed alpha-cutoff frequency and it is more appropriate to use the expression

$$f_c = \frac{1}{2\pi C_c(r_b + R_c)}$$

where $r_b \equiv$ base resistance. This cutoff frequency could be raised by increasing the collector voltage, but the allowable power dissipation in the mounting determines an upper limit for this voltage. It should be noted that an increase in the doping of the collector material would raise the cutoff since the spreading resistance is inversely proportional to N_a, while the junction capacity for constant collector voltage is only proportional to $N_a^{1/2}$.

The low-frequency alpha of the transistor ranged from 0.95 to 0.99 with some exceptional units as high as 0.998. The factors to be considered here are the emitter efficiency γ and the transport factor β. The transport factor is dependent upon the lifetime in the base region, the recombination velocity at the surface immediately surrounding the emitter, and the geometry. The geometrical factor of the ratio of the emitter dimensions to the base layer thickness is >10, indicating that solutions for a planar geometry may be assumed.[8] If a lifetime in the base region of 1 microsecond and a surface recombination velocity of 2,000 cm/sec is assumed a perturbation calculation[9] gives

$$\beta = 0.995$$

The high value of β obtained with what is estimated to be a low base region lifetime and a high surface recombination velocity indicates that the observed low frequency alpha is most probably limited by the emitter injection efficiency. As for the emitter injection efficiency, within the accuracy to which the impurity concentrations in the emitter regrowth layer and the base region are known, together with the thicknesses of these two regions, the calculated efficiency is consistent with the experimentally observed values.

Considerations of Transit Time

An examination of what agreement exists between the alpha-cutoff frequency and the physical measurements of the base region involves the mechanism of transport of minority carriers through the active regions of the transistor. The "active regions" include the space charge

region of the collector junction. The transit time through this region[10] is no longer a negligible factor. A short calculation will show that with -10 volts on the collector junction, the space charger layer is about 4×10^{-4} cm thick and that the frequency cutoff associated with transport through this region is approximately 3,000 mc/sec.

The remaining problem is the transport of minority carriers through the base region. Depending upon the boundary conditions existing at the surface of the germanium during the diffusion process, considerable gradients of the impurity density in the surface layer are possible. However, the problem of what boundary conditions existed during the diffusion process employed in the fabrication of these transistors will not be discussed here because of the many uncertainties involved. Some qualitative idea is necessary though of how electric fields arising from impurity gradients may affect the frequency behavior of a transistor in the limit of low injection.

If one assumes a constant electric field as would result from an exponential impurity gradient in the base region of a transistor, then the continuity equation may be solved for the distribution of minority carriers.[4] From the hole distribution one can obtain an expression for the transport factor β and it has the form

$$\beta = e^{\eta} \frac{Z}{\eta \sinh Z + Z \cosh Z}$$

where

$$\eta \equiv \frac{1}{2} \ln \frac{N_e}{N_c} = \frac{1}{2} \frac{qE}{kT} w,$$

$$Z \equiv [i\varphi + \eta^2]^{1/2}$$

$$\varphi = \omega \frac{w^2}{D_p}$$

$N_e \equiv$ donor density in base region at emitter junction

$N_c \equiv$ donor density in base region at collector junction

$E \equiv$ electric field strength

$D_p \equiv$ diffusion constant for holes

$w \equiv$ width of the base layer

A plot of this function for various values of η is shown in Fig. 3. For $\eta = 0$, the above expression reduces to the well known case of a uniformly doped base region. The important feature to be noted in Fig. 3 is that relatively small gradients of the impurity distribution in the base layer can produce a considerable enhancement of the frequency response.

It is instructive to calculate what the alpha-cutoff frequency would be for a base region with a uniform distribution of impurity. The effective thickness of the base layer may be estimated by decreasing the measured thickness of the surface layer by the penetration of the space charge region of the collector and the depth of the alloyed emitter structure. Using a value for the diffusion constant of holes in the base region appropriate to a donor density of about 10^{17}/cc,

$$300 \text{ mc/s} \leqq f_\alpha \leqq 800 \text{ mc/s}$$

This result implies that the frequency enhancement due to "built-in" fields is at most a factor of two. In addition it was observed that the alpha-cutoff frequency was a function of the emitter current as shown in Fig. 4. This variation indicates that at least intermediate injection

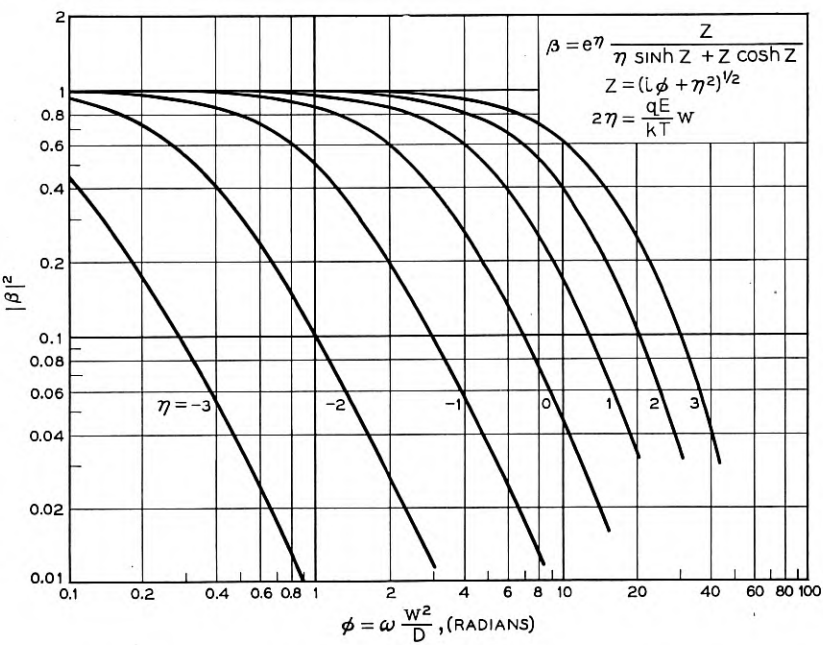

Fig. 3 — The variation of $|\beta|$ versus frequency for various values of a uniform drift field in the base region.

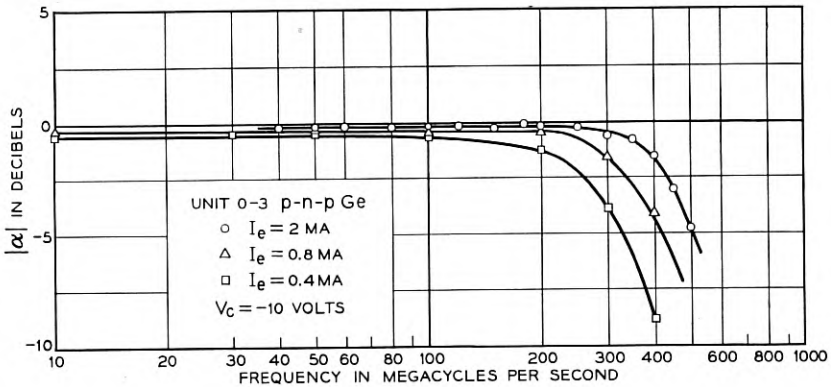

Fig. 4 — The variation of the alpha-cutoff frequency as a function of emitter current.

levels exist in the range of emitter current shown in Fig. 4. The conclusion to be drawn then is that electric fields produced by impurity gradients in the base region are not the dominant factor in the transport of minority carriers in these transistors.

The emitter current for a low level of injection could not be determined by measuring f_α versus I_e because the high input impedance at very low levels was shorted by the input capacity of the header and socket. Thus at very small emitter currents the measured cutoff frequency was due to an emitter cutoff and was roughly proportional to the emitter current. At $I_e \geqq 1$ ma this effect is small, but here at least intermediate levels of injection already exist.

A further attempt to measure the effect of any "built-in" fields by turning the transistor around and measuring the inverse alpha proved fruitless for two reasons. The unfavorable geometrical factor of a large collector area an a small emitter area as well as a poor injection efficiency gave an alpha of only

$$\alpha = 0.1$$

Secondly, the injection efficiency turns out in this case to be proportional to $\omega^{-1/2}$ giving a cutoff frequency of less than 1 mc/sec. The square-root dependence of the injection efficiency on frequency may be readily seen. The electron current injected into the collector body may be expressed as

$$J_e = qD_nN\left[\frac{1 + i\omega\tau_e}{L_e^2}\right]^{1/2}$$

where $q \equiv$ electronic charge

$D_n \equiv$ diffusion constant of electrons

$$N = \frac{q}{kT} v_1 n_c$$

$v_1 \equiv$ voltage across collector junction

$n_c \equiv$ density of electrons on the p-type side of the collector junction

$\tau_e \equiv$ lifetime of electrons in collector body

$L_e \equiv$ diffusion length of electrons in the collector body

Since the inverse cutoff frequency is well below that associated with the base region, we may regard the injected hole current as independent of the frequency in this region. The injection efficiency is low so that

$$\gamma \approx \frac{J_p}{J_e} \ll 1$$

Thus at a frequency where

$$\omega\tau_e \gg 1$$

then

$$\gamma \propto \omega^{-1/2}$$

An interesting feature of these transistors was the very high current densities at which the emitter could be operated without appreciable loss of injection efficiency. Fig. 5 shows the transmission of a 50 millimicrosecond pulse up to currents of 18 milliamperes which corresponds to a current density of 1800 amperes/cm^2. The injection efficiency should remain high as long as the electron density at the emitter edge of the base region remains small compared to the acceptor density in the emitter regrowth layer. When high injection levels are reached the injected hole density at the emitter greatly exceeds the donor density in the base region. In order to preserve charge neutrality then

$$p \approx n$$

where $p \equiv$ hole density

$n \equiv$ electron density

As the injected hole density is raised still further the electron density will eventually become comparable to the acceptor density in the emitter regrowth layer. The density of acceptors in the emitter regrowth

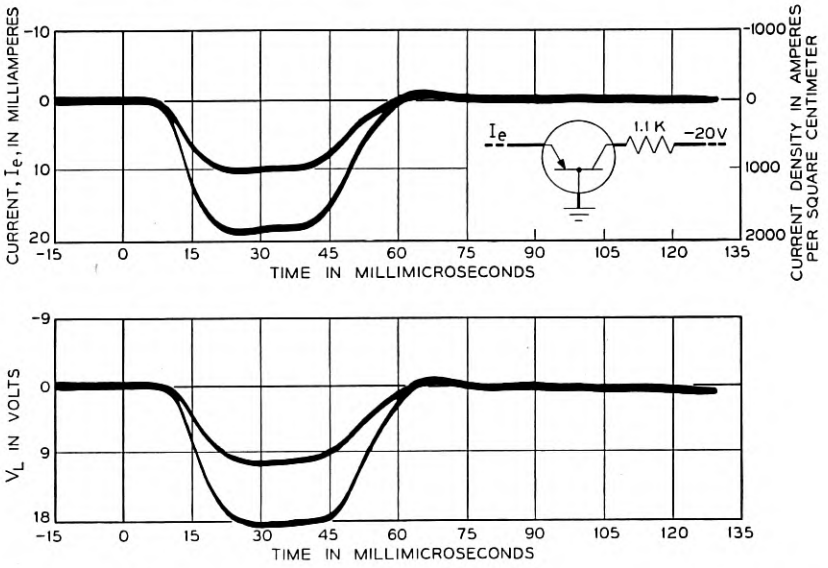

Fig. 5 — Transmission of a 50 millimicrosecond pulse at emitter currents up to 18 ma by a typical unit. (Courtesy of F. K. Bowers).

region is of the order of

$$N_A \approx 10^{20}/\text{cc}$$

and this is to be compared with injected hole density at the base region side of the emitter junction. The relation between the injected hole density and the current density may be approximated by[8]

$$J_p = \frac{2qD_p p_1}{w}$$

where p_1 = hole density at emitter side of base region

w = width of base region

A short calculation indicates that the emitter efficiency should remain high at a current density of an order of magnitude higher than 1,800 amp/cm^2. The measurements were not carried to higher current densities because the voltage drop across the spreading resistance in the collector was producing saturation of the collector junction.

CONCLUSIONS

Impurity diffusion is an extremely powerful tool for the fabrication of high frequency transistors. Moreover, of the 50-odd transistors which

were made in the laboratory, the characteristics were remarkably uniform considering the variations usually encountered at such a stage of development. It appears that diffusion process is sufficiently controllable that the thickness of the base region can be reduced to half that of the units described here. Therefore, with no change in the other design parameters, outside of perhaps a different mounting, units with a 1000 mc/s cutoff frequency should be possible.

ACKNOWLEDGMENT

The author wishes to acknowledge the help of P. W. Foy and W. Wiegmann who aided in the construction of the transistors, D. E. Thomas who designed the electrical equipment needed to characterize these units, and J. Klein who helped with the electrical measurements. The numerical evaluation of alpha for drift fields was done by Lillian Lee whose assistance is gratefully acknowledged.

REFERENCES

1. C. S. Fuller, Phys. Rev., **86,** pp. 136–137, 1952.
2. J. Saby and W. C. Dunlap, Jr., Phys. Rev., **90,** p. 630, 1953.
3. W. Shockley, private communication.
4. H. Krömer, Archiv. der Elek. Übertragung, **8,** No. 5, pp. 223–228, 1954.
5. R. A. Logan and M. Schwartz, Phys. Rev., **96,** p. 46, 1954
6. L. B. Valdes, Proc. I.R.E., **42,** pp. 420–427, 1954.
7. W. L. Bond and F. M. Smits, to be published.
8. E. S. Rittner, Pnys. Rev., **94,** p. 1161, 1954.
9. W. M. Webster, Proc. I.R.E., **42,** p. 914, 1954.
10. J. M. Early, B.S.T.J., **33,** pp. 517–533, 1954.

Waveguide Investigations with Millimicrosecond Pulses

By A. C. BECK

(Manuscript received October 11, 1955)

Pulse techniques have been used for many waveguide testing purposes. The importance of increased resolution by means of short pulses has led to the development of equipment to generate, receive and display pulses about 5 or 6 millimicroseconds long. The equipment is briefly described and its resolution and measuring range are discussed. Dominant mode waveguide and antenna tests are described and illustrated. Applications to multimode waveguides are then considered. Mode separation, delay distortion and its equalization, and mode conversion are discussed, and examples are given. The resolution obtained with this equipment provides information that is difficult to get by any other means, and its use has proved to be very helpful in waveguide investigations.

CONTENTS

1. INTRODUCTION

Pulse testing techniques have been employed to advantage in waveguide investigations in numerous ways. The importance of better resolution through the use of short pulses has always been apparent and, from the first, equipment was employed which used as short a pulse as possible. Radar-type apparatus using magnetrons and a pulse width of about one-tenth microsecond has seen considerable use in waveguide research, and many of the results have been published.[1, 2]

To improve the resolution, work was initiated some time ago by S. E. Miller to obtain measuring equipment which would operate with much shorter pulses. As a result, pulses about 5 or 6 millimicroseconds long became available at a frequency of 9,000 mc. In a pulse of this length there are less than 100 cycles of radio frequency energy, and the signal occupies less than ten feet of path length in the transmission medium. The RF bandwidth required is about 500 mc. In order to obtain such bandwidths, traveling wave tubes were developed by J. R. Pierce and members of the Electronics Research Department of the Laboratories. The completed amplifiers were designed by W. W. Mumford. N. J. Pierce, R. W. Dawson and J. W. Bell assisted in the design and construction phases, and G. D. Mandeville has been closely associated in all of this work.

2. PULSE GENERATION

These millimicrosecond pulses have been produced by two different types of generators. In the first equipment, a regenerative pulse generator of the type suggested by C. C. Cutler of the Laboratories was used.[3] This was a very useful device, although somewhat complicated and hard to keep in adjustment. A brief description of it will permit comparisons with a simpler generator which was developed a little later.

A block diagram of the regenerative pulse generator is shown in Fig. 1. The fundamental part of the system is the feedback loop drawn with heavy lines in the lower central part of the figure. This includes a traveling wave amplifier, a waveguide delay line about sixty feet long, a crystal expander, a band-pass filter, and an attenuator. This combination forms an oscillator which produces very short pulses of microwave energy. Between pulses, the expander makes the feedback loop loss too high for oscillation. Each time the pulse circulates around the loop it tends to shorten, due to the greater amplification of its narrower upper part caused by the expander action, until it uses the entire available bandwidth. A 500-mc gaussian band-pass filter is used in the feedback loop of this generator to determine the final bandwidth. An automatic gain control operates with the expander to limit the pulse amplitude, thus preventing amplifier compression from reducing the available expansion.

To get enough separation between outgoing pulses for reflected pulse measurements with waveguides, the repetition rate would need to be too low for a practical delay line length in the loop. Therefore a 12.8-mc fundamental rate was chosen, and a gated traveling wave tube amplifier was used to reduce it to a 100-kc rate at the output. This amplifier is kept in a cutoff condition for 127 pulses, and then a gate pulse restores

it to the normal amplifying condition for fifty millimicroseconds, during which time the 128th pulse is passed on to the output of the generator as shown on Fig. 1.

The synchronizing system is also shown on Fig. 1. A 100-kc quartz crystal controlled oscillator with three cathode follower outputs is the basis of the system. One output goes through a seven stage multiplier to get a 12.8-mc signal, which is used to control a pulser for synchronizing the circulating loop. Another output controls the gate pulser for the output traveling wave amplifier. Accurate timing of the gate pulse is obtained by adding the 12.8-mc pulses through a buffer amplifier to the gate pulser. The third output synchronizes the indicator oscilloscope sweep to give a steady pattern on the screen.

Although this equipment was fairly satisfactory and served for many

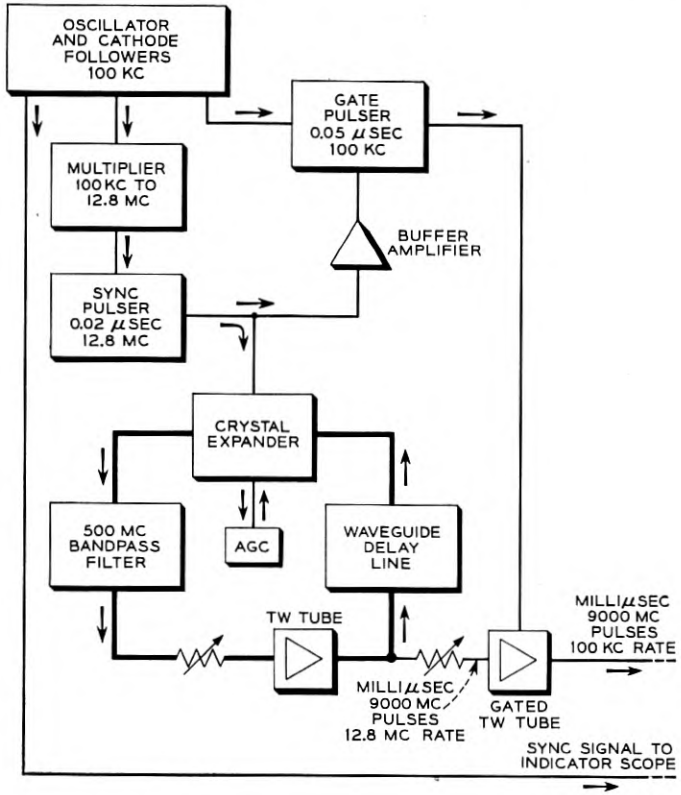

FIG. 1 — Block diagram of the regenerative pulse generator.

testing purposes, it was rather complex and there were some problems in its construction and use. It was difficult to obtain suitable microwave crystals to match the waveguide at low levels in the expander. This would make it even more difficult to build this type of pulse generator for higher frequency ranges. Stability also proved to be a problem. The frequency multiplier had to be very well constructed to avoid phase shift due to drifting. The gate pulser also required care in design and construction in order to get a stable and flat output pulse. It was somewhat troublesome to keep the gain adjusted for proper operation, and the gate pulse time adjustment required some attention. The pulse frequency could not be changed. For these reasons, and in order to get a smaller, lighter and less complicated pulse generator, work was carried out to produce pulses of about the same length by a simpler method.

If the gated output amplifier of Fig. 1 were to have a CW instead of a pulsed input, a pulse of microwave energy would nevertheless appear at the output because of the presence of the gating pulse. This gating pulse is applied to the beam forming electrode of the tube to obtain the gating action. If the beam forming electrode could be pulsed from cutoff to its normal operating potential for a very short time, very short pulses of output energy could be obtained from a continuous input signal. However, it is difficult to obtain millimicrosecond video gating pulses of sufficient amplitude for this purpose at a 100-kc repetition rate.

A traveling-wave tube amplifies normally only when the helix is within a small voltage range around its rated dc operating value. For voltages either above or below this range, the tube is cut off. When the helix voltage is raised through this range into the cutoff region beyond it, and then brought back again, two pulses are obtained, one during a small part of the rise time and the other during a small part of the return time. If the rise and fall times are steep, very short pulses can be obtained. Fig. 2 shows the pulse envelopes photographed from the indicator scope screen when this is done. For the top trace, the helix was biased 300 volts negatively from its normal operating potential, then pulsed to its correct operating range for about 80 millimicroseconds, during which time normal amplification of the CW input signal was obtained. The effect of further increasing the helix video pulse amplitude in the positive direction is shown by the succeeding lower traces. The envelope dips in the middle, then two separated pulses remain — one during a part of the rise time and one during a part of the fall time of helix voltage. The pulses shown on the bottom trace have shortened to about six millimicroseconds in length. The helix pulse had a positive amplitude of about 500 volts for this trace.

Since only one of these pulses can be used to get the desired repetition rate, it is necessary to eliminate the other pulse. This is done in a similar manner to that used for gating out the undesired pulses in the regenerative pulse generator. However, it is not necessary to use another amplifier, as was required there, since the same tube can be used for this purpose, as well as for producing the microwave pulses. Its beam forming electrode is biased negatively about 250 volts with respect to the cathode, and then is pulsed to the normal operating potential for about 50 millimicroseconds during the time of the first short pulse obtained by gating the helix. Thus, the beam forming electrode potential has been returned to the cutoff value during the second helix pulse, which is therefore eliminated.

A block diagram of the resulting double-gated pulse generator is shown in Fig. 3. Comparison with Fig. 1 shows that it is simpler than the regenerative pulse generator, and it has also proved more satisfactory in operation. It can be used at any frequency where a signal source and a traveling-wave amplifier are available, and the pulse

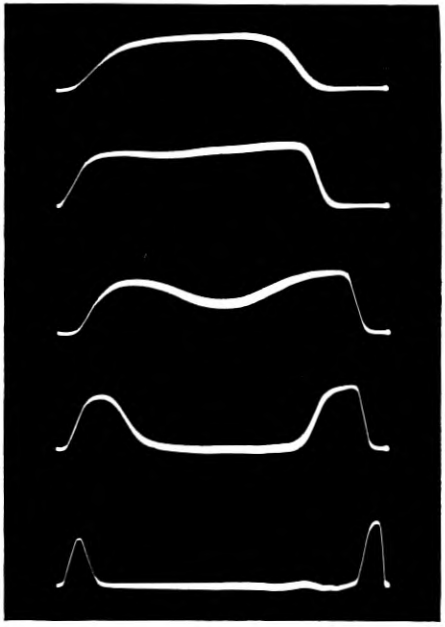

Fig. 2 — Envelopes of microwave pulses at the output of a traveling wave amplifier with continuous wave input and helix gating. The gating voltage is higher for the lower traces.

frequency can be set anywhere within the bandwidth of the traveling-wave amplifier by tuning the klystron oscillator.

The pulse center frequency is shifted from that of the klystron oscillator frequency by this helix gating process. An over-simplified but helpful explanation of this effect can be obtained by considering that the microwave signal voltage on the helix causes a bunching of the electron stream. This bunching has the same periodicity as the microwave signal voltage when the dc helix potential is held constant. However, since the helix voltage is continuously increased in the positive direction during the time of the first pulse, the average velocity of the last bunches of electrons becomes higher than that of the earlier bunches in the pulse, because the later electrons come along at the time of higher positive helix voltage. This tends to shorten the total length of the series of bunches, resulting in a shorter wavelength at the output end of the helix and therefore a higher output microwave frequency. On the second pulse, obtained when the helix voltage returns toward zero, the process is reversed, the bunching is stretched out, and the frequency is decreased. This second pulse is, however, gated out in this arrangement by the beam-forming electrode pulsing voltage. The result for this particular tube and pulse length is an effective output frequency approximately 150 mc higher than the oscillator frequency, but this figure is not constant over the range of pulse frequencies available within the amplifier bandwidth.

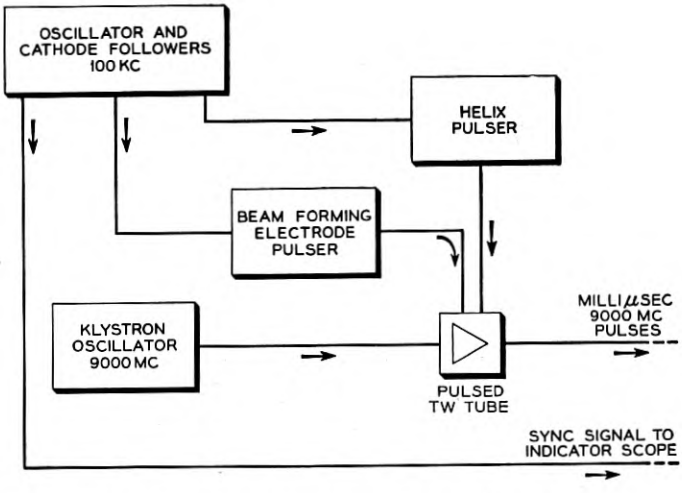

Fig. 3 — Block diagram of the double-gated traveling wave tube millimicrosecond pulse generator.

3. RECEIVER AND INDICATOR

The receiving equipment is shown in Fig. 4. It uses two traveling-wave amplifiers in cascade. A wide band detector and a video amplifier then follow, and the signal envelope is displayed by connecting it to the vertical deflecting plates of a 5 XP type oscilloscope tube. The video amplifier now consists of two Hewlett Packard wide band distributed amplifiers, having a baseband width of about 175 mc. The second one of these has been modified to give a higher output voltage. The sweep circuits for this oscilloscope have been built especially for this use, and produce a sweep speed in the order of 6 feet per microsecond. An intensity pulser is used to eliminate the return trace. These parts of the system are controlled by a synchronizing output from the pulse generator 100-kc oscillator. A precision phase shifter is used at the receiver for the same purpose that a range unit is employed in radar systems. This has a dial, calibrated in millimicroseconds, which moves the position of a pulse appearing on the scope and makes accurate measurement of pulse delay time possible.

Fig. 4 also shows the appearance of the pulses obtained with this equipment. The pulse on the left-hand side of this trace came from the

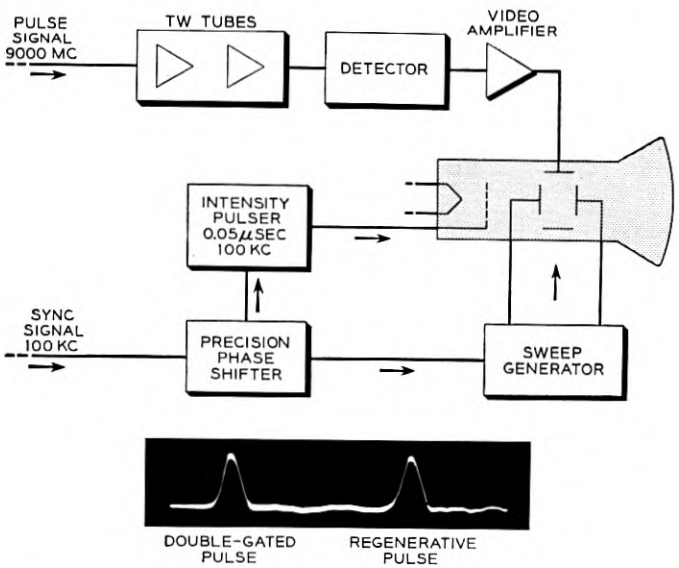

Fig. 4 — Block diagram of millimicrosecond pulse receiver and indicator. The indicator trace photograph shows pulses from each type of generator.

newer double-gated pulse generator, while the pulse on the right was produced by the regenerative pulse generator. It can be seen that they appear to have about the same pulse width and shape. This is partly due to the fact that the video amplifier bandwidth is not quite adequate to show the actual shape, since in both cases the pulses are slightly shorter than can be correctly reproduced through this amplifier. The ripples on the base line following the pulses are also due to the video amplifier characteristics when used with such short pulses.

4. RESOLUTION AND MEASURING RANGE

Fig. 5 shows a piece of equipment which was placed between the pulse generator and the receiver to show the resolution which can be obtained. This waveguide hybrid junction has its branch marked 1 connected to the pulse generator and branch 3 connected to the receiver. If the two side branches marked 2 and 4 were terminated, substantially no energy would be transmitted from the pulser straight through to the receiver. However, a short circuit placed on either side branch will send energy through the system to the receiver. Two short circuits were so placed that the one on branch 4 was 4 feet farther away from the hybrid junction than the one on branch 2. The pulse appearing first is produced by a signal traveling from the pulse generator to the short circuit on branch 2 and then through to the receiver, as shown by the path drawn with short dashes. A second pulse is produced by the signal which travels

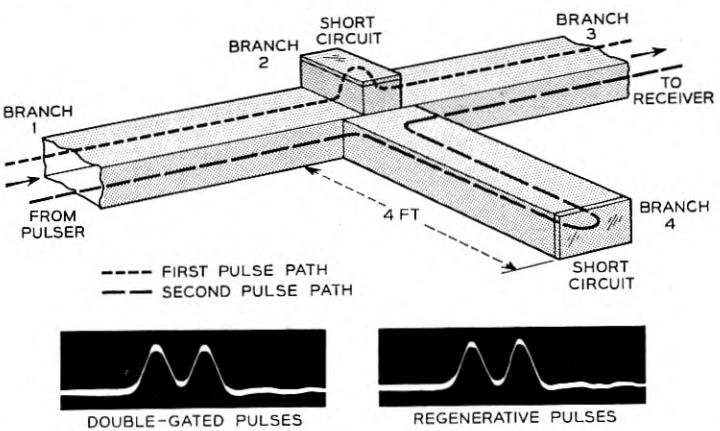

Fig. 5 — Waveguide hybrid circuit used to demonstrate resolution of millimicrosecond pulses. Trace photographs of pulses from each type of generator are shown.

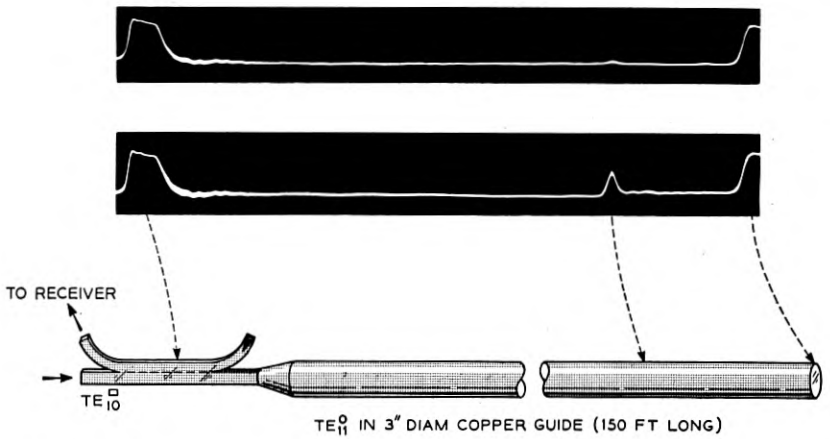

Fig. 6 — Waveguide arrangement and oscilloscope trace photos showing presence and location of defective joint. The dominant mode (TE_{11}) was used with its polarization changed 90 degrees for the two trace photos.

from the pulse generator through branch 4 to the short circuit and then to the receiver as shown by the long dashed line. This pulse has traveled 8 feet farther in the waveguide than the first pulse. This would be equivalent to seeing separate radar echoes from two targets about 4 feet apart. Resolution tests made in this way with the pulses from the regenerative pulse generator, and from the double-gated pulse generator, are shown on Fig. 5. With our video amplifier and viewing equipment, there is no appreciable difference in the resolution obtained using either type of pulse generator.

The measuring range is determined by the power output of the gated amplifier at saturation and by the noise figure of the first tube in the receiver. In this equipment the saturation level is about 1 watt, and the noise figure of the first receiver tube is rather poor. As a result, received pulses about 70 db below the outgoing pulse can be observed, which is enough range for many measurement purposes.

5. DOMINANT MODE WAVEGUIDE TESTS

Fig. 6 shows the use of this equipment to test 3″ round waveguides such as those installed between radio repeater equipment and an antenna. This particular 150-foot line had very good soldered joints and was thought to be electrically very smooth. The signal is sent in through a transducer to produce the dominant TE_{11} mode. The receiver is connected through a directional coupler on the sending end to look for any

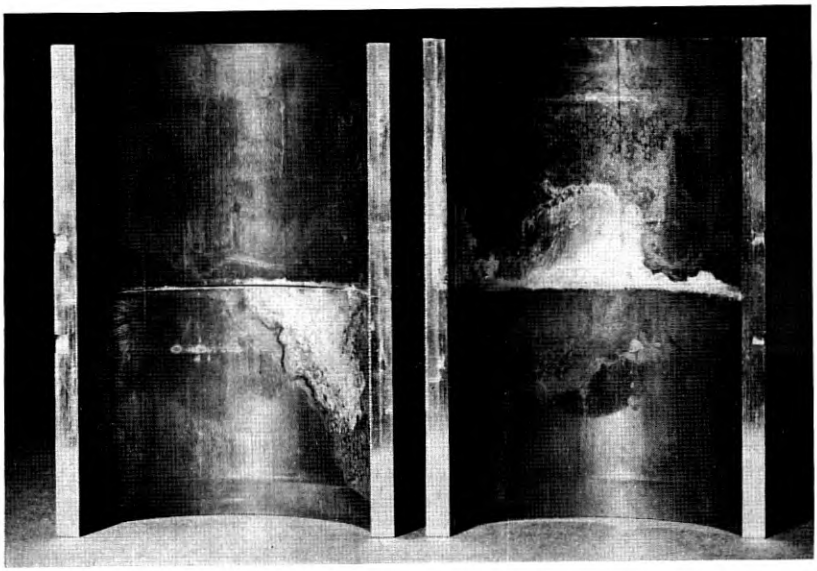

Fig. 7 — Defective joint caused by imperfect soldering which gave the reflection shown on Fig. 6.

reflections from imperfections in the line. The overloaded signal at the left of the oscilloscope trace is produced by leakage directly through the directional coupler. The overloaded signal on the other end of this trace is produced by the reflection from the short circuit piston at the far end of the waveguide. The signal between these two, which is about 45 db down from the input signal, is produced by an imperfect joint in the waveguide. The signal polarization was oriented so that a maximum reflection was obtained in the case of the lower trace. In the other trace, the polarization was changed by 90°. It is seen that this particular joint produces a stronger reflection for one polarization than for the other. By use of the precision phase shifter in the receiver the exact location of this defect was found and the particular joint that was at fault was sawed out. Fig. 7 shows this joint after the pipe had been cut in half through the middle. The guide is quite smooth on the inside in spite of the discoloration of some solder that is shown here, but on the left-hand side of the illustration the open crack is seen where the solder did not run in properly. This causes the reflected pulse that shows on the trace. The fact that this crack is less than a semi-circumference in length causes the echo to be stronger for one polarization than for the other.

Fig. 8 shows the same test for a 3″ diameter aluminum waveguide 250 feet long. This line was mounted horizontally in the test building with compression couplings used at the joints. The line expanded on warm days but the friction of the mounting supports was so great that it pulled open at some of the joints when the temperature returned to normal. These open joints produced reflected pulses from 40 to 50 db down, which are shown here. They come at intervals equal to the length of one section of pipe, about 12 feet. Some of these show polarization effects where the crack was more open on one side than on the other, but others are almost independent of polarization. These two photographs of the trace were taken with the polarization changed 90°.

Fig. 9 shows the same test for a 3″ diameter galvanized iron waveguide. This line had shown fairly high loss using CW for measurements. The existence of a great many echoes from random distances indicates a rough interior finish in the waveguide. Fig. 10 shows the kind of inperfections in the zinc coating used for galvanizing which caused these reflections.

6. TESTING ANTENNA INSTALLATIONS

The use of this equipment in testing waveguide and antenna installations for microwave radio repeater systems is shown in Fig. 11. This particular work was done in cooperation with A. B. Crawford's antenna research group at Holmdel, who designed the antenna system. A directional coupler was used to observe energy reflections from the system under test. In this installation a 3″ diameter round guide carrying the TE_{11} mode was used to feed the antenna. Two different waveguide

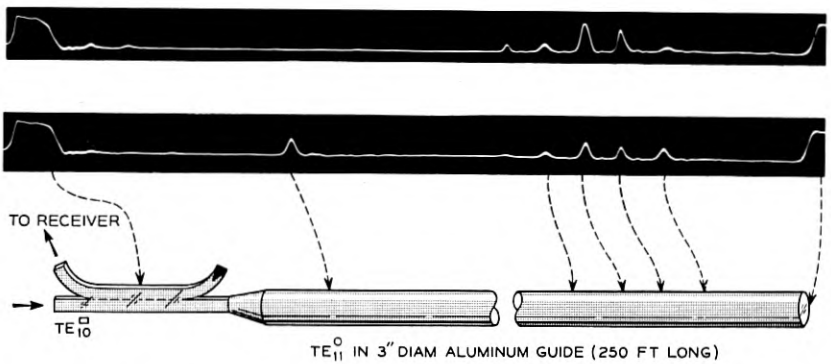

Fig. 8 — Reflections from several defective joints in a dominant (TE_{11}) mode waveguide. The two trace photos are for polarizations differing by 90 degrees.

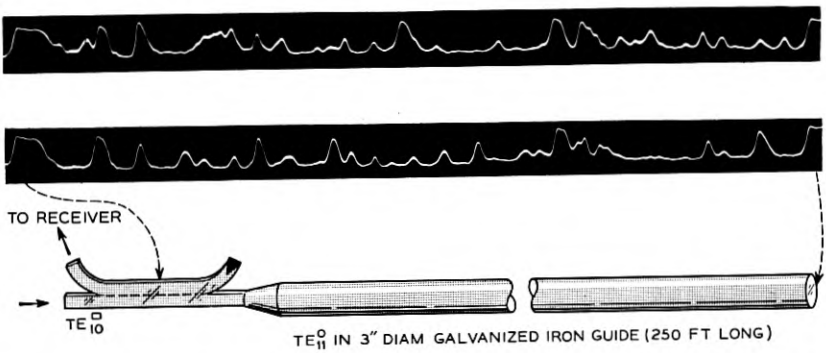

FIG. 9 — Multiple reflections from a dominant (TE_{11}) mode waveguide with a rough inside surface. The two trace photos are for polarizations differing by 90 degrees.

joints are shown here. In addition, a study was being made of the return loss of the transition piece at the throat of the antenna which connected the 3″ waveguide to the square section of the horn. The waveguide sections are about 10 feet long. The overloaded pulse at the left on the traces is the leakage through the directional coupler. The

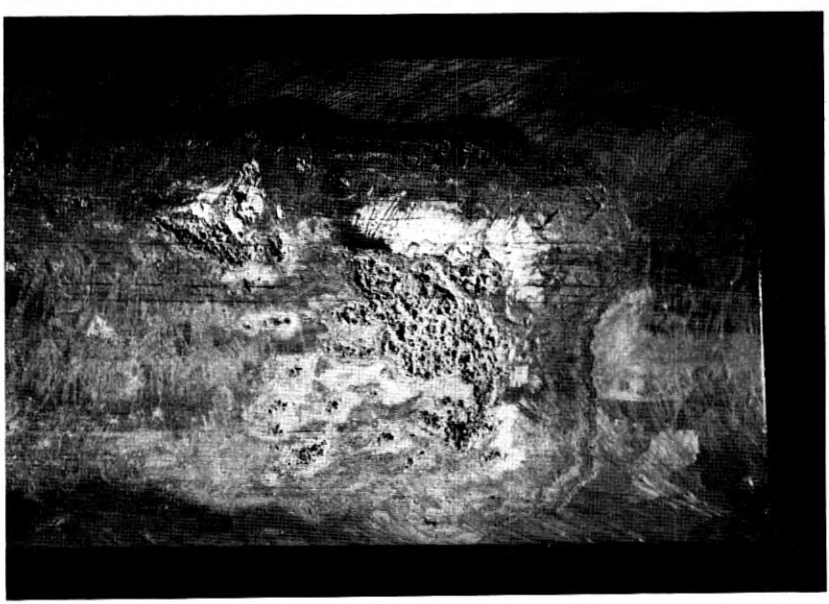

Fig. 10 — Rough inside surface of a galvanized iron waveguide which produced the reflections shown on Fig. 9.

other echoes are associated with the parts of the system from which they came by the dashed lines and arrows on the figure. A clamped joint in the line gave the reflection shown next following the initial overloaded pulse. A well made threaded coupling in which the ends of the pipe butted squarely is seen to have a very much lower reflection, scarcely observable on this trace. Since there is always reflection from the mouth and upper reflector parts of this kind of antenna, it is not possible to measure a throat transition piece alone by conventional CW methods, as the total reflected power from the system is measured. Here, use of the resolution of this short pulse equipment completely separated the reflection of the transition piece from all other reflections and made a measurement of its performance possible. In this particular case, the reflection from the transition is more than 50 db down from the incident signal which represents very good design. As can be seen,

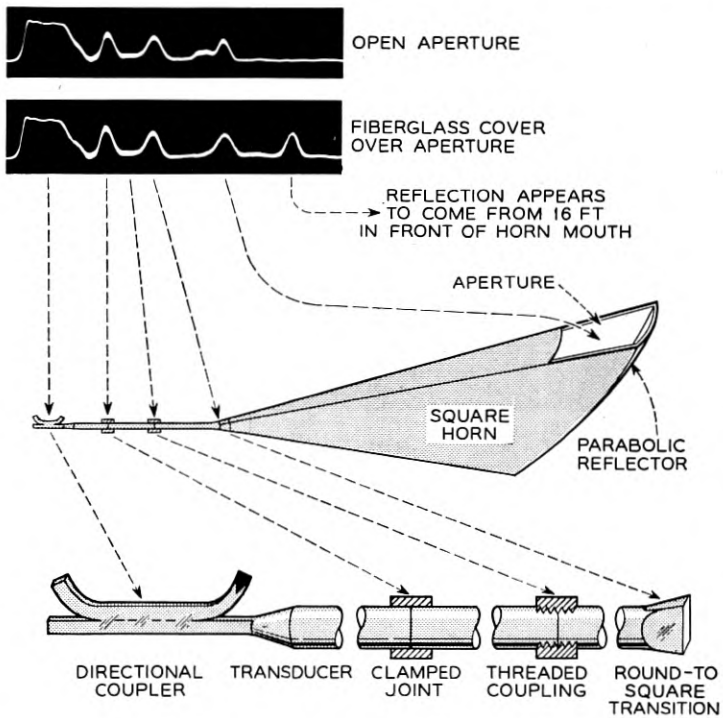

Fig. 11 — Waveguide and antenna arrangement with trace photos showing reflections from joints, transition section, and cover.

the reflection from the parabolic reflector and mouth is also quite low, and this characterizes a good antenna installation.

The extra reflected pulse on the right of the lower trace on Fig. 11 appeared when a fiberglas weatherproof cover was installed over the open mouth of the horn. This cover by itself would normally produce a troublesome reflection. However, in this antenna, it is a continuation of one of the side walls of the horn. Consequently, outgoing signals strike it at an oblique angle. Reflected energy from it is not focused by the parabolic section back at the waveguide, so the overall reflected power in the waveguide was found to be rather low. However, measuring it with this equipment, we found that an extra reflection appeared to come from a point 16 feet out in front of the mouth of the horn when the cover was in place. This is accounted for by the fact that energy reflected obliquely from this cover bounces back and forth inside the horn before getting back into the waveguide, thus traveling the extra distance that makes the measurement seem to show that it comes from 16 feet out in front.

7. SEPARATION OF MODES ON A TIME BASIS

If a pulse of energy is introduced into a moderate length of round waveguide to excite a number of modes which travel with different group velocities, and then observed farther along the line, or reflected from a piston at the end and observed at the beginning, separate pulses will be seen corresponding to each mode that is sent. This is illustrated

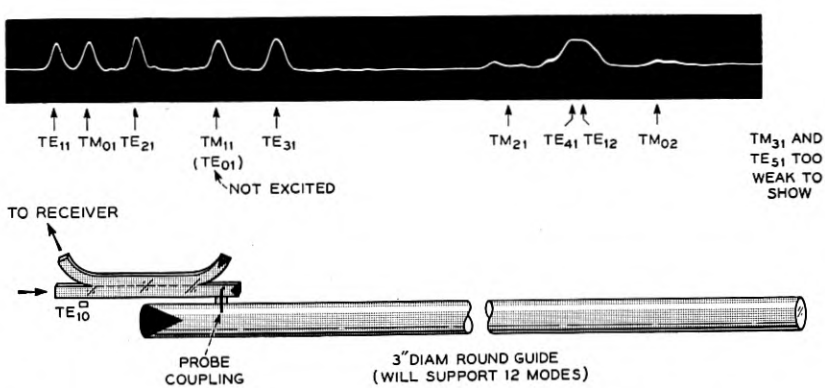

FIG. 12 — Arrangement for showing mode separation on a time basis in a multimode waveguide. The pulses in the trace photo have all traveled to the piston and back. The earlier outgoing pulse due to directional coupler unbalance is not shown.

in Fig. 12. In this arrangement energy was sent into the round line from a probe inserted in the side of the guide. This couples to all of the 12 modes which can be supported, with the exception of the TE_{01} circular electric mode. The sending end of the round guide was terminated. A directional coupler is connected to the sending probe so that the return from the piston at the far end can be observed on the receiver. Because of the different time that each mode takes to travel one round trip in this waveguide, which was 258 feet long, separate pulses are seen for each mode. The pulses in this figure have been marked to show which mode is being received.

The time of each pulse referred to the outgoing pulse was measured and found to check very well with the calculated time. The formula for the time of transit in the waveguide for any mode is:

$$T = \frac{L}{0.98322\sqrt{1 - v_{nm}^2}}$$

where T = time in millimicroseconds

L = length of pulse travel in feet

$v_{nm} = \lambda/\lambda_c$

λ = operating wavelength in air

λ_c = cutoff wavelength of guide for the mode involved.

TABLE I — CALCULATED AND MEASURED VALUE OF TIME FOR ONE ROUND TRIP

Mode Number	Mode Designation	Time in Millimicroseconds	
		Calculated	Measured
1	TE_{11}	545	545
2	TM_{01}	561	561
3	TE_{21}	587	587
4	TM_{11}	634	634
5	TE_{01}	634	—
6	TE_{31}	665	665
7	TM_{21}	795	793
8	TE_{41}	835	838
9	TE_{12}	838	—
10	TM_{02}	890	890
11	TM_{31}	1461	—
12	TE_{51}	1519	—

The calculated and measured value of time for one round trip is given in Table I.

In this experiment the operating wavelength was 3.35 centimeters. This was obtained by measurements based on group velocity in a number of guides as well as information about the pulse generator components. It represents an effective wavelength giving correct time of travel. The pulse occupies such a wide bandwidth that a measurement of its wavelength is difficult by the usual means.

The dashes in the measured column indicate that the mode was not excited by the probe or was too weak to measure. These modes do not appear on the oscilloscope trace photograph.

The relative pulse heights can be calculated from a knowledge of the probe coupling factors and the line loss. The probe coupling factors as given by M. Aronoff in unpublished work are expressed by the following:

For TE_{nm} modes:

$$P = 2.390 \frac{n^2}{K_{nm}^2 - n^2} \frac{\lambda_{g_{nm}}}{\lambda_{g_{11}}}$$

For TM_{nm} modes:

$$P = 1.195 \epsilon_n \frac{\lambda}{\lambda_{g_{11}}} \frac{\lambda}{\lambda_{g_{nm}}}$$

where

P = ratio of probe coupling power in mode nm to that in mode TE_{11}

n = first index of mode being calculated

K_{nm} = Bessel function zero value for mode being calculated $= \pi d/\lambda_c$

λ = wavelength in air

λ_g = wavelength in the guide for the mode involved

λ_c = cutoff wavelength of guide for the mode involved

$\epsilon_n = 1$ for $n = 0$

$\epsilon_n = 2$ for $n \neq 0$

d = waveguide diameter

Formulas for guide loss as given by S. A. Schelkunoff on page 390 of his book *Electromagnetic Waves* for this case where the resistivity of the aluminum guide is 4.14×10^{-6} ohms per cm cube are:

For TE_{nm} modes:

$$\alpha = 3.805 \left(\frac{n^2}{K_{nm}^2 - n^2} + v_{nm}^2 \right) (1 - v_{nm}^2)^{-1/2}$$

For TM_{nm} modes:

$$\alpha = 3.805(1 - v_{nm}^2)^{-1/2}$$

where:

α = attenuation of this aluminum guide in db

n = first index of mode being calculated

K_{nm} = Bessel function zero value for mode being calculated = $\pi d/\lambda_c$

$v_{nm} = \lambda/\lambda_c$

λ = operating wavelength in air

λ_c = cutoff wavelength of guide for the mode involved

d = waveguide diameter

Table II gives the calculated probe coupling factor, line loss, and relative pulse height for each mode. In the calculation of the latter, wave ellipticity and loss due to mode conversion were neglected, but the heat loss given by the preceding formulas has been increased 20 per cent for all modes, to take account of surface roughness. Relative pulse heights were obtained by subtracting the relative line loss from twice the relative probe coupling factor. The relative line loss is the number in the table minus 2.33 db, the loss for the TE_{11} mode.

The actual pulse heights on the photo of the trace on Fig. 12 are in fair agreement with these calculated values. Differences are probably due to polarization rotation in the guide (wave ellipticity) and conversion to other modes, effects which were neglected in the calculations, and which are different for different modes.

Calculated pulse heights with this guide length, except for modes near cutoff, vary less than the probe coupling factors, because line loss is high when tight probe coupling exists. This is to be expected, since both are the result of high fields near the guide walls.

The table of round trip travel time shows that the TE_{41} and TE_{12} modes are separated by only three millimicroseconds after the round trip in this waveguide. They would not be resolved as separate pulses by this equipment. However, the table of calculated pulse heights shows that the TE_{41} pulse should be about 22 db higher than the TE_{12} pulse.

TABLE II — CALCULATED PROBE COUPLING FACTOR, LINE LOSS AND PULSE HEIGHT FOR EACH MODE

Mode Number	Mode Designation	Relative Probe Coupling Factor, db	1.2 × Theoretical Line Loss, db	Calculated Relative Pulse Heights, db
1	TE_{11}	0	2.33	0
2	TM_{01}	+0.32	4.88	−1.91
3	TE_{21}	+2.86	4.85	+3.20
4	TM_{11}	+2.80	5.51	+2.42
5	TE_{01}	$-\infty$	1.73	$-\infty$
6	TE_{31}	+4.82	8.21	+3.76
7	TM_{21}	+1.82	6.92	−0.95
8	TE_{41}	+6.80	13.86	+2.07
9	TE_{12}	−8.73	4.70	−19.83
10	TM_{02}	−1.68	7.74	−8.77
11	TM_{31}	−0.82	12.71	−12.02
12	TE_{51}	+10.14	32.09	−9.48

Since the TE_{12} pulse is so weak, it would not show on the trace even if it were resolved on a time basis. Coupling to the TM_{02} mode is rather weak, and the gain was increased somewhat at its position on the trace to show its time location.

8. DELAY DISTORTION

Another effect of the wide bandwidth of the pulses used with this equipment can be observed in Fig. 12. The pulses that have traveled for a longer time in the guide are in the modes closer to cutoff, and are on the right-hand side of the oscilloscope trace. They are broadened and distorted compared with the ones on the left-hand side. This effect is due to delay distortion in the guide. This can be explained by reference to Fig. 13. On this figure the ratio of group velocity to the velocity in an unbounded medium is shown plotted as a function of frequency for each of the modes that can be propagated. The bandwidth of the transmitted pulse is indicated by the vertical shaded area. It will be noticed that the spacing of the pulses on the oscilloscope trace on Fig. 12 from left to right in time corresponds to the spacing of the group velocity curves in the bandwidth of the pulse from top to bottom. Delay distortion on these curves is shown by the slope of the line across the pulse bandwidth. If the line were horizontal, showing the same group velocity at all points in the band, there would be no delay distortion. The greater the difference in group velocity at the two edges of the band, the greater the delay distortion. The curves of Fig. 13 indicate

that there should be increasing amounts of delay distortion reading from top to bottom for the pulse bandwidth used in these experiments. The effect of this delay distortion is to cause a broadening of the pulse. Examination of the pulse pattern of Fig. 12 shows that the later pulses corresponding in mode designation to the lower curves of Fig. 13 do indeed show a broadening due to the increased delay distortion. One method of reducing the effect of delay distortion is to use frequency division multiplex so that each signal uses a smaller bandwidth. Another way, suggested by D. H. Ring, is to invert the band in a section of the waveguide between one pair of repeaters compared with that between an adjacent pair of repeaters so that the slope is, in effect, placed in the opposite direction, and delay distortion tends to cancel out, to a first order at least.

The quantitative magnitude of delay distortion has been expressed by S. Darlington in terms of the modulating base-band frequency needed to generate two side frequencies which suffer a relative phase error of 180° in traversing the line. This would cause cancellation of a single frequency AM signal, and severe distortion using any of the

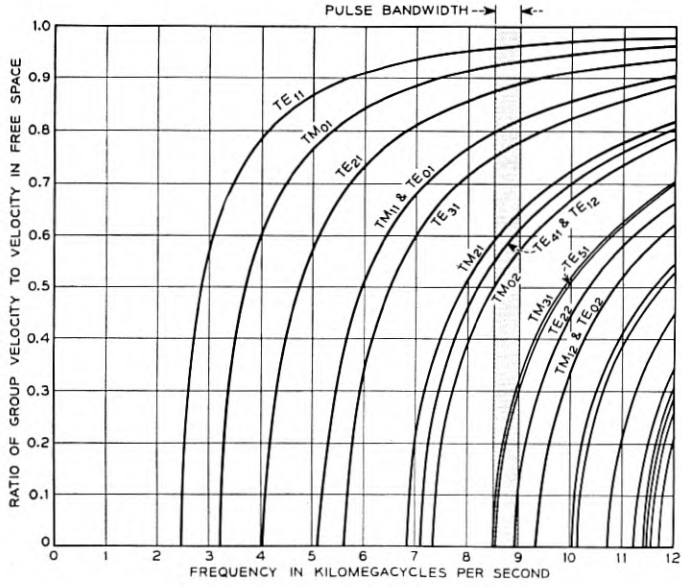

Fig. 13 — Theoretical group velocity vs. frequency curves for the 3″ diameter waveguide used for the tests shown on Fig. 12. The vertical shaded area gives the bandwidth for the millimicrosecond pulses employed in that arrangement.

ordinary modulation methods. Darlington gives this formula:

$$fB = f\left(\frac{\lambda}{2L}\right)^{1/2} \frac{(1 - v_{nm}{}^2)^{3/4}}{v_{nm}}$$

where:

fB = base bandwidth for 180° out of phase sidebands

f = operating frequency (in same units as fB)

λ = wavelength in air

L = waveguide length (in same units as λ)

$v_{nm} = \lambda/\lambda_c$

λ_c = cutoff wavelength for the mode involved

With this equipment, the base bandwidth of the pulse is about 175 mc, and when fB from the formula above is about equal to or less than this, pulse distortion should be observed. The following Table III gives fB calculated from this formula for the arrangement shown on Fig. 12.

It is interesting to note that pulses in the TM_{11} and TE_{31} modes, for which fB is less than the 175-mc pulse bandwidth, are broadened, but not badly distorted. For the higher modes, where fB is much less than 175 mc, broadening and severe distortion are evident. Another example is given in the next section.

9. DELAY DISTORTION EQUALIZATION

If the distance which a pulse travels in a waveguide is increased, its delay distortion also increases. Since the group velocity at one edge of the band is different than at the other edge of the band, the amount by which the two edges get out of phase with each other increases with the total length of travel, causing increased distortion and pulse broadening. The Darlington formula in the previous section shows that fB varies inversely as the square root of the length of travel. This effect is shown on Fig. 14. In this arrangement the transmitter was connected to the end of a 3″ diameter round waveguide 107 feet long through a small hole in the end plate. A mode filter was used so that only the TE_{01} mode would be transmitted in this waveguide. Through another small hole in the end plate polarized 90° from the first one, and rotated 90° around the plate, a directional coupler was connected as shown. The direct through guide of this directional coupler could be short circuited with a waveguide shorting switch. Energy reflected from this

TABLE III — CALCULATED VALUES OF fB FOR THE ARRANGEMENT SHOWN IN FIG. 12

Mode Number	Mode Designation	fB Megacycles	Remarks
1	TE_{11}	324.0	
2	TM_{01}	237.7	
3	TE_{21}	174.9	
4	TM_{11}	124.1	
5	TE_{01}	124.1	Not excited
6	TE_{31}	105.2	
7	TM_{21}	65.9	
8	TE_{41}	59.1	
9	TE_{12}	58.6	Very weakly excited
10	TM_{02}	51.8	
11	TM_{31}	21.3	Not observed
12	TE_{51}	20.0	Not observed

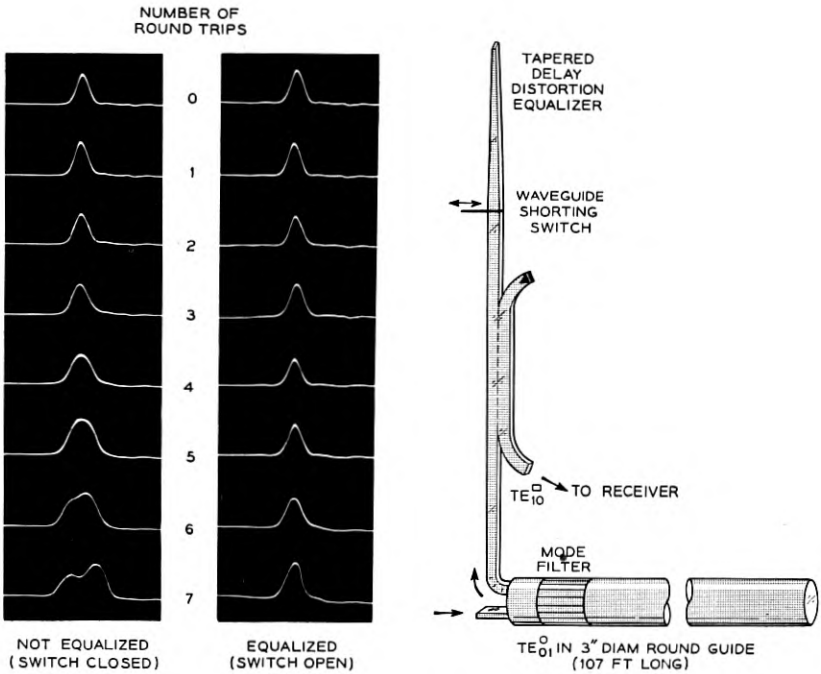

Fig. 14 — The left-hand series of pulses shows the build up of delay distortion with increasing number of round trips in a long waveguide. The right-hand series shows the improvement obtained with the tapered delay distortion equalizer shown at the right.

switch was then taken through the directional coupler to the receiver as shown by the output arrow. The series of pulses at the left-hand photograph of the oscilloscope traces was taken with this waveguide shorting switch closed. The top pulse shows the direct leakage across the inside of the end plate before it has traveled through the 3″ round guide. The next pulse is marked one round trip, having gone therefore 214 feet in the TE_{01} mode in the round waveguide. The successive pulses have traveled more round trips as shown by the number in the center between the two photographs. The effect of increased delay distortion broadening and distorting the pulse can be seen as the numbers increase. The values of fB from the Darlington formula in the previous section for these lengths are given in Table IV.

It will be noticed that pulse broadening, and eventually severe distortion, occurs as fB decreases much below the 175-mc pulse bandwidth. The effect is gradual, and not too bad a pulse shape is seen until fB is about half the pulse bandwidth, although broadening is very evident earlier.

When the waveguide short-circuiting switch was opened so that the tapered delay distortion equalizer was used to reflect the energy, instead of the switch, the series of pulses at the right was observed on the indicator. It will be noted that there is much less distortion of these pulses, particularly toward the bottom of the series. The ones at the top have less distortion than would be expected, probably because of frequency modulation of the injected pulse. The equalizer consists of a long gradually tapered section of waveguide which has its size reduced to a point beyond cutoff for the frequencies involved. Reflection takes place at the point of cutoff in this tapered guide. For the high frequency part of the pulse bandwidth, this point is farther away from the shorting switch than for the low frequency part of the bandwidth. Consequently, the high frequency part of the pulse travels farther in one round trip into this tapered section and back than the low frequency part of

TABLE IV — VALUES OF fB FROM THE DARLINGTON FORMULA FOR THE ARRANGEMENT SHOWN IN FIG. 14

Round Trip Number	fB Megacycles	Round Trip Number	fB Megacycles
1	185.8	6	75.8
2	131.4	7	70.2
3	107.3	8	65.7
4	92.9	9	61.9
5	83.1	10	58.7

the pulse. This increased time of travel compensates for the shorter time of travel of the high frequency edge of the band in the 3″ round waveguide, so equalization takes place. Since this waveguide close to cutoff introduces considerable delay distortion by itself, the taper effect must be made larger in order to secure the equalization. This can be done by making the taper sufficiently gradual. This type of equalizer introduces a rather high loss in the system. For this reason it might be used to predistort the signal at an early level in a repeater system. Equalization by this method was suggested by J. R. Pierce.

10. MEASURING MODE CONVERSION FROM ISOLATED SOURCES

One of the important uses of this equipment has been for the measurement of mode conversion. W. D. Warters has cooperated in developing techniques and carrying out such measurements. One of the problems in the design of mode filters used for suppressing all modes except the circular electric ones in round multimode guides is mode conversion. Since these mode filters have circular symmetry, conversion can take place only to circular electric modes of order higher than the TE_{01} mode. This conversion is, however, a troublesome one, since these higher order circular modes cannot be suppressed by the usual type of filter.

An arrangement for measuring mode conversion at such mode filters from the TE_{01} to the TE_{02} mode is being used with the short pulse equipment. This employs a 400-foot long section of the 5″ diameter line. Because the coupled-line transducer available had too high a loss to TE_{02}, a combined $TE_{01} - TE_{02}$ transducer was assembled. It uses one-half of the round waveguide to couple to each mode. Fig. 15 shows this device.

The use of this transducer and line is illustrated in Fig. 16. Pulses in the TE_{01} mode are sent into the waveguide by the upper section of the transducer as shown. Some of the TE_{01} energy goes directly across to the TE_{02} transducer and appears as the outgoing pulse with a level down about 32 db. This is useful as a time reference in the system and is shown as the outgoing pulse in the photo of the oscilloscope trace above. The main energy in the TE_{01} mode propagates down the line as shown by dashed line 2, which is the path of this wave. Most of this energy goes all the way to the reflecting piston at the far end and then returns to the TE_{02} transducer where it gives a pulse which is marked TE_{01} round trip on the trace photograph above. Two thirds of the way from the sending end to the piston, the mode filter being measured is inserted in the line. When the TE_{01} mode energy comes to this mode filter, a small amount of it is converted to the TE_{02} mode. This

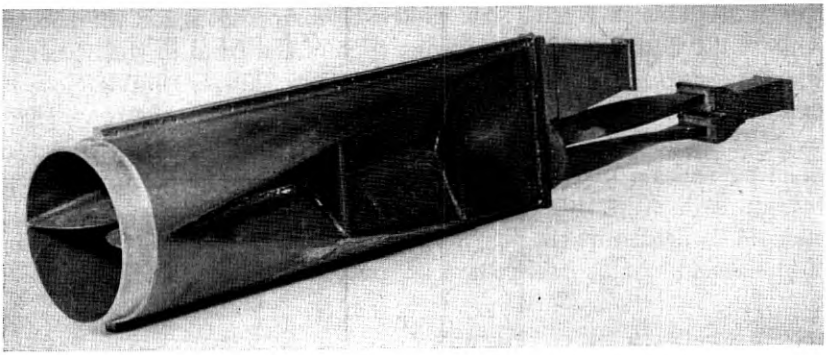

Fig. 15 — A special experimental transducer for injecting the TE_{01} mode and receiving the converted TE_{02} mode in a 5″ diameter waveguide.

continues to the piston by path 4 (with dashed lines and crosses) and then returns and is received by the TE_{02} part of the transducer. This appears on the trace photo as the TE_{02} first conversion. When the main TE_{01} energy reflected by the piston comes back to the mode filter, conversion again takes place to TE_{02}. This is shown by path 3 having dashed lines and circles. This returns to the TE_{02} part of the transducer and appears on the trace photo as the TE_{02} second conversion. In addition, a small amount of energy in the TE_{02} mode is generated by the TE_{01} upper part of the transducer. It is shown by path 5, having

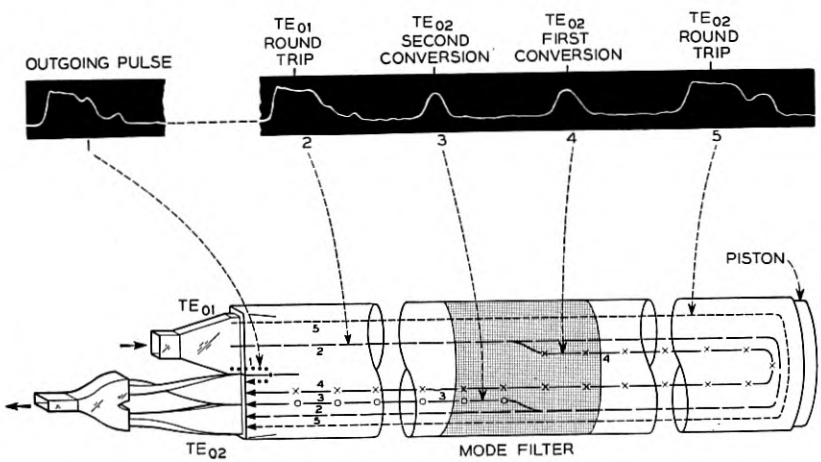

Fig. 16 — Trace photos and waveguide paths traveled when measuring TE_{01} to TE_{02} mode conversion at a mode filter with the transducer shown on Fig. 15.

short dashes. This goes down through the waveguide to the far end piston and back, and is received by the TE_{02} transducer and shown as the pulse marked TE_{02} round trip. The pulse marked TE_{01} round trip has a time separation from the outgoing pulse which is determined by the group velocity of TE_{01} waves going one round trip in the guide. The TE_{02} round trip pulse appears at a time corresponding to the group velocity of the TE_{02} mode going one round trip in the guide. Spacing the mode filter two-thirds of the way down produces the two conversion pulses equally spaced between these two as shown in Fig. 16. The first conversion pulse appears at a time which is the sum of the time taken for the TE_{01} to go down to the filter and the TE_{02} to go from the filter to the piston and back to the receiver. Because of the slower velocity of the TE_{02}, this appears at the time shown, since it was in the TE_{02} mode for a longer time than it was in the TE_{01} mode. The second conversion, which happened when TE_{01} came back to the mode filter, comes earlier in time than the first conversion, since the path for this signal was in the TE_{01} mode longer than it was in the TE_{02} mode. This arrangement gives very good time separation, and makes possible a measurement of the amount of mode conversion taking place in the mode filters. Mode conversion from TE_{01} to TE_{02} as low as 50 to 55 db down, can be measured with this equipment.

Randomly spaced single discontinuities in long waveguides can be located by this technique if they are separated far enough to give individually resolved short pulses in the converted mode. Fig. 17 shows

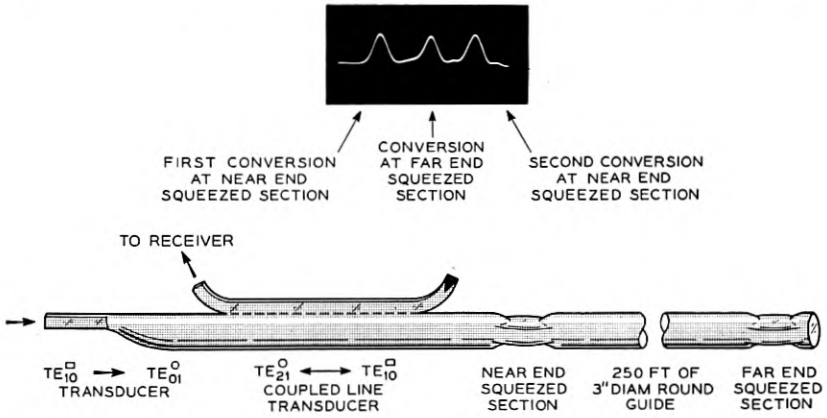

Fig. 17 — Arrangement used to explain the measurement and location of mode conversion from isolated sources. A deliberately squeezed section was placed at each end of the long waveguide, producing the pulses shown in the trace photo.

an arrangement having oval sections deliberately placed in the waveguide in order to explain the method. Pure TE_{01} excitation is used, and the converted TE_{21} mode observed with a coupled line transducer giving an output for that mode alone.

Let us consider first what would happen with the far-end squeezed section alone, omitting the near-end squeezed section from consideration. The injected TE_{01} mode signal would then travel down the 250 feet of 3″ diameter round waveguide to the far end with substantially no mode conversion at the level being measured. At this point it goes through the squeezed section. Conversion now takes place from the TE_{01} mode to the TE_{21} mode. Both these modes after reflection from the piston travel back up the waveguide to the sending end. The group velocity of the TE_{21} mode is higher than the group velocity of the TE_{01} mode, so energy in these two modes separates, and if a coupling system were used to receive energy in both modes, two pulses would appear, with a time separation between them. In this case, since the receiver is connected to the line through the coupled line transducer which is responsive only to the TE_{21} mode, only one pulse is seen, that due to this mode alone. This is the center pulse in the trace photograph at the top of Fig. 17. If only one mode conversion point at the far end of the guide exists, only this one pulse is seen at the receiver. It would be spaced a distance away from the injected outgoing pulse that corresponds in time to one trip of the TE_{01} mode down to the far end and one trip of the TE_{21} mode from the far end back to the receiver.

Now let us consider what would happen if the near-end squeezed section alone were present. When the TE_{01} wave passes the oval section just beyond the coupled line transducer, conversion takes place, and the energy travels down the line in both the TE_{01} and the TE_{21} modes, at a higher group velocity in the TE_{21} mode. These two signals are reflected by the piston at the far end and return to the sending end. The TE_{21} signal comes through the coupled line transducer and appears as the pulse at the left of the photo shown on Fig. 17. Now the TE_{01} energy has lagged behind the TE_{21} energy, and when it gets back to the near-end squeezed section, a second mode conversion takes place, and TE_{21} mode energy is produced which comes through the coupled line transducer and appears at the receiver at the time of the right hand pulse. The spacing between these two pulses is equal to the difference in round trip times between the two modes.

In general, for a single conversion source occurring at any point in the line, two pulses will appear on the scope. The spacing between these pulses corresponds to the difference in group velocity between the modes

from the point of the discontinuity down to the piston at the far end, and then back to the discontinuity. If the discontinuity is at the far end, this time difference becomes zero, and a single pulse is seen. By making a measurement of the pulse spacing, the location of a single conversion point can be determined.

In the arrangement illustrated in Fig. 17, two isolated sources of conversion existed. They were spaced far enough apart so that they were resolved by this equipment, and all three pulses were observed. The two outside pulses were due to the first conversion point. The center pulse was caused by the other squeeze, which was right at the reflecting piston. If this conversion point had been located back some distance from the piston, it would have produced two conversion pulses whose spacing could be used to determine the location of the conversion point.

The coupled-line transducers are calibrated for coupling loss by sending the pulse through a directional coupler into the branch normally used for the output to the receiver. This gives a return loss from the directional coupler equal to twice the transducer loss plus the round trip line loss.

11. MEASURING DISTRIBUTED MODE CONVERSION IN LONG WAVEGUIDES

Measurements of mode conversion from TE_{01} to a number of other modes have been made with 5″ diameter guides using this equipment. The arrangement of Fig. 18 was set up for this purpose. This is the same as Fig. 17, except that a long taper was used at the input end of the 5″ waveguide, and a movable piston installed at the remote end.

One of the converted modes studied with this apparatus arrangement was the TM_{11} mode, which is produced by bends in the guide. This mode has the same velocity in the waveguide as the TE_{01} mode. Therefore energy components converted at different points in the line stay in phase with the injected TE_{01} mode from which they are converted. There is never any time separation between these modes, and a single

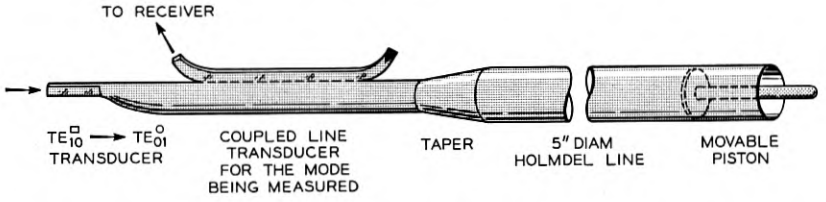

Fig. 18 — Arrangement used for measuring mode conversion in the 5″ diameter waveguides at Holmdel.

narrow pulse like the transmitted one is all that appears on the indicator oscilloscope. It is not possible from this to get any information about the location or extent of the conversion points in the line. Moving the far end piston does not change the relative phases of the modes, so no changes are seen in indicator pattern or pulse level as the piston is moved. For the Holmdel waveguides, which are about 500 feet long, the total round trip TM_{11} mode converted level varies from 32 to 36 db below the input TE_{01} mode level over a frequency range from 8,800 to 9,600 mc per second.

All the other modes have velocities that are different than that of the TE_{01} mode. When mode conversion takes place at many closely spaced points along the waveguide, the pulses from the various sources overlap, and phasing effects take place. In general, a filled-in pulse much longer than the injected one is observed. The maximum possible, but not necessary, pulse length is equal to the difference in time required for the TE_{01} mode and the converted mode to travel the total waveguide length being observed. The phasing effects within the broadened pulse change its height and shape as a function of frequency and line length.

Measurements of mode conversion from TE_{01} to TE_{31} in these waveguides illustrate distributed sources and piston phasing effects. The TE_{31} mode has a group velocity 1.4 per cent slower than the TE_{01} mode. For a full round trip in the 500-foot lines, assuming conversion at the imput end, this causes a time separation of about two and one half pulse widths between these two modes. The received pulse is about two and a half times as long as the injected pulse, indicating rather closely spaced sources over the whole line length. For one far-end piston position, the received pattern is shown as the upper trace in Fig. 19. As the piston is moved, the center depressed part of the trace gradually

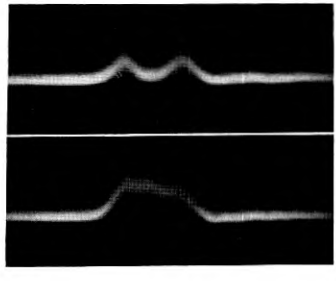

Fig. 19 — Received pulse patterns with the arrangement of Fig. 18 used for studying conversion to the TE_{31} mode.

rises until the pattern shown in the lower trace is seen. As the piston is moved farther in the same direction the trace gradually changes to have the appearance of the upper photo again. Moving the far-end piston changes the phase of energy on the return trip, and thus it can be made to add to, or nearly cancel out, conversion components that originated ahead of the piston. When the time separation becomes great enough to prevent overlapping in the pulse width, phasing effects cannot take place, therefore, the beginning and end of the spread-out received pulse are not affected by moving the piston. Energy converted at the sending end of the guide travels the full round trip to the piston and back in the slower TE_{31} mode, and thus appears at the latest time, which is at the right-hand end of the received pulse. Conversion at the piston end returns at the center of the pulse, and conversion on the return trip comes at earlier times, at the left-hand part of the pulse. The TE_{01} mode has less loss in the guide than the TE_{31} mode. Since the energy in the earlier part of the received pulse spent a greater part of the trip in the lower loss TE_{01} mode before conversion, the output is higher here, and slopes off toward the right, where the later returning energy has gone for a longer distance in the higher loss mode. The pulse height at the maximum shows the converted energy from that part of the line to be between 30 and 35 db below the incident TE_{01} energy level over the measured bandwidth.

Measurements of mode conversion from TE_{01} to TE_{21} in these waveguides show these same effects, and also a phasing effect as a function of frequency. The TE_{21} mode has a group velocity 2.4 per cent faster than the TE_{01} mode. For a full round trip in the guides, this is a time separation of about four pulse widths between the modes. At one frequency and one far-end piston position, the TE_{21} response shown as the top trace of Fig. 20 was obtained. Moving the far-end piston gradually changed this to the second trace from the top, and further piston motion changed it back again. This is the same kind of piston phasing effect observed in the TE_{31} mode conversion studies. The irregular top of this broadened pulse indicates fewer conversion points than for the TE_{31} mode, or phasing effects along the guide length. Since the TE_{21} mode has a higher group velocity than the TE_{01} mode, energy converted at the beginning of the guide returns at the earlier or left-hand part of the pulse, and conversions on the return trip, having traveled longer in the slower TE_{01} mode, are on the right-hand side of the pulse. This is just the reverse of the situation for the TE_{31} mode. Since the loss in the TE_{21} mode is higher than in the TE_{01} mode, the right side of this broadened pulse is higher than the left side, as the energy in the left side has

gone further in the higher loss TE_{21} mode. Conversions from the piston end of the guide return in the center of the pulse, and only in this region do piston phasing effects appear. As the frequency is changed the pattern changes, until it reaches the extreme shape shown in the next-to-the-bottom trace, with this narrower pulse coming at a time corresponding to the center of the broadened pulse at the top. Further frequency change in the same direction returns the shape to that of the top traces. At the frequency giving the received pulse shown on the next-to-the-bottom trace, moving the far-end piston causes a gradual change to the shape shown on the lowest trace. This makes it appear as if the mode conversion were coming almost entirely from the part of the guide near the piston end at this frequency. The upper traces appear to show that more energy is converted at the transducer end of the waveguide at that frequency. It would seem that at certain frequencies some phase cancellation is taking place between conversion points spaced closely enough to overlap within the pulse width. At frequencies between the ones giving traces like this, the appearance is more like that shown for the TE_{31} mode on Fig. 19 except for the slope across the top of the pulse being reversed. The highest part of this TE_{21} pulse is

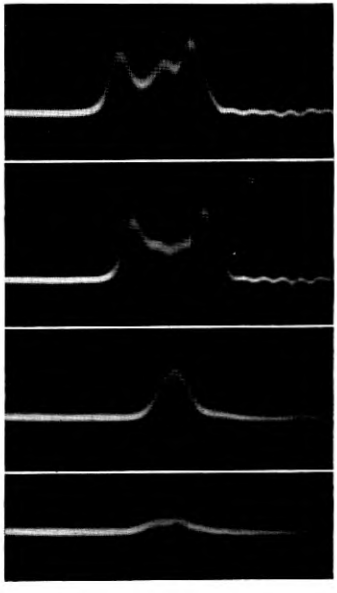

Fig. 20 — Received pulse patterns with the arrangement of Fig. 18 used for studying conversion to the TE_{21} mode.

24 to 27 db below the injected TE_{01} pulse level for the 5″ diameter Holmdel waveguides.

12. CONCLUDING REMARKS

The high resolution obtainable with this millimicrosecond pulse equipment provides information difficult to obtain by any other means. These examples of its use in waveguide investigations indicate the possibilities of the method in research, design and testing procedures. It is being used for many other similar purposes in addition to the illustrations given here, and no doubt many more uses will be found for such short pulses in the future.

REFERENCES

1. S. E. Miller and A. C. Beck, Low-loss Waveguide Transmission, Proc. I.R.E., **41**, pp. 348–358, March, 1953.
2. S. E. Miller, Waveguide As a Communication Medium, B. S. T. J., **33**, pp. 1209–1265, Nov., 1954.
3. C. C. Cutler, The Regenerative Pulse Generator, Proc. I.R.E., **43**, pp. 140–148, Feb., 1955.
4. S. E. Miller, Coupled Wave Theory and Waveguide Applications, B. S. T. J., **33**, pp. 661–719, May, 1954.

Experiments on the Regeneration of Binary Microwave Pulses

By O. E. DeLANGE

(Manuscript received September 7, 1955)

A simple device has been produced for regenerating binary pulses directly at microwave frequencies. To determine the capabilities of such devices one of them was included in a circulating test loop in which pulse groups were passed through the device a large number of times. Results indicate that even in the presence of serious noise and bandwidth limitations pulses can be regenerated many times and still show no noticeable deterioration. Pictures of circulated pulses are included which illustrate performance of the regenerator.

INTRODUCTION

The chief advantage of a transmission system employing binary pulses resides in the possibility of regenerating such pulses at intervals along the route of transmission to prevent the accumulation of distortion due to noise, bandwidth limitations and other effects. This makes it possible to take the total allowable deterioration of signal in each section of a long relay system rather than having to make each link sufficiently good to prevent total accumulated distortion from becoming excessive. This has been pointed out by a number of writers.[1-2]

W. M. Goodall[3] has shown the feasibility of transmitting television signals in binary form. Such transmission requires a considerable amount of bandwidth; a seven digit system, for example, would require transmission of seventy million pulses per second. This need for wide bands makes the microwave range an attractive one in which to work. S. E. Miller[4] has pointed out that a binary system employing regeneration might prove to be especially advantageous in waveguide transmission.

[1] B. M. Oliver, J. R. Pierce and, C. E. Shannon, The Philosophy of PCM, Proc. I. R. E., Nov., 1948.

[2] L. A. Meacham and E. Peterson, An Experimental Multichannel Pulse Code Modulation System of Toll Quality, B. S. T. J., Jan. 1948.

[3] W. M. Goodall, Television by Pulse Code Modulation, B. S. T. J., Jan., 1951.

[4] S. E. Miller, Waveguide as a Communication Medium, B. S. T. J., Nov., 1954.

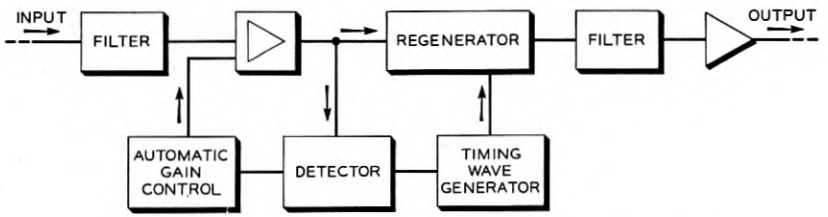

Fig. 1 — A typical regenerative repeater shown in block form.

That the Bell System is interested in the long-distance transmission of television and other broad-band signals is evident from the number of miles of such broad-band circuits, both coaxial cable and microwave radio,[5] now in service. These circuits provide high-grade transmission because each repeater was designed to have a very flat frequency characteristic and linear phase over a considerable bandwidth. Furthermore, these characteristics are very carefully maintained. For a binary pulse system employing regeneration the requirements on flatness of band and linearity of phase can be relaxed to a considerable degree. The components for such a system should, therefore, be simpler and less expensive to build and maintain. Reduced maintenance costs might well prove to be the chief virtue of the binary system.

Since the chief advantage of a binary system lies in the possibility of regeneration it is obvious that a very important part of such a system is the regenerative repeater employed. Fig. 1 shows in block form a typical broad-band, microwave repeater. Here the input, which might come from either a radio antenna or from a waveguide, is first passed through a proper microwave filter then amplified, probably by a traveling-wave amplifier. The amplified pulses of energy are regenerated, filtered, amplified and sent on to the next repeater. The experiment to be described here deals primarily with the block labeled "Regenerator" on Fig. 1.

In these first experiments one of our main objectives was to keep the repeater as simple as possible. This suggests regeneration of pulses directly at microwave frequency, which for this experiment was chosen to be 4 kmc. It was suggested by J. R. Pierce and W. D. Lewis, both of Bell Telephone Laboratories, that further simplification might be made possible by accepting only partial instead of complete regeneration. This suggestion was adopted.

For the case of complete regeneration each incoming pulse inaugurates a new pulse, perfect in shape and correctly timed to be sent on to the

[5] A. A. Roetken, K. D. Smith and R. W. Friis, The TD-2 System, B. S. T. J., Oct., 1951, Part II.

next repeater. Thus noise and other disturbing effects are completely eliminated and the output of each repeater is identical to the original signal which entered the system. For the case of partial regeneration incoming pulses are retimed and reshaped only as well as is possible with simple equipment. Obviously the difference between complete and partial regeneration is one of degree.

One object of the experiment was to determine how well such a partial regenerator would function and what price must be paid for employing partial instead of complete regeneration. The regenerator developed consists simply of a waveguide hybrid junction with a silicon crystal diode in each side arm. It appears to meet the requirement of simplicity in that it combines the functions of amplitude slicing and pulse retiming in one unit. A detailed description of this unit will be given later. Although the purpose of this experiment was to determine what could be accomplished in a very simple repeater we must keep in mind that superior performance would be obtained from a regenerator which approached more nearly the ideal. For some applications the better regenerator might result in a more economical system even though the regenerator itself might be more complicated and more expensive to produce.

METHOD OF TESTING

The regeneration of pulses consists of two functions. The first function is that of removing amplitude distortions, the second is that of restoring each pulse to its proper time. The retiming problem divides into two parts the first of which is the actual retiming process and the second that of obtaining the proper timing pulses with which to perform this function. In a practical commercial system timing information at a repeater would probably be derived from the incoming signal pulses. There are a number of problems involved in this recovery of timing pulses. These are being studied at the present time but were avoided in the experiment described here by deriving such information from the local synchronizing gear.

Since the device we are dealing with only partially regenerates pulses it is not enough to study the performance of a single unit — we should like to have a large number operating in tandem so that we can observe what happens to pulses as they pass through one after another of these regenerators. To avoid the necessity of building a large number of units the pulse circulating technique of simulating a chain of repeaters was employed. Fig. 2 shows this circulating loop in block form.

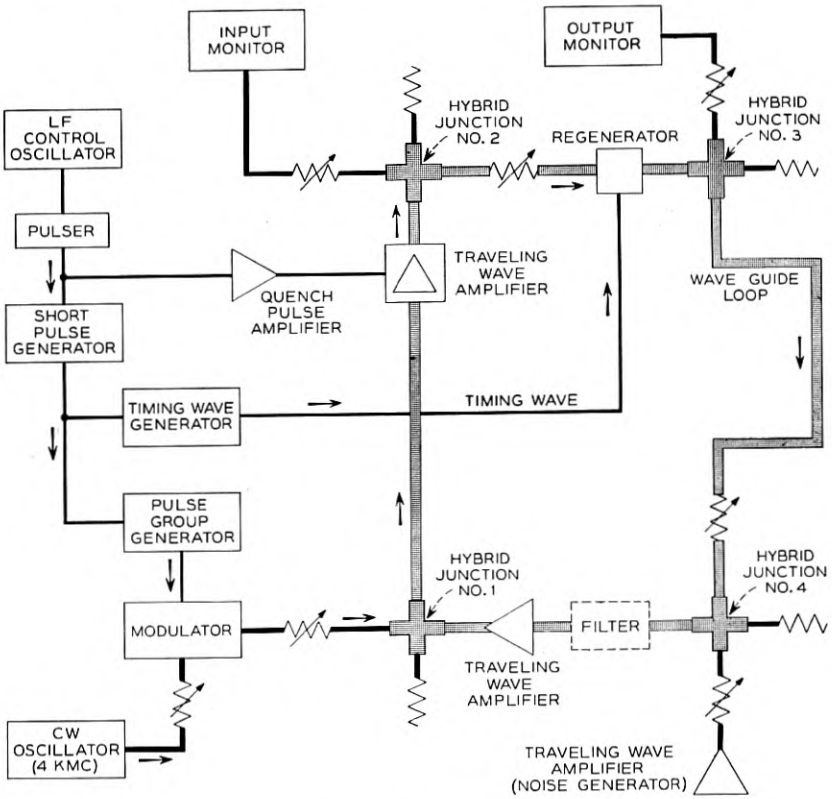

Fig. 2 — The circulating loop.

To provide RF test pulses for this loop the output of a 4 kmc, cw oscillator is gated by baseband pulse groups in a microwave gate or modulator. The resultant microwave pulses are fed into the loop (heavy line) through hybrid junction No. 1. They are then amplified by a traveling-wave amplifier the output of which is coupled to the pulse regenerator through another hybrid junction (No. 2). The purpose of this hybrid is to provide a position for monitoring the input to the regenerator. A monitoring position at the output of the regenerator is provided by a third hybrid, the main output of which feeds a considerable length of waveguide which provides the necessary loop delay. At the far end of the waveguide another hybrid (No. 4) makes it possible to feed noise, which is derived from a traveling-wave amplifier, into the loop. The combined output after passing through a band pass filter is ampli-

fied by another traveling-wave amplifier and fed back into the loop input thus completing the circuit.

The synchronizing equipment starts out with an oscillator going at approximately 78 kc. A pulse generator is locked in step with this oscillator. The output of the pulser is a negative 3 microsecond pulse as shown in Fig. 3A. After being amplified to a level of about 75 volts this pulse is applied to the helix of the first traveling-wave tube to reduce the gain of this tube during the 3-microsecond interval. Out of each 12.8μsec interval pulses are allowed to circulate for 9.8μsec but are blocked for the remaining 3μsec thus allowing the loop to return to the quiescent condition once during each period as shown on Figs. 3A and 3C.

The 3μsec pulse also synchronizes a short-pulse generator. This unit delivers pulses which are about 25 millimicroseconds long at the base and spaced by 12.8μsec, i.e., with a repetition frequency of 78 kc. See Fig. 3B.

In order to simulate a PCM system it was decided to circulate pulse

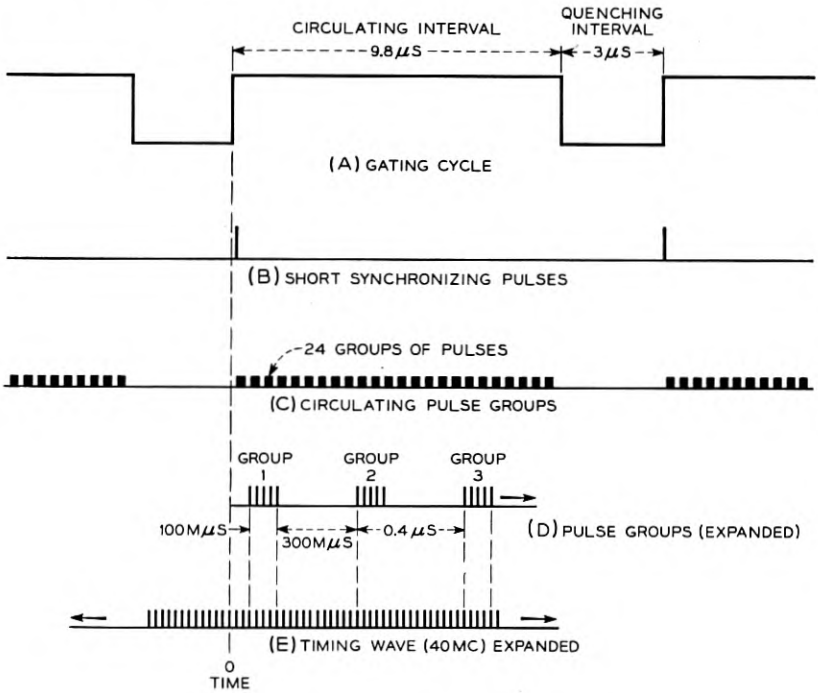

Fig. 3 — Timing events in the circulating loop.

groups rather than individual pulses through the system. These were derived from the pulse group generator which is capable of delivering any number up to 5 pulses for each short input pulse. These pulses are about 15 milli-microseconds long at the base and spaced 25 milli-microseconds apart. The amplitude of each of these pulses can be adjusted independently to any value from zero to full amplitude making it possible to set up any combination of the five pulses. These are the pulses which are used to gate, or modulate, the output of the 4-kmc oscillator.

The total delay around the waveguide loop including TW tubes, etc., was 0.4μsec or 400 milli-microseconds. This was sufficient to allow time between pulse groups and yet short enough that groups could circulate 24 times in the available 9.8μsec interval. This can be seen from Figs. 3C and 3D. The latter figure shows an expanded view of circulating pulse groups. The pulses in Group 1 are inserted into the loop at the beginning of each gating cycle, the remaining groups result from circulation around the loop.

When all five pulses are present in the pulse groups the pulse repetition frequency is 40 mc. (Pulse interval 25 milli-microseconds). For this condition timing pulses should be supplied to the regenerator at the rate of 40 million per second. These pulses are supplied continuously and not in groups as is the case with the circulating pulses. See Fig. 3E. In order to maintain time coincidence between the circulating pulses and the timing pulses the delay around the loop must be adjusted to be an exact multiple of the pulse spacing. In this experiment the loop delay is equal to 16-pulse intervals. Since timing pulses are obtained by harmonic generation from the quenching frequency as will be discussed later this frequency must be an exact submultiple of pulse repetition frequency. In this experiment the ratio is 512 to 1.

Although the above discussion is based on a five-pulse group and 40-mc repetition frequency it turned out that for most of the experiments described here it was preferable to drop out every other pulse, leaving three to a group and resulting in a 20-mc repetition frequency. The one exception to this is the limited-band-width experiment which will be described later.

For all of the experiments described here timing pulses were derived from the 78-kc quenching frequency by harmonic generation. A pulse with a width of 25 milli-microseconds and with a 78-kc repetition frequency as shown in Fig. 3B supplied the input to the timing wave generator. This generator consists of several stages of limiting amplifiers all tuned to 20 mc, followed by a locked-in 20-mc oscillator. The output of the amplifier consists of a train of 20-mc sine waves with constant ampli-

tude for most of the 12.8μsec period but falling off somewhat at the end of the period. This train locks in the oscillator which oscillates at a constant amplitude over the whole period and at a frequency of 20 mc. Timing pulses obtained from the cathode circuit of the oscillator tube provided the timing waves for most of the experiments. For the experiment where a 40-mc timing wave was required it was obtained from the 20 mc train by means of a frequency doubler. For this case it is necessary for the output of the timing wave generator to remain constant in amplitude and fixed in phase for the 512-pulse interval between synchronizing pulses.

In spite of the stringent requirements placed upon the timing equipment it functioned well and maintained synchronism over adequately long periods of time without adjustment.

PERFORMANCE OF REGENERATOR

Performance of the regenerator under various conditions is recorded on the accompanying illustrations of recovered pulse envelopes. The first experiment was to determine the effects of disturbances which arise at only one point in a system. Such effects were simulated by adding disturbances along with the group of pulses as they were fed into the circulating loop from the modulator. This is equivalent to having them occur at only the first repeater of the chain.

Some of the first experiments also involved the use of extraneous pulses to represent noise or distortion since these pulses could be synchronized and thus studied more readily than could random effects. In Fig. 4A the first pulse at the left represents a desired digit pulse with its amplitude increased by a burst of noise, the second pulse represents a clean digit pulse, and the third pulse a burst of noise. This group is at the input to the regenerator. Fig. 4B shows the same group of pulses after traversing the regenerator once. The pulses are seen to be shortened due to the gating, or retiming, action. There is also seen to be some amplitude correction, i.e. the two desired pulses are of more nearly the same amplitude and the undesired pulse has been reduced in relative amplitude. After a few trips through the regenerator the pulse group was rendered practically perfect and remained so for the rest of the twenty-four trips around the loop. Fig. 4C shows the group after 24 trips. In another experiment pulses were circulated for 100 trips without deterioration. Nothing was found to indicate that regeneration could not be repeated indefinitely.

Figs. 5A and 5B represent the same conditions as those of 4A and 4B

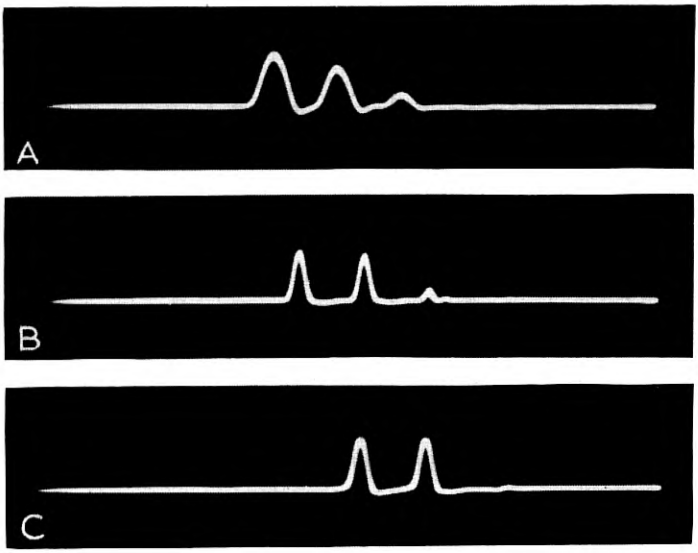

Fig. 4 — Effect of regeneration on disturbances which occur at only one repeater. A — Input to regenerator, original signal. B — Output of regenerator, first trip. C — Output of regenerator, 24th trip.

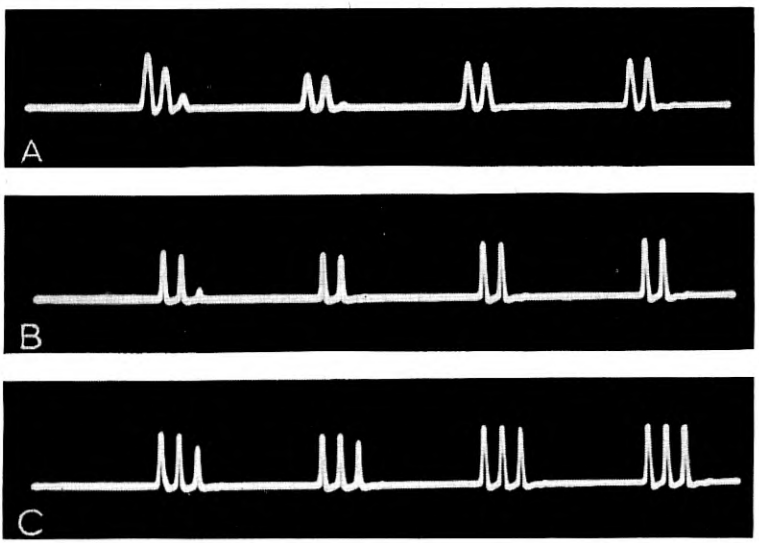

Fig. 5 — Effect of regeneration on disturbances which occur at only one repeater. A — Input to regenerator, first four groups. B — Output of regenerator, first four groups. C — Output of regenerator, increased input level.

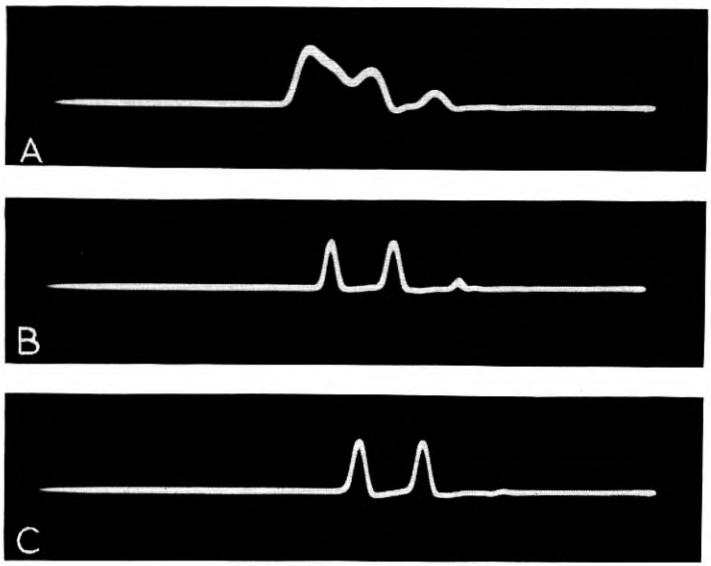

Fig. 6 — Effect of regeneration on disturbances which occur at only one repeater. A — Input to regenerator, original signal. B — Output of regenerator, first trip. C — Output of regenerator, 24th trip.

except that the oscilloscope sweep has been contracted in order to show the progressive effects produced by repeated passage of the signal through the regenerator. Fig. 5B shows that after the pulses have passed through the regenerator only twice all visible effects of the disturbances have been removed. Fig. 5C shows the effect of simply increasing the RF pulse input to the regenerator by approximately 4 db. The small "noise" pulse which in the previous case was quickly dropped out because of being below the slicing level has now come up above the slicing level and so builds up to full amplitude after only a few trips through the regenerator. Note that in the cases shown in Figs. 4 and 5 discrimination against unwanted pulses has been purely on an amplitude basis since the gate has been unblocked to pulses with amplitudes above the slicing level whenever one of these disturbing pulses was present.

For Fig. 6A conditions are the same as for Fig. 4A except that an additional pulse has been added to simulate intersymbol noise or interference. Fig. 6B indicates that after only one trip through the regenerator the effect of the added pulse is very small. After a few trips the effect is completely eliminated leaving a practically perfect group which continues on for 24 trips as shown by Fig. 6C. For the intersymbol pulse, discrimination is on a time basis since this interference occurs at a time

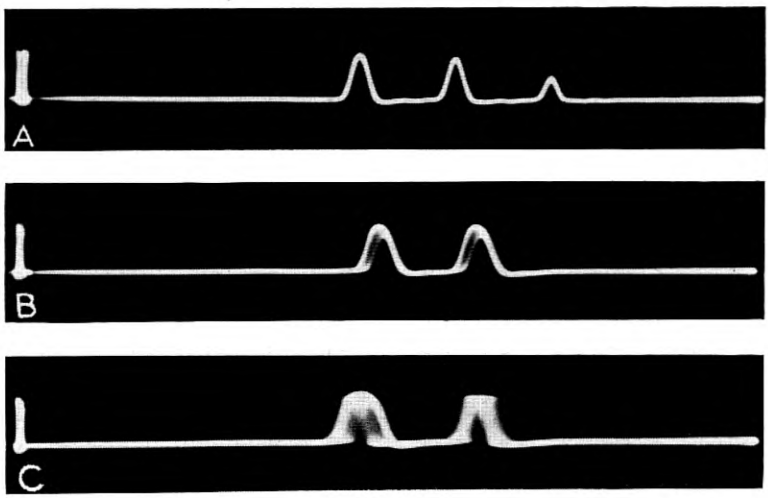

Fig. 7 — Effect of regenerating in amplitude without retiming. A — Output of regenerator, no timing, firt trip. B — Output of regenerator, no timing, 10th trip. Output of regenerator, no timing, 23rd trip.

when no gating pulse is present and hence finds the gate blocked regardless of amplitude.

To show the need for retiming the pictures shown on Figs. 7 and 8 were taken. These were taken with the amplitude slicer in operation but with the pulses not being retimed. Figs. 7A, 7B and 7C, respectively, show the output of the slicer for the first, tenth and twenty-third trips. After ten trips, there is noticeable time jitter caused by residual noise in the system; after 23 trips this jitter has become severe though pulses are still recognizable. It should be pointed out that for this experiment no noise was purposely added to the system and hence the signal-to-noise ratio was much better than that which would probably be encountered in an operating system. For such a system we would expect time jitter effects to build up much more rapidly. For Fig. 8 conditions are the same as for Fig. 7 except that the pulse spacing is decreased by the addition of an extra pulse at the input. Now, after ten trips, time jitter is bad and after 23 trips the pulse group has become little more than a smear. This increased distortion is probably due to the fact that less jitter is now required to cause overlap of pulses. There may also be some effects due to change of duty cycle. For Fig. 9 there was neither slicing nor retiming of pulses. Here, pulse groups deteriorate very rapidly to nothing more than blobs of energy. Note that there is an increase of

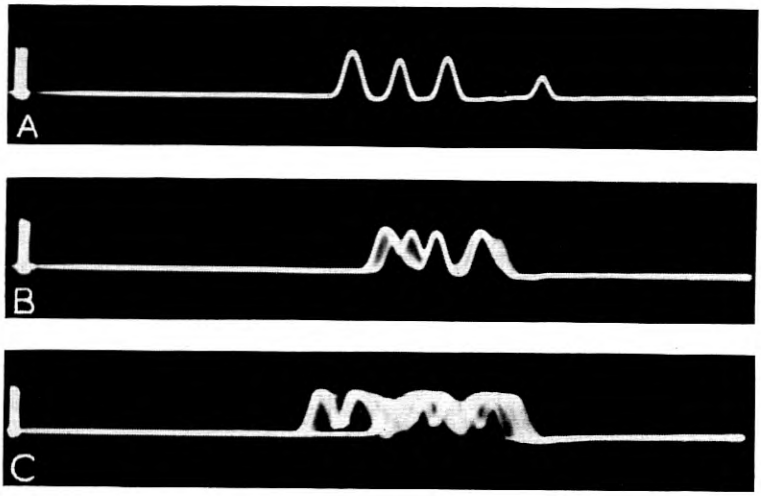

Fig. 8 — Effect of regenerating in amplitude without retiming. A — Output of regenerator, no timing, first trip. B — Output of regenerator, no timing, 10th trip. C — Output of regenerator, no timing, 23rd trip.

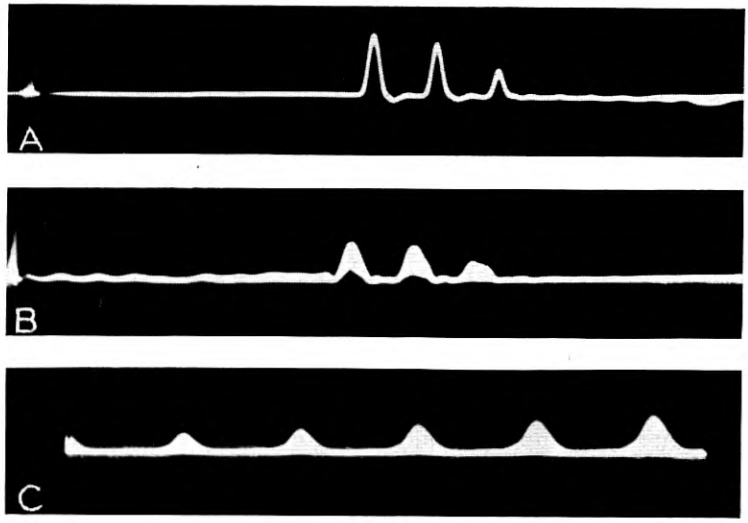

Fig. 9 — Pulses circulating through the loop without regeneration. A — Original input. B — 4th trip without regeneration. C — 20th to 24th trip without regeneration.

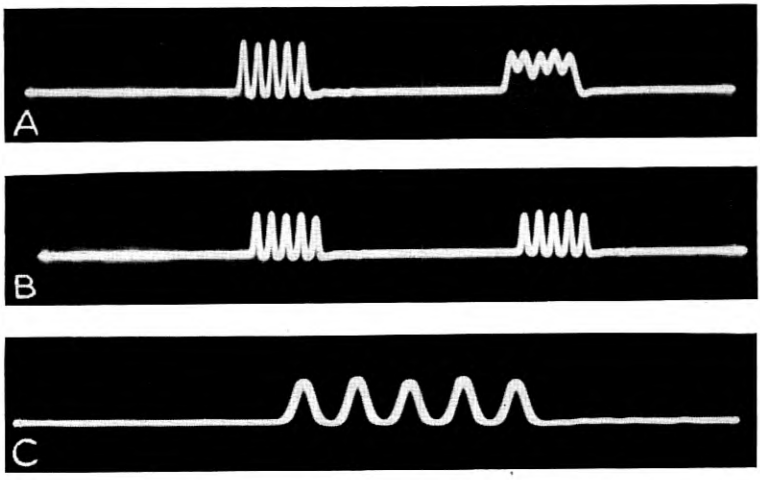

Fig. 10 — The regeneration of band-limited pulses. A — Input to regenerator, first two groups. B — Output of regenerator, first two groups. C — Output of regenerator, 24th trip.

amplitude with each trip around the loop indicating that loop gain was slightly greater than unity. Without the slicer it is difficult to set the gain to exactly unity and the amplitude tends to either increase or decrease depending upon whether the gain is greater or less than unity. Results indicated by the pictures of Fig 9 are possibly not typical of a properly functioning system but do show what happened in this particular system when regeneration was dispensed with.

Another important function of regeneration is that of overcoming band-limiting effects. Figs. 10 and 11 show what can be accomplished. For this experiment the pulse groups inserted into the loop were as shown at the left in Fig. 10A. These pulses were 15 milli-microseconds wide at the base and spaced by 25 milli-microseconds which corresponds to a repetition frequency of 40 mc. After passing through a band-pass filter these pulses were distorted to the extent shown at the right in Fig. 10A. From the characteristic of the filter, as shown on Fig. 12, it is seen that the bandwidth employed is not very different from the theoretical minimum required for double sideband transmission. This minimum characteristic is shown by the dashed lines on Fig. 12. Fig. 10B shows that at the output of the regenerator the effects of band limiting have been removed. This is borne out by Fig. 10C which shows that after 24 trips the code group was still practically perfect. It should be pointed out that the pulses traversed the filter once for each trip around the loop,

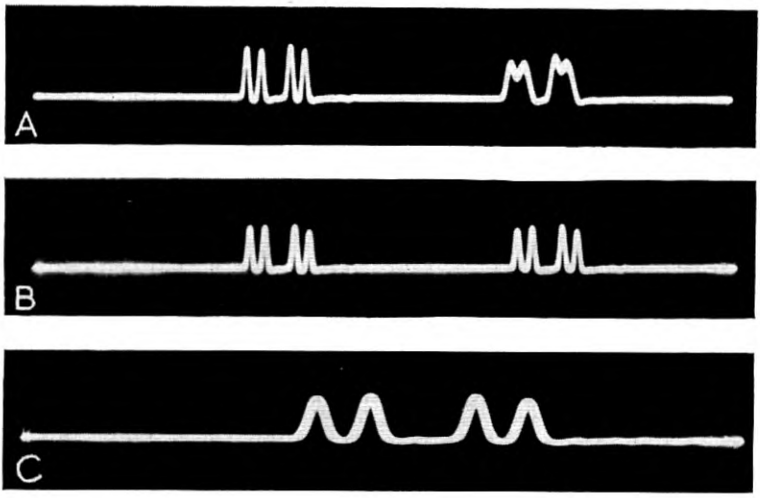

Fig. 11 — The regeneration of band-limited pulses. A — Input to regenerator, first two groups. B — Output of regenerator, first two groups. C — Output of regenerator, 24th trip.

that is for each trip the input to the regenerator was as shown at the right of Fig. 10A and the output as shown by Fig. 10B. It is important to note that Fig. 12 represents the frequency characteristic of a single link of the simulated system. The pictures of Fig. 11 show the same experiment but this time with a different code group. Any code group which we could set up with our five digit pulses was transmitted equally well.

In order to determine the breaking point of the experimental system, broad-band noise obtained from a traveling-wave amplifier was added into the system as shown on Fig. 2. The breaking point of the system is the noise level which is just sufficient to start producing errors at the output of the system.* The noise is seen to be band-limited in exactly the same way as the signal. With the system adjusted to operate properly the level of added noise was increased to the point where errors became barely discernible after 24 trips around the loop. Noise level was now reduced slightly (no errors discernible) and the ratio of rms signal to rms noise measured. Fig. 13A shows the input to the regenerator for the 23rd and 24th trips with this amount of noise added. Note that the noise has

* The type of noise employed has a Gaussian amplitude distribution and therefore there was actually no definite breaking point — the rate at which errors occurred increased continuously as noise amplitude was increased. The breaking point was taken as the noise level at which errors became barely discernible on the viewing oscilloscope. More accurate measurements made in other experiments indicate that this is a fairly satisfactory criterion.

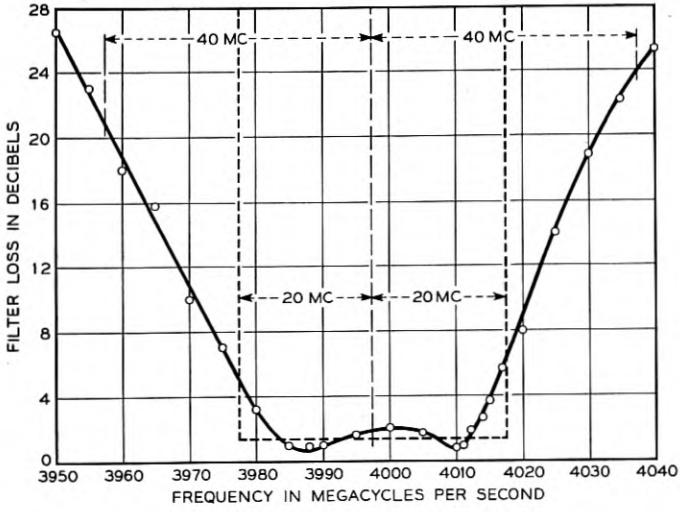

Fig. 12 — Characteristics of the band-pass microwave filter.

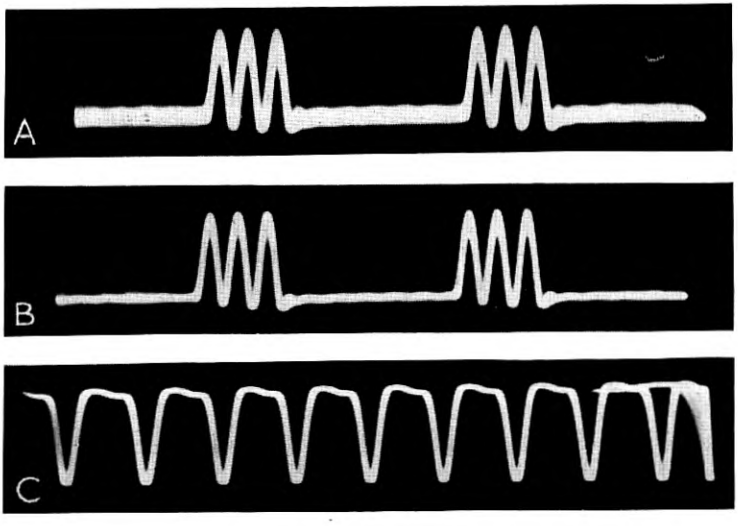

Fig. 13. — The regeneration of pulses in the presence of broad-band, random noise added at each repeater. A — Input to regenerator, 23rd and 24th trips, broad-band noise added. B — Input to regenerator, 23rd and 24th trips, no added noise. C — 20-mc timing wave.

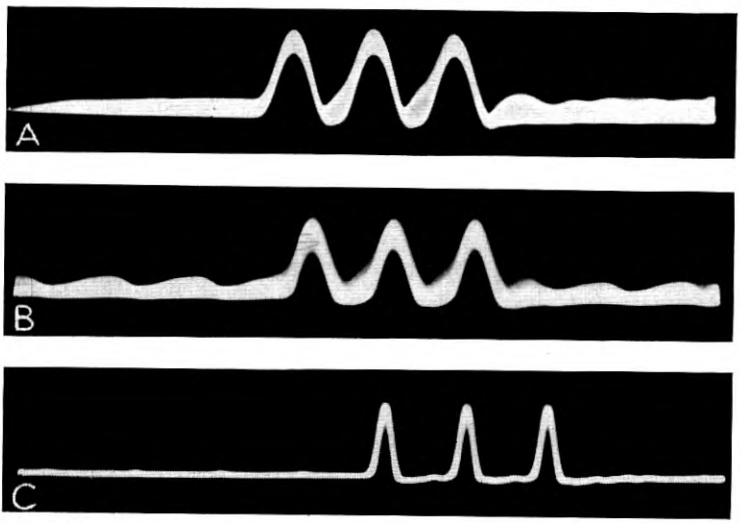

Fig. 14 — The regeneration of pulses in the presence of interference occurring at each repeater. A — Original signal with added modulated carrier interference. B — Input to regenerator, 24th trip, modulated carrier interference. C — Output of regenerator, 24th trip, modulated carrier interference.

produced a considerable broadening of the oscilloscope trace. Fig. 13B shows the same pulse groups with no added noise. These photographs are included to give some idea as to how bad the noise was at the breaking point of the system. Of course maximum noise peaks occur rather infrequently and do not show on the photograph. At the output of the regenerator effects due to noise were barely discernible. This output looked so much like that shown at Fig. 14C that no separate photograph is shown for it.

Figs. 14A, 14B and 14C show the effects of a different type of interference upon the system. This disturbance was produced by adding into the system a carrier of exactly the same frequency as the signal carrier (4 kmc) but modulated by a 14-mc wave, a frequency in the same order as the pulse rate. Here again the level of the interference was adjusted to be just below the breaking point of the system. A comparison between Figs. 14B and 14C gives convincing evidence that the regenerator has substantially restored the waveform.

For the case of the interfering signal a ratio of signal to interference of 10 db on a peak-to-peak basis was measured when the interference was just below the breaking point of the system. This, of course, is 4 db above the theoretical value for a perfect regenerator. For the case of

broad-band random noise an rms signal to noise ratio of 20 db was measured.* This compares with a ratio of 18 db as measured by Messrs. Meacham and Peterson for a system employing complete regeneration and a single repeater.†

Recently, A. F. Dietrich repeated the circulating loop experiment at a radio frequency of 11 kmc. His determinations of required signal-to-noise ratios are substantially the same as those reported here. From the various experiments we conclude that for a long chain of properly functioning regenerative repeaters of the type discussed here practically perfect transmission is obtained as long as the signal-to-noise ratio at the input to each repeater is 20 db or better on an rms basis. In an operating system it might be desirable to increase this ratio to 23 db to take care of deficiencies in automatic gain controls, power changes, etc.

From the experiments we also conclude that the price we pay for using partial instead of complete regeneration is about 3 to 4 db increase in the required signal-to-noise ratio. In a radio system which provides a fading margin this penalty would be less since the probability that two or more adjacent links will reach maximum fades simultaneously is very small. Under these conditions only one repeater at a time would be near the breaking point and the system would behave much as though the repeater provided complete regeneration.

TIMING

Although we have considered the problem of retiming of signal pulses up to now we have not discussed the problem of obtaining the necessary timing pulses to perform this function, but have simply assumed that a source of such pulses was available. As was mentioned earlier timing pulses would probably be derived from the signal pulses in a practical system. These pulses would be fed into some narrow band amplifier tuned to pulse repetition frequency. The output of this circuit could be made to be a sine wave at repetition frequency if gaps between the input pulses were not too great. Timing pulses could be derived from this sine wave. This timing equipment could be similar to that used in these experiments and described earlier. Further study of the problems of obtaining timing information is being made.

* For Gaussian noise it is not possible to specify a theoretical value of minimum S/N ratio without specifying the tolerable percentage of errors. For the number of errors detectable on the oscilloscope it seems rasonable to assume a 12 db peak factor for the noise. The peak factor for the signal is 3 db. The 6 db peak S/N which would be required for an ideal regenerator then becomes 15 db on an rms basis.

† L. A. Meacham and E. Peterson, B. S. T. J., p. 43, Jan., 1948.

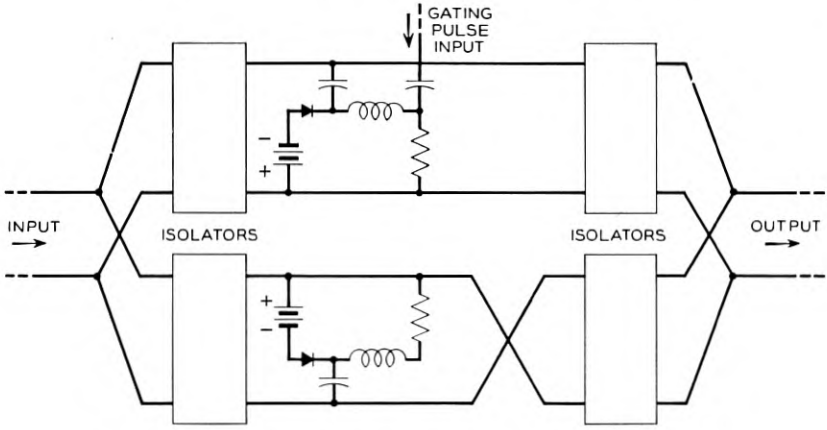

Fig. 15A — Low-frequency equivalent of the partial regenerator.

DESCRIPTION OF REGENERATOR

This device regenerates pulses by performing on them the operations of "slicing" and retiming.

An ideal slicer is a device with an input-output characteristics such as shown by the dashed lines of Fig. 15C. It is seen that for all input levels below the so-called slicing level transmission through the device is zero but that for all amplitudes greater than this value the output level is finite and constant. Thus, all input voltages which are less than the slicing level have no effect upon the output whereas all input voltages greater than the slicing level produce the same amplitude of output. Normally conditions are adjusted so that the slicing level is at one-half

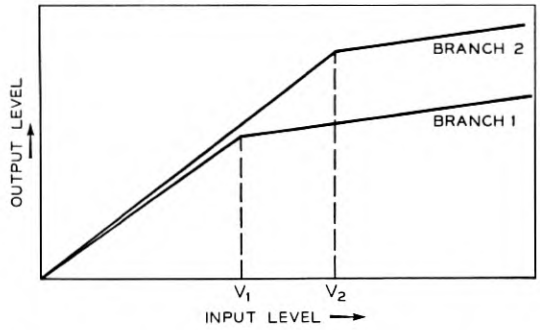

Fig. 15B — Characteristics of the separate branches with differential bias.

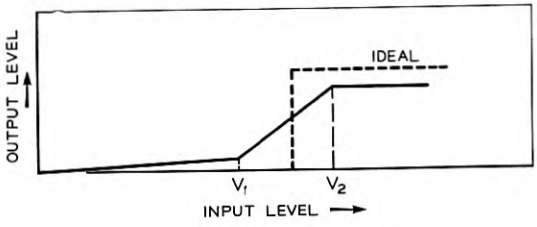

Fig. 15C — Resultant output with differential bias.

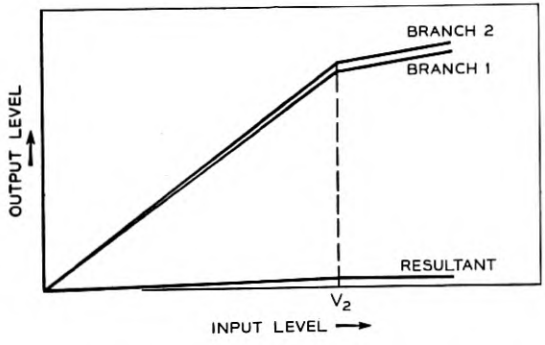

Fig. 15D — Characteristics of the separate branches and resultant output with equal biases.

of peak pulse amplitude — then at the output of the slicer there will be no effect whatsoever from disturbances unless these disturbances exceed half of the pulse amplitude. It is this slicing action which removes the amplitude effects of noise. Time jitter effects are removed by retiming, i.e., the device is made to have high loss regardless of input level except at those times when a gating pulse is present.

Fig. 15A shows schematically a low-frequency equivalent of the regenerator used in these experiments. Here an input line divides into two identical branches isolated from each other and each with a diode shunted across it. The outputs of the two branches are recombined through necessary isolators to form a single output. The phase of one branch is reversed before recombination, so that the final output is the difference between the two individual outputs.

Fig. 15B shows the input-output characteristics of the two branches when the diodes are biased back to be non-conducting by means of bias voltages V_1 and V_2 respectively. For low levels the input-output characteristic of both branches will be linear and have a 45° slope. As soon

as the input voltage in a branch reaches a value equal to that of the back bias the diode will start to conduct, thus absorbing power and decrease the slope of the characteristic. The output of Branch 1 starts to flatten off when the input reaches the value V_1, while the output of Branch 2 does not flatten until the input reaches the value V_2. The combined output, which is equal to the differences of the two branch outputs, is then that shown by the solid line of Fig. 15C and is seen to have a transition region between a low output and a high output level. If the two branches are accurately balanced and if the signal voltage is large compared to the differential bias $V_2 - V_1$ the transition becomes sharp and the device is a good slicer.

If the two diodes are equally biased as shown on Fig. 15D the outputs of the two branches should be nearly equal regardless of input and the total output, which is the difference between the two branch outputs, will always be small.

Fig. 16 shows a microwave equivalent of the circuit of Fig. 15A. In the microwave structure lengths of wave-guide replace the wire lines and branching, recombining and isolation are accomplished by means of hybrid junctions. The hybrid shown here is of the type known as the 1A junction.

Fig. 17 shows another equivalent microwave structure employing only one hybrid. This is the type used in the experiments described here. The output consists of the combined energies reflected from the two side arms of the junction. With the junction connected as shown phase relationships are such that the output is the difference between the reflec-

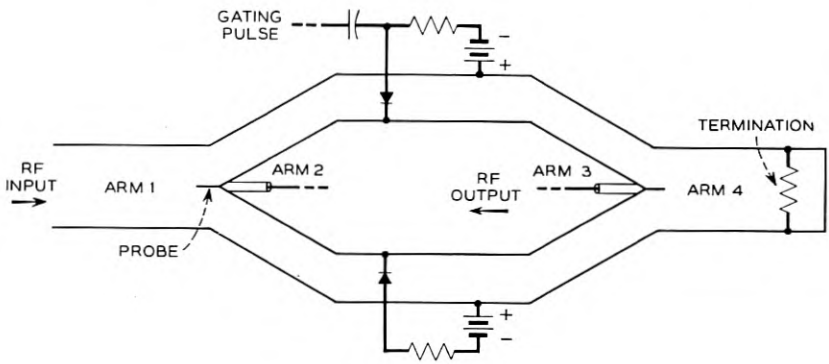

Fig. 16 — Microwave regenerator.

tions from the two side arms so that when conditions in the two arms are identical there is no output. The crystal diodes coupled to the side arms are equivalent to those shunted across the two lines of Fig. 15A.

Fig. 18, which is a plot of the measured input-output characteristic of the regenerator used in the loop test, shows how the device acts as a combined slicer and retimer. Curve A, obtained with equal biases on the two diodes, is the characteristic with no gating pulse applied i.e. the diodes are normally biased in this manner. It is seen that this condition produces the maximum of loss through the device. By shifting one diode bias so as to produce a differential of 0.5 volt the characteristic changes to that of Curve B. This differential bias can be supplied by the timing pulse in such a way that this pulse shifts the characteristic from that shown at A to that shown at B thus decreasing the loss through the device by some 12 to 15 db during the time the pulse is present. In this way the regenerator is made to act as a gate — though not an ideal one.

We see from curve B that with the differential bias the device has the characteristic of a slicer — though again not ideal. For lower levels of input there is a region over which the input-output characteristic is square law with a one db change of input producing a two db change of output. This region is followed by another in which limiting is fairly pronounced. At the 8-db input level, which is the point at which limiting sets in, the loss through the regenerator was measured to be approximately 12 db. The characteristic shown was found to be reproducible both in these experiments at 4 kmc and in those by A. F. Dietrich at 11 kmc.

For a perfect slicer only an infinitesimal change of input level is re-

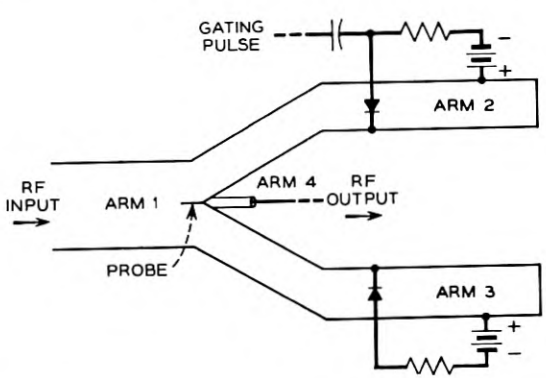

Fig. 17 — Microwave regenerator employing a single hybrid junction.

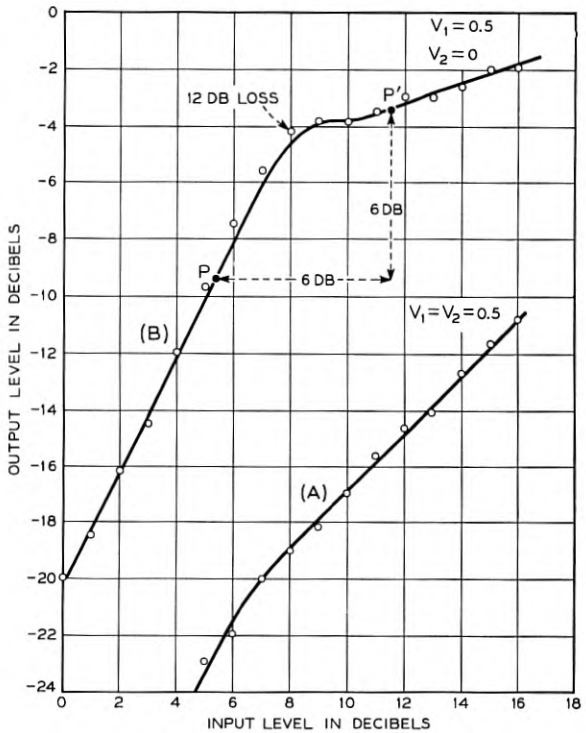

Fig. 18 — Static characteristics of the regenerator employed in these experiments.

quired to change the output from zero to maximum. The input level at which this transition takes place is the slicing level and has a very definite value. For a characteristic such as that shown on Fig. 18 this point is not at all definite and the question arises as to how one determines the slicing level for such a device. Obviously this point should be somewhere on the portion of the characteristic where expansion takes place. In the case of the circulating loop the slicing level is the level for which total gain around the loop is exactly equal to unity. Why this is so can be seen from Fig. 19 which is a plot of gain versus input level for a repeater containing a slicer with a characteristic as shown by curve B of Fig. 18. Amplifiers are necessary in the loop to make up for loss through the regenerator and other components. For Fig. 19 we assume that these amplifiers have been adjusted so that gain around the loop is exactly unity for an input pulse having a peak amplitude corresponding to the

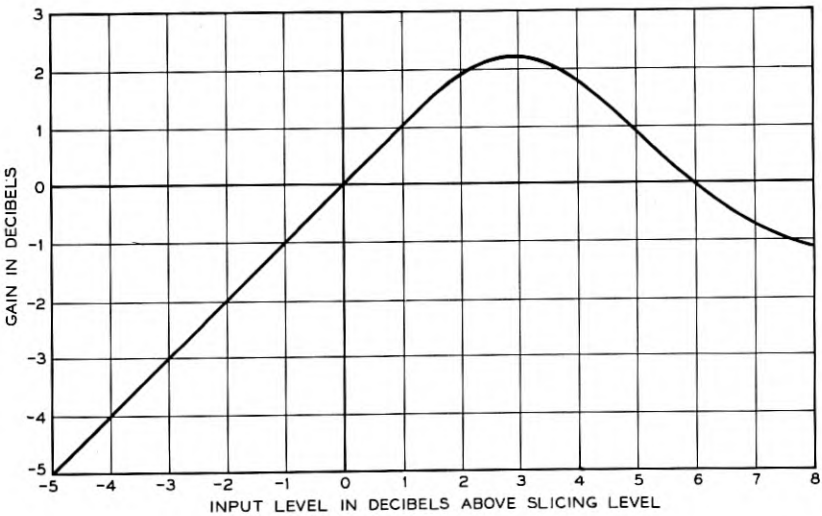

Fig 19 — Gain characteristics of a repeater providing partial regeneration.

point P' of Fig. 18. On Fig. 19 all other levels are shown in reference to this unity-gain value.

From Fig. 19 it is obvious that a pulse which starts out in the loop with a peak amplitude exactly equal to the reference, or slicing level, will continue to circulate without change of amplitude since for this level there is unity gain around the loop. A pulse with amplitude greater than the slicing level will have its amplitude increased by each passage through a regenerator until it eventually reaches a value of +6 db. It will continue to circulate at this amplitude, for here also the gain around the loop is unity.* Any pulse with peak amplitude less than the reference level will have its amplitude decreased by successive trips through the regenerator and eventually go to zero. We also see that the greater the departure of the amplitude of a pulse from the slicing level the more effect the regenerator has upon it. This means that the device acts much more powerfully on low level noise than on noise with pulse peaks near the slicing level. As examples consider first the case of noise peaks only 1 db below slicing level at the input (peak S/N = 7 db). At this level there is a 1 db loss through the repeater so that at the output the noise peaks will be 2 db below reference to give a S/N ratio of 8 db. Next

* Note that the +6-db level is at a point of stable equilibrium whereas at the slicing level equilibrium is unstable.

consider noise with a peak level 5 db below slicing level (S/N = 11 db) at the input. The loss at this level is 5 db resulting in a noise level 10 db below reference to give a S/N ratio of 16 db. We see that a 4 db improvement in S/N ratio at the input results in an 8 db improvement in this ratio at the output.

Everything which was said above concerning the circulating loop applies equally to a chain of identical repeaters. To set the effective slicing level at half amplitude at each repeater in a chain one would first find two points on the slicer characteristics such as P and P' of Fig. 18. The point P should be in the region of expansion and P' in the limiting region. Also the points should be so chosen that a 6 db increase of input from that at point P results in a 6 db increase in output at the point P'. If now at each repeater we adjust pulse peak amplitude at the slicer input to a value corresponding to that at point P' we will have unity gain from one repeater to the next at levels corresponding to pulse peaks. We will also have unity gain at levels corresponding to one half of pulse amplitude. The effective slicing level is thus set at half amplitude. Obviously the procedure for setting the slicing level at some value other than half amplitude would be practically the same. It should be pointed out that although half amplitude is the preferred slicing level for baseband pulses this is not the case for carrier pulses. W. R. Bennett of Bell Telephone Laboratories has shown that for carrier pulses the probability that noise of a given power will reduce signal pulses below half amplitude is less than the probability that this same noise will exceed half amplitude. This comes about from the fact that for effective cancellation there must be a 180° phase relationship between noise and pulse carrier. For this reason the slicing level should be set slightly above half amplitude for a carrier pulse system.

The difference in performance between a perfect slicer and one with characteristics such as shown on Fig. 18 are as follows: For the perfect slicer no effects from noise or other disturbances are passed from one repeater to the next. For the case of the imperfect regenerator some effects are passed on and so tend to accumulate in a chain of repeaters. To prevent this accumulated noise from building up to the breaking point of the system it is necessary to make the signal-to-noise ratio at each repeater somewhat better than that which would be required with the ideal slicer. For the case of random noise the required S/N ratio seems to be about 5 or 6 db above the theoretical value. This is due in part to slicer deficiency and in part to other system imperfections.

CONCLUSIONS

It is possible to build a simple device for regenerating pulses directly at microwave frequencies. A long chain of repeaters employing this regenerator should perform satisfactorily as long as the rms signal-to-noise ratio at each repeater is maintained at a value of 20 db or greater. There are a number of remaining problems which must be solved before we have a complete regenerative repeater. Some of these problems are: (1) Recovery of information for retiming from the incoming pulse train; (2) Automatic gain or level control to set the slicing level at each repeater; (3) Simple, reliable, economical, broad-band microwave amplifiers. (4) Proper filters — both for transmitting and receiving. Traveling-wave tube development should eventually result in amplifiers which will meet all of the requirements set forth in (3) above. Any improvements which can be made in the regenerator without adding undue complications would also be advantageous.

ACKNOWLEDGMENTS

A. F. Dietrich assisted in setting up the equipment described here and in many other ways. The experiment would not have been possible without traveling-wave tubes and amplifiers which were obtained through the cooperation of M. E. Hines, C. C. Cutler and their associates. I wish to thank W. M. Goodall, and J. R. Pierce for many valuable suggestions.

Crossbar Tandem as a Long Distance Switching System

By A. O. ADAM

(Manuscript received March 4, 1955)

Major toll switching features are being added to the crossbar tandem switching system for use at many of the important long distance switching centers of the nationwide network. These include automatic selection of one of several alternate routes to a particular destination, storing and sending forward digits as required, highly flexible code conversion for transmitting digits different from those received, and a translating arrangement to select the most direct route to a destination. The system is designed to serve both operator and customer dialed long distance traffic.

INTRODUCTION

The crossbar tandem switching system,[1] originally designed for switching between local dial offices, will now play an important role in nationwide dialing. New features are now available or are being developed that will permit this system to switch all types of traffic. As a result, crossbar tandem offices will have widespread use at many of the important switching centers of the nationwide switching network.

This paper briefly reviews the crossbar tandem switching system and its application for local switching, followed by discussion of the general aspects of the nationwide switching plan and of the major new features required to adapt crossbar tandem to this plan.

CROSSBAR TANDEM OFFICES USED FOR LOCAL SWITCHING

Crossbar tandem offices are now used in many of the large metropolitan areas throughout the country for interconnecting all types of local dial offices. In these applications they perform three major functions. Basically, they permit economies in trunking by combining small amounts of

traffic to and from the local offices into larger amounts for routing over common trunk groups to gain increased efficiency resulting in fewer over-all trunks.

A second important function is to permit handling calls economically between different types of local offices which are not compatible from the standpoint of intercommunication by direct pulsing. Crossbar tandem offices serve to connect these offices and to supply the conversion from one type of pulsing to another where such incompatibilities exist.

The third major function is that of centralization of equipment or services. For example, centralization of expensive charging equipment at a crossbar tandem office results in efficient use of such equipment and over-all lower cost as compared with furnishing this equipment at each local office requiring it. Examples of such equipment are remote control of zone registration and centralized automatic message accounting.[2] Centralization of other services such as weather bureau, time-of-day and similar services can be furnished.

The first crossbar tandem offices were installed in 1941 in New York, Detroit and San Francisco. These offices were equipped to interconnect local panel and No. 1 crossbar central offices in the metropolitan areas, and to complete calls to manual central offices in the same areas. The war years slowed both development and production and it was not until the late 40's that many features now in use were placed in service. These later features enable customers in step-by-step local central offices on the fringes of the metropolitan areas to interconnect on a direct dialing basis with metropolitan area customers in panel, crossbar, manual and step-by-step central offices. This same development also permitted central offices in strictly step-by-step areas to be interconnected by a crossbar tandem office where direct interconnecting was not economical. Facilities were also made available in the crossbar tandem system for completing calls from switchboards where operators use dials or multifrequency key pulsing sets.

Since a crossbar tandem office usually has access to all of the local offices in the area in which it is installed, it is attractive for handling short and long haul terminating traffic. The addition of toll terminal equipment at Gotham Tandem in New York City in 1947 permitted operators in New York State and northern New Jersey as well as distant operators to dial or key pulse directly into the tandem equipment for completion of calls to approximately 350 central offices in the New York metropolitan area. This method of completing these calls without the aid of the inward operators was a major advance in using tandem switching equipment for speeding completion of out-of-town calls.

CROSSBAR TANDEM SWITCHING ARRANGEMENT

The connections in a crossbar tandem office are established through crossbar switches mounted on incoming trunk link and outgoing office link frames shown on Fig. 1. The connections set up through these switches are controlled by equipment common to the crossbar tandem office which is held only long enough to set up each individual connection. Senders and markers are the major common control circuits.

The sender's function is to register the digits of the called number, transmit the called office code to the marker and then, as subsequently directed by the marker, control the outpulsing to the next office.

The marker's function is to receive the code digits from the sender for translation, return information to the sender concerning the details of the call, select an idle outgoing trunk to the called destination and close the transmission path through the crossbar switches from the incoming to the outgoing trunk.

GENERAL ASPECTS OF NATIONWIDE DIALING

Operator distance dialing, now used extensively throughout the country, as well as customer direct distance dialing are based on the division of the United States and Canada into numbering plan areas, interconnected by a national network through some 225 Control Switching Points (CSP's) equipped with automatic toll switching systems.

An essential element of the nationwide dialing program is a universal numbering plan[3] wherein each customer will have a distinctive number which does not conflict with the number of any other customer. The method employed is to divide the United States and Canada geographi-

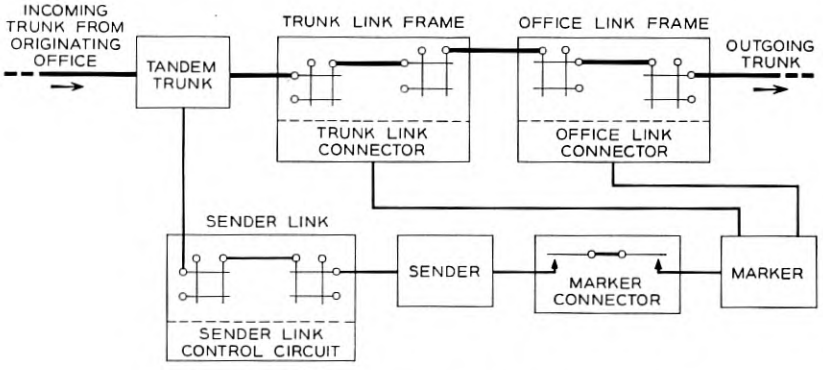

Fig. 1 — Crossbar tandem switching arrangement.

cally into more than 100 numbering plan areas and to give each of these a distinctive three digit code with either a 1 or 0 as the middle digit. Each numbering plan area will contain 500 or fewer local central offices each of which will be assigned a distinctive three-digit office code. Thus each of the telephones in the United States and Canada will have, for distance dialing purposes, a distinct identity consisting of a three digit area code, an office code of two letters and a numeral, and a station number of four digits. Under this plan, a customer will dial 7 digits to reach another customer in the same numbering area and 10 digits to reach a customer in a different numbering area.

A further requirement for nationwide dialing of long distance calls is a fundamental plan[4] for automatic toll switching. The plan provides a systematic method of interconnecting all the local central offices and toll switching centers in the United States and Canada. As shown on Fig. 2, several local central offices or "end offices" are served by a single toll center or toll point that has trunks to a "home" primary center which serves a group of toll centers. Each primary center, has trunks to a "home" sectional center which serves a larger area of the country. Similarly, the entire toll dialing territory is divided into eleven very large areas called regions, each having a regional center to serve all the sectional centers in the region. One of the regional centers, probably St. Louis, Missouri, will be designated the national center. The homing arrangements are such that it is not necessary for end offices, toll centers, toll points and primary centers to home on the next higher ranking office since the complete final route chain is not necessary. For example, end offices may be served directly from any of the higher ranking switching centers also shown in Fig. 2.

Collectively, the national center, the regional centers, the sectional centers and the primary centers will constitute the control switching points for nationwide dialing. The basic switching centers and homing arrangements are illustrated in Fig. 3.

TANDEM CROSSBAR FEATURES FOR NATIONWIDE DIALING

The broad objective in developing new features for crossbar tandem is to provide a toll switching system that can be used in cities where the large capacity and the full versatility of the No. 4 toll crossbar switching system[5] may not be economical.

The application of crossbar tandem two-wire switching systems at primary and sectional centers has been made possible by the extended use of high speed carrier systems. The echoes at the 2-wire crossbar tandem switching offices can be effectively reduced by providing a high

office balance and by the use of impedance compensators and fixed pads. A well balanced two-wire switching system, proper assignment of intertoll trunk losses, and the use of carrier circuits with high speed of propagation will permit through switching with little or no impairment from an echo standpoint.

The new features for crossbar tandem will provide arrangements necessary for operation at control switching points (CSP's). These include automatic alternate routing, the ability to store and send forward

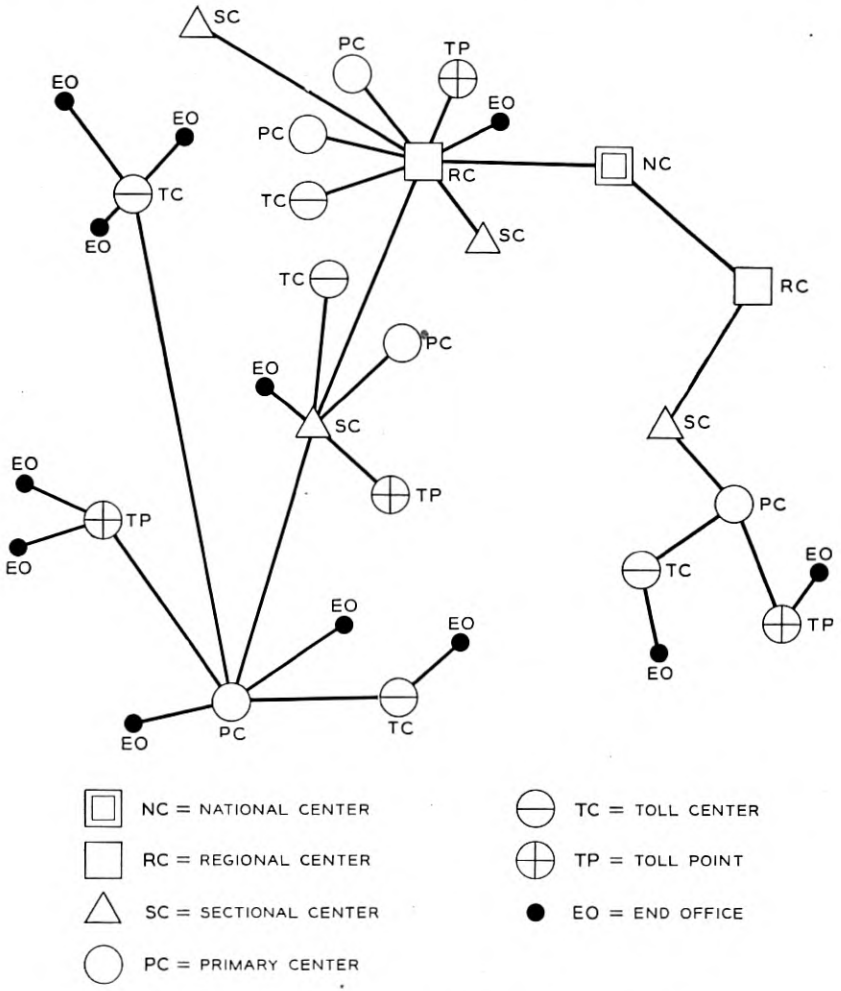

Fig. 2 — Homing arrangement for local central offices and toll centers.

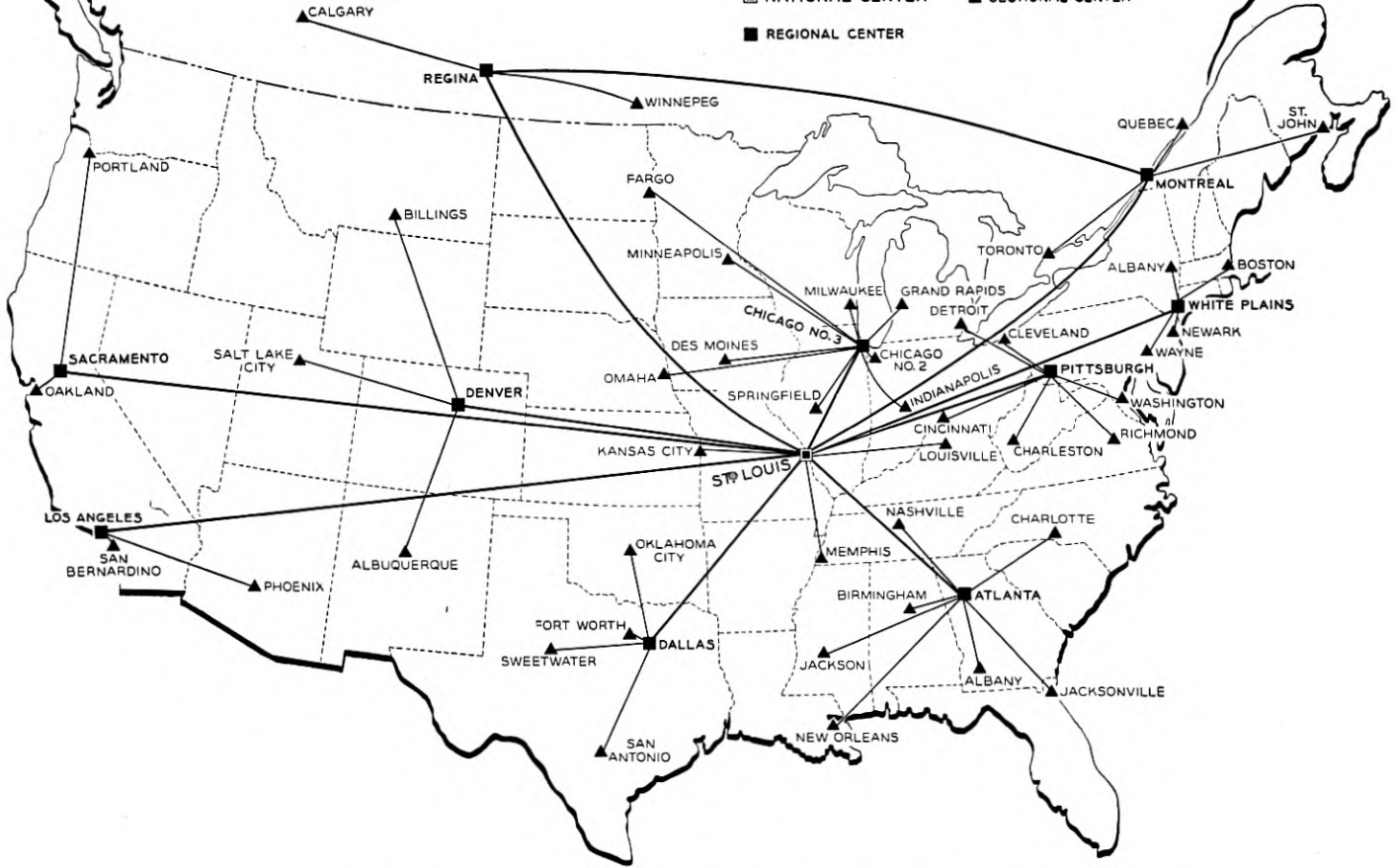

Fig. 3 — Today's vi[illegible] of the basic toll switching network in 1965.

digits as required, highly flexible code conversion (transmitting forward different digits for the area or office code instead of the dialed digits), prefixing digits ahead of the called office code, and six-digit translation.

ALTERNATE ROUTING

The control switching points will be interconnected by a final or "backbone" network of intertoll trunks engineered so that very few calls will be delayed. In addition, direct circuits between individual switching offices of all classes will be provided as warranted by the traffic density. These are called "high-usage" groups and are not engineered to handle all the traffic offered to them during the busy hour. Traffic offered to a high-usage group which finds all trunks busy will be automatically rerouted to alternate routes[6,7] consisting of other high-usage groups or to the final trunk group. The ability of the crossbar tandem equipment at the control switching point to select one of several alternate routes automatically, when all choices in the first route are busy, contributes to the economy of the plant and provides additional protection against complete interruption of service when all circuits on a particular route are out of service.

Fig. 4 shows a hypothetical example of alternate routing when a crossbar tandem office at South Bend, Indiana, receives a call destined for Youngstown, Ohio. To select an idle path, using this plan, the switching equipment at South Bend first tests the direct trunks to Youngstown. If these are all busy, it tests the direct trunks to Cleveland where the call would be completed over the final group to Youngstown. If the group to Cleveland is also busy, South Bend would test the group

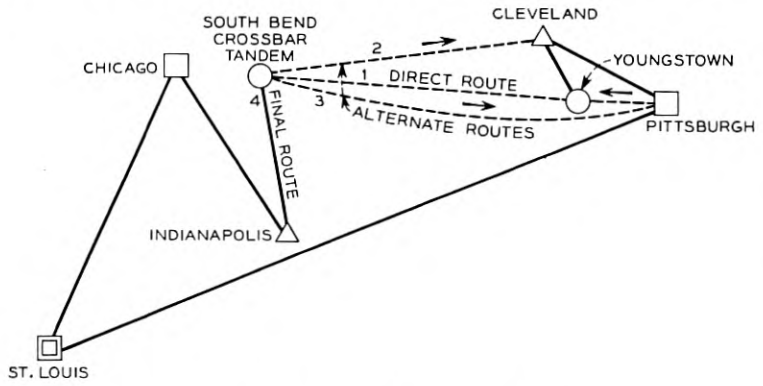

Fig. 4 — Toll network — alternate routing.

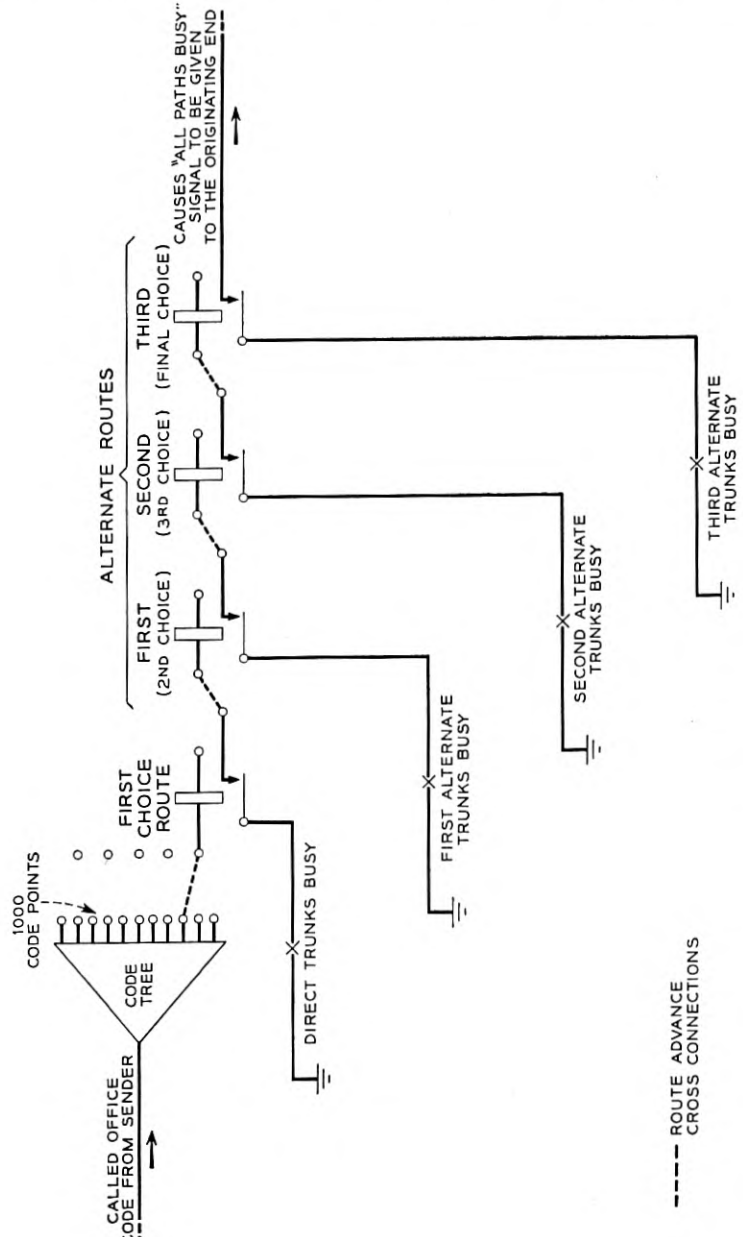

Fig. 5 — Method used for alternate routing.

to Pittsburgh and on its last attempt it would test the final group to Indianapolis. If the call were routed to Pittsburgh or Indianapolis, the switching equipment at these points would attempt by first choice and alternate routes to reach Youngstown. The final choice backbone route would be via Indianapolis, Chicago, St. Louis, Pittsburgh, Cleveland to Youngstown. Should all the trunks in any of the final groups tested be busy no further attempt to complete the call is made. It is unlikely that so many alternate routes would be provided in actual practice since crossbar tandem can test only a maximum of 240 trunks on each call and, in the case illustrated, the final trunk group to Indianapolis may be quite large.

The method employed by the crossbar tandem marker in selecting the direct route and subsequent alternate routes is shown in simplified form on Fig. 5. As a result of the translating operation, the marker selects the first choice route relay, corresponding to the called destination. Each route relay has a number of contacts which are connected to supply all the information required for proper routing of the call. Several of these contacts are used to indicate the equipment location of the trunks and the number of trunks to be tested. The marker tests all of the trunks in the direct route and if they are busy, the search for an idle trunk continues in the first alternate route which is brought into play from the "route advance" cross-connection shown on the sketch. As many as three alternate routes in addition to the first choice route can be tested in this manner.

STORING AND SENDING FORWARD DIGITS AS REQUIRED

The crossbar tandem equipment at control switching points must store all the digits received and send forward as many as are required to complete the call.

The called number recorded at a switching point is in the form of ABX-XXXX if the call is to be completed in the same numbering plan area. If the called destination is in another area, the area code XOX or XIX precedes the 7 digit number. The area codes XOX or XIX and the local office code ABX are the digits used for routing purposes and are sufficient to complete the call regardless of the number of switching points involved. Each control switching point is arranged to advance the call towards its destination when these codes are received. If the next switching point is not in the numbering area of the called telephone, the complete ten-digit number is needed to advance the call toward its destination. If the next switching point is in the num-

bering area of the called telephone the area code is not needed and seven digits will suffice for completing the call.

For example, suppose a call is originated by a customer in South Bend, Indiana, destined for customer NAtional 4-1234 in Washington, D.C. If it is assumed that the route to Washington is via a switching center in Pittsburgh, then the crossbar tandem equipment at South Bend pulses forward to Pittsburgh 202-NA4-1234, 202 being the area code for the District of Columbia. Pittsburgh in turn will delete the area code and send NA4-1234 to the District of Columbia terminating area.

As another example, suppose the crossbar tandem office at South Bend receives a call from some foreign area destined to a nearby step-by-step end office in Michigan. The crossbar tandem equipment receives and stores a ten-digit number comprising the area code and the seven digits for the office code and station number. Assuming that direct trunks to the step-by-step end office in Michigan are available, the area code and office code are deleted and the line number only is pulsed forward. To meet all conditions, the equipment is arranged to permit deletion of either the first three, four, five or six digits of a ten-digit number.

CODE CONVERSION

At the present time, some step-by-step primary centers reach other offices by the use of routing codes that are different from those assigned under the national numbering plan. This arrangement is used to obtain economies in switching equipment of the step-by-step plant and is accetpable with operator originated calls. However, with the introduction of customer direct distance dialing, it is essential that the codes used by customers be in accordance with the national numbering plan. The crossbar tandem control switching point must then automatically provide the routing codes needed by the intermediate step-by-step primary centers. This is accomplished by the code conversion feature which substitutes the arbitrary digits required to reach the called office through the step-by-step systems. Fig. 6 illustrates an application of this feature. It shows a crossbar tandem office arranged for completing calls through a step-by-step toll center to a local central office, GArden 8, in an adjacent area. A call reaching the crossbar tandem office for a customer in this office arrives with the national number, 218-GA8-1234. To complete this call, the crossbar tandem equipment deletes the area code 218 and pulses forward the local office code and number. If the

call is switched to an alternate route via the step-by-step primary center, it will be necessary for the crossbar tandem equipment to delete the area code 218 and substitute the arbitrary digits 062 to direct the call through the switches at the primary center, since the toll center requires the full seven digit number for completing the call.

PREFIXING DIGITS

It may be necessary to route a call from one area to another and back to the original area for completion. Such a situation arises on a call from Amarillo to Lubbock, Texas, both in area 915 when the crossbar tandem switching equipment finds all of the direct paths from Amarillo to Lubbock busy as illustrated on Fig. 7. The call could be routed to Lubbock via Oklahoma City which is in area 405. A seven-digit number for example, MAin 2-1234, is received in the crossbar tandem office at Amarillo. Assuming that the call is to be switched out of the 915 area through the 405 area and back to the 915 area for completion, it is necessary for the crossbar tandem office in Amarillo to prefix 915 to the MAin 2-1234 number so that the switching equipment in Oklahoma City will know that the call is for the 915 area and not for the 405 area.

Prefixing digits may also be needed at crossbar tandem offices to route calls through step-by-step primary centers. The crossbar tandem office in Fig. 8 receives the seven digit number MA2-1234 for a call to a

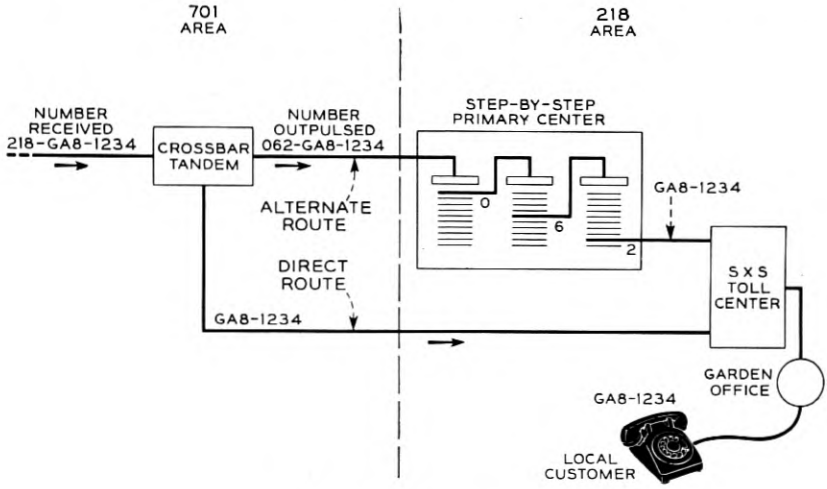

Fig. 6 — Code conversion.

customer in the Madison office in the same area. However, since the toll center needs the full seven digit number for completing the call and since the step-by-step switches at the primary center "use up" two digits (04) for its switching, the crossbar tandem equipment must prefix 04 to the seven digit number.

METHOD OF DETERMINING DIGITS TO BE TRANSMITTED

The circuitry involved for transmitting digits as received, prefixing, code conversion and for deletion involves both marker and sender functions. The senders have ten registers (1 to 10) for storing incoming digits and three registers (AA, AB, AC) for storing the arbitrary digits that are used for prefixing and code conversion.

On a ten-digit call into a crossbar tandem switching center the area code XOX, the office code ABX and the station number XXXX are stored in the inpulsing or receiving registers of the sender. The code digits XOX-ABX are sent to the marker which translates them to determine which of the digits received by the sender should be outpulsed. It also determines whether arbitrary digits should be transmitted ahead of the digits received and, if so, the value of the arbitrary digits to be stored in the sender registers AA, AB and AC. Case 1 of Fig. 9 assumes that a ten-digit number has been stored in the sender registers 1 to 10

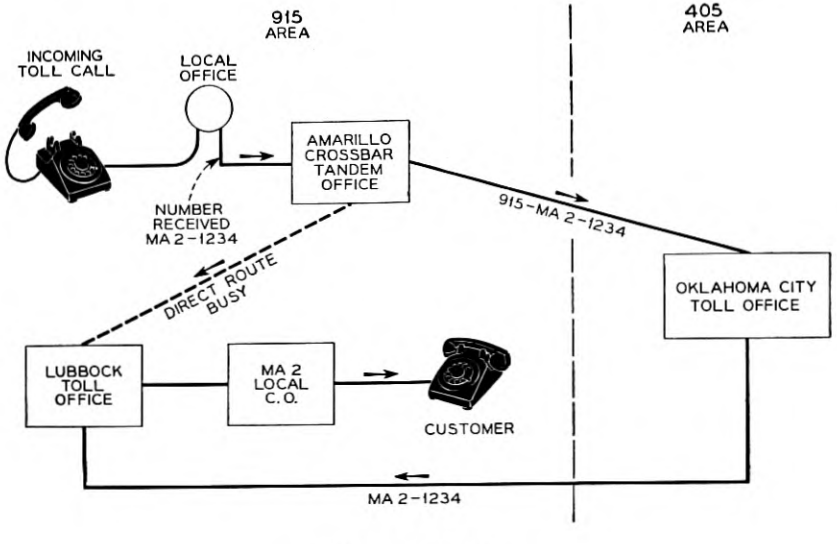

Fig. 7 — Prefixing.

and that the marker has informed the sender the called number is to be sent as received. The outpulsing control circuit is connected to each register in turn through the steering circuit S1, S2, etc. and sends the digits stored.

Case 2 illustrates a situation where the sender has stored ten digits in registers 1 to 10 and received information from the marker to delete the digits in registers 1 to 3 inclusive and to substitute the arbitrary digits stored in registers AA, AB and AC. The outpulsing circuit is first connected to register AA through steering circuit PS1, then to AB through PS2, continuing in a left to right sequence until all digits are outpulsed.

Case 3 covers a condition where the sender has stored seven digits and has obtained information from the marker to prefix the two digits stored in registers AB and AC. Outpulsing begins at the AB register through steering circuit PS2 and then advances through steering circuit PS3 to the AC register, continuing in a left to right sequence until all digits have been transmitted.

These are only a few of the many combinations that are used to give the crossbar tandem control switching equipment complete pulsing flexibility.

SIX-DIGIT TRANSLATION

Six-digit translation will be another feature added to the crossbar tandem system. When only three digits are translated, it is necessary to direct all calls to a foreign area over a single route. The ability to translate six digits permits the establishment of two or more routes from the switching center to or towards the foreign area. This is shown in Fig.

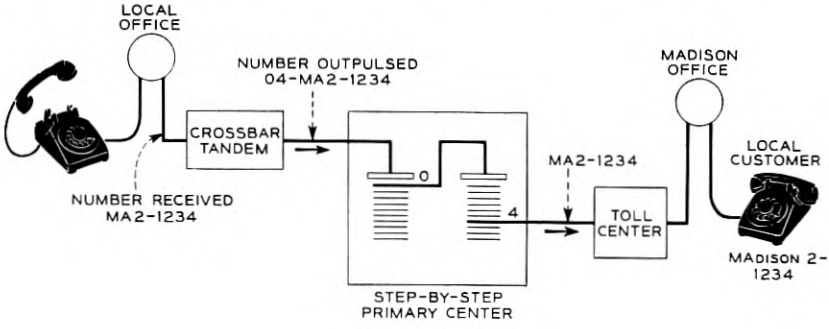

Fig. 8 — Prefixing.

10 with Madison and Milwaukee, Wisconsin, in area 414 and Belle Plaine Crossbar Tandem in Chicago, Illinois, in area 312. An economical trunking plan may provide for direct circuits from Chicago to each place. If only three-digit translation were provided in the Chicago switching equipment, the route to both places would be selected as a result of the translation of the 414 area code alone and, therefore, calls to central offices reached through Madison, would need to be routed via Milwaukee. This involves not only the extra trunk mileage, but also the use of an extra switching point. With six-digit translation, both the area code and the central office code are analyzed, making it possible to select the direct route to either city.

Six-digit translation in crossbar tandem will involve primarily the use of a foreign area translator and a marker. The translator will have a capacity for translation of five foreign areas and for 60 routes to each area. Since the translator holding time is very short, one translator is sufficient to handle all of the calls requiring six-digit translation, but two are always provided for hazard and maintenance reasons.

On a call requiring six-digit translation the first three digits are

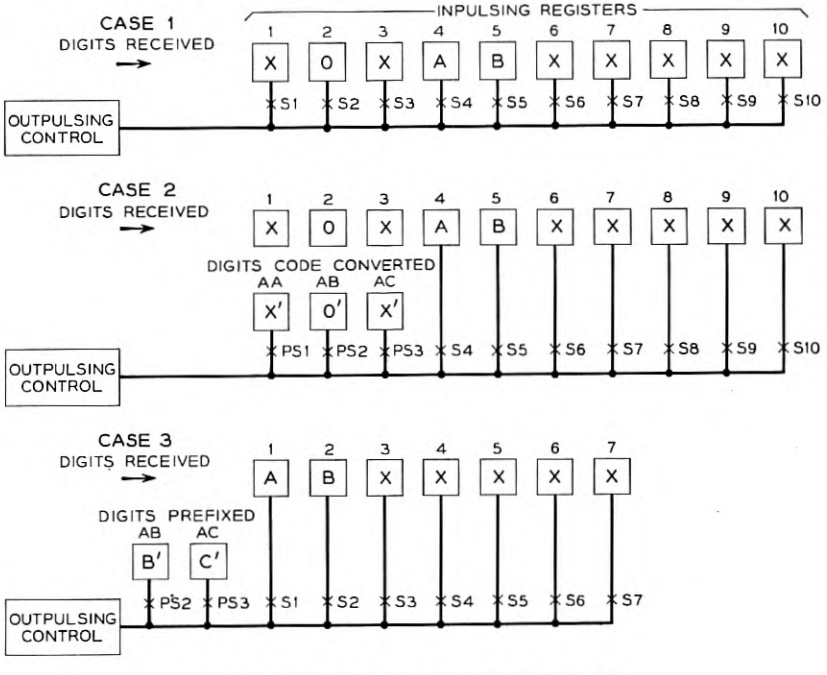

Fig. 9 — Method used for outpulsing digits.

translated in the marker and the second three digits in a foreign area translator which is associated with the marker. Fig. 11 shows, in simplified form, how this translation is accomplished.

The first three digits, corresponding to the area code, are received by a relay code tree in the marker which translates it into one of a thousand code points. This code point is cross-connected to the particular relay of the five area relays A0–A4 which has been assigned to the called area. A foreign area translator is now connected to the marker and a corresponding area relay is operated in it. The translator also receives the called office code from the sender via the marker and by means of a relay code tree similar to that in the marker translates the office code to one of a thousand code points. This code point plus the area relay is sufficient to determine the actual route to be used. As shown on the sketch, wires from each of the code points are threaded through transformers, two for each area. When the marker is ready to receive the route information, a surge of current is sent through one of these threaded wires which produces a voltage in the output winding to ionize the T- and U- tubes. Only the tubes associated with the area involved in the translation pass current to operate one each of the eight T- and U-relays. This information is passed to the marker and registered on corresponding tens and units relays. These operate a route relay which

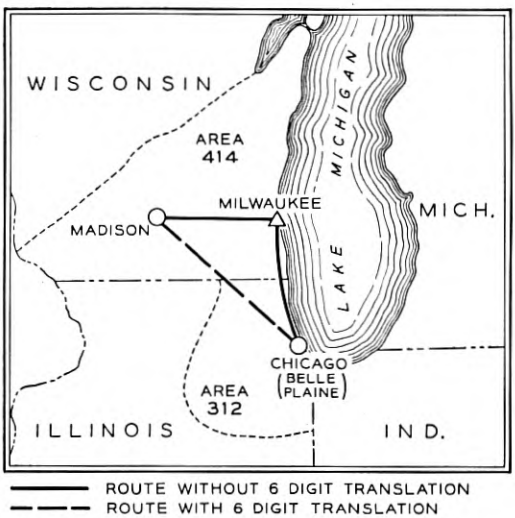

Fig. 10 — Six-digit translation.

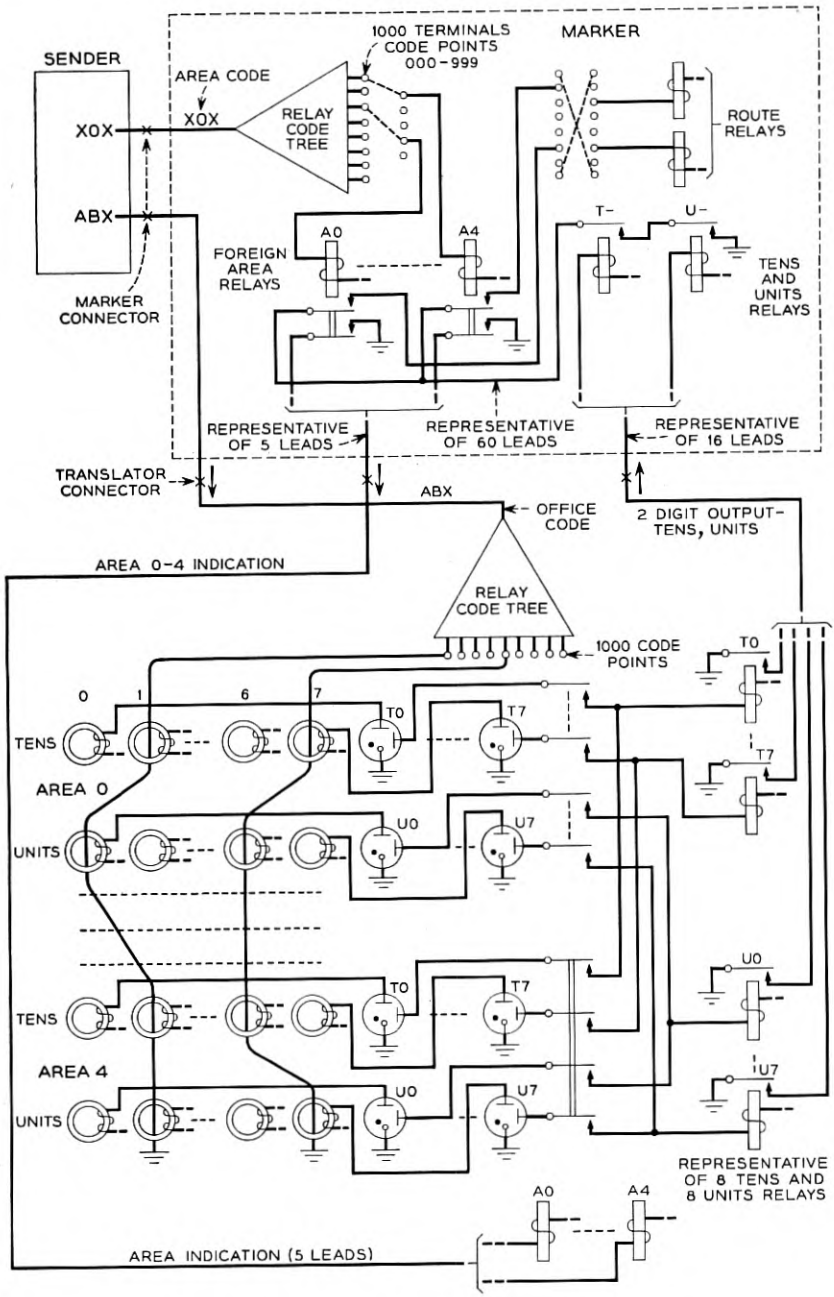

Fig. 11 — Method used for foreign area translation.

provides all the information necessary for routing the call to the central office involved.

CUSTOMER DIRECT DISTANCE DIALING

Crossbar tandem will provide arrangements permitting customers in step-by-step offices to dial their own calls anywhere in the country. Centralized automatic message accounting previously mentioned will be used for charging purposes. While the basic plan for direct distance dialing provides for the dialing of either seven or ten digits, it will be necessary for the customer in step-by-step areas to prefix a three-digit directing code, such as 112, to the called number. This directing code is required to direct the call through the step-by-step switches to the crossbar tandem office so that the seven or ten digit number can be registered in the crossbar tandem office.

When a customer in a step-by-step office originates a call to a distant customer whose national number is 915-CH3-1234, he first dials the directing code 112 and then the ten-digit number. The dialing of 112 causes the selectors in the step-by-step office to select an outgoing trunk to the crossbar tandem office. The incoming trunk in the crossbar tandem office has quick access to a three-digit register. The register must be connected during the interval between the last digit of the directing code and the first digit of the national number to insure registration of this number. This arrangement is used to permit the customer to dial all digits without delay and avoids the use of a second dial tone. If this arrangement were not used, the customer would be required to wait after dialing the 112 until the trunk in the tandem crossbar office could gain access to a sender through the sender link circuit which would then signal the customer to resume dialing by returning dial tone.

After recording the 915 area code digits in the case assumed, the CH3-1234 portion of the number is registered directly in the tandem sender which has been connected to the trunk while the customer was dialing 915. When the sender is attached to the trunk, it signals the three-digit register to transfer the 915 area code digits to it via a connector circuit. Thus when dialing is complete, the entire number 915-CH3-1234 is registered in the sender.

Crossbar tandem is being arranged to serve customers of panel and No. 1 crossbar offices for direct distance dialing. At the present time, ten digit direct distance dialing is not available to these customers because the digit storing equipments in these offices are limited to eight digits. Developments now under way, will provide arrangements for expanding the digit capacity in the local offices so that ultimately

calls from customers in panel and No. 1 crossbar offices may be routed through crossbar tandem or other equivalent offices to telephones anywhere in the country.

CONCLUSION

The new features developed for crossbar tandem will adapt it to switching all types of traffic at many important switching centers of the nationwide toll network. Of the 225 important toll switching centers now contemplated, it is expected that about 80 of these will be equipped with crossbar tandem.

REFERENCES

1. Collis, R. E., Crossbar Tandem System, A.I.E.E. Trans., **69**, pp. 997–1004, 1950.
2. King, G. V., Centralized Automatic Message Accounting, B.S.T.J., **33**, pp. 1331–1342, 1952.
3. Nunn, W. H., Nationwide Numbering Plan, B.S.T.J., **31**, pp. 851–859, 1952.
4. Pilliod, J. J., Fundamental Plans for Toll Telephone Plant, B.S.T.J., **31**, pp. 832–850, 1952.
5. Shipley, F. F., Automatic Toll Switching Systems, B.S.T.J., **31**, pp. 860–882, 1952.
6. Truitt, C. J., Traffic Engineering Techniques for Determining Trunk Requirements in Alternate Routing Trunk Networks, B.S.T.J., **33**, pp. 277–302, 1954.
7. Clos, C., Automatic Alternate Routing of Telephone Traffic, Bell Laboratories Record, **32**, pp. 51–57, Feb. 1954.

Growing Waves Due to Transverse Velocities

By J. R. PIERCE and L. R. WALKER

(Manuscript received March 30, 1955)

This paper treats propagation of slow waves in two-dimensional neutralized electron flow in which all electrons have the same velocity in the direction of propagation but in which there are streams of two or more velocities normal to the direction of propagation. In a finite beam in which electrons are reflected elastically at the boundaries and in which equal dc currents are carried by electrons with transverse velocities $+u_1$ and $-u_1$, there is an antisymmetrical growing wave if

$$\omega_p^2 \sim (\pi u_1/W)^2$$

and a symmetrical growing wave if

$$\omega_p^2 \sim \tfrac{4}{3}(\pi u_1/W)^2$$

Here ω_p is plasma frequency for the total charge density and W is beam width.

INTRODUCTION

It is well-known that there can be growing waves in electron flow when the flow is composed of several streams of electrons having different velocities in the direction of propagation of the waves.[1-5] While Birdsall[6] considers the case of growing waves in electron flow consisting of streams which cross one another, the growing waves which he finds apparently occur when two streams have different components of velocity in the direction of propagation.

This paper shows that there can be growing waves in electron flow consisting of two or more streams with the same component of velocity in the direction of wave propagation but with different components of velocity transverse to the direction of propagation. Such growing waves can exist when the electric field varies in strength across the flow. Such waves could result in the amplification of noise fluctuations in electron flow. They could also be used to amplify signals.

Actual electron flow as it occurs in practical tubes can exhibit transverse velocities. For instance, in Brillouin flow, [7, 8] if we consider electron motion in a coordinate system rotating with the Larmor frequency we see that electrons with transverse velocities are free to cross the beam repeatedly, being reflected at the boundaries of the beam. The transverse velocities may be completely disorganized thermal velocities, or they may be larger and better-organized velocities due to aberrations at the edges of the cathode or at lenses or apertures. Two-dimensional Brillouin flow allows similar transverse motions.

It would be difficult to treat the case of Brillouin or Brillouin-like flow with transverse velocities. Here, simpler cases with transverse velocities will be considered. The first case treated is that of infinite ion-neutralized two-dimensional flow with transverse velocities. The second case treated is that of two-dimensional flow in a beam of finite width in which the electrons are elastically reflected at the boundaries of the beam. Growing waves are found in both cases, and the rate of growth may be large.

In the case of the finite beam both an antisymmetric mode and a symmetric mode are possible. Here, it appears, the current density required for a growing wave in the symmetric mode is about $\frac{4}{3}$ times as great as the current density required for a growing wave in the antisymmetric mode. Hence, as the current is increased, the first growing waves to arise might be antisymmetric modes, which could couple to a symmetrical resonator or helix only through a lack of symmetry or through high-level effects.

1. Infinite two-dimensional flow

Consider a two-dimensional problem in which the potential varies sinusoidally in the y direction, as $\exp(-j\beta z)$ in the z direction and as $\exp(j\omega t)$ with time. Let there be two electron streams, each of a negative charge ρ_0 and each moving with the velocity u_0 in the z direction, but with velocities u_1 and $-u_1$ respectively in the y direction. Let us denote ac quantities pertaining to the first stream by subscripts 1 and ac quantities pertaining to the second stream by subscripts 2. The ac charge density will be denoted by ρ, the ac velocity in the y direction by $\dot{y}$, and the ac velocity in the z direction by $\dot{z}$. We will use linearized or small-signal equations of motion.[9] We will denote differentiation with respect to y by the operator D.

The equation of continuity gives

$$j\omega\rho_1 = -D(\rho_1 u_1 + \rho_0 \dot{y}_1) + j\beta(\rho_1 u_0 + \rho_0 \dot{z}_1) \tag{1.1}$$

$$j\omega\rho_2 = -D(-\rho_2 u_1 + \rho_0 \dot{y}_2) + j\beta(\rho_2 u_0 + \rho_0 \dot{z}_2) \tag{1.2}$$

Let us define

$$d_1 = j(\omega - \beta u_0) + u_1 D \tag{1.3}$$

$$d_2 = j(\omega - \beta u_0) - u_1 D \tag{1.4}$$

We can then rewrite (1.1) and (1.2) as

$$d_1 \rho_1 = \rho_0(-D\dot{y}_1 + j\beta\dot{z}_1) \tag{1.5}$$

$$d_2 \rho_2 = \rho_0(-D\dot{y}_2 + j\beta\dot{z}_2) \tag{1.6}$$

We will assume that we are dealing with slow waves and can use a potential V to describe the field. We can thus write the linearized equations of motion in the form

$$d_1 \dot{z}_1 = -j \frac{e}{m} \beta V \tag{1.7}$$

$$d_2 \dot{z}_2 = -j \frac{e}{m} \beta V \tag{1.8}$$

$$d_1 \dot{y}_1 = \frac{e}{m} DV \tag{1.9}$$

$$d_2 \dot{y}_2 = \frac{e}{m} DV \tag{1.10}$$

From (1.5) to (1.10) we obtain

$$d_1^2 \rho_1 = -\frac{e}{m} \rho_0 (D^2 - \beta^2) V \tag{1.11}$$

$$d_2^2 \rho_2 = -\frac{e}{m} \rho_0 (D^2 - \beta^2) V \tag{1.12}$$

Now, Poisson's equation is

$$(D^2 - \beta^2) V = -\frac{\rho_1 + \rho_2}{\epsilon} \tag{1.13}$$

From (1.11) to (1.13) we obtain

$$(D^2 - \beta^2) V = -\tfrac{1}{2}\omega_p^2 \left(\frac{1}{d_1^2} + \frac{1}{d_2^2} \right) (D^2 - \beta^2) V \tag{1.14}$$

$$\omega_p^2 = \frac{-2 \frac{e}{m} \rho_0}{\epsilon} \tag{1.15}$$

Here ω_p is the plasma frequency for the charge of both beams.

Either

$$(D^2 - \beta^2)V = 0 \tag{1.16}$$

or else

$$1 = \frac{-\omega_p^{\,2}}{2}\frac{(d_1^{\,2} + d_2^{\,2})}{d_1^{\,2}\,d_2^{\,2}} \tag{1.17}$$

We will consider this second case.

We should note from (1.3) and (1.4) that

$$d_1^{\,2} = u_1^{\,2}D^2 - (\omega - \beta u_0)^2 + 2jD(\omega - \beta u_0)u_1 \tag{1.18}$$

$$d_2^{\,2} = u_1^{\,2}D^2 - (\omega - \beta u_0)^2 - 2jD(\omega - \beta u_0)u_1 \tag{1.19}$$

$$d_1^{\,2} + d_2^{\,2} = 2[u_1^{\,2}D^2 - (\omega - \beta u_0)^2] \tag{1.20}$$

$$d_1^{\,2}d_2^{\,2} = [u_1^{\,2}D^2 + (\omega - \beta u_0)^2]^2 \tag{1.21}$$

Thus, (1.17) becomes

$$1 = \frac{-\omega_p^{\,2}[u_1^{\,2}D^2 - (\omega - \beta u_0)^2]}{[u_1^{\,2}D^2 + (\omega - \beta u_0)^2]^2} \tag{1.22}$$

If the quantities involved vary sinusoidally with y as $\cos \gamma y$ or $\sin \gamma y$, then

$$D^2 = -\gamma^2 \tag{1.23}$$

Our equation becomes

$$1 = \frac{\omega_p^{\,2}}{\gamma^2 u_1^{\,2}}\frac{\left[1 + \left(\dfrac{\omega - \beta u_0}{\gamma u_1}\right)^2\right]}{\left[1 - \left(\dfrac{\omega - \beta u_0}{\gamma u_1}\right)^2\right]^2} \tag{1.24}$$

What happens if we have many transverse velocities? If we refer back to (1.14) we see that we will have an equation of the form

$$1 = \sum -\tfrac{1}{2}\omega_{pn}^{\,2}\left(\frac{d_{1n}^{\,2} + d_{2n}^{\,2}}{d_{1n}^{\,2}\,d_{2n}^{\,2}}\right) \tag{1.25}$$

Here $\omega_{pn}^{\,2}$ is a plasma frequency based on the density of electrons having transverse velocities $\pm u_n$. Equation (1.25) can be written

$$1 = \sum \frac{\omega_{pn}^{\,2}}{\gamma^2 u_n^{\,2}}\frac{\left[1 + \dfrac{(\omega - \beta u_0)^2}{\gamma^2 u_n^{\,2}}\right]}{\left[1 - \dfrac{(\omega - \beta u_0)^2}{\gamma^2 u_n^{\,2}}\right]^2} \tag{1.26}$$

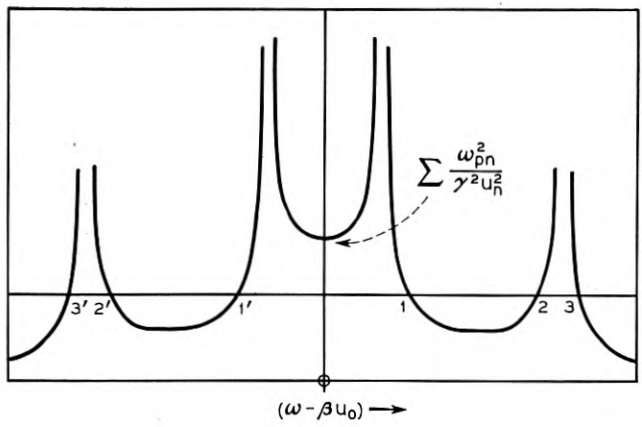

Fig. 1

Suppose we plot the left-hand and the right-hand sides of (1.26) versus $(\omega - \beta u_0)$. The general appearance of the left-hand and right-hand sides of (1.26) is indicated in Fig. 1 for the case of two velocities u_n. There will always be two unattenuated waves at values of $(\omega - \beta u_0)^2 > \gamma^2 u_e^2$ where u_e is the extreme value of u_n; these correspond to intersections 3 and 3′ in Fig. 2. The other waves, two per value of u_n, may be unattenuated or a pair of increasing and decreasing waves, depending on the values of the parameters. If

$$\sum \frac{\omega_{pn}^2}{\gamma^2 u_n^2} > 1$$

there will be at least one pair of increasing and decreasing waves.

It is not clear what will happen for a Maxwellian distribution of velocities. However, we must remember that various aberrations might give a very different, strongly peaked velocity distribution.

Let us consider the amount of gain in the case of one pair of transverse velocities, $\pm u_1$. The equation is now

$$\frac{\gamma^2 u_1^2}{\omega_p^2} = \frac{\left[1 + \left(\frac{\omega - \beta u_0}{\gamma u_1}\right)^2\right]}{\left[1 - \left(\frac{\omega - \beta u_0}{\gamma u_1}\right)^2\right]^2} \tag{1.27}$$

Let

$$\beta = \frac{\omega}{u_0} + j\frac{\gamma u_1 \epsilon}{u_0} \tag{1.28}$$

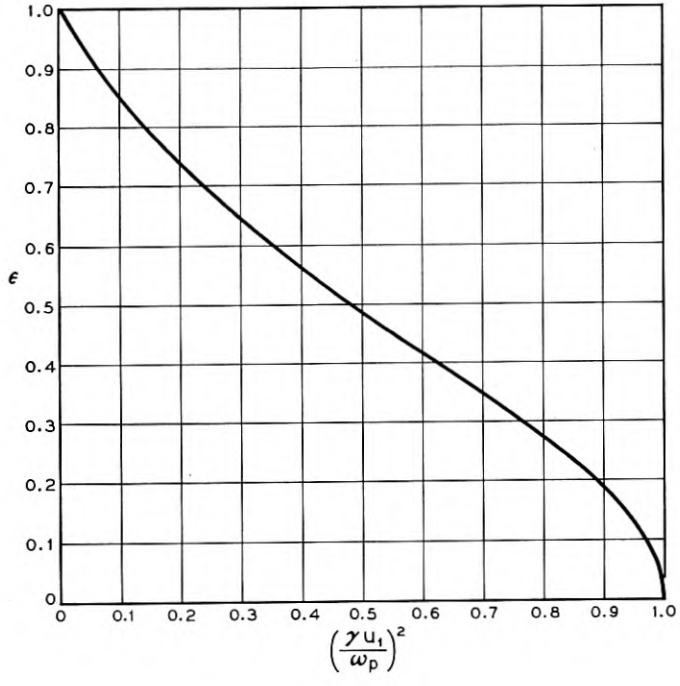

Fig. 2

This relation defines ϵ. Equation (1.27) becomes

$$\frac{\gamma^2 u_1^2}{\omega_p^2} = \frac{1 - \epsilon^2}{(1 + \epsilon^2)^2} \tag{1.29}$$

In Fig. 2, ϵ is plotted versus the parameter $\gamma^2 u_1^2/\omega_p^2$. We see that as the parameter falls below unity, ϵ increases, at first rapidly, and then more slowly, reaching a value of ± 1 as the parameter goes to zero (as ω_p^2 goes to infinity, for instance).

It will be shown in Section 2 of this paper that these results for infinite flow are in some degree an approximation to the results for flow in narrow beams. It is therefore of interest to see what results they yield if applied to a beam of finite width.

If the beam has a length L, the voltage gain is

$$e^{\epsilon\gamma(u_1/u_0)L} \tag{1.30}$$

The gain G in db is

$$G = 8.7 \frac{\gamma u_1 L}{u_0} \epsilon \text{ db} \tag{1.31}$$

Let the width of the beam be W. We let

$$\gamma = \frac{n\pi}{W} \tag{1.32}$$

Thus, for $n = 1$, there is a half-cycle variation across the beam. From (1.31) and (1.32)

$$G = 27.3 \left(\frac{u_1}{u_0}\frac{L}{d}\right) n\epsilon \text{ db} \tag{1.33}$$

Now L/u_0 is the time it takes the electrons to go from one end of the beam to the other, while W/u_1 is the time it takes the electrons to cross the beam. If the electrons cross the beam N times

$$N = \frac{u_1}{u_0}\frac{L}{W} \tag{1.34}$$

Thus,

$$G = 27.3\, Nn\epsilon \text{ db} \tag{1.35}$$

While for a given value of ϵ the gain is higher if we make the phase vary many times across the beam, i.e., if we make n large, we should note that to get any gain at all we must have

$$\begin{aligned} \omega_p^2 &> \gamma^2 u_1^2 \\ \omega_p^2 &> \left(\frac{n\pi u_1}{W}\right)^2 \end{aligned} \tag{1.36}$$

If we increase ω_p^2, which is proportional to current density, so that ω_p^2 passes through this value, the gain will rise sharply just after ω_p^2 passes through this value and will rise less rapidly thereafter.

2. A Two-Dimensional Beam of Finite Width.

Let us assume a beam of finite width in the y-direction; the boundaries lying at $y = \pm y_0$. It will be assumed also that electrons incident upon these boundaries are elastically reflected, so that electrons of the incident stream (1 or 2) are converted into those of the other stream (2 or 1). The condition of elastic reflection implies that

$$\dot{y}_1 = -\dot{y}_2 \tag{2.1}$$

$$\dot{z}_1 = \dot{z}_2 \quad \text{at } y = \pm y_0 \tag{2.2}$$

and, in addition, that

$$\rho_1 = \rho_2 \quad \text{at } y = \pm y_0 \tag{2.3}$$

since there is no change in the number of electrons at the boundary.

The equations of motion and of continuity (1.7–1.12) may be satisfied by introducing a single quantity, ψ, such that

$$V = d_1^2\, d_2^2 \psi \tag{2.4}$$

$$\dot{z}_1 = -j \frac{e}{m} \beta\, d_1\, d_2^2 \psi \tag{2.5}$$

$$\dot{z}_2 = -j \frac{e}{m} d_2^2\, d_1 \psi \tag{2.6}$$

$$\dot{y}_1 = \frac{e}{m} d_1\, d_2 D\psi \tag{2.7}$$

$$\dot{y}_2 = \frac{e}{m} d_1^2\, d_2 D\psi \tag{2.8}$$

$$\rho_1 = -\frac{e}{m} \rho_0 (D^2 - \beta^2)\, d_2^2 \psi \tag{2.9}$$

$$\rho_2 = -\frac{e}{m} \rho_0 (D^2 - \beta^2)\, d_1^2 \psi \tag{2.10}$$

Then, if we introduce the symbol, Ω, for $\omega - \beta u_0$

$$\dot{y}_1 + \dot{y}_2 = 2j \frac{e}{m} d_1\, d_2 D\Omega\psi \tag{2.11}$$

$$\dot{z}_1 - \dot{z}_2 = 2j \frac{e}{m} d_1\, d_2 u_1 D\psi \tag{2.12}$$

$$\rho_1 - \rho_2 = 2j \frac{e}{m} \rho_0 (D^2 - \beta^2) u_1 \Omega D\psi \tag{2.13}$$

It is clear that if

$$D\psi = D^3\psi = 0 \qquad y = \pm y_0 \tag{2.14}$$

the conditions for elastic reflection will be satisfied. The equation satisfied by ψ may now be found from Poisson's equation, (1–13), and is

$$(D^2 - \beta^2)\, d_1^2\, d_2^2 \psi = \frac{e\rho_0}{m\epsilon} (D^2 - \beta^2)(d_1^2 + d_2^2)\psi$$

or

$$(D^2 - \beta^2)[(u_1^2 D^2 + \Omega^2)^2 + \omega_p^2 (u_1^2 D^2 - \Omega^2)] = 0 \tag{2.15}$$

which is of the sixth degree in D. So far four boundary conditions have been imposed. The remaining necessary pair arise from matching the

internal fields to the external ones. For $y > y_0$

$$V = V_0 e^{-j\beta z} \cdot e^{-\beta y} \tag{2.16}$$

and

$$\frac{\partial V}{\partial y} + \beta V = 0 \qquad \text{at } y = y_0$$

Similarly

$$\frac{\partial V}{\partial y} - \beta V = 0 \qquad \text{at } y = -y_0 \tag{2.17}$$

The most familiar procedure now would be to look for solutions of (2.15) of the form, e^{cy}. This would give the sextic for c

$$(c^2 - \beta^2)[(u_1^2 c^2 + \Omega^2)^2 + \omega_p^2(u_1^2 c^2 - \Omega^2)] = 0 \tag{2.18}$$

with the roots $c = \pm\beta, \pm c_1, \pm c_2$, let us say. We could then express ψ as a linear combination of these six solutions and adjust the coefficients to satisfy the six boundary equations. In this way a characteristic equation for β would be obtained. From the symmetry of the problem this has the general form $F(\beta, c_1) = F(\beta, c_2)$, where c_1 and c_2 are found from (2.18). The discussion of the problem in these terms is rather laborious and, if we are concerned mainly with examining qualitatively the onset of increasing waves, another approach serves better.

From the symmetry of the equations and of the boundary conditions we see that there are solutions for ψ (and consequently for V and ρ) which are even in y and again some which are odd in y. Consider first the even solutions. We will assume that there is an even function, $\psi_1(y)$, periodic in y with period $2y_0$, which coincides with $\psi(y)$ in the open interval, $-y_0 < y < y_0$ and that $\psi_1(y)$ has a Fourier cosine series representation:

$$\psi_1(y) = \sum_1^\infty c_n \cos \lambda_n y \qquad \lambda_n = \frac{n\pi}{y_0} \qquad n = 0, 1, 2, \cdots \tag{2.19}$$

ψ inside the interval satisfies (2.15), so we assume that $\psi_1(y)$ obeys

$$(D^2 - \beta^2)[(u_1^2 D^2 + \Omega^2)^2 + \omega_p^2(u_1^2 D^2 - \Omega^2)]\psi_1 = \sum_{m=-\infty}^{+\infty} \delta(y - \overline{2m+1}y_0) \tag{2.20}$$

where δ is the familiar δ-function. Since $D\psi$ and $D^3\psi$ are required to vanish at the ends of the interval and ψ, $D^2\psi$ and $D^4\psi$ are even it follows that all

of these functions are continuous. We assume that $\psi_1 = \psi$, $D\psi_1 = D\psi$, $D^2\psi_1 = D^2\psi$, $D^3\psi_1 = D^3\psi$ and $D^4\psi_1 = D^4\psi$ at the ends of the intervals. From (2.20), $u_1^4 D^5\psi_1 \to -\frac{1}{2}$ as $y \to y_0$.

Since

$$\sum_{-\infty}^{+\infty} \delta(y - \overline{2m+1}y_0) = \frac{1}{2y_0} + \frac{1}{y_0}\sum_{1}^{\infty}(-1)^n \cos \lambda_n y \tag{2.21}$$

we obtain from (2.20)

$$2y_0\psi_1 = -\left(\frac{1}{\beta^2\Omega^2(\Omega^2 - \omega_p^2)} + 2\sum_{1}^{\infty}(-1)^n \frac{\cos \lambda_n y}{(\beta^2 + \lambda_n^2)[(\Omega^2 - u_1^2\lambda_n^2)^2 - \omega_p^2(\Omega^2 + u_1^2\lambda_n^2)]}\right) \tag{2.22}$$

Since

$$\frac{\partial V}{\partial y} + \beta V = (D + \beta)(u_1^2 D^2 + \Omega^2)^2\psi,$$

using (2.4), the condition for matching to the external field,

$$\frac{\partial V}{\partial y} + \beta V = 0,$$

yields, using $D\psi = D^3\psi = 0$ and $u_1^4 D^5\psi = -\frac{1}{2}$, the relation

$$(u_1^2 D^2 + \Omega^2)^2\psi_1 = \tfrac{1}{2}\beta \quad \text{at } y = y_0.$$

Applying this to (2.22), we then obtain, finally,

$$\frac{y_0}{\beta} = \frac{1}{\beta^2[\Omega^2 - \omega_p^2]} + 2\sum_{1}^{\infty}\frac{(\Omega^2 - u_1^2\lambda_n^2)^2}{(\beta^2 + \lambda_n^2)[(\Omega^2 - u_1^2\lambda_n^2)^2 - \omega_p^2(\Omega^2 + u_1^2\lambda_n^2)]} \tag{2.23}$$

For the odd solution we use a function, $\psi_2(y)$, equal to $\psi(y)$ in $-y_0 < y < y_0$ and representable by a sine series. To ensure the vanishing of $D\psi$ and $D^3\psi$ at $y = \pm y_0$ it is appropriate to use the functions, $\sin \mu_n y$, where $\mu_n = (n + \frac{1}{2})\pi/y_0$. The period is now $4y_0$ and we define $\psi_2(y)$ in $y_0 < y < 3y_0$ by the relation $\psi_2(y) = \psi(2y_0 - y)$ and in $-3y_0 < y < -y_0$ by $\psi_2(y) = \psi(-2y_0 - y)$. Thus, we write

$$\psi_2(y) = \sum_{0}^{\infty} d_n \sin \mu_n y \qquad \mu_n = (n + \tfrac{1}{2})\pi/y_0$$

$\psi_2(y)$ will be supposed to satisfy

$$(D^2 - \beta^2)[(u_1^2 D^2 + \Omega^2)^2 + \omega_p^2(u_1^2 D^2 - \Omega^2)[\psi_2 = \sum_{m=-\infty}^{+\infty} [\delta(y - \overline{4m+1}y_0) - \delta(y - \overline{4m-1}y_0)] \tag{2.24}$$

The extended definition of ψ_2 (outside $-y_0 < y < y_0$) is such that we may again take $\psi_1 = \psi, \cdots, D^4\psi_1 = D^4\psi$ at the ends of the interval. $u_1^4 D^5 \psi_1$ is still equal to $-\frac{1}{2}$ at $y = y_0$. Now

$$\sum_{-\infty}^{+\infty} [\delta(y - \overline{4m+1}y_0) - \delta(y - \overline{4m-1}y_0)] = \frac{1}{y_0} \sum (-1)^n \sin \mu_n y \tag{2.25}$$

so from (2.24) we may find

$$y_0 \psi_2 = -\sum_0^\infty \frac{(-1)^n \sin \mu_n y}{(\beta^2 + \mu_n^2)[(\Omega^2 - u_1^2\mu_n^2)^2 - \omega_p^2(\Omega^2 + u_1^2\mu_n^2)]} \tag{2.26}$$

Matching to the external field as before gives

$$(u_1^2 D^2 + \Omega^2)^2 \psi_2 = \frac{1}{2\beta} \qquad \text{at } y = y_0$$

and applied to (2.26) we have

$$-\frac{y_0}{2\beta} = \sum_0^\infty \frac{(\Omega^2 - u_1^2\mu_n^2)^2}{(\beta^2 + \mu_n^2)[(\Omega^2 - u_1^2\mu_n^2)^2 - \omega_p^2(\Omega^2 + u_1^2\mu_n^2)]} \tag{2.27}$$

The equations (2.23) and (2.27) for the even and odd modes may be rewritten using the following reduced variables.

$$z = \frac{\beta y_0}{\pi}$$

$$k = \frac{\omega y_0}{\pi u_1} - \frac{u_0}{u_1} z$$

$$\delta^2 = \frac{\omega_p^2 y_0^2}{\pi^2 u_1^2}$$

(2.23) becomes

$$\frac{k^2}{k^2 - \delta^2} + 2 \sum_{n=1}^\infty \frac{z^2}{z^2 + n^2} \cdot \frac{(n^2 - k^2)^2}{(n^2 - k^2)^2 - \delta^2(n^2 + k^2)} = -\pi z \tag{2.28}$$

and (2.27) transforms to

$$2 \sum_{n=0}^\infty \frac{z^2}{z^2 + (n + \frac{1}{2})^2} \cdot \frac{[(n + \frac{1}{2})^2 - k^2]^2}{[(n + \frac{1}{2})^2 - k^2]^2 - \delta^2[(n + \frac{1}{2})^2 + k^2]} = -\pi z \tag{2.29}$$

We shall assume in considering (2.28) and (2.29) that the beam is sufficiently wide for the transit of an electron from one side to the other to take a few RF cycles. The number of cycles is in fact, $\omega y_0/\pi u_1$, and, hence, from the definition of z, we see that for values of k less than 2, perhaps, z is certainly positive.

Let us consider (2.29) first since it proves to be the simpler case. If we transfer the term πz to the right hand side, it follows from the observation that z is positive (for modest values of k), that it is necessary to make the sum negative. The sum may be studied qualitatively by sketching in the $k^2 - \delta^2$ plane the lines on which the individual terms go to infinity, given by

$$\delta^2 = \frac{[(n + \tfrac{1}{2})^2 - k^2]^2}{(n + \tfrac{1}{2})^2 + k^2} \tag{2.30}$$

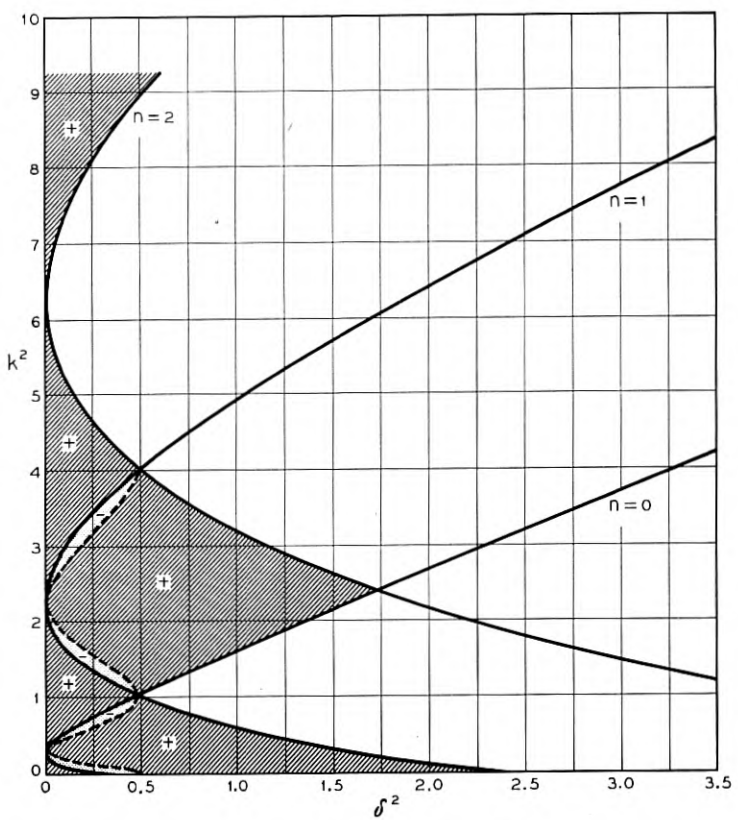

Fig. 3

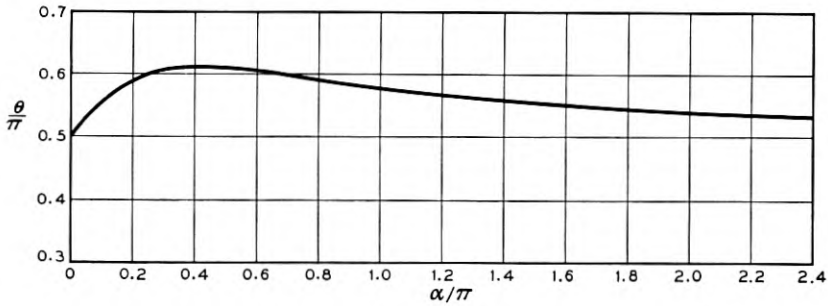

Fig. 4

Fig. 3 shows a few such curves ($n = 0, 1, 2$). To the right of such curves the individual term in question is negative, except on the line, $k^2 = (n + \frac{1}{2})^2$, where it attains the value of zero. Approaching the curves from the right the terms go to $-\infty$. On the left of the curves the function is positive and goes to $+\infty$ as the curve is approached from the

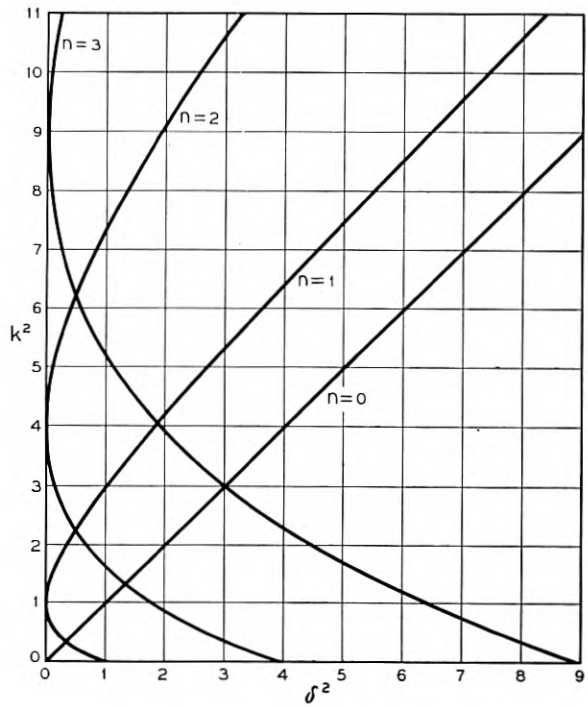

Fig. 5

left. Clearly in the regions marked + which lie to the left of every curve given by (2.30), the sum is positive and we cannot have roots. Let us examine the sum in the region to the right of the $n = 0$ curve and to the left of all others. On the line, $k^2 = \frac{1}{4}$, the sum is positive, since the first term is zero. On any other line, $k^2 =$ constant, the sum goes from $+\infty$ at the $n = 1$ curve monotonically to $-\infty$ at the $n = 0$ curve, so that somewhere it must pass through 0. This enables us to draw the zero-sum contours qualitatively in this region and they are indicated in Fig. 3. We are now in a position to follow the variation in the sum as k varies at fixed δ^2. It is readily seen that for $\delta^2 < 0.25$, because $-\pi z$ is negative in the region under consideration, there will be four real roots, two for positive, two for negative k. For δ^2 slightly greater than 0.25, the sum has

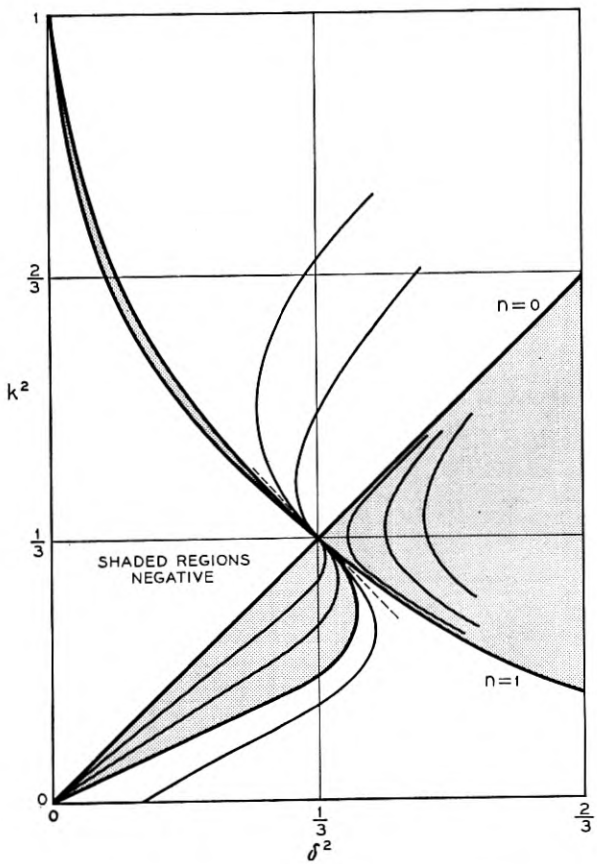

Fig. 6A

a deep minimum for $k = 0$, so that there are still four real roots unless z is very large. For z fixed, as δ^2 increases, the depth of the minimum decreases and there will finally occur a δ^2 for which the minimum is so shallow that two of the real roots disappear. Call $z(0)$ the value of z for $k = 0$, write the sum as $\Sigma(\delta^2, k^2)$ and suppose that $\Sigma(\delta_0^2, 0) = -\pi z(0)$, then for small k we have

$$\Sigma(\delta^2, k^2) = -\pi z(0) + (\delta^2 - \delta_0^2)\frac{\partial \Sigma}{\partial \delta^2} + k^2 \frac{\partial \Sigma}{\partial k^2} = -\pi z(0) - \frac{u_1}{u_0} k$$

$$k^2 - \frac{u_1/u_0}{\dfrac{\partial \Sigma}{\partial k^2}} k = \frac{\dfrac{\partial \Sigma}{\partial \delta^2}}{\dfrac{\partial \Sigma}{\partial k^2}} (\delta^2 - \delta_0^2)$$

$$k = \frac{u_1/u_0}{2\dfrac{\partial \Sigma}{\partial k^2}} \pm \sqrt{\frac{\dfrac{\partial \Sigma}{\partial \delta^2}}{\dfrac{\partial \Sigma}{\partial k^2}} (\delta^2 - \delta_0^2) + \left(\frac{u_1/u_0}{2\dfrac{\partial \Sigma}{\partial k^2}}\right)^2}$$

The roots become complex when

$$\delta^2 = \delta_0^2 - \frac{(u_1/u_0)^2}{4\dfrac{\partial \Sigma}{\partial \delta^2}\dfrac{\partial \Sigma}{\partial k^2}}$$

Since u_1/u_0 may be considered small (say 10 per cent) it is sufficient to look for the values of δ_0^2.

When $k^2 = 0$ we have

$$-\pi z = 2\sum \frac{z^2}{z^2 + (n + \frac{1}{2})^2} \cdot \frac{(n + \frac{1}{2})^2}{(n + \frac{1}{2})^2 - \delta^2}$$

$$= \frac{2z^2}{z^2 + \delta^2} \sum_0^\infty \left(\frac{\delta^2}{(n + \frac{1}{2})^2 - \delta^2} + \frac{z^2}{(n + \frac{1}{2})^2 + z^2} \right)$$

$$= \frac{\pi z^2}{z^2 + \delta^2} (\delta \tan \pi\delta + z \tanh \pi z)$$

Fig. 4 shows the solution of this equation for various $z(0)$ or $\omega y_0/\pi u_0$. Clearly the threshold δ is rather insensitive to variations in $\omega y_0/\pi u_0$.

Equation (2.28) may be examined by a similar method, but here some complications arise. Fig. 5 shows the infinity curves for $n = 0, 1, 2, 3$; the $n = 0$ term being of the form $k^2/k^2 - \delta^2$. The lowest critical region in δ^2 is the neighborhood of the point $k^2 = \delta^2 = \frac{1}{3}$, which is the intersection of the $n = 0$ and $n = 1$ lines. To obtain an idea of the behavior of

the left hand side (l.h.s.) of (2.28) in this area we first see how the point $k^2 = \delta^2 = \frac{1}{3}$ can be approached so that the l.h.s. remains finite. If we put $k^2 = \frac{1}{3} + \varepsilon$ and $\sigma^2 = \frac{1}{3} + c\varepsilon$ and expand the first two dominant terms of (2.28), then adjust c to keep the result finite as $\varepsilon \to 0$ we find

$$c = \frac{1}{4}\frac{3z^2 - 5}{3z^2 + 1}$$

c varies from $-\frac{5}{4}$ to $\frac{1}{4}$ as z goes from 0 to ∞, changing sign at $z^2 = \frac{5}{3}$. Every curve for which the l.h.s. is constant makes quadratic contact with the line $\delta^2 - \frac{1}{3} = c(k^2 - \frac{1}{3})$ at $k^2 = \delta^2 = \frac{1}{3}$. If we remember that the l.h.s. is positive for $k^2 = 0$, $0 < \delta^2 < 1$ and for $k^2 = 1$, $0 < \delta^2 < 1$,

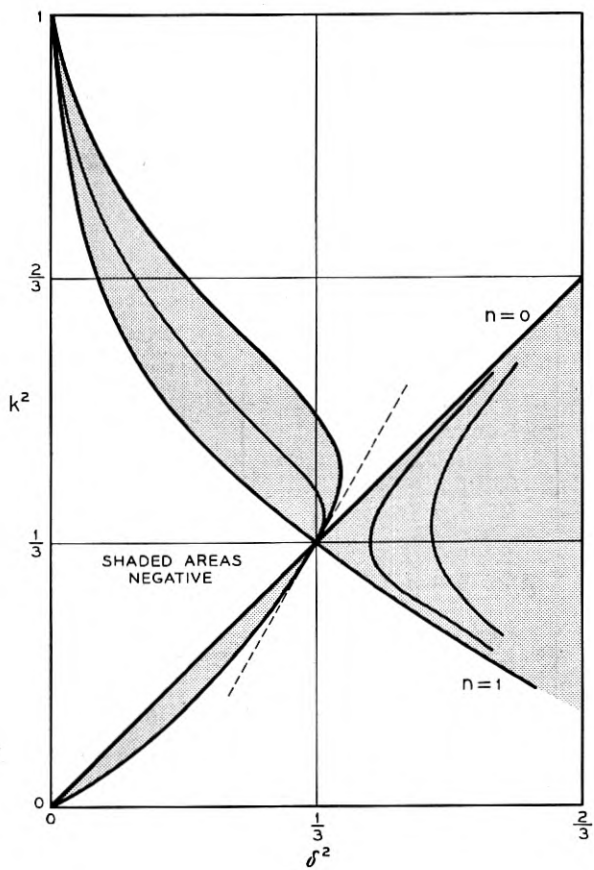

Fig. 6B

since there are no negative terms in the sum for these ranges and again that the l.h.s. must change sign between the $n = 0$ and $n = 1$ lines for any k^2 in the range $0 < k^2 < 1$ (since it varies from $\mp\infty$ to $\pm\infty$), this information may be combined with that about the immediate vicinity of $\delta^2 = k^2 = \frac{1}{3}$ to enable us to draw a line on which the l.h.s. is zero. This is indicated in Figs. 6A and 6B for small z and large z respectively. It will be seen that the zero curve and, in fact, all curves on which the l.h.s. is equal to a negative constant are required to have a vertical tangent at some point. This point may be above or below $k^2 = \frac{1}{3}$ (depending upon the sign of c or the size of z) but always at a $\delta^2 > \frac{1}{3}$. For $\delta^2 < \frac{1}{3}$ there are no regions where roots can arise as we can readily see by considering how the l.h.s. varies with k^2 at fixed δ^2. For a fixed $\delta^2 > \frac{1}{3}$ we have, then, either for $k^2 > \frac{1}{3}$ or $k^2 < \frac{1}{3}$, according to the size of z, a negative minimum which becomes indefinitely deep as $\delta^2 \to \frac{1}{3}$. Thus, since the negative terms on the right-hand side are not sensitive to small changes in δ^2, we must expect to find, for a fixed value of the l.h.s., two real solutions of (2.28) for some values of δ^2 and no real solutions for some larger value of δ^2, since the negative minimum of the l.h.s. may be made as shallow as we like by increasing δ^2. By continuity then we expect to find pairs of complex roots in this region. Rather oddly these roots, which will exist certainly for δ^2 sufficiently close to $\frac{1}{3} + 0$, will disappear if δ^2 is sufficiently increased.

REFERENCES

1. L. S. Nergaard, Analysis of a Simple Model of a Two-Beam Growing-Wave Tube, RCA Review, **9,** pp. 585–601, Dec., 1948.
2. J. R. Pierce and W. B. Hebenstreit, A New Type of High-Frequency Amplifier, B. S. T. J., **28,** pp. 23–51, Jan., 1949.
3. A. V. Haeff, The Electron-Wave Tube — A Novel Method of Generation and Amplification of Microwave Energy, Proc. I.R.E., **37,** pp. 4–10, Jan., 1949.
4. G. G. Macfarlane and H. G. Hay, Wave Propagation in a Slipping Stream of Electrons, Proc. Physical Society Sec. B, **63,** pp. 409–427, June, 1950.
5. P. Guénard and H. Huber, Étude Expérimentale de L'Interaction par Ondes de Charge d'Espace au Sein d'Un Faisceau Électronique se Deplaçant dans Des Champs Electrique et Magnétique Croisés, Annales de Radioélectricite, **7,** pp. 252–278, Oct., 1952.
6. C. K. Birdsall, Double Stream Amplification Due to Interaction Between Two Oblique Electron Streams, Technical Report No. 24, Electronics Research Laboratory, Stanford University.
7. L. Brillouin, A Theorem of Larmor and Its Importance for Electrons in Magnetic Fields, Phys. Rev., **67,** pp. 260–266, 1945.
8. J. R. Pierce, Theory and Design of Electron Beams, 2nd Ed., Chapter 9, Van Nostrand, 1954.
9. J. R. Pierce, Traveling-Wave Tubes, Van Nostrand, 1950.

Coupled Helices

By J. S. COOK, R. KOMPFNER and C. F. QUATE

(Received September 21, 1955)

An analysis of coupled helices is presented, using the transmission line approach and also the field approach, with the objective of providing the tube designer and the microwave circuit engineer with a basis for approximate calculations. Devices based on the presence of only one mode of propagation are briefly described; and methods for establishing such a mode are given. Devices depending on the simultaneous presence of both modes, that is, depending on the beat wave phenomenon, are described; some experimental results are cited in support of the view that a novel and useful class of coupling elements has been discovered.

CONTENTS

GLOSSARY OF SYMBOLS

a	Mean radius of inner helix
b	Mean radius of outer helix
b	Capacitive coupling coefficient
$B_{10,\ 20}$	shunt susceptance of inner and outer helices, respectively
$B_{1,\ 2}$	Shunt susceptance plus mutual susceptance of inner and outer helices, respectively, $B_{10} + B_m$, $B_{20} + B_m$
B_m	Mutual susceptance of two coupled helices
c	Velocity of light in free space
d	Radial separation between helices, b-a
D	Directivity of helix coupler
E	Electric field intensity
F	Maximum fraction of power transferable from one coupled helix to the other
$F(\gamma a)$	Impedance parameter
$I_{1,\ 2}$	RF current in inner and outer helix, respectively
K	Impedance in terms of longitudinal electric field on helix axis and axial power flow
L	Minimum axial distance required for maximum energy transfer from one coupled helix to the other, $\lambda_b/2$
P	Axial power flow along helix circuit
r	Radial coordinate
$\bar{r}$	Radius where longitudinal component of electric field is zero for transverse mode (about midway between a and b)
R	Return loss
s	Radial separation between helix and adjacent conducting shield
t	Time
$V_{1,\ 2}$	RF potential of inner and outer helices, respectively
x	Inductive coupling coefficient
$X_{10,\ 20}$	Series reactance of inner and outer helices, respectively
$X_{1,\ 2}$	Series reactance plus mutual reactance of inner and outer helices, respectively, $X_{10} + X_m$, $X_{20} + X_m$
X_m	Mutual reactance of two coupled helices
z	Axial coordinate
$Z_{1,\ 2}$	Impedance of inner and outer helix, respectively
$\alpha_{1,\ 2}$	Attenuation constant of inner and outer helices, respectively
β	General circuit phase constant; or mean circuit phase constant, $\sqrt{\beta_1\beta_2}$
β_0	Free space phase constant
$\beta_{10,\ 20}$	Axial phase constant of inner and outer helices in absence of coupling, $\sqrt{B_{10}X_{10}}$, $\sqrt{B_{20}X_{20}}$

$\beta_{1,2}$ May be considered as axial phase constant of inner and outer helices, respectively
β_b Beat phase constant
β_c Coupling phase constant, (identical with β_b when $\beta_1 = \beta_2$)
$\beta_{c\epsilon}$ Coupling phase constant when there is dielectric material between the helices
β_d Difference phase constant, $|\beta_1 - \beta_2|$
β_ϵ Axial phase constant of single helix in presence of dielectric
$\beta_{t,\ell}$ Axial phase constant of transverse and longitudinal modes, respectively
γ Radial phase constant
$\gamma_{t,\ell}$ Radial phase constant of transverse and longitudinal modes, respectively
Γ Axial propagation constant
$\Gamma_{t,\ell}$ Axial propagation constant for transverse and longitudinal coupled-helix modes, respectively
ε Dielectric constant
ε' Relative dielectric constant, $\varepsilon/\varepsilon_0$
ε_0 Dielectric constant of free space
λ General circuit wavelength; or mean circuit wavelength, $\sqrt{\lambda_1\lambda_2}$
λ_0 Free space wavelength
$\lambda_{1,2}$ Axial wavelength on inner and outer helix, respectively
λ_b Beat wavelength
λ_c Coupling wavelength (identical with λ_b when $\beta_1 = \beta_2$)
ψ Helix pitch angle
$\psi_{1,2}$ Pitch angle of inner and outer helix, respectively
ω Angular frequency

1. INTRODUCTION

Since their first appearance, traveling-wave tubes have changed only very little. In particular, if we divide the tube, somewhat arbitrarily, into circuit and beam, the most widely used circuit is still the helix, and the most widely used transition from the circuits outside the tube to the circuit inside is from waveguide to a short stub or antenna which, in turn, is attached to the helix, either directly or through a few turns of increased pitch. Feedback of signal energy along the helix is prevented by means of loss, either distributed along the whole helix or localized somewhere near the middle. The helix is most often supported along its whole length by glass or ceramic rods, which also serve to carry a conducting coating ("aquadag"), acting as the localized loss.

We therefore find the following circuit elements within the tube envelope, fixed and inaccessible once and for all after it has been sealed off:

1. The helix itself, determining the beam voltage for optimum beam-circuit interaction;

2. The helix ends and matching stubs, etc., all of which have to be positioned very precisely with relation to the waveguide circuits in order to obtain a reproducible match;

3. The loss, in the form of "aquadag" on the support rods, which greatly influences the tube performance by its position and distribution.

In spite of the enormous bandwidth over which the traveling-wave tube is potentially capable of operating — a feature new in the field of microwave amplifier tubes — it turns out that the positioning of the tube in the external circuits and the necessary matching adjustments are rather critical; moreover the overall bandwidths achieved are far short of the obtainable maximum.

Another fact, experimentally observed and well-founded in theory, rounds off the situation: The electro-magnetic field surrounding a helix, i.e., the slow wave, under normal conditions, does not radiate, and is confined to the close vicinity of the helix, falling off in intensity nearly exponentially with distance from the helix. A typical traveling-wave tube, in which the helix is supported by ceramic rods, and the whole enclosed by the glass envelope, is thus practically inaccessible as far as RF fields are concerned, with the exception of the ends of the helix, where provision is made for matching to the outside circuits. Placing objects such as conductors, dielectrics or distributed loss close to the tube is, in general, observed to have no effect whatsoever.

In the course of an experimental investigation into the propagation of space charge waves in electron beams it was desired to couple into a long helix at any point chosen along its length. Because of the feebleness of the RF fields outside the helix surrounded by the conventional supports and the envelope, this seemed a rather difficult task. Nevertheless, if accomplished, such a coupling would have other and even more important applications; and a good deal of thought was given to the problem.

Coupled concentric helices were found to provide the solution to the problem of coupling into and out of a helix at any particular point, and to a number of other problems too.

Concentric coupled helices have been considered by J. R. Pierce,[1] who has treated the problem mainly with transverse fields in mind. Such fields were thought to be useful in low-noise traveling-wave tube devices. Pierce's analysis treats the helices as transmission lines coupled uniformly over their length by means of mutual distributed capacitance and inductance. Pierce also recognized that it is necessary to wind the

two helices in opposite directions in order to obtain well defined transverse and axial wave modes which are well separated in respect to their velocities of propagation.

Pierce did not then give an estimate of the velocity separation which might be attainable with practical helices, nor did anybody (as far as we are aware) then know how strong a coupling one might obtain with such helices.

It was, therefore, a considerable (and gratifying) surprise[2, 3] to find that concentric helices of practically realizable dimensions and separations are, indeed, very strongly coupled when, and these are the important points,

(*a*) They have very nearly equal velocities of propagation when uncoupled, and when

(b) They are wound in opposite senses.

It was found that virtually complete power transfer from outer to inner helix (or vice versa) could be effected over a distance of the order of *one* helix wavelength (normally between $\frac{1}{10}$ and $\frac{1}{20}$ of a free-space wavelength.

It was also found that it was possible to make a transition from a coaxial transmission line to a short (outer) helix and thence through the glass surrounding an inner helix, which was fairly good over quite a considerable bandwidth. Such a transition also acted as a directional coupler, RF power coming from the coaxial line being transferred to the inner helix predominantly in one direction.

Thus, one of the shortcomings of the "conventional" helix traveling-wave tube, namely the necessary built-in accuracy of the matching parameters, was overcome by means of the new type of coupler that might evolve around coupled helix-to-helix systems.

Other constructional and functional possibilities appeared as the work progressed, such as coupled-helix attenuators, various types of broadband couplers, and schemes for exciting pure transverse (slow) or longitudinal (fast) waves on coupled helices.

One central fact emerged from all these considerations: by placing part of the circuit outside the tube envelope with complete independence from the helix terminations inside the tube, coupled helices give back to the circuit designer a freedom comparable only with that obtained at much lower frequencies. For example, it now appears entirely possible to make one type of traveling wave tube to cover a variety of frequency bands, each band requiring merely different couplers or outside helices, the tube itself remaining unchanged.

Moreover, one tube may now be made to fulfill a number of different

functions; this is made possible by the freedom with which couplers and attenuators can be placed at any chosen point along the tube.

Considerable work in this field has been done elsewhere. Reference will be made to it wherever possible. However, only that work with which the authors have been intimately connected will be fully reported here. In particular, the effect of the electron beam on the wave propagation phenomena will not be considered.

2. THEORY OF COUPLED HELICES

2.1 *Introduction*

In the past, considerable success has been attained in the understanding of traveling wave tube behavior by means of the so-called "transmission-line" approach to the theory. In particular, J. R. Pierce used it in his initial analysis and was thus able to present the solution of the so-called traveling-wave tube equations in the form of 4 waves, one of which is an exponentially growing forward traveling wave basic to the operation of the tube as an amplifier.

This transmission-line approach considers the helix — or any slow-wave circuit for that matter — as a transmission line with distributed capacitance and inductance with which an electron beam interacts. As the first approximation, the beam is assumed to be moving in an RF field of uniform intensity across the beam.

In this way very simple expressions for the coupling parameter and gain, etc., are obtained, which give one a good appreciation of the physically relevant quantities.

A number of factors, such as the effect of space charge, the non-uniform distribution of the electric field, the variation of circuit impedance with frequency, etc., can, in principle, be calculated and their effects can be superimposed, so to speak, on the relatively simple expressions deriving from the simple transmission line theory. This has, in fact, been done and is, from the design engineer's point of view, quite satisfactory.

However, physicists are bound to be unhappy over this state of affairs. In the beginning was Maxwell, and therefore the proper point to start from is Maxwell.

So-called "Field" theories of traveling-wave tubes, based on Maxwell's equation, solved with the appropriate boundary conditions, have been worked out and their main importance is that they largely confirm the results obtained by the inexact transmission line theory. It is, however, in the nature of things that field theories cannot give answers in terms of

simple closed expressions of any generality. The best that can be done is in the form of curves, with step-wise increases of particular parameters. These can be of considerable value in particular cases, and when exactness is essential.

In this paper we shall proceed by giving the "transmission-line" type theory first, together with the elaborations that are necessary to arrive at an estimate of the strength of coupling possible with coaxial helices. The "field" type theory will be used whenever the other theory fails, or is inadequate. Considerable physical insight can be gotten with the use of the transmission-line theory; nevertheless recourse to field theory is necessary in a number of cases, as will be seen.

It will be noted that in all the calculations to be presented the presence of an electron beam is left out of account. This is done for two reasons: Its inclusion would enormously complicate the theory, and, as will eventually be shown, it would modify our conclusions only very slightly. Moreover, in practically all cases which we shall consider, the helices are so tightly coupled that the velocities of the two normal modes of propagation are very different, as will be shown. Thus, only when the beam velocity is very near to either one or the other wave velocity, will growing-wave interaction take place between the beam and the helices. In this case conventional traveling wave tube theory may be used.

A theory of coupled helices in the presence of an electron beam has been presented by Wade and Rynn,[4] who treated the case of weakly coupled helices and arrived at conclusions not at variance with our views.

2.2 *Transmission Line Equations*

Following Pierce we describe two lossless helices by their distributed series reactances X_{10} and X_{20} and their distributed shunt susceptances B_{10} and B_{20}. Thus their phase constants are

$$\beta_{10} = \sqrt{B_{10}X_{10}}$$

$$\beta_{20} = \sqrt{B_{20}X_{20}}$$

Let these helices be coupled by means of a mutual distributed reactance X_m and a mutual susceptance B_m, both of which are, in a way which will be described later, functions of the geometry.

Let waves in the coupled system be described by the factor

$$e^{j\omega t}e^{-\Gamma z}$$

where the Γ's are the propagation constants to be found.

The transmission line equations may be written:

$$\begin{aligned} \Gamma I_1 - jB_1V_1 + jB_mV_2 &= 0 \\ \Gamma V_1 - jX_1I_1 + jX_mI_2 &= 0 \\ \Gamma I_2 - jB_2V_2 + jB_mV_1 &= 0 \\ \Gamma V_2 - jX_2I_a + jX_mI_1 &= 0 \end{aligned} \tag{2.2.1}$$

where

$$\begin{aligned} B_1 &= B_{10} + B_m \\ X_1 &= X_{10} + X_m \\ B_2 &= B_{20} + B_m \\ X_2 &= X_{20} + X_m \end{aligned}$$

I_1 and I_2 are eliminated from the (2.2.1) and we find

$$\frac{V_2}{V_1} = \frac{+(\Gamma^2 + X_1B_1 + X_mB_m)}{X_1B_m + B_2X_m} \tag{2.2.2}$$

$$\frac{V_1}{V_2} = \frac{+(\Gamma^2 + X_2B_2 + X_mB_m)}{X_2B_m + B_1X_m} \tag{2.2.3}$$

These two equations are then multiplied together and an expression for Γ of the 4th degree is obtained:

$$\begin{aligned} \Gamma^4 + (X_1B_1 + X_2B_2 + 2X_mB_m)\Gamma^2 \\ + (X_1X_2 - X_m^2)(B_1B_2 - B_m^2) = 0 \end{aligned} \tag{2.2.4}$$

We now define a number of dimensionless quantities:

$$\frac{B_m^2}{B_1B_2} = b^2 = (\text{capacitive coupling coefficient})^2$$

$$\frac{X_m^2}{X_1X_2} = x^2 = (\text{inductive coupling coefficient})^2$$

$$B_1X_1 = \beta_1^2, \qquad B_2X_2 = \beta_2^2$$

$$X_1B_1X_2B_2 = \beta^4 = (\text{mean phase constant})^4$$

With these substitutions we obtain the general equation for Γ^2

$$\begin{aligned} \Gamma^2 = \beta^2\Bigg[-\frac{1}{2}\left(\frac{\beta^2}{\beta_2^2} + \frac{\beta^2}{\beta_1^2} + 2bx\right) \\ \pm \sqrt{\frac{1}{4}\left(\frac{\beta^2}{\beta_2^2} + \frac{\beta^2}{\beta_1^2} + 2bx\right)^2 - (1 - x^2)(1 - b^2)}\Bigg] \end{aligned} \tag{2.2.5}$$

If we make the same substitutions in (2.2.2) we find

$$\frac{V_2}{V_1} = \sqrt{\frac{Z_2}{Z_1}}\left[\frac{\Gamma^2 + \beta_1^2 + \beta^2 bx}{\beta(\beta_1 b + \beta_2 x)}\right] \tag{2.2.6}$$

where the Z's are the impedances of the helices, i.e.,

$$Z_n = \sqrt{X_n/B_n}$$

2.3 *Solution for Synchronous Helices*

Let us consider the particular case where $\beta_1 = \beta_2 = \beta$. From (2.2.5) we obtain

$$\Gamma^2 = -\beta^2[1 + xb \pm (x + b)] \tag{2.3.1}$$

Each of the above values of Γ^2 characterizes a normal mode of propagation involving both helices. The two square roots of each Γ^2 represent waves going in the positive and negative directions. We shall consider only the positive roots of Γ^2, denoted Γ_t and Γ_ℓ, which represent the forward traveling waves.

$$\Gamma_{t,\ell} = j\beta\sqrt{1 + xb \pm (x + b)} \tag{2.3.2}$$

If $x > 0$ and $b > 0$

$$|\Gamma_t| > |\beta|, |\Gamma_\ell| < |\beta|$$

Thus Γ_t represents a normal mode of propagation which is slower than the propagation velocity of either helix alone and can be called the "slow" wave. Similarly Γ_ℓ represents a "fast" wave. We shall find that, in fact, x and b are numerically equal in most cases of interest to us; we therefore write the expressions for the propagation constants

$$\begin{aligned}\Gamma_t &= j\beta[1 + \tfrac{1}{2}(x + b)] \\ \Gamma_\ell &= j\beta[1 - \tfrac{1}{2}(x + b)]\end{aligned} \tag{2.3.3}$$

If we substitute (2.3.3) into (2.2.6) for the case where $\beta_1 = \beta_2 = \beta$ and assume, for simplicity, that the helix self-impedances are equal, we find that for $\Gamma = \Gamma_t$

$$\frac{V_2}{V_1} = -1$$

for $\Gamma = \Gamma_\ell$

$$\frac{V_2}{V_1} = +1$$

Thus, the slow wave is characterized by equal voltages of unlike sign on the two helices, and the fast wave by equal voltages of like sign. It follows that the electric field in the annular region between two such coupled concentric helices will be transverse for the slow wave and longitudinal for the fast. For this reason the slow and fast modes are often referred to as the transverse and longitudinal modes, respectively, as indicated by our subscripts.

It should be noted here that we arbitrarily chose b and x positive. A different choice of signs cannot alter the fact that the transverse mode is the slower and the longitudinal mode is the faster of the two.

Apart from the interest in the separate existence of the fast and slow waves as such, another object of interest is the phenomenon of the simultaneous existence of both waves and the interference, or spatial beating, between them.

Let V_2 denote the voltage on the outer helix; and let V_1, the voltage on the inner halix, be zero at $z = 0$. Then we have, omitting the common factor $e^{j\omega t}$,

$$\begin{aligned} V_1 &= V_{t1}e^{-\Gamma_t z} + V_{\ell 1}e^{-\Gamma_\ell z} \\ V_2 &= V_{t2}e^{-\Gamma_t z} + V_{\ell 2}e^{-\Gamma_\ell z} \end{aligned} \tag{2.3.4}$$

Since at $z = 0$, $V_1 = 0$, $V_{t1} = -V_{\ell 1}$. For the case we have considered we have found $V_{t1} = -V_{t2}$ and $V_{\ell 1} = V_{\ell 2}$. We can write (2.3.4) as

$$\begin{aligned} V_1 &= \frac{V}{2}(e^{-\Gamma_\ell z} - e^{-\Gamma_t z}) \\ V_2 &= \frac{V}{2}(e^{-\Gamma_\ell z} + e^{-\Gamma_t z}) \end{aligned} \tag{2.3.5}$$

V_2 can be written

$$\begin{aligned} V_2 &= \frac{V}{2}e^{-1/2(\Gamma_t+\Gamma_\ell)z}[e^{+1/2(\Gamma_t-\Gamma_\ell)z} + e^{-1/2(\Gamma_t-\Gamma_\ell)z}] \\ &= Ve^{-1/2(\Gamma_t+\Gamma_\ell)z}\cos[-j\tfrac{1}{2}(\Gamma_t - \Gamma_\ell)z] \end{aligned}$$

In the case when $x = b$, and $\beta_1 = \beta_2 = \beta$

$$V_2 = Ve^{-j\beta z}\cos[\tfrac{1}{2}(x + b)\beta z] \tag{2.3.6}$$

Correspondingly, it can be shown that the voltage on the inner helix is

$$V_1 = jVe^{-j\beta z}\sin[\tfrac{1}{2}(x + b)\beta z] \tag{2.3.7}$$

The last two equations exhibit clearly what we have called the spatial beat phenomenon, a wave-like transfer of power from one helix to the

other and back. We started, arbitrarily, with all the voltage on the outer helix at $z = 0$, and none on the inner; after a distance, z', which makes the argument of the cosine $\pi/2$, there is no voltage on the outer helix and all is on the inner.

To conform with published material let us define what we shall call the "coupling phase-constant" as

$$\beta_c = \beta(b + x) \tag{2.3.8}$$

From (2.3.3) we find that for $\beta_1 = \beta_2 = \beta$, and $x = b$,

$$\Gamma_t - \Gamma_\ell = j\beta_c$$

2.4 *Non-Synchronous Helix Solutions*

Let us now go back to the more general case where the propagation velocities of the (uncoupled) helices are not equal. Equation (2.2.5) can be written:

$$\Gamma^2 = -\beta^2 [1 + (1/2)\Delta + xb \pm \sqrt{(1 + xb)\Delta + (1/4)\Delta^2 + (b + x)^2}] \tag{2.4.1}$$

where

$$\Delta \equiv \left[\frac{\beta_2 - \beta_1}{\beta}\right]^2$$

In the case where $x = b$, (2.4.1) has an exact root.

$$\Gamma_{t,\ell} = j\beta [\sqrt{1 + \Delta/4} \pm 1/2 \sqrt{\Delta + (x + b)^2}] \tag{2.4.2}$$

We shall be interested in the difference between Γ_t and Γ_ℓ,

$$\Gamma_t - \Gamma_\ell = j\beta \sqrt{\Delta + (x + b)^2} \tag{2.4.3}$$

Now we substitute for Δ and find

$$\Gamma_t - \Gamma_\ell = j \sqrt{(\beta_1 - \beta_2)^2 + \beta^2 (b + x)^2} \tag{2.4.4}$$

Let us define the "beat phase-constant" as:

$$\beta_b = \sqrt{(\beta_1 - \beta_2)^2 + \beta^2(b + x)^2}$$

so that

$$\Gamma_t - \Gamma_\ell = j\beta_b \tag{2.4.5}$$

Further, let us define

$$\beta_d = | \beta_1 - \beta_2 |$$

and call this the "difference phase-constant," i.e., the hase constant corresponding to two uncoupled waves of the same frequency but differing phase velocities. We can thus state the relation between these phase constants:

$$\beta_b^2 = \beta_d^2 + \beta_c^2 \tag{2.4.6}$$

This relation is identical (except for notation) with expression (33) in S. E. Miller's paper.[5] In this paper Miller also gives expressions for the voltage amplitudes in two coupled transmission systems in the case of unequal phase velocities. It turns out that in such a case the power transfer from one system to the other is necessarily incomplete. This is of particular interest to us, in connection with a number of practical schemes. In our notation it is relatively simple, and we can state it by saying that the maximum fraction of power transferred is

$$F = \left(\frac{\beta_c}{\beta_b}\right)^2 \tag{2.4.7}$$

or, in more detail,

$$F = \frac{\beta_c^2}{\beta_d^2 + \beta_c^2} = \frac{\beta^2(b + x)^2}{(\beta_1 - \beta_2)^2 + \beta^2(b + x)^2}$$

This relationship can be shown to be a good approximation from (2.2.6), (2.3.4), (2.4.2), on the assumption that $b \approx x$ and $Z_1 \approx Z_2$, and the further assumption that the system is lossless; that is,

$$|V_2|^2 + |V_1|^2 = \text{constant} \tag{2.4.8}$$

We note that the phase velocity difference gives rise to two phenomena: It reduces the coupling wavelength and it reduces the amount of power that can be transferred from one helix to the other.

Something should be said about the case where the two helix impedances are not equal, since this, indeed, is usually the case with coupled concentric helices. Equation (2.4.8) becomes:

$$\frac{|V_2|^2}{Z_2} + \frac{|V_1|^2}{Z_1} = \text{constant} \tag{2.4.9}$$

Using this relation it is found from (2.3.4) that

$$\frac{V_2}{V_1}\sqrt{\frac{Z_1}{Z_2}} = \pm\sqrt{\frac{1}{F}}\,(1 \pm \sqrt{1 - F}) \tag{2.4.10}$$

When this is combined with (2.2.6) it is found that the impedances drop out with the voltages, and that "F" is a function of the β's only. In other

words, complete power transfer occurs when $\beta_1 = \beta_2$ regardless of the relative impedances of the helices.

The reader will remember that β_{10} and β_{20}, not β_1 and β_2, were defined as the phase constants of the helices in the absence of each other. If the assumption that $b \approx x$ is maintained, it will be found that all of the derived relationships hold true when β_{n0} is substituted for β_n. In other words, throughout the paper, β_1 and β_2 may be treated as the phase constants of the inner and outer helices, respectively. In particular it should be noted that if these quantities are to be measured experimentally each helix must be kept in the same environment as if the helices were coupled; only the other helix may be removed. That is, if there is dielectric in the annular region between the coupled helices, β_1 and β_2 must each be measured in the presence of that dielectric.

Miller also has treated the case of lossy coupled transmission systems. The expressions are lengthy and complicated and we believe that no substantial error is made in simply applying his conclusions to our case.

If the attenuation constants α_1 and α_2 of the two transmission systems (helices) are equal, no change is required in our expressions; when they are unequal the total available power (in both helices) is most effectively reduced when

$$\frac{\alpha_1 - \alpha_2}{\beta_c} \approx 1 \tag{2.4.11}$$

This fact may be made use of in designing coupled helix attenuators.

2.5 *A Look at the Fields*

It may be advantageous to consider sketches of typical field distributions in coupled helices, as in Fig. 2.1, before we go on to derive a quantitative estimate of the coupling factors actually obtainable in practice.

Fig. 2.1(a) shows, diagrammatically, electric field lines when the coupled helices are excited in the fast or "longitudinal" mode. To set up this mode only, one has to supply voltages of like sign and equal amplitudes to both helices. For this reason, this mode is also sometimes called the "(++) mode."

Fig. 2.1(b) shows the electric field lines when the helices are excited in the slow or "transverse" mode. This is the kind of field required in the transverse interaction type of traveling wave tube. In order to excite this mode it is necessary to supply voltages of equal amplitude and opposite signs to the helices and for this reason it is sometimes called the "(+−) mode." One way of exciting this mode consists in connecting one

helix to one of the two conductors of a balanced transmission line ("Lecher"-line) and the other helix to the other.

Fig. 2.1(c) shows the electric field configuration when fast and slow modes are both present and equally strongly excited. We can imagine the two helices being excited by a voltage source connected to the outer

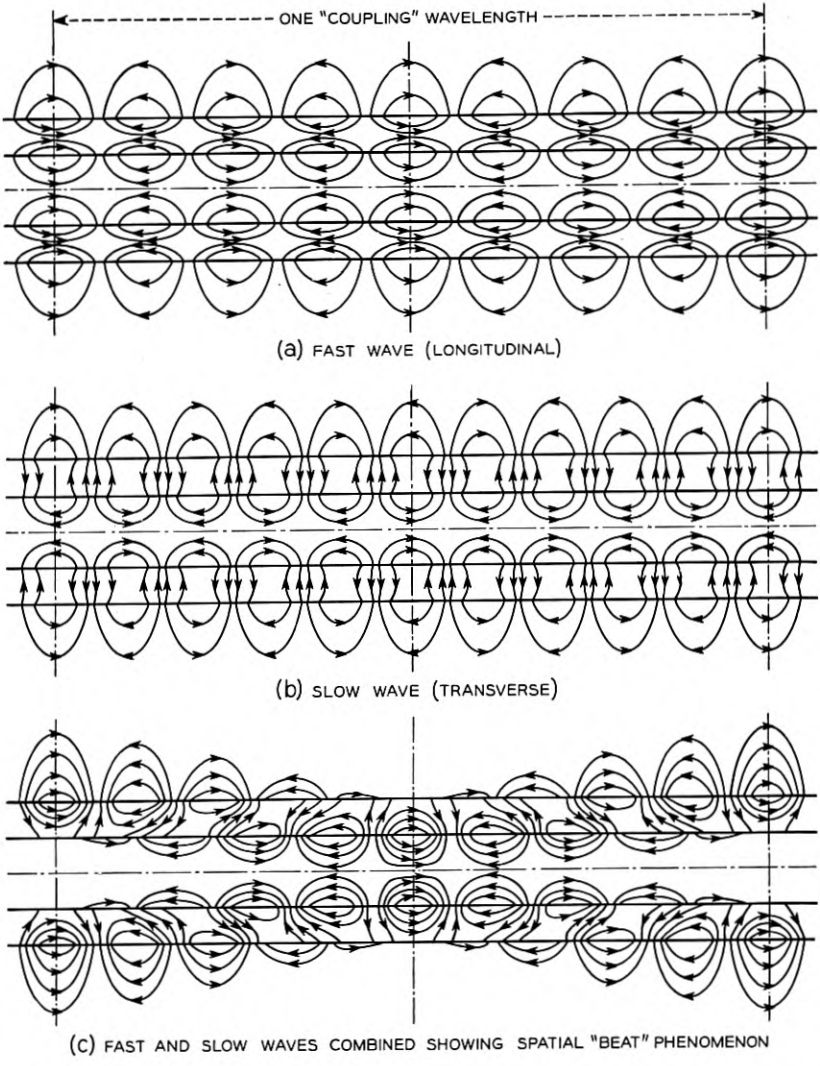

Fig. 2.1 — Typical electric field distributions in coupled coaxial helices when they are excited in: (a) the in-phase or longitudinal mode, (b) the out-of-phase or transverse mode, and (c) both modes equally.

helix only at the far left side of the sketch. One, perfectly legitimate, view of the situation is that the RF power, initially all on the outer helix, leaks into the inner helix because of the coupling between them, and then leaks back to the outer helix, and so forth.

Apart from noting the appearance of the stationary spatial beat (or interference) phenomenon these additional facts are of interest:

1) It is a simple matter to excite such a beat-wave, for instance, by connecting a lead to either one or the other of the helices, and

2) It should be possible to discontinue either one of the helices, at points where there is no current (voltage) on it, without causing reflections.

2.6 *A Simple Estimate of b and x*

How strong a coupling can one expect from concentric helices in practice? Quantitatively, this is expressed by the values of the coupling factors x and b, which we shall now proceed to estimate.

A first crude estimate is based on the fact that slow-wave fields are known to fall off in intensity somewhat as $e^{-\beta r}$ where β is the phase constant of the wave and r the distance from the surface guiding the slow wave. Thus a unit charge placed, say, on the inner helix, will induce a charge of opposite sign and of magnitude

$$e^{-\beta(b-a)}$$

on the outer helix. Here b = mean radius of the outer helix and a = mean radius of the inner. We note that the shunt mutual admittance coupling factor is negative, irrespective of the directions in which the helices are wound. Because of the similarity of the magnetic and electric field distributions a current flowing on the inner helix will induce a similarly attenuated current, of amplitude

$$e^{-\beta(b-a)}$$

on the outer helix. The direction of the induced current will depend on whether the helices are wound in the same sense or not, and it turns out (as one can verify by reference to the low-frequency case of coaxial coupled coils) that the series mutual impedance coupling factor is negative when the helices are oppositely wound.

In order to obtain the greatest possible coupling between concentric helices, both coupling factors should have the same sign. This then requires that the helices should be wound in opposite directions, as has been pointed out by Pierce.

When the distance between the two helices goes to zero, that is to say,

if they lie in the same surface, it is clear that both coupling factors b and x will go to unity.

As pointed out earlier in Section 2.3, the choice of sign for b is arbitrary. However, once a sign for b has been chosen, the sign of x is necessarily the opposite when the helices are wound in the same direction, and vice versa. We shall choose, therefore,

$$\begin{aligned} b &= +e^{-\beta(b-a)} \\ x &= \mp e^{-\beta(b-a)} \end{aligned} \tag{2.6.1}$$

the sign of the latter depending on whether the helices are wound in the same direction or not.

In the case of unequal velocities, β, the propagation constant, would be given by

$$\beta = \sqrt{\beta_1 \beta_2} \tag{2.6.2}$$

2.7 *Strength of Coupling versus Frequency*

The exponential variation of coupling factors with respect to frequency (since $\beta = \omega/v$) has an important consequence. Consider the expression for the coupling phase constant

$$\beta_c = \beta(b + x) \tag{2.3.8}$$

or

$$| \beta_c | = 2\beta e^{-\beta(b-a)} \tag{2.7.1}$$

The coupling wavelength, which is defined as

$$\lambda_c = \left| \frac{2\pi}{\beta_c} \right| \tag{2.7.2}$$

is, therefore,

$$\lambda_c = \frac{\pi}{\beta} e^{\beta(b-a)}$$

or

$$\lambda_c = \frac{\lambda}{2} e^{(2\pi/\lambda)(b-a)} \tag{2.7.3}$$

where λ is the (slowed-down) RF wavelength on either helix. It is convenient to multiply both sides of (2.7.1) with a, the inner helix radius, in order to obtain a dimensionless relation between β_c and β:

$$\beta_c a = 2\beta a e^{-\beta a((b/a)-1)} \tag{2.7.4}$$

This relation is plotted on Fig. 2.2 for several values of b/a.

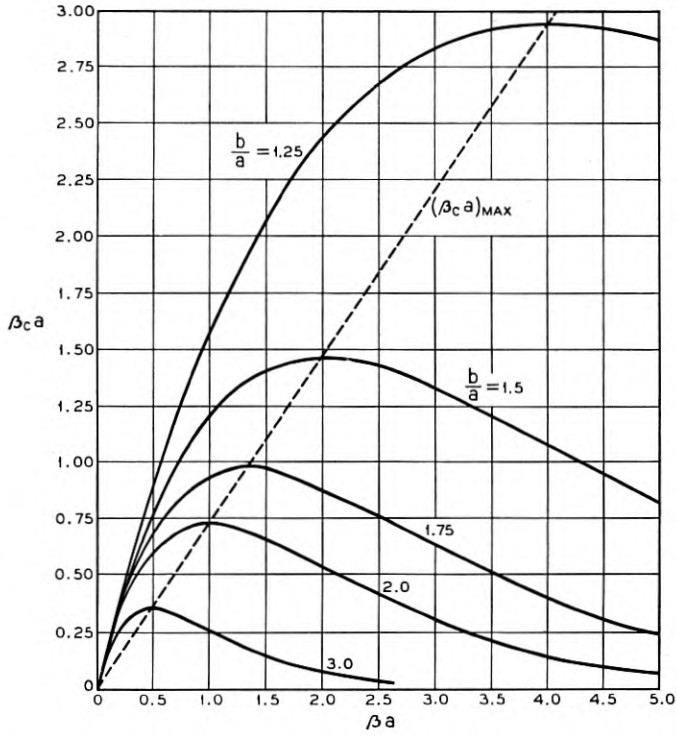

Fig. 2.2 — Coupling phase-constant plotted as a function of the single helix phase-constant for synchronous helices for several values of b/a. These curves are based on simple estimates made in Section 2.7.

There are two opposing tendencies determining the actual physical length of a coupling beat-wavelength:

1) It tends to grow with the RF wavelength, being proportional to it in the first instance;

2) Because of the tighter coupling possible as the RF wavelength increases in relation to the helix-to-helix distance, the coupling beat-wavelength tends to shrink.

Therefore, there is a region where these tendencies cancel each other, and where one would expect to find little change of the coupling beat-wavelength for a considerable change of RF frequency. In other words, the "bandwidth" over which the beat-wavelength stays nearly constant can be large.

This is a situation naturally very desirable and favorable for any device in which we rely on power transfer from one helix to the other by

means of a length of overlap between them an integral number of half beat-wavelengths long. Obviously, one will design the helices in such a way as to take advantage of this situation.

Optimum conditions are easily obtained by differentiating β_c with respect to β and setting $\partial\beta_c/\partial\beta$ equal to zero. This gives for the optimum conditions

$$\beta_{\text{opt}} = \frac{1}{b - a} \tag{2.7.5}$$

or

$$\beta_{c\,\text{opt}} = \frac{2e^{-1}}{b - a} = 2e^{-1}\beta_{\text{opt}} \tag{2.7.6}$$

Equation (2.7.5), then, determines the ratio of the helix radii if it is required that deviations from a chosen operating frequency shall have least effect.

2.8 *Field Solutions*

In treating the problem of coaxial coupled helices from the transmission line point of view one important fact has not been considered, namely, the dispersive character of the phase constants of the separate helices, β_1 and β_2. By dispersion we mean change of phase velocity with frequency. If the dispersion of the inner and outer helices were the same it would be of little consequence. It is well known, however, that the dispersion of a helical transmission line is a function of the ratio of helix radius to wavelength, and thus becomes a parameter to be considered. When the theory of wave propagation on a helix was solved by means of Maxwell's equations subject to the boundary condition of a helically conducting cylindrical sheath, the phenomenon of dispersion first made its appearance. It is clear, therefore, that a more complete theory of

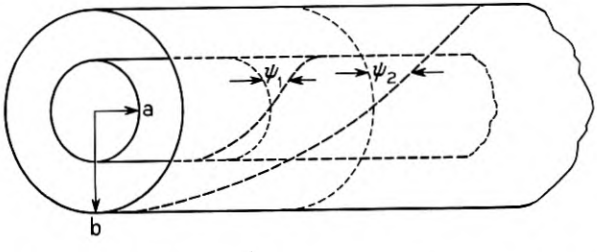

Fig. 2.3 — Sheath helix arrangement on which the field equations are based.

coupled helices will require similar treatment, namely, Maxwell's equations solved now with the boundary conditions of two cylindrical helically conducting sheaths. As shown on Fig. 2.3, the inner helix is specified by its radius a and the angle ψ_1 made by the direction of conductivity with a plane perpendicular to the axis; and the outer helix by its radius b (not to be confused with the mutual coupling coefficient b) and its corresponding pitch angle ψ_2. We note here that oppositely wound helices require opposite signs for the angles ψ_1 and ψ_2; and, further, that helices with equal phase velocities will have pitch angles of about the same absolute magnitude.

The method of solving Maxwell's equations subject to the above mentioned boundary conditions is given in Appendix I. We restrict ourselves here to giving some of the results in graphical form.

The most universally used parameter in traveling-wave tube design is a combination of parameters:

$$\beta_0 a \cot \psi_1$$

where $\beta_0 = 2\pi/\lambda_0$, λ_0 being the free-space wavelength, a the radius of the inner helix, and ψ_1 the pitch angle of the inner helix. The inner helix is chosen here in preference to the outer helix because, in practice, it will be part of a traveling-wave tube, that is to say, inside the tube envelope. Thus, it is not only less accessible and changeable, but determines the important aspects of a traveling-wave tube, such as gain, power output, and efficiency.

The theory gives solutions in terms of radial propagation constants which we shall denote γ_t and γ_ℓ (by analogy with the transverse and longitudinal modes of the transmission line theory). These propagation constants are related to the axial propagation constants β_t and β_ℓ by

$$\gamma_n = \sqrt{\beta_n^2 - \beta_0^2}$$

Of course, in transmission line theory there is no such thing as a radial propagation constant. The propagation constant derived there and denoted Γ corresponds here to the axial propagation constant $j\beta$. By analogy with (2.4.5) the beat phase constant should be written

$$\beta_b = \beta_t - \beta_\ell$$

However, in practice β_0 is usually much smaller than β and we can therefore write with little error

$$\beta_b = \gamma_t - \gamma_\ell$$

for the beat phase constant. For practical purposes it is convenient to

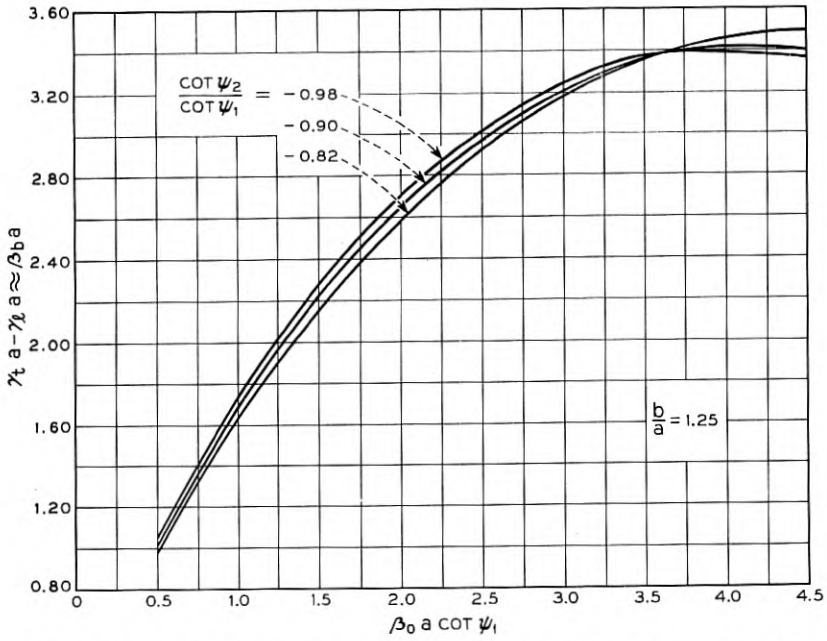

Fig. 2.4.1 — Beat phase-constant plotted as a function of $\beta_0 a \cot \psi_1$. These curves result from the solution of the field equations given in the appendix. For $b/a = 1.25$.

normalize in terms of the inner helix radius, a:

$$\beta_b a = \gamma_t a - \gamma_l a$$

This has been plotted as a function of $\beta_0\ a \cot \psi_1$ in Fig. 2.4, which should be compared with Fig. 2.2. It will be seen that there is considerable agreement between the results of the two methods.

2.9 *Bifilar Helix*

The failure of the transmission line theory to take into account dispersion is well illustrated in the case of the bifilar helix. Here we have two identical helices wound in the same sense, and at the same radius. If the two wires are fed in phase we have the normal mode characterized by the sheath helix model whose propagation constant is the familiar Curve A of Fig. 2.5. If the two wires of the helix are fed out of phase we have the bifilar mode; and, since that is a two wire transmission system, we shall have a TEM mode which, in the absence of dielectric, propagates along the wire with the velocity of light. Hence, the propagation constant for this mode is simply $\beta_0 a \cot \psi$ and gives rise to the horizontal

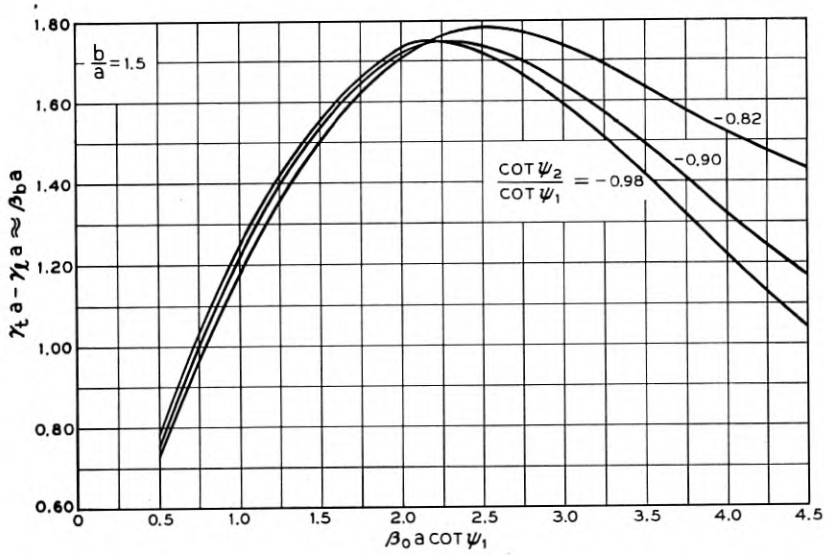

Fig. 2.4.2 — Beat phase-constant plotted as a function of $\beta_0 a \cot \psi_1$. These curves result from the solution of the field equations given in the appendix. For $b/a = 1.5$.

line of Curve B in Fig. 2.5. Again the coupling phase constant β_c is given by the difference of the individual phase constants:

$$\beta_c a = \beta_0 a \cot \psi - \gamma a \tag{2.9.1}$$

which is plotted in Fig. 2.6. Now note that when $\beta_0 \ll \gamma$ this equation is accurate, for it represents a solution of the field equations for the helix.

From the simple unsophisticated transmission line point of view no coupling between the two helices would, of course, have been expected, since the two helices are identical in every way and their mutual capacity and inductance should then be equal and opposite.

Experiments confirm the essential correctness of (2.9.1). In one experiment, which was performed to measure the coupling wavelength for the bifilar helices, we used helices with a $\cot \psi = 3.49$ and a radius of 0.036 cm which gave a value, at 3,000 mc, of $\beta_0 a \cot \psi = 0.51$. In these experiments the coupling length, L, defined by

$$(\beta_0 a \cot \psi - \gamma a) \frac{L}{a} = \pi$$

was measured to be $15.7a$ as compared to a value of $13.5a$ from Fig. 2.6. At 4,000 mc the measured coupling length was $14.6a$ as compared to

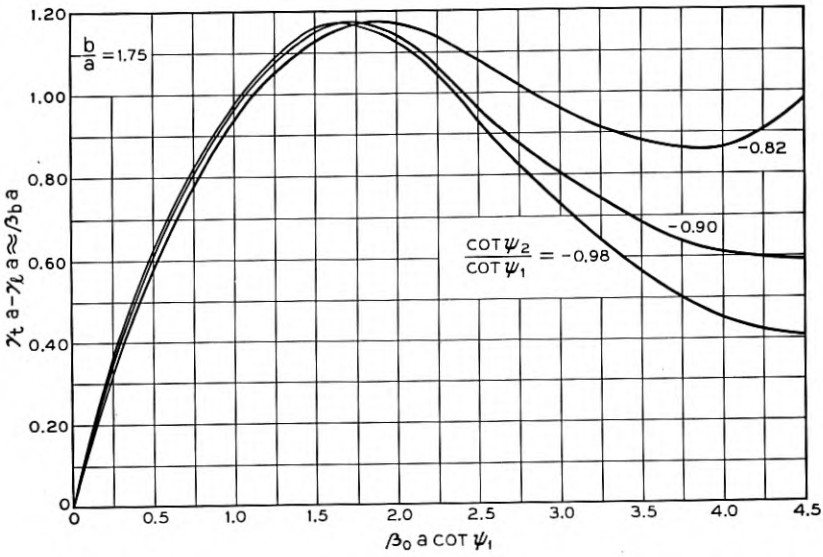

Fig. 2.4.3 — Beat phase-constant plotted as a function of $\beta_0 a \cot \psi_1$. These curves result from the solution of the field equations given in the appendix. For $b/a = 1.75$.

12.6a computed from Fig. 2.6, thus confirming the theoretical prediction rather well. The slight increase in coupling length is attributable to the dielectric loading of the helices which were supported in quartz tubing. The dielectric tends to decrease the dispersion and hence reduce β_c. This is discussed further in the next section.

2.10 *Effect of Dielectric Material between Helices*

In many cases which are of interest in practice there is dielectric material between the helices. In particular when coupled helices are used with traveling-wave tubes, the tube envelope, which may be of glass, quartz, or ceramic, all but fills the space between the two helices.

It is therefore of interest to know whether such dielectric makes any difference to the estimates at which we arrived earlier. We should not be surprised to find the coupling strengthened by the presence of the dielectric, because it is known that dielectrics tend to rob RF fields from the surrounding space, leading to an increase in the energy flow through the dielectric. On the other hand, the dielectric tends to bind the fields closer to the conducting medium. To find a qualitative answer to this question we have calculated the relative coupling phase constants for two sheath helices of infinite radius separated by a distance "d" for 1)

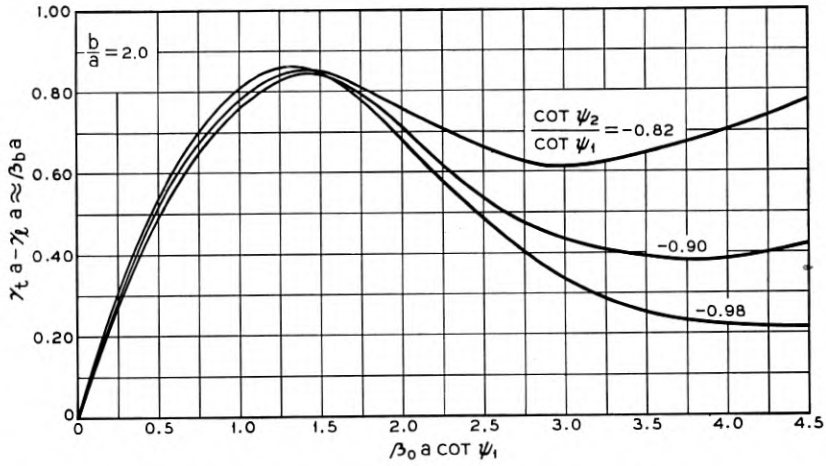

Fig. 2.4.4 — Beat phase-constant plotted as a function of $\beta_0 a \cot \psi_1$. These curves result from the solution of the field equations given in the appendix. For $b/a = 2.0$.

the case with dielectric between them having a relative dielectric constant $\epsilon' = 4$, and 2) the case of no dielectric. The pitch angles of the two helices were ψ and $-\psi$, respectively; i.e., the helices were assumed to be synchronous, and wound in the opposite sense.

Fig. 2.7 shows a plot of the ratio of $\beta_{c\epsilon}/\beta_\epsilon$ to β_c/β versus $\beta_0 (d/2) \cot \psi$,

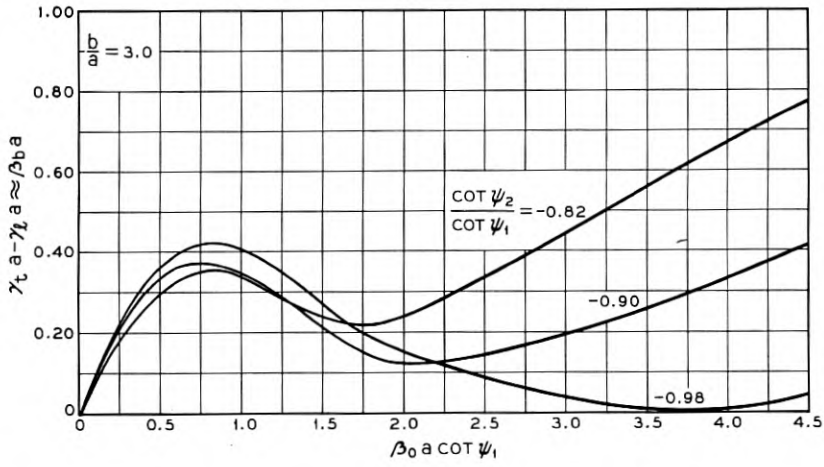

Fig. 2.4.5 — Beat phase-constant plotted as a function of $\beta_0 a \cot \psi_1$. These curves result from the solution of the field equations given in the appendix. For $b/a = 3.0$.

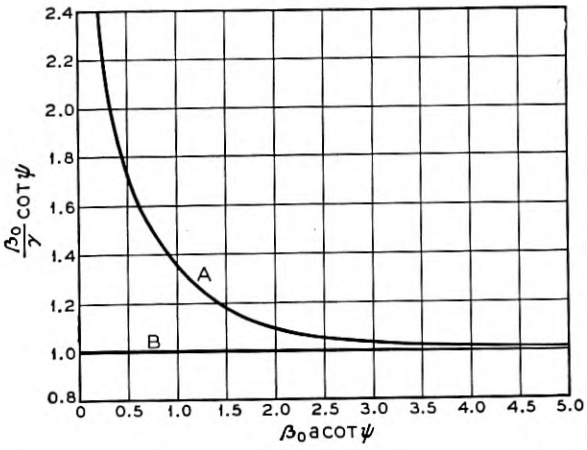

Fig. 2.5 — Propagation constants for a bifilar helix plotted as a function of $\beta_0 a \cot \psi_1$. The curves illustrate, (A) the dispersive character of the in-phase mode and, (B) the non-dispersive character of the out-of-phase mode.

where $\beta_{c\epsilon}$ is the coupling phase-constant in the presence of dielectric, β_ϵ is the phase-constant of each helix alone in the presence of the same dielectric, β_c is the coupling phase-constant with no dielectric, and β is the phase constant of each helix in free space. In many cases of interest $\beta_0(d/2) \cot \psi$ is greater than 1.2. Then

$$\frac{\beta_{c\epsilon}/\beta_\epsilon}{\beta_c/\beta} = \left[\frac{3\varepsilon' + 1}{2\varepsilon' + 2}\right] e^{-(\sqrt{2\varepsilon'+2}-2)\beta_0 (d/2) \cot \psi} \qquad (2.10.1)$$

Appearing in the same figure is a similar plot for the case when there is a conducting shield inside the inner helix and outside the outer, and separated a distance, "s," from the helices. Note that

$$d \equiv b - a.$$

It appears from these calculations that the effect of the presence of dielectric between the helices depends largely on the parameter β_0 $(d/2)$ cot ψ. For values of this parameter larger than 0.3 the coupling wavelength tends to increase in terms of circuit wavelength. For values smaller than 0.3 the opposite tends to happen. Note that the curve representing (2.10.1) is a fair approximation down to $\beta_0(d/2)$ cot $\psi = 0.6$ to the curve representing the exact solution of the field equations. J. W. Sullivan, in unpublished work, has drawn similar conclusions.

2.11 *The Conditions for Maximum Power Transfer*

The transmission line theory has led us to expect that the most efficient power transfer will take place if the phase velocities on the two helices, prior to coupling, are the same. Again, this would be true were it not for the dispersion of the helices. To evaluate this effect we have used the field equation to determine the parameter of the coupled helices which gives maximum power transfer. To do this we searched for combinations of parameters which give an equal current flow in the helix sheath for either the longitudinal mode or the transverse mode. This was suggested by L. Stark, who reasoned that if the currents were equal for the individual modes the beat phenomenon would give points of zero RF current on the helix.

The values of $\cot \psi_2/\cot \psi_1$ which are required to produce this condition are plotted in Fig. 2.8 for various values of b/a. Also there are shown values of $\cot \psi_2/\cot \psi_1$ required to give equal axial velocities for the helices before they are coupled. It can be seen that the uncoupled velocity of the inner helix must be slightly slower than that of the outer.

A word of caution is necessary for these curves have been plotted without considering the effects of dielectric loading, and this can have a rather marked effect on the parameters which we have been discussing. The significant point brought out by this calculation is that the optimum

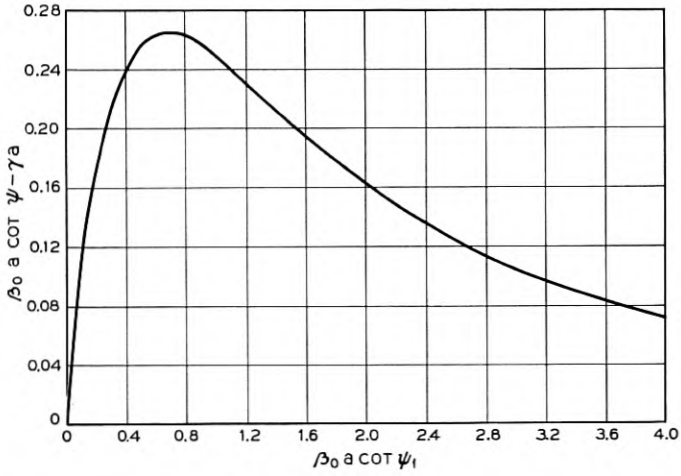

Fig. 2.6 — The coupling phase-constant which results from the two possible modes of propagation on a bifilar helix shown as a function of $\beta_0 a \cot \psi_1$.

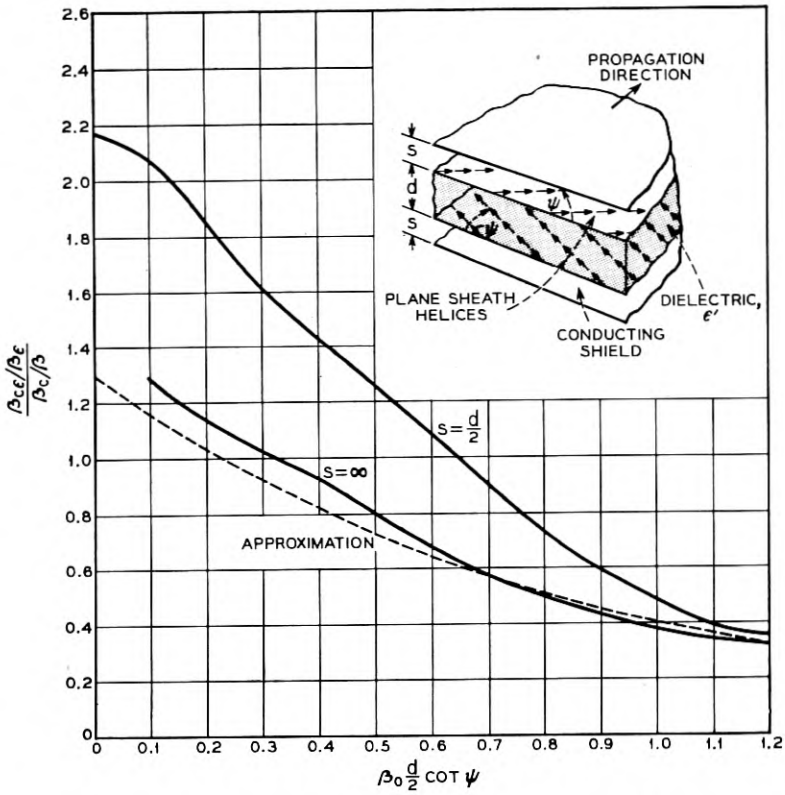

FIG. 2.7 — The effect of dielectric material between coupled infinite radius sheath helices on their relative coupling phase-constant shown as a function of $\beta_0 d/2 \cot \psi_1$. The effect of shielding on this relation is also indicated.

condition for coupling is not necessarily associated with equal velocities on the uncoupled helices.

2.12 *Mode Impedance*

Before leaving the general theory of coupled helices something should be said regarding the impedance their modes present to an electron beam traveling either along their axis or through the annular space between them. The field solutions for cross wound, coaxially coupled helices, which are given in Appendix I, have been used to compute the impedances of the transverse and longitudinal modes. The impedance, K, is defined, as usual, in terms of the longitudinal field on the axis and the power flow along the system.

$$K = \frac{E_z^2}{\beta^2 P} = \left(\frac{\beta}{\beta_0}\right)^{1/3} \left(\frac{\gamma}{\beta}\right)^{4/3} F(\gamma a)$$

In Fig. 2.9, $F(\gamma a)$, for various ratios of inner to outer radius, is plotted for both the transverse and longitudinal modes together with the value of $F(\gamma a)$ for the single helix ($b/a = \infty$). We see that the longitudinal mode has a higher impedance with cross wound coupled helices than does a single helix. We call attention here to the fact that this is the same phenomenon which is encountered in the contrawound helix[6], where the structure consists of two oppositely wound helices of the same radius.

As defined here, the transverse mode has a lower impedance than the single helix. This, however, is not the most significant comparison; for it is the transverse field midway between helices which is of interest in the transverse mode. The factor relating the impedance in terms of the transverse field between helices to the longitudinal field on the axis is $E_r^2(\bar{r})/E_z^2(0)$, where $\bar{r}$ is the radius at which the longitudinal component of the electric field E_z, is zero for the transverse mode. This factor, plotted in Fig. 2.10 as a function of $\beta_0 a \cot \psi_r$, shows that the impedance in terms of the transverse field at $\bar{r}$ is interestingly high.

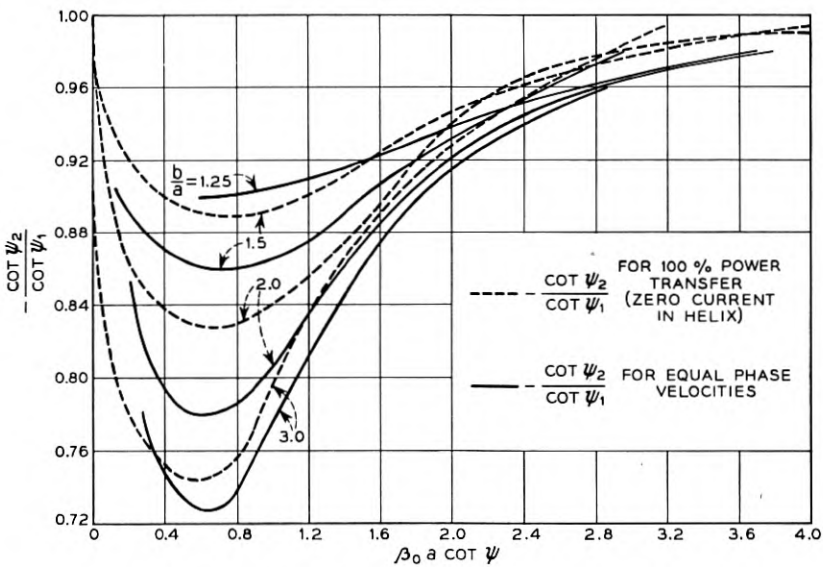

Fig. 2.8 — The values of cot ψ_2/cot ψ_1 required for complete power transfer plotted as a function of $\beta_0 a$ cot ψ_1 for several values of b/a. For comparison, the value of cot ψ_2/cot ψ_1 required for equal velocities on inner and outer helices is also shown.

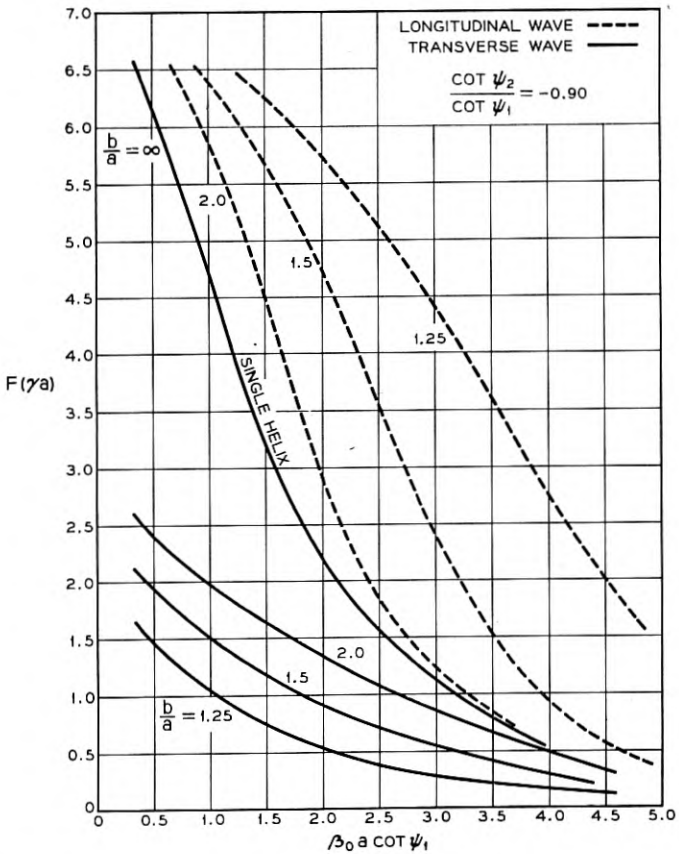

Fig. 2.9 — Impedance parameter, $F(\gamma a)$, associated with both transverse and longitudinal modes shown for several values of b/a. Also shown is $F(\gamma a)$ for a single helix.

It is also of interest to consider the impedance of the longitudinal mode in terms of the longitudinal field between the two helices. The factor, $E_z^2(\bar{r})/E_z^2(0)$, relating this to the axial impedance is plotted in Fig. 2.11. We see that rather high impedances can also be obtained with the longitudinal field midway between helices. This, in conjunction with a hollow electron beam, should provide efficient amplification.[7]

3. APPLICATION OF COUPLED HELICES

When we come to describe devices which make use of coupled helices we find that they fall, quite naturally, into two separate classes. One

class contains those devices which depend on the presence of only one of the two normal modes of propagation. The other class of devices depends on the simultaneous presence, in roughly equal amounts, of *both* normal modes of propagation, and is, in general, characterized by the words "spatial beating." Since spatial beating implies energy surging to and fro between inner and outer helix, there is no special problem in exciting both modes simultaneously. Power fed exclusively to one or the other

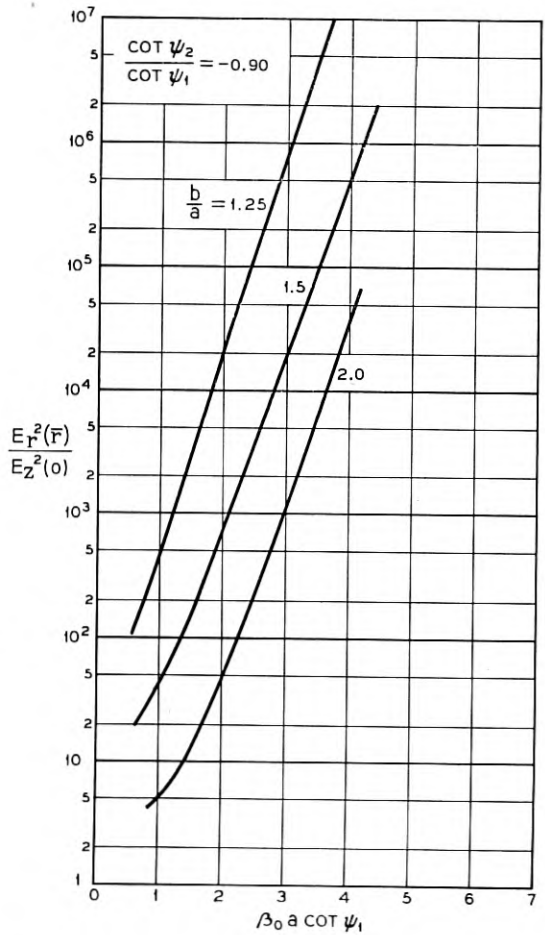

Fig. 2.10 — The relation between the impedance in terms of the transverse field between coupled helices excited in the out-of-phase mode, and the impedance in terms of the longitudinal field on the axis shown as a function of $\beta_0 a \cot \psi_1$.

helix will inevitably excite both modes equally. When it is desired to excite one mode exclusively a more difficult problem has to be solved. Therefore, in section 3.1 we shall first discuss methods of exciting one mode only before going on to discuss in sections 3.2 and 3.3 devices using one mode only.

In section 3.4 we shall discuss devices depending on the simultaneous presence of both modes.

3.1 *Excitation of Pure Modes*

3.1.1 *Direct Excitation*

In order to set up one or the other normal mode on coupled helices, voltages with specific phase and amplitudes (or corresponding currents)

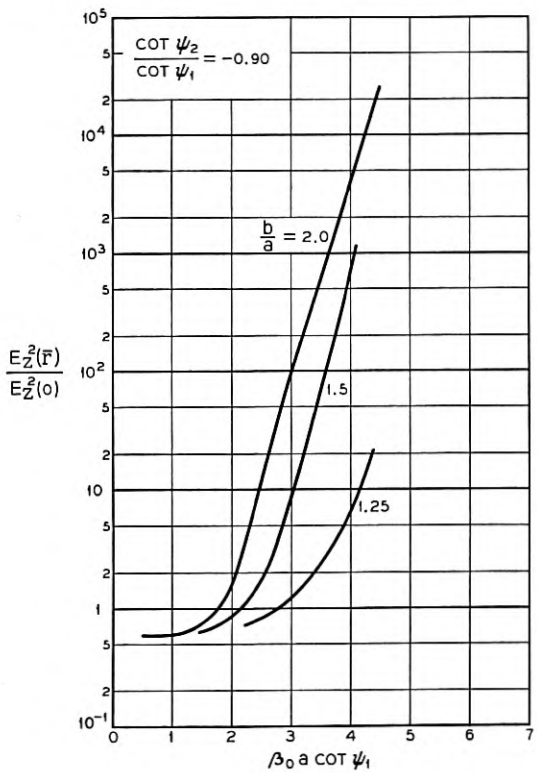

Fig. 2.11 — The relation between the impedance in terms of the longitudinal field between coupled helices excited in the in-phase mode, and the impedance in terms of the longitudinal field on the axis shown as a function of $\beta_0 a \cot \psi_1$.

have to be supplied to each helix at the input end. A natural way of doing this might be by means of a two-conductor balanced transmission line (Lecher-line), one conductor being connected to the inner helix, the other to the outer helix. Such an arrangement would cause something like the transverse (+ −) mode to be set up on the helices. If the two conductors and the balanced line can be shielded from each other starting some distance from the helices then it is, in principle, possible to introduce arbitrary amounts of extra delay into one of the conductors. A delay of one half period would then cause the longitudinal (+ +) mode to be set up in the helices. Clearly such a coupling scheme would not be broad-band since a frequency-independent delay of one half period is not realizable.

Other objections to both of these schemes are: Balanced lines are not generally used at microwave frequencies; it is difficult to bring leads through the envelope of a TWT without causing reflection of RF energy and without unduly encumbering the mechanical design of the tube plus circuits; both schemes are necessarily inexact because helices having different radii will, in general, require different voltages at either input in order to be excited in a pure mode.

Thus the practicability, and success, of any general scheme based on the existence of a pure transverse or a pure longitudinal mode on coupled helices will depend to a large extent on whether elegant coupling means are available. Such means are indeed in existence as will be shown in the next sections.

3.1.2 *Tapered Coupler*

A less direct but more elegant means of coupling an external circuit to either normal mode of a double helix arrangement is by the use of the so-called "tapered" coupler.[8, 9, 10] By appropriately tapering the relative propagation velocities of the inner and outer helices, outside the interaction region, one can excite either normal mode by coupling to one helix only.

The principle of this coupler is based on the fact that any two coupled transmission lines support two, and only two, normal modes, regardless of their relative phase velocities. These normal modes are characterized by unequal wave amplitudes on the two lines if the phase velocities are not equal. Indeed the greater the phase velocity difference and/or the smaller the coupling coefficient between the lines, the more their wave amplitudes diverge. Furthermore, the wave amplitude on the line with the slower phase velocity is greater for the out-of-phase or transverse normal mode, and the wave amplitude on the faster line is greater

for the longitudinal normal mode. As the ratio of phase constant to coupling constant approaches infinity, the ratio of the wave amplitudes on the two lines does also. Finally, if the phase velocities of, or coupling between, two coupled helices are changed gradually along their length the normal modes existing on the pair roughly maintain their identity even though they change their character. Thus, by properly tapering the phase velocities and coupling strength of any two coupled helices one can cause the two normal modes to become two separate waves, one existing on each helix.

For instance, if one desires to extract a signal propagating in the in-phase, or longitudinal, normal mode from two concentric helices of equal phase velocity, one might gradually increase the pitch of the outer helix and decrease that of the inner, and at the same time increase the diameter of the outer helix to decrease the coupling, until the longitudinal mode exists as a wave on the outer helix only. At such a point the outer helix may be connected to a coaxial line and the signal brought out.

This kind of coupler has the advantage of being frequency insensitive; and, perhaps, operable over bandwidths upwards of two octaves. It has the disadvantage of being electrically, and sometimes physically, quite long.

3.1.3 *Stepped Coupler*

There is yet a third way to excite only one normal mode on a double helix. This scheme consists of a short length at each end of the outer helix, for instance, which has a pitch slightly different from the rest. This has been called a "stepped" coupler.

The principle of the stepped coupler is this: If two coupled transmission lines have unlike phase velocities then a wave initiated in one line can never be completely transferred to the other, as has been shown in Section 2.4. The greater the velocity difference the less will be the maximum transfer. One can choose a velocity difference such that the maximum power transfer is just one half the initial power. It is a characteristic of incomplete power transfer that at the point where the maximum transfer occurs the waves on the two lines are exactly either in-phase or out-of-phase, depending on which helix was initially excited. Thus, the conditions for a normal mode on two equal-velocity helices can be produced at the maximum transfer point of two unlike velocity helices by initiating a wave on only one of them. If at that point the helix pitches are changed to give equal phase velocities in both helices, with equal current or voltage amplitude on both helices, either one or the other of the two normal modes will be propagated on the two helices from there on. Although the

pitch and length of such a stepped coupler are rather critical, the requirements are indicated in the equations in Section 2.4.

The useful bandwidth of the stepped coupler is not as great as that of the tapered variety, but may be as much as an octave. It has however the advantage of being very much shorter and simpler than the tapered coupler.

3.2 *Low-Noise Transverse-Field Amplifier*

One application of coupled helices which has been suggested from the very beginning is for a transverse field amplifier with low noise factor. In such an amplifier the RF structure is required to produce a field which is purely transverse at the position of the beam. For the transverse mode there is always such a cylindrical surface where the longitudinal field is zero and this can be obtained from the field equation of Appendix II. In Fig. 3.1 we have plotted the value of the radius $\bar{r}$ at which the longitudinal field is zero for various parameters. The significant feature of this plot is that the radius which specifies zero longitudinal field is not constant with frequency. At frequencies away from the design frequency the electron beam will be in a position where interaction with longitudinal components might become important and thus shotnoise power will be introduced into the circuit. Thus the bandwidth of the amplifier over which it has a good noise factor would tend to be limited. However, this effect can be reduced by using the smallest practicable value of b/a.

Section 2.12 indicates that the impedance of the transverse mode is very high, and thus this structure should be well suited for transverse field amplifiers.

3.3 *Dispersive Traveling-Wave Tube*

Large bandwidth is not always essential in microwave amplifiers. In particular, the enormous bandwidth over which the traveling-wave tube is potentially capable of amplifying has so far found little application, while relatively narrow bandwidths (although quite wide by previous standards) are of immediate interest. Such a relatively narrow band, if it is an inherent electronic property of the tube, makes matching the tube to the external circuits easier. It may permit, for instance, the use of non-reciprocal attenuation by means of ferrites in the ferromagnetic resonance region. It obviates filters designed to deliberately reduce the band in certain applications. Last, but not least, it offers the possibility of trading bandwidth for gain and efficiency.

A very simple method of making a traveling-wave tube narrow-band

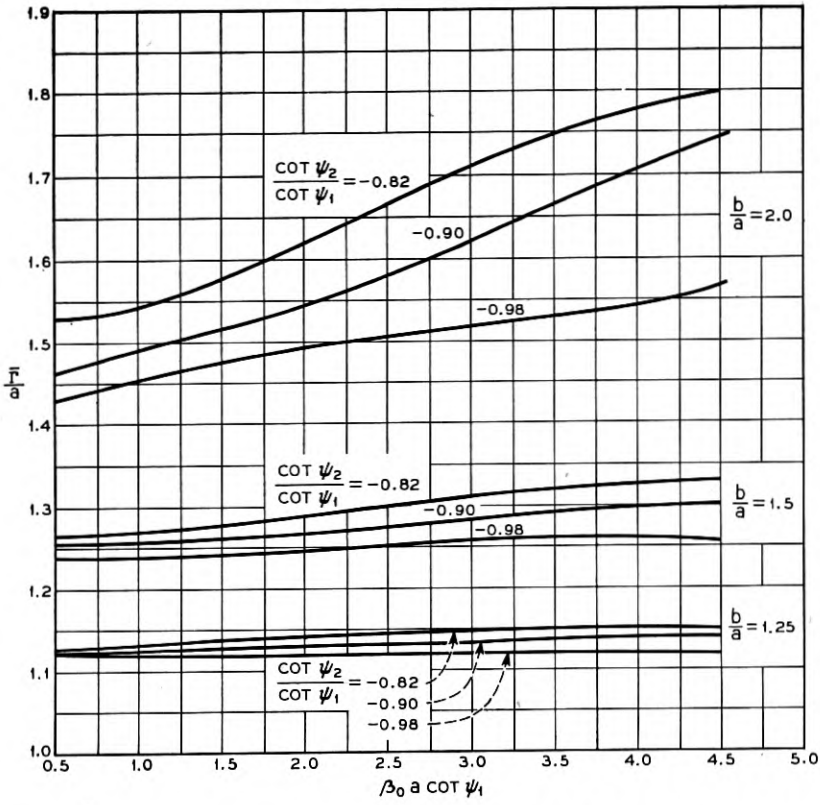

Fig. 3.1 — The radius $\bar{r}$ at which the longitudinal field is zero for transversely excited coupled coaxial helices.

is by using a dispersive circuit, (i.e. one in which the phase velocity varies significantly with frequency). Thus, we obtain an amplifier that can be *tuned* by varying the beam voltage; being dispersive we should also expect a low group velocity and therefore higher circuit impedance.

Calculations of the phase velocities of the normal modes of coupled concentric helices presented in the appendix show that the fast, longitudinal or (++) mode is highly dispersive. Given the geometry of two such coupled helices and the relevant data on an electron beam, namely current, voltage and beam radius, it is possible to arrive at an estimate of the dependence of gain on frequency.

Experiments with such a tube showed a bandwidth 3.8 times larger than the simple estimate would show. This we ascribe to the presence

of the dielectric between the helices in the actual tube, and to the neglect of power propagated in the form of spatial harmonics.

Nevertheless, the tube operated satisfactorily with distributed non-reciprocal ferrite attenuation along the whole helix and gave, at the center frequency of 4,500 mc/s more than 40 db stable gain.

The gain fell to zero at 3,950 mc/s at one end of the band and at 4,980 mc/s at the other. The forward loss was 12 db. The backward loss was of the order of 50 db at the maximum gain frequency.

3.4 *Devices Using Both Modes*

In this section we shall discuss applications of the coupled-helix principle which depend for their function on the simultaneous presence of both the transverse and the longitudinal modes. When present in substantially equal magnitude a spatial beat-phenomenon takes place, that is, RF power transfers back and forth between inner and outer helix.

Thus, there are points, periodic with distance along each helix, where there is substantially no current or voltage; at these points a helix can be terminated, cut-off, or connected to external circuits without detriment.

The main object, then, of all devices discussed in this section is power *transfer* from one helix to the other; and, as will be seen, this can be accomplished in a remarkably efficient, elegant, and broad-band manner.

3.4.1 *Coupled-Helix Transducer*

It is, by now, a well known fact that a good match can be obtained between a coaxial line and a helix of proportions such as used in TWT's. A wire helix in free space has an effective impedance of the order of 100 ohms. A conducting shield near the helix, however, tends to reduce the helix impedance, and a value of 70 or even 50 ohms is easily attained. Provided that the transition region between the coaxial line and the helix does not present too abrupt a change in geometry or impedance, relatively good transitions, operable over bandwidths of several octaves, can be made, and are used in practice to feed into and out of tubes employing helices such as TWT's and backward-wave oscillators.

One particularly awkward point remains, namely, the necessity to lead the coaxial line through the tube envelope. This is a complication in manufacture and requires careful positioning and dimensioning of the helix and other tube parts.

Coupled helices offer an opportunity to overcome this difficulty in the form of the so-called coupled-helix transducer, a sketch of which is shown in Fig. 3.2. As has been shown in Section 2.3, with helices having

the same velocity an overlap of one half of a beat wavelength will result in a 100 per cent power transfer from one helix to the other. A signal introduced into the outer helix at point A by means of the coaxial line will be all on the inner helix at point B, nothing remaining on the outer helix. At that point the outer helix can be discontinued, or cut off; since there is no power there, the seemingly violent discontinuity represented by the "open" end of the helix will cause no reflection of power. In practice, unfortunately, there are always imperfections to consider, and there will often be some power left at the end of the coupler helix. Thus, it is desirable to terminate the outer helix at this point non-reflectively, as, for instance, by a resistive element of the right value, or by connecting to it another matched coaxial line which in turn is then non-reflectively terminated.

It will be seen, therefore, that the coupled-helix transducer can, in principle, be made into an efficient device for coupling RF energy from a coaxial line to a helix contained in a dielectric envelope such as a glass tube. The inner helix will be energized predominantly in one direction, namely, the one away from the input connection. Conversely, energy traveling initially in the inner helix will be transferred to the outer, and made available as output in the respective coaxial line. Such a coupled-helix transducer can be moved along the tube, if required. As long as the outer helix completely overlaps the inner, operation as described above should be assured. By this means a new flexibility in design, operation and adjustment of traveling-wave tubes is obtained which could not be achieved by any other known form of traveling-wave tube transducer.

Naturally, the applications of the coupled-helix transducer are not restricted to TWT's only, nor to 100 per cent power transfer. To obtain

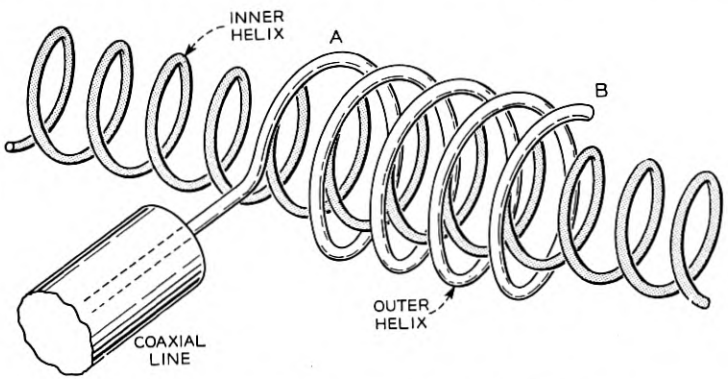

Fig. 3.2 — A simple coupled helix transducer.

power transfer of proportions other than 100 per cent two possibilities are open: either one can reduce the length of the synchronous coupling helix appropriately, or one can deliberately make the helices non-synchronous. In the latter case, a considerable measure of broad-banding can be obtained by making the length of overlap again equal to one half of a beat-wavelength, while the fraction of power transferred is determined by the difference of the helix velocities according to 2.4.7. An application of the principle of the coupled-helix transducer to a variable delay line has been described by L. Stark[12] in an unpublished memorandum.

Turning again to the complete power transfer case, we may ask: How broad is such a coupler?

In Section 2.7 we have discussed how the radial falling-off of the RF energy near a helix can be used to broad-band coupled-helix devices which depend on relative constancy of beat-wavelength as frequency is varied. On the assumption that there exists a perfect broad-band match between a coaxial line and a helix, one can calculate the performance of a coupled-helix transducer of the type shown in Fig. 3.2.

Let us define a center frequency ω, at which the outer helix is exactly one half beat-wavelength, λ_b, long. If ω is the frequency of minimum beat wavelength then at frequencies ω_1 and ω_2, larger and smaller, respectively, than ω, the outer helix will be a fraction δ shorter than $\frac{1}{2}\lambda_b$, (Section 2.7). Let a voltage amplitude, V_2, exist at the point where the outer helix is joined to the coaxial line. Then the magnitude of the voltage at the other end of the outer helix will be $| V_2 \cdot \sin(\pi\delta/2) |$ which means that the power has not been completely transferred to the inner helix. Let us assume complete reflection at this end of the outer helix. Then all but a fraction of the reflected power will be transferred to the inner helix in a *reverse* direction. Thus, we have a first estimate for the "directivity" defined as the ratio of forward to backward power (in db) introduced into the inner helix:

$$D = \left| 10 \log \sin^2\left(\frac{\pi\delta}{2}\right) \right| \tag{3.4.1.1}$$

We have assumed a perfect match between coaxial line and outer helix; thus the power reflected back into the coaxial line is proportional to $\sin^4(\pi\delta/2)$. Thus the reflectivity defined as the ratio of reflected to incident power is given in db by

$$R = 10 \log \sin^4\left(\frac{\pi\delta}{2}\right) \tag{3.4.1.2}$$

For the sake of definiteness, let us choose actual figures: let $\beta a = 2.0$. and $b/a = 1.5$. And let us, arbitrarily, demand that R always be less than -20 db.

This gives $\sin(\pi\delta/2) < 0.316$ and $\pi\delta/2 < 18.42°$ or 0.294 radians, $\delta < 0.205$. With the optimum value of $\beta_c a = 1.47$, this gives the minimum permissible value of $\beta_c a$ of $1.47/(1 + 0.205) = 1.22$. From the graph on Fig. 2.2 this corresponds to values of βa of 1.00 and 3.50. Therefore, the reflected power is down 20 db over a frequency range of $\omega_2/\omega_1 = 3.5$ to one. Over the same range, the directivity is better than 10 to one. Suppose a directivity of better than 20 db were required. This requires $\sin(\pi\delta/2) = 0.10$, $\delta = 0.0638$ and is obtained over a frequency range of approximately two to one. Over the same range, the reflected power would be down by 40 db.

In the above example the full bandwidth possibilities have not been used since the coupler has been assumed to have optimum length when $\beta_c a$ is maximum. If the coupler is made longer so that when $\beta_c a$ is maximum it is electrically short of optimum to the extent permissible by the quality requirements, then the minimum allowable $\beta_c a$ becomes even smaller. Thus, for $b/a = 1.5$ and directivity 20 db or greater the realizable bandwidth is nearly three to one.

When the coupling helix is non-reflectively terminated at both ends, either by means of two coaxial lines or a coaxial line at one end and a resistive element at the other, the directivity is, ideally, infinite, irrespective of frequency; and, similarly, there will be no reflections. The power transfer to the inner helix is simply proportional to $\cos^2(\pi\delta/2)$. Thus, under the conditions chosen for the example given above, the coupled-helix transducer can approach the ideal transducer over a considerable range of frequencies.

So far, we have inspected the performance and bandwith of the coupled-helix transducer from the most optimistic theoretical point of view. Although a more realistic approach does not change the essence of our conclusions, it does modify them. For instance, we have neglected dispersion on the helices. Dispersion tends to reduce the maximum attainable bandwidth as can be seen if Fig. 2.4.2 rather than Fig. 2.2 is used in the example cited above. The dielectric that exists in the annular region between coupled concentric helices in most practical couplers may also affect the bandwidth.

In practice, the performance of coupled-helix transducers has been short of the ideal. In the first place, the match from a coaxial line to a helix is not perfect. Secondly, a not inappreciable fraction of the RF power on a real wire helix is propagated in the form of spatial harmonic

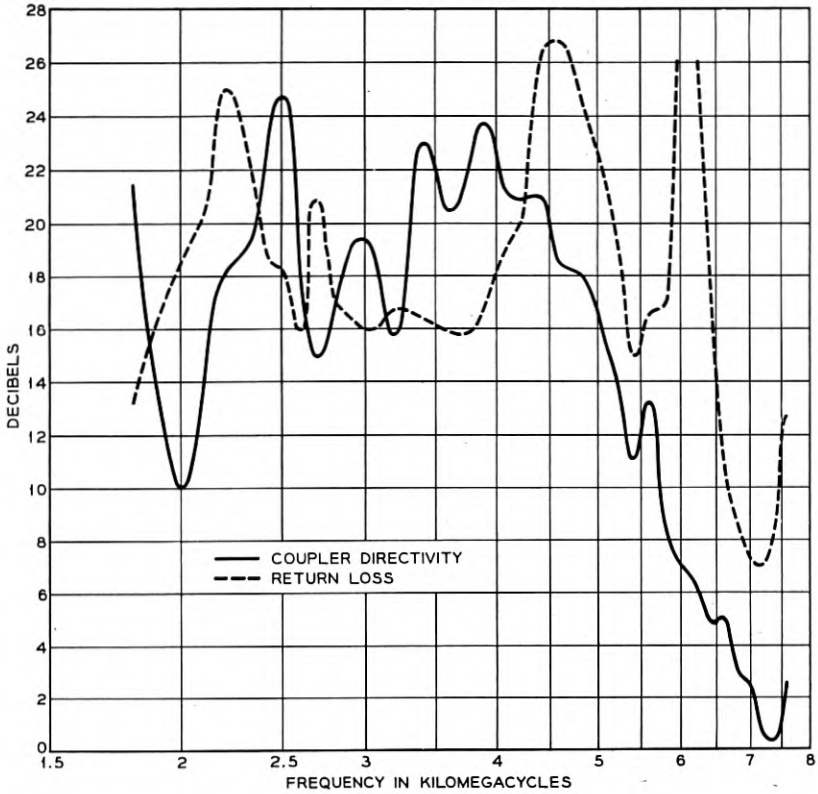

Fig. 3.3 — The return loss and directivity of an experimental 100 per cent coupled-helix transducer.

wave components which have variations with angle around the helix-axis, and coupling between such components on two helices wound in opposite directions must be small. Finally, there are the inevitable mechanical inaccuracies and misalignments.

Fig. 3.3 shows the results of measurements on a coupled-helix transducer with no termination at the far end.

3.4.2 *Coupled-Helix Attenuator*

In most TWT's the need arises for a region of heavy attenuation somewhere between input and output; this serves to isolate input and output, and prevents oscillations due to feedback along the circuit. Because of the large bandwidth over which most TWT's are inherently capable of amplifying, substantial attenuation, say at least 60 db, is

required over a bandwidth of maybe 2 octaves, or even more. Furthermore, such attenuation should present a very good match to a wave on the helix, particularly to a wave traveling backwards from the output of the tube since such a wave will be amplified by the output section of the tube.

Another requirement is that the attenuator should be physically as short as possible so as not to increase the length of the tube unnecessarily.

Finally, such attenuation might, with advantage, be made movable during the operation of the tube in order to obtain optimum performance, perhaps in respect of power output, or linearity, or some other aspect.

Coupled-helix attenuators promise to perform these functions satisfactorily.

A length of outer helix (synchronous with the inner helix) one half of a beat wavelength long, terminated at either end non-reflectively, forms a very simple, short, and elegant solution of the coupled-helix attenuator problem. A notable weakness of this form of attenuator is its relatively narrow bandwidth. Proceeding, as before, on the assumption that the attenuator is a fraction δ larger or smaller than half a beat wavelength at frequencies ω_1 and ω_2 on either side of the center frequency ω, we find that the fraction of power transferred from the inner helix to the attenuator is then given by $(1 - \sin^2 (\pi\delta/2))$. The attenuation is thus simply

$$A = \sin^2 \left(\frac{\pi\delta}{2}\right)$$

For helices of the same proportions as used before in Section 3.4.1, we find that this will give an attenuation of at least 20 db over a frequency band of two to one. At the center frequency, ω_0, the attenuation is infinite; — in theory.

Thus to get higher attenuation, it would be necessary to arrange for a sufficient number of such attenuators in tandem along the TWT. Moreover, by properly staggering their lengths within certain ranges a wider attenuation band may be achieved. The success of such a scheme largely depends on the ability to terminate the helix ends non-reflectively. Considerable work has been done in this direction, but complete success is not yet in sight.

Another basically different scheme for a coupled-helix attenuator rests on the use of distributed attenuation along the coupling helix. The difficulty with any such scheme lies in the fact that *unequal* attenuation in the two coupled helices reduces the coupling between them and the more they differ in respect to attenuation, the less the coupling. Naturally, one

would wish to have as little attenuation as practicable associated with the inner helix (inside the TWT). This requires the attenuating element to be associated with the outer helix. Miller[5] has shown that the maximum total power reduction in coupled transmission systems is obtained when

$$\left| \frac{\alpha_1 - \alpha_2}{\beta_b} \right| \approx 1$$

where α_1 and α_2 are the attenuation constants in the respective systems, and β_b the beat phase constant. If the inner helix is assumed to be lossless, the attenuation constant of the outer helix has to be effectively equal to the beat wave phase constant. It turns out that 60 db of attenuation requires about 3 beat wavelengths (in practice 10 to 20 helix wavelengths). The total length of a typical TWT is only 3 or 4 times that, and it will be seen, therefore, that this scheme may not be practical as the only means of providing loss.

Experiments carried out with outer helices of various resistivities and thicknesses by K. M. Poole (then at the Clarendon Laboratory, Oxford, England) tend to confirm this conclusion. P. D. Lacy[11] has described a coupled helix attenuator which uses a multifilar helix of resistance material together with a resistive sheath between the helices.

Experiments were performed at Bell Telephone Laboratories with a TWT using a resistive sheath (graphite on paper) placed between the outer helix and the quartz tube enclosing the inner helix. The attenuations were found to be somewhat less than estimated theoretically. The attenuator helix was movable in the axial direction and it was instructive to observe the influence of attenuator position on the power output from the tube, particularly at the highest attainable power level. As one might expect, as the power level is raised, the attenuator has to be moved nearer to the input end of the tube in order to obtain maximum gain and power output. In the limit, the attenuator helix has to be placed right close to the input end, a position which does not coincide with that for maximum low-level signal gain. Thus, the potential usefulness of the feature of mobility of coupled-helix elements has been demonstrated.

4. CONCLUSION

In this paper we have made an attempt to develop and collect together a considerable body of information, partly in the form of equations, partly in the form of graphs, which should be of some help to workers in the field of microwave tubes and devices. Because of the crudity of the assumptions, precise agreement between theory and experiment has not

been attained nor can it be expected. Nevertheless, the kind of physical phenomena occurring with coupled helices are, at least, qualitatively described here and should permit one to develop and construct various types of devices with fair chance of success.

ACKNOWLEDGEMENTS

As a final note the authors wish to express their appreciation for the patient work of Mrs. C. A. Lambert in computing the curves, and to G. E. Korb for taking the experimental data.

Appendix I

I. Solution of Field Equations

In this section there is presented the field equations for a transmission system consisting of two helices aligned with a common axis. The propagation properties and impedance of such a transmission system are discussed for various ratios of the outer helix radius to the inner helix radius. This system is capable of propagating two modes and as previously pointed out one mode is characterized by a longitudinal field midway between the two helices and the other is characterized by a transverse field midway between the two helices.

The model which is to be treated and shown in Fig. 2.3 consists of an inner helix of radius a and pitch angle ψ_1 which is coaxial with the outer helix of radius b and pitch angle ψ_2. The sheath helix model will be treated, wherein it is assumed that helices consist of infinitely thin sheaths which allow for current flow only in the direction of the pitch angle ψ.

The components of the field in the region inside the inner helix, between the two helices and outside the outer helix can be written as follows — inside the inner helix

$$H_{z_1} = B_1 I_0(\gamma r) \tag{1}$$

$$E_{z_2} = B_2 I_0(\gamma r) \tag{2}$$

$$H_{\varphi_2} = j \frac{\omega \varepsilon}{\gamma} B_2 I_1(\gamma r) \tag{3}$$

$$H_{r_1} = \frac{j\beta}{\gamma} B_1 I_1(\gamma r) \tag{4}$$

$$E_{\varphi_1} = -j \frac{\omega \mu}{\gamma} B_1 I_1(\gamma r) \tag{5}$$

$$E_{r_2} = \frac{j\beta}{\gamma} B_2 I_1(\gamma r) \tag{6}$$

and between the two helices

$$H_{z_3} = B_3 I_0(\gamma r) + B_4 K_0(\gamma r) \tag{7}$$

$$E_{z_5} = B_5 I_0(\gamma r) + B_6 K_0(\gamma r) \tag{8}$$

$$H_{\varphi_5} = \frac{j\omega\varepsilon}{\gamma} [B_5 I_1(\gamma r) - B_6 K_1(\gamma r)] \tag{9}$$

$$H_{r_3} = \frac{j\beta}{\gamma} [B_3 I_1(\gamma r) - B_4 K_1(\gamma r)] \tag{10}$$

$$E_{\varphi_3} = -j \frac{\omega\mu}{\gamma} [B_3 I_1(\gamma r) - B_4 K_1(\gamma r)] \tag{11}$$

$$E_{r_5} = \frac{j\beta}{\gamma} [B_5 I_1(\gamma r) - B_6 K_1(\gamma r)] \tag{12}$$

and outside the outer helix

$$H_{z_7} = B_7 K_0(\gamma r) \tag{13}$$

$$E_{z_8} = B_8 K_0(\gamma r) \tag{14}$$

$$H_{\varphi_8} = -j \frac{\omega\varepsilon}{\gamma} B_8 K_1(\gamma r) \tag{15}$$

$$H_{r_7} = \frac{-j\beta}{\gamma} B_7 K_1(\gamma r) \tag{16}$$

$$E_{\varphi_7} = j \frac{\omega\mu}{\gamma} B_7 K_1(\gamma r) \tag{17}$$

$$E_{r_8} = \frac{-j\beta}{\gamma} B_8 K_1(\gamma r) \tag{18}$$

With the sheath helix model of current flow only in the direction of wires we can specify the usual boundary conditions that at the inner and outer helix radius the tangential electric field must be continuous and perpendicular to the wires, whereas the tangential component of magnetic field parallel to the current flow must be continuous. These can be written as

$$E_z \sin\psi + E_\varphi \cos\psi = 0 \tag{19}$$

E_z, E_φ and $(H_z \sin\psi + H_\varphi \cos\psi)$ be equal on either side of the helix.

By applying these conditions to the two helices the following equations are obtained for the various coefficients.

First, we will define a more simple set of parameters. We will denote

$$I_0(\gamma a) \text{ by } I_{01} \qquad \text{and} \qquad I_0(\gamma b) \text{ by } I_{02}\text{, etc.}$$

Further let us use the notation introduced by Humphrey, Kite and James[11] in his treatment of coaxial helices.

$$\begin{aligned} P_{01} &\equiv I_{01}K_{01} \qquad P_{02} \equiv I_{02}K_{02} \qquad R_0 \equiv I_{01}K_{02} \\ P_{11} &\equiv I_{11}K_{11} \qquad P_{12} \equiv I_{12}K_{12} \qquad R_1 \equiv I_{11}K_{12} \end{aligned} \tag{20}$$

and define a common factor (C.F.) by the equation

$$\text{C.F.} = -\left[\frac{(\beta_0 a \cot \psi_2)^2}{(\gamma a)^2} P_{01}P_{02} - \frac{(\beta_0 a \cot \psi_1)^2}{(\gamma a)^2} \frac{\cot \psi_2}{\cot \psi_1} R_1R_0 + R_0^2 - P_{01}P_{01}\right] \tag{21}$$

With all of this we can now write for the coefficients of equations 1 through 18:

$$\frac{B_1}{B_2} = -j \sqrt{\frac{\varepsilon}{\mu}} \frac{\gamma a}{\beta_0 a \cot \psi_1} \frac{I_{01}}{I_{02}} \tag{22}$$

$$\frac{B_3}{B_2} = -j \sqrt{\frac{\varepsilon}{\mu}} \frac{\beta_0 a \cot \psi_1}{\gamma a} \frac{I_{01}K_{12}}{\text{C.F.}} \left[\frac{(\beta_0 a \cot \psi_1)^2}{(\gamma a)^2} R_1 - \frac{\cot \psi_2}{\cot \psi_1} R_0\right] \tag{23}$$

$$\frac{B_4}{B_2} = -j \sqrt{\frac{\varepsilon}{\mu}} \frac{\beta_0 a \cot \psi_1}{\gamma a} \frac{I_{01}I_{11}}{\text{C.F.}} \left[\frac{(\beta_0 a \cot \psi_2)^2}{(\gamma a)^2} P_{12} - P_{02}\right] \tag{24}$$

$$\frac{B_5}{B_2} = -\frac{R_0}{\text{C.F.}} \left[R_0 - \frac{(\beta_0 a \cot \psi_1)^2}{(\gamma a^2)} \frac{\cot \psi_2}{\cot \psi_1} R_1\right] \tag{25}$$

$$\frac{B_6}{B_2} = -\frac{I_{01}^2}{\text{C.F.}} \left[\frac{(\beta_0 a \cot \psi_2)^2}{(\gamma a)^2} P_{12} - P_{02}\right] \tag{26}$$

$$\frac{B_7}{B_2} = j \sqrt{\frac{\varepsilon}{\mu}} \frac{\beta_0 a \cot \psi_1}{\gamma a} \frac{1}{\text{C.F.}} \frac{I_{01}}{K_{12}} \left[P_{02}R_1 - \frac{\cot \psi_2}{\cot \psi_1} P_{12}R_0\right] \tag{27}$$

$$\frac{B_8}{B_2} = \frac{(\beta_0 a \cot \psi_1)^2}{(\gamma a)^2} \frac{\cot \psi_2}{\cot \psi_1} \frac{I_{01}^2}{\text{C.F.}R_0} \left[P_{02}R_1 - \frac{\cot \psi_2}{\cot \psi_1} P_{12}R_0\right] \tag{28}$$

The last equation necessary for the solution of our field problem is the transcendental equation for the propagation constant, γ, which can be

written

$$\left[R_0 - \frac{(\beta_0 a \cot \psi_1)^2}{(\gamma a)^2} \frac{\cot \psi_2}{\cot \psi_1} R_1\right]^2 = \left[P_{02} - \frac{(\beta_0 a \cot \psi_2)^2}{(\gamma a)^2} P_{12}\right]\left[P_{01} - \frac{(\beta_0 a \cot \psi_1)^2}{(\gamma a)^2} P_{11}\right] \tag{29}$$

The solutions of this equation are plotted in Fig. 4.1.

There it is seen that there are two values of γ, one, γ_t, denoting the slow mode with transverse fields between helices and the other, γ_ℓ, denoting the fast mode with longitudinal fields midway between the two helices.

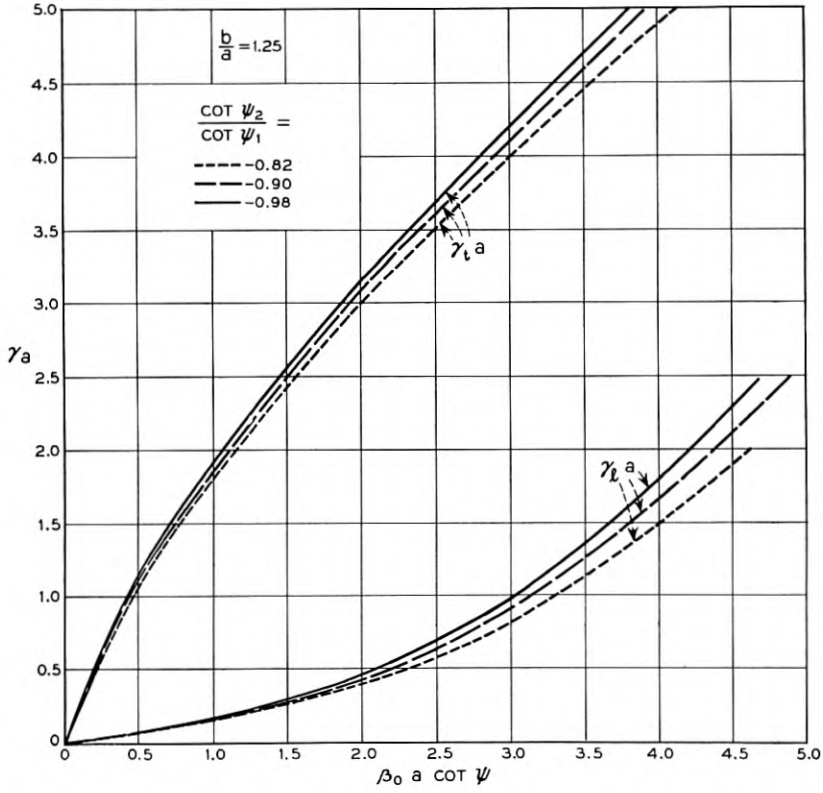

Fig. 4.1.1 — The radial propagation constants associated with the transverse and longitudinal modes on coupled coaxial sheath helices given as a function of $\beta_0 a \cot \psi_1$ for several values of $b/a = 1.25$.

These equations can now be used to compute the power flow as defined by

$$P = \tfrac{1}{2}\, Re \int E \times H^* \, dA \tag{30}$$

which can be written in the form

$$\left[\frac{E_z^{\,2}(0)}{\beta^2 P}\right]^{\frac{1}{3}} = \frac{\beta}{\beta_0}\left(\frac{\gamma}{\beta}\right)^4 F(\gamma a, \gamma b) \tag{31}$$

where

$$\begin{aligned}
[F(\gamma a, \gamma b)]^{-3} = \frac{(\gamma a)^2}{240}\frac{I_{01}^{\,2}}{(\text{C.F.})^2}\Bigg\{ & \frac{\left(I_{01}^{\,2} + \dfrac{(\beta_0 a \cot \psi_1)^2}{(\gamma a)^2} I_{11}^{\,2}\right)}{I_{01}^{\,2} I_{11}^{\,2}\left(\dfrac{\beta_0 a \cot \psi_1}{\gamma a}\right)^2} \frac{(I_{11}^{\,2} - I_{01}I_{21})(\text{C.F.})^2}{} \\
& - \left(K_{02}^{\,2} + \frac{(\beta_0 a \cot \psi_1)^2}{(\gamma a)^2} K_{12}^{\,2}\right)\left(R_0 - \frac{(\beta_0 a \cot \psi_1)^2}{(\gamma a)^2}\frac{\cot \psi_2}{\cot \psi_1} R_1\right)^2 \\
& \left[\left(\frac{b}{a}\right)^2 (I_{02}I_{22} - I_{12}^{\,2}) + (I_{11}^{\,2} - I_{01}I_{21})\right] \\
& + \left(R_0 - \frac{(\beta_0 a \cot \psi_1)^2}{(\gamma a)^2}\frac{\cot \psi_2}{\cot \psi_1} R_1\right)^2 \left(P_{02} - \frac{(\beta_0 a \cot \psi_2)^2}{(\gamma a)^2} P_{12}\right) \\
& \left[\left(\frac{b}{a}\right)^2 (2I_{12}K_{12} + I_{02}K_{22} + I_{22}K_{02}) - (2I_{11}K_{11} + I_{01}K_{21} + I_{21}K_{01})\right] \\
& - \left[I_{01}^{\,2} + \frac{(\beta_0 a \cot \psi_1)^2}{(\gamma a)^2} I_{11}^{\,2}\right]\left[P_{02} - \frac{(\beta_0 a \cot \psi_2)^2}{(\gamma a)^2} P_{12}\right]^2 \\
& \left[\left(\frac{b}{a}\right)^2 (K_{02}K_{22} - K_{12}^{\,2}) - (K_{01}K_{21} - K_{11}^{\,2})\right] \\
& + \frac{(\beta_0 a \cot \psi_1)^2}{(\gamma a)^2 K_{12}^{\,2} R_0^{\,2}}\left(\frac{b}{a}\right)^2 \left[R_0^{\,2} + \frac{(\beta_0 a \cot \psi_2)^2}{(\gamma a)^2} I_{01}^{\,2} K_{12}^{\,2}\right] \\
& \left[P_{02}R_1 - \frac{\cot \psi_2}{\cot \psi_1} P_{12}R_0\right]^2 [K_{02}K_{22} - K_{12}^{\,2}]\Bigg\}
\end{aligned} \tag{32}$$

In (32) we find the power in the transverse mode by using values of

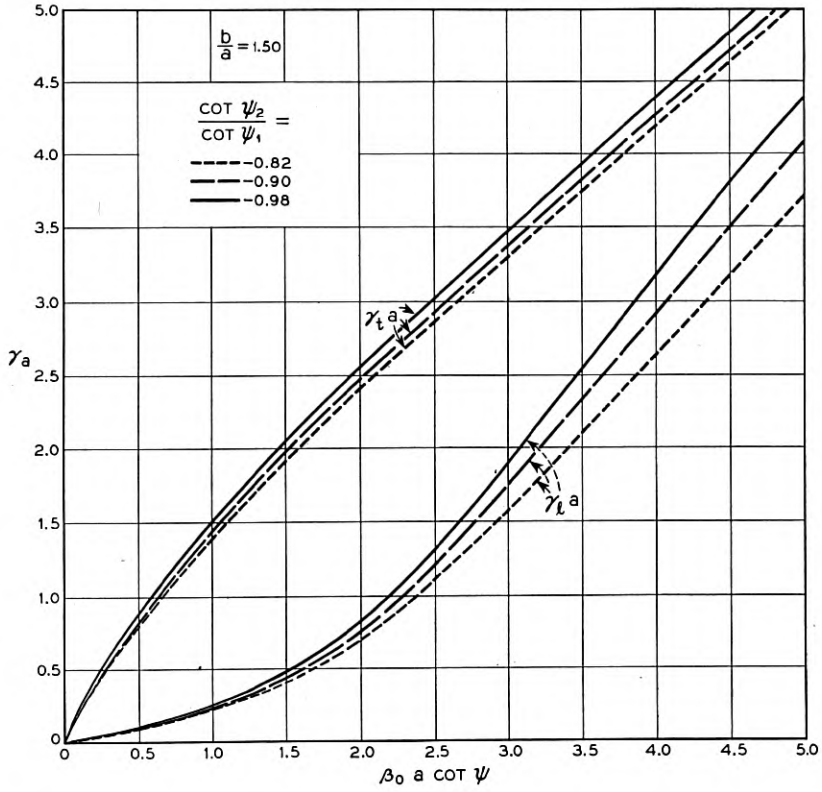

Fig. 4.1.2 — The radial propagation constants associated with the transverse and longitudinal modes on coupled coaxial sheath helices given as a function of $\beta_0 a \cot \psi_1$ when $b/a = 1.50$.

γ_t obtained from (29) and similarly the power in the longitudinal mode is found by using values of γ_t.

II. FINDING $\bar{r}$

When coaxial helices are used in a transverse field amplifier, only the transverse field mode is of interest and it is important that the helix parameters be adjusted such that there is no longitudinal field at some radius, $\bar{r}$, where the cylindrical electron beam will be located. This condition can be expressed by equating E_z to zero at $r = \bar{r}$ and from (8)

$$B_5 I_0(\gamma \bar{r}) + B_6 K_0(\gamma \bar{r}) = 0 \tag{33}$$

which can be written with (25) and (26) as

$$K_{02}\left[R_0 - \frac{(\beta_0 a \cot \psi_1)^2}{(\gamma a)^2}\frac{\cot \psi_2}{\cot \psi_1} R_1\right] I_0(\gamma \bar{r}) = I_{01}\left[P_{02} - \frac{(\beta_0 a \cot \psi_2)^2}{(\gamma a)^2} P_{12}\right] K_0(\gamma \bar{r}) \tag{34}$$

This equation together with (29) enables one to evaluate $\bar{r}/a$ versus $\beta_0 a \cot \psi_1$ for various ratios of b/a and $\cot \psi_2/\cot \psi_1$. The results of these calculations are shown in Fig. 3.1.

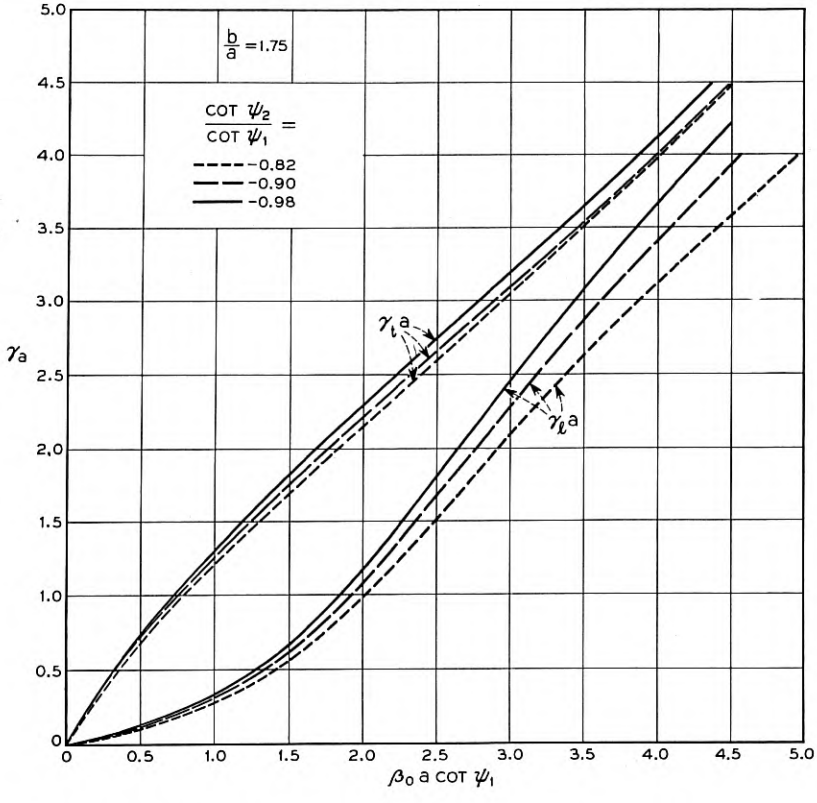

Fig. 4.1.3 — The radial propagation constants associated with the transverse and longitudinal modes on coupled coaxial sheath helices given as a function of $\beta_0 a \cot \psi_1$ when $b/a = 1.75$.

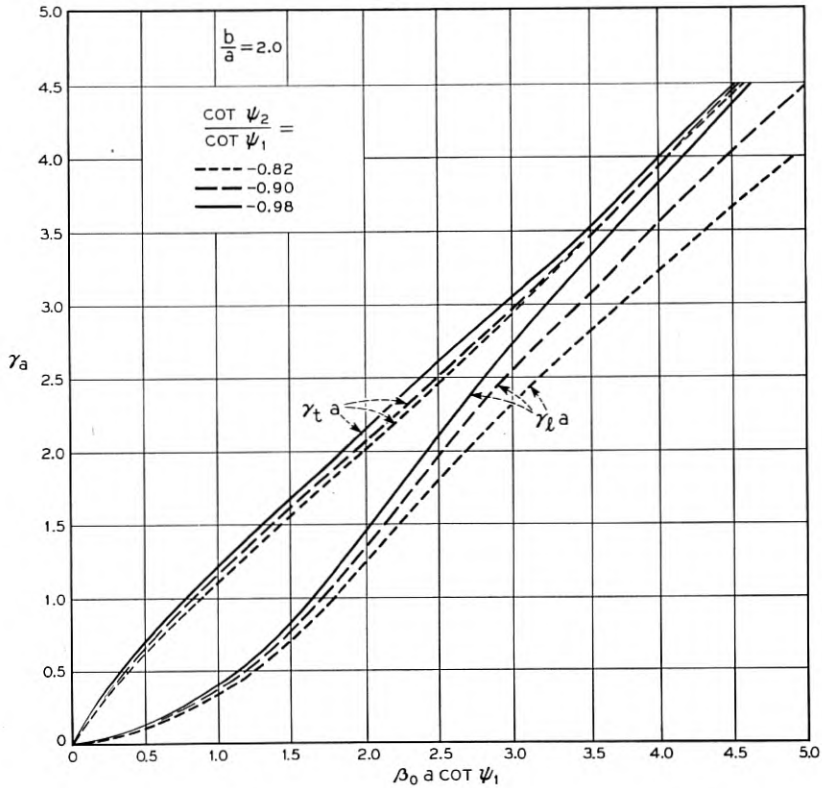

Fig. 4.1.4 — The radial propagation constants associated with the transverse and longitudinal modes on coupled coaxial sheath helices given as a function of $\beta_0 a \cot \psi_1$ when $b/a = 2.0$.

III. COMPLETE POWER TRANSFER

For coupled helix applications we require the coupled helix parameters to be adjusted so that RF power fed into one helix alone will set up the transverse and longitudinal modes equal in amplitude. For this condition the power from the outer helix will transfer completely to the inner helix. The total current density can be written as the sum of the current in the longitudinal mode and the transverse mode. Thus for the inner helix we have

$$J_a = J_{at} e^{-j\beta_t z} + J_{at} e^{-j\beta_t z} \tag{35}$$

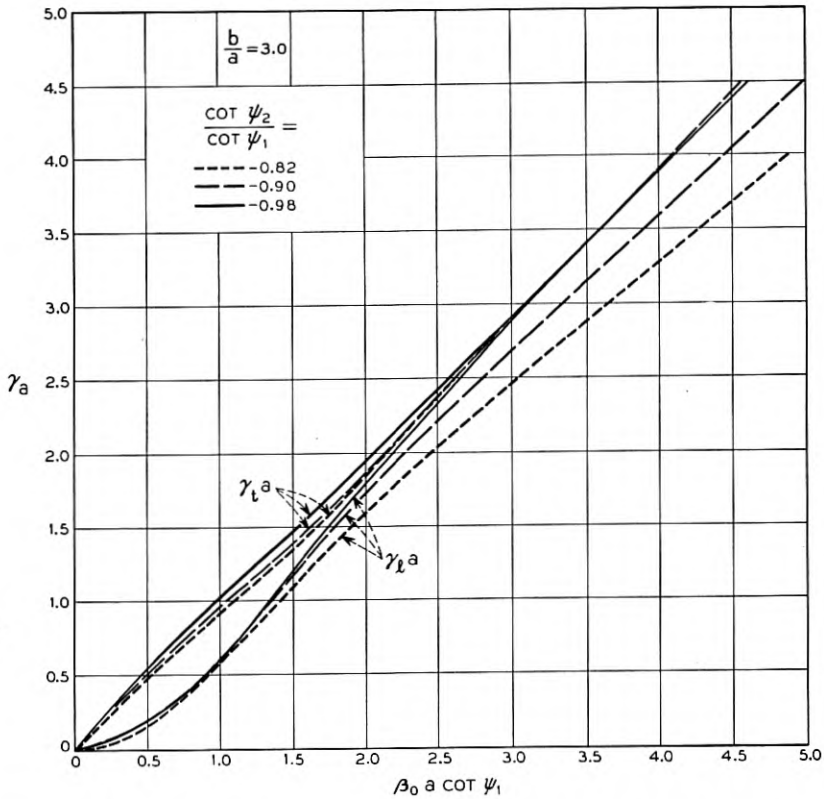

Fig. 4.1.5 — The radial propagation constants associated with the transverse and longitudinal modes on coupled coaxial sheath helices given as a function of $\beta_0 a \cot \psi_1$ when $b/a = 3.0$.

and for the outer helix

$$J_b = J_{bt}e^{-j\beta_t z} + J_{bt}e^{-j\beta_t z} \tag{36}$$

For complete power transfer we ask that

$$J_{bt} = J_{bt}$$

when J_a is zero at the input ($z = 0$)

$$J_{at} = -J_{at}$$

or

$$\frac{J_{bt}}{J_{at}} = -\frac{J_{bt}}{J_{at}} \tag{37}$$

Now J_{at} is equal to the discontinuity in the tangential component of magnetic field which can be written at $r = a$

$$J_{at} = (H_{z3} \cos \psi_1 - H_{\varphi 5} \sin \psi_1) - (H_{z1} \cos \psi_1 - H_{\varphi 2} \sin \psi_1)$$

which can be written as

$$J_{at} = -(H_{z1} - H_{z3})_{at}(\cot \psi_1 + \tan \psi_1) \sin \psi_1 \tag{38}$$

and similarily at $r = b$

$$J_{bt} = -(H_{z7} - H_{z3})_{bt}(\cot \psi_2 + \tan \psi_2) \sin \psi_2 \tag{39}$$

Equations (38) and (39) can be combined with (37) to give as the condition for complete power transfer

$$A_t = -A_t \tag{40}$$

where

$$A = \frac{(I_{12}K_{02} + I_{02}K_{12})\left(P_{01} - \dfrac{(\beta_0 a \cot \psi_1)^2}{(\gamma a)^2} P_{11}\right)}{(I_{01}K_{11} + I_{11}K_{01})\left(R_0 - \dfrac{(\beta_0 a \cot \psi_1)^2}{(\gamma a)^2} \dfrac{\cot \psi_2}{\cot \psi_1} R_1\right)} \tag{41}$$

In (40) A_t is obtained by substituting γ_t into (41) and A_t is obtained by substituting γ_t into (41).

The value of $\cot \psi_2 / \cot \psi_1$ necessary to satisfy (40) is plotted in Fig. 2.8.

In addition to $\cot \psi_2 / \cot \psi_1$ it is necessary to determine the interference wavelength on the helices and this can be readily evaluated by considering (36) which can now be written

$$J_b = J_{bt}(e^{-j\beta_t z} + e^{-j\beta_t z})$$

or

$$J_b = J_{bt} e^{-j((\beta_t + \beta_t)z/2)} \cos \frac{(\beta_t - \beta_t)}{2} z \tag{48}$$

and

$$J_b = J_{bt} e^{-j((\beta_t + \beta_t)z/2)} \cos \tfrac{1}{2}\beta_b z \tag{49}$$

where we have defined

$$\beta_b a = (\gamma_t a - \gamma_t a) \tag{50}$$

This value of β_b is plotted versus $\beta_0 a \cot \psi_1$ in Fig. 2.4.

BIBLIOGRAPHY

1. J. R. Pierce, Traveling Wave Tubes, p. 44, Van Nostrand, 1950.
2. R. Kompfner, Experiments on Coupled Helices, A. E. R. E. Report No. G/M98, Sept., 1951.
3. R. Kompfner, Coupled Helices, paper presented at I. R. E. Electron Tube Conference, 1953, Stanford, Cal.
4. G. Wade and N. Rynn, Coupled Helices for Use in Traveling-Wave Tubes, I.R.E. Trans. on Electron Devices, Vol. ED-2, p. 15, July, 1955.
5. S. E. Miller, Coupled Wave Theory and Waveguide Applications, B.S.T.J., **33,** pp. 677–693, 1954.
6. M. Chodorow and E. L. Chu, The Propagation Properties of Cross-Wound Twin Helices Suitable for Traveling-Wave Tubes, paper presented at the Electron Tube Res. Conf., Stanford Univ., June, 1953.
7. G. M. Branch, A New Slow Wave Structure for Traveling-Wave Tubes, paper presented at the Electron Tube Res. Conf., Stanford Univ., June, 1953.
   G. M. Branch, Experimental Observation of the Properties of Double Helix Traveling-Wave Tubes, paper presented at the Electron Tube Res. Conf., Univ. of Maine, June, 1954.
8. J. S. Cook, Tapered Velocity Couplers, B.S.T.J. **34,** p. 807, 1955.
9. A. G. Fox, Wave Coupling by Warped Normal Modes, B.S.T.J., **34,** p. 823, 1955.
10. W. H. Louisell, Analysis of the Single Tapered Mode Coupler, B.S.T.J., **34,** p. 853.
11. B. L. Humphreys, L. V. Kite, E. G. James, The Phase Velocity of Waves in a Double Helix, Report No. 9507, Research Lab. of G.E.C., England, Sept., 1948.
12. L. Stark, A Helical-Line Phase Shifter for Ultra-High Frequencies, Technical Report No. 59, Lincoln Laboratory, M.I.T., Feb., 1954.
13. P. D. Lacy, Helix Coupled Traveling-Wave Tube, Electronics, **27,** No. 11, Nov., 1954.

Statistical Techniques for Reducing the Experiment Time in Reliability Studies

By MILTON SOBEL

(Manuscript received September 19, 1955)

Given two or more processes, the units from which fail in accordance with an exponential or delayed exponential law, the problem is to select the particular process with the smallest failure rate. It is assumed that there is a common guarantee period of zero or positive duration during which no failures occur. This guarantee period may be known or unknown. It is desired to accomplish the above goal in as short a time as possible without invalidating certain predetermined probability specifications. Three statistical techniques are considered for reducing the average experiment time needed to reach a decision.

1. One technique is to increase the initial number of units put on test. This technique will substantially shorten the average experiment time. Its effect on the probability of a correct selection is generally negligible and in some cases there is no effect.

2. Another technique is to replace each failure immediately by a new unit from the same process. This replacement technique adds to the bookkeeping of the test, but if any of the population variances is large (say in comparison with the guarantee period) then this technique will result in a substantial saving in the average experiment time.

3. A third technique is to use an appropriate sequential procedure. In many problems the sequential procedure results in a smaller average experiment time than the best non-sequential procedure regardless of the true failure rates. The amount of saving depends principally on the "distance" between the smallest and second smallest failure rates.

For the special case of two processes, tables are given to show the probability of a correct selection and the average experiment time for each of three types of procedures.

Numerical estimates of the relative efficiency of the procedures are given by computing the ratio of the average experiment time for two procedures of different type with the same initial sample size and satisfying the same probability specification.

INTRODUCTION

This paper is concerned with a study of the advantages and disadvantages of three statistical techniques for reducing the average duration of life tests. These techniques are:

1. Increasing the initial number of units on test.
2. Using a replacement technique.
3. Using a sequential procedure.

To show the advantages of each of these techniques, we shall consider the problem of deciding which of two processes has the smaller failure rate. Three different types of procedures for making this decision will be considered. They are:

R_1, A nonsequential, nonreplacement type of procedure
R_2, A nonsequential, replacement type of procedure
R_3, A sequential, replacement type of procedure

Within each type we will consider different values of n, the initial number of units on test for each process. The effect of replacement is shown by comparing the average experiment time for procedures of type 1 and 2 with the same value of n and comparable probabilities of a correct selection. The effect of using a sequential rule is shown by comparing the average experiment time for procedures of type 2 and 3 with the same value of n and comparable probabilities of a correct selection.

ASSUMPTIONS

1. It is assumed that failure is clearly defined and that failures are recognized without any chance of error.

2. The lifetime of individual units from either population is assumed to follow an exponential density of the form

$$\begin{aligned} f(x;\theta,g) &= \frac{1}{\theta}\, e^{-(x-g)/\theta} && \text{for } x \geqq g \\ f(x;\theta,g) &= 0 && \text{for } x < g \end{aligned} \tag{1}$$

where the location parameter $g \geqq 0$ represents the common guarantee period and the scale parameter $\theta > 0$ represents the *unknown* parameter which distinguishes the two different processes. Let $\theta_1 \geqq \theta_2$ denote the *ordered* values of the unknown parameter θ for the two processes; then the *ordered* failure rates are given by

$$\lambda_1 = 1/(\theta_1 + g) \leqq \lambda_2 = 1/(\theta_2 + g) \tag{2}$$

3. It is not known which process has the parameter θ_1 and which has the parameter θ_2.

4. The parameter g is assumed to be the same for both processes. It may be known or unknown.

5. The initial number n of units put on test is the same for both processes.

6. All units have independent lifetimes, i.e., the test environment is not such that the failure of one unit results in the failure of other units on test.

7. Replacements used in the test are assumed to come from the same population as the units they replace. If the replacement units have to sit on a shelf before being used then it is assumed that the replacements are not affected by shelf-aging.

CONCLUSIONS

1. Increasing the initial sample size n has at most a negligible effect on the probability of a correct selection. It has a substantial effect on the average experiment time for all three types of procedures. If the value of n is doubled, then the average time is reduced to a value less than or equal to half of its original value.

2. The technique of replacement always reduces the average experiment time. This reduction is substantial when $g = 0$ or when the population variance of either process is large compared to the value of g. This decrease in average experiment time must always be weighed against the disadvantage of an increase in bookkeeping and the necessity of having the replacement units available for use.

3. The sequential procedure enables the experimenter to make rational decisions as the evidence builds up without waiting for a predetermined number of failures. It has a shorter average experiment time than non-sequential procedures satisfying the same specification. This reduction brought about by the sequential procedure increases as the ratio α of the two failure rates increases. In addition the sequential procedure always terminates with a decision that is clearly convincing on the basis of the observed results, i.e., the à posteriori probability of a correct selection is always large at the termination of the experiment.

SPECIFICATION OF THE TEST

Each of the three types of procedures is set up so as to satisfy the same specification described below. Let α denote the true value of the ratio θ_1/θ_2 which by definition must be greater than, or equal to, one. It turns out that in each type of procedure the probability of a correct selection depends on θ_1 and θ_2 only through their ratio α.

1. The experimenter is asked to specify the smallest value of α (say it is $\alpha^* > 1$) that is worth detecting. Then the interval $(1, \alpha^*)$ represents a zone of indifference such that if the true ratio α lies therein then we would still like to make a correct selection, but the loss due to a wrong selection in this case is negligible.

2. The experimenter is also asked to specify the minimum value $P^* > \frac{1}{2}$ that he desires for the probability of a correct selection whenever $\alpha \geqq \alpha^*$. In each type of procedure the rules are set up so that the probability of a correct selection for $\alpha = \alpha^*$ is as close to P^* as possible without being less than P^*.

The two constants $\alpha^* > 1$ and $\frac{1}{2} < P^* < 1$ are the only quantities specified by the experimenter. Together they make up the *specification* of the test procedure.

EFFICIENCY

If two procedures of different type have the same value of n and satisfy the same specification then we shall regard them as comparable and their relative efficiency will be measured by the ratio of their average experiment times. This ratio is a function of the true α but we shall consider it only for selected values of α, namely, $\alpha = 1$, $\alpha = \alpha^*$ and $\alpha = \infty$.

PROCEDURES OF TYPE R_1 — NONSEQUENTIAL, NONREPLACEMENT

"The same number n of units are put on test for each of the two processes. Experimentation is continued until either one of the two samples produces a predetermined number r ($r \leqq n$) of failures. Experimentation is then stopped and the process with fewer than r failures is chosen to be the better one."

TABLE I — PROBABILITY OF A CORRECT SELECTION — PROCEDURE TYPE R_1

($\alpha = 2$, any $g \geqq 0$, to be used to obtain r for $\alpha^* = 2$)

n	$r = 1$	$r = 2$	$r = 3$	$r = 4$
1	0.667	—	—	—
2	0.667	0.733	—	—
3	0.667	0.738	0.774	—
4	0.667	0.739	0.784	0.802
10	0.667	0.741	0.789	0.825
20	0.667	0.741	0.790	0.826
∞	0.667	0.741	0.790	0.827

Note: The value for $r = 0$ is obviously 0.500 for any n.

We shall assume that the number n of units put on test is determined by non-statistical considerations such as the availability of units, the availability of sockets, etc. Then the only unspecified number in the above procedure is the integer r. This can be determined from a table of probabilities of a correct selection to satisfy any given specification (α^*, P^*). If, for example, $\alpha^* = 2$ then we can enter Table I. If n is given to be 4 and we wish to meet the specification $\alpha^* = 2$, $P^* = 0.800$ then we would enter Table I with $n = 4$ and select $r = 4$, it being the smallest value for which $P \geqq P^*$.

The table above shows that for the given specification we would also have selected $r = 4$ for any value of n. In fact, we note that the probability of a correct selection depends only slightly on n. The given value of n and the selected value of r then determine a particular procedure of type R_1, say, $R_1(n, r)$.

The average experiment time for each of several procedures $R_1(n, r)$ is given in Table II for the three critical values of the true ratio α, namely, $\alpha = 1$, $\alpha = \alpha^*$ and $\alpha = \infty$. Each of the entries has to be multiplied by θ_2, the smaller of the two θ values, and added to the common guarantee period g. For $n = \infty$ the entry should be zero $(+g)$ but it was found convenient to put in place of zero the leading term in the asymptotic expansion of the expectation in powers of $1/n$. Hence the entry for $n = \infty$ can be used for any large n, say, $n \geqq 25$ when $r \leqq 4$.

We note in Table II the undesirable feature that for each procedure the average experiment time increases with α for fixed θ_2. For the sequential procedure we shall see later that the average experiment time is greater at $\alpha = \alpha^*$ than at either $\alpha = 1$ or $\alpha = \infty$. This is intuitively more desirable since it means that the procedure spends more time when the choice is more difficult to make and less time when we are indifferent or when the choice is easy to make.

PROCEDURES OF TYPE R_2 — NONSEQUENTIAL, REPLACEMENT

"Such procedures are carried out exactly as for procedures of R_1 except that failures are immediately replaced by new units from the same population."

To determine the appropriate value of r for the specification $\alpha^* = 2$, $P^* = 0.800$ when $g = 0$ we use the last row of Table I, i.e., the row marked $n = \infty$, and select $r = 4$. The probability of a correct selection for procedures of type R_2 is exactly the same for all values of n and depends only on r. Furthermore, it agrees with the probability for procedures of type R_1 with $n = \infty$ so that it is not necessary to prepare a separate table.

TABLE II — AVERAGE EXPERIMENT TIME — PROCEDURE TYPE R_1

(Multiply entry by θ_2 and add g)

n	$r = 1$			$r = 2$			$r = 3$			$r = 4$		
	$\alpha = 1$	$\alpha = 2$	$\alpha = \infty$	$\alpha = 1$	$\alpha = 2$	$\alpha = \infty$	$\alpha = 1$	$\alpha = 2$	$\alpha = \infty$	$\alpha = 1$	$\alpha = 2$	$\alpha = \infty$
1	0.500	0.667	1.000	—	—	—	—	—	—	—	—	—
2	0.250	0.333	0.500	0.917	1.200	1.500	—	—	—	—	—	—
3	0.167	0.222	0.333	0.517	0.675	0.833	1.217	1.572	1.833	—	—	—
4	0.125	0.167	0.250	0.363	0.474	0.583	0.735	0.944	1.083	1.449	1.854	2.083
10	0.050	0.067	0.100	0.132	0.172	0.211	0.231	0.297	0.336	0.347	0.439	0.479
20	0.025	0.033	0.050	0.064	0.084	0.103	0.109	0.139	0.158	0.157	0.200	0.217
∞	$0.500/n$	$0.667/n$	$1.000/n$	$1.250/n$	$1.630/n$	$2.000/n$	$2.063/n$	$2.642/n$	$3.000/n$	$2.906/n$	$3.669/n$	$4.000/n$

TABLE III — VALUE OF r REQUIRED TO MEET THE SPECIFICATION (α^*, P^*) FOR PROCEDURES OF TYPE R_2 ($g = 0$)

P^*	α^*												
	1.05	1.10	1.15	1.20	1.25	1.30	1.35	1.40	1.45	1.50	2.00	2.50	3.00
0.50	0	0	0	0	0	0	0	0	0	0	0	0	0
0.55	14	4	2	2	1	1	1	1	1	1	1	1	1
0.60	55	15	7	5	3	3	2	2	2	1	1	1	1
0.65	126	33	16	10	7	5	4	3	3	3	1	1	1
0.70	232	61	29	17	12	9	7	6	5	4	2	1	1
0.75	383	101	47	28	19	14	11	9	7	6	3	2	1
0.80	596	157	73	43	29	21	17	13	11	9	4	2	2
0.85	903	238	111	65	44	32	25	20	16	14	5	3	3
0.90	1381	363	169	100	67	49	37	30	25	21	8	5	4
0.95	2274	597	278	164	110	80	61	49	40	34	12	7	5
0.99	4549	1193	556	327	219	160	122	98	80	68	24	14	10

It is also unnecessary to prepare a separate table for the average experiment time for procedures of type R_2 since for $g = 0$ the exact values can be obtained by substituting the appropriate value of n in the expressions appearing in Table II in the row marked $n = \infty$. For example, for $n = 2$, $r = 1$ and $\alpha = 1$ the exact value for $g = 0$ is $0.500\ \theta_2/2 = 0.250\ \theta_2$, and for $n = 3$, $r = 4$, $\alpha = \infty$ the exact value for $g = 0$ is $4.000\ \theta_2/3 = 1.333\ \theta_2$. It should be noted that for procedures of type R_2 we need not restrict our attention to the cases $r \leqq n$ but can also consider $r > n$.

Table III shows the value of r required to meet the specification (α^*, P^*) with a procedure of type R_2 for various selected values of α^* and P^*.

PROCEDURES OF TYPE R_3 — SEQUENTIAL, REPLACEMENT

Let $D(t)$ denote the absolute difference between the number of failures produced by the two processes at any time t. The sequential procedure is as follows:

"Stop the test as soon as the inequality

$$D(t) \geqq \frac{ln\ [P^*/(1 - P^*)]}{ln\ \alpha^*} \tag{3}$$

is satisfied. Then select the population with the smaller number of failures as the better one."

To get the best results we will choose (α^*, P^*) so that the right hand member of the inequality (3) is an integer. Otherwise we would be operating with a higher value of P^* (or a smaller value of α^*) than was specified.

TABLE IV — AVERAGE EXPERIMENT TIME AND PROBABILITY OF A CORRECT SELECTION — PROCEDURE TYPE R_3

($\alpha^* = 2$, $P^* = 0.800$, $g = 0$)

(Multiply each average time entry by θ_2)

n	$\alpha = 1$	$\alpha = 2$	$\alpha = \infty$
1	2.000	2.400	2.000
2	1.000	1.200	1.000
3	0.667	0.800	0.667
4	0.500	0.600	0.500
10	0.200	0.240	0.200
20	0.100	0.120	0.100
∞	$2.000/n$	$2.400/n$	$2.000/n$
Probability.....	0.500	0.800	1.000

For example, we might choose $\alpha^* = 2$ and $P^* = 0.800$. For procedures of type R_3 the probability of a correct selection is again completely independent of n; here it depends only on the true value of the ratio α. The average experiment time depends strongly on n and only to a limited extent on the true value of the ratio α. Table IV gives these quantities for $\alpha = 1$, $\alpha = 2$, and $\alpha = \infty$ for the particular specification $\alpha^* = 2$, $P^* = 0.800$ and for the particular value $g = 0$.

EFFICIENCY

We are now in a position to compare the efficiency of two different types of procedures using the same value of n. The efficiency of R_1 relative to R_2 is the reciprocal of the ratio of their average experiment time. This is given in Table V for $\alpha^* = 2$, $P^* = 0.800$, $r = 4$ and $n = 4, 10, 20$ and ∞. By Table I the value $P^* = 0.800$ is not attained for $n < 4$.

In comparing the sequential and the nonsequential procedures it was found that the slight excesses in the last column of Table I over 0.800

TABLE V — EFFICIENCY OF TYPE R_1 RELATIVE TO TYPE R_2

($\alpha^* = 2$, $P^* = 0.800$, $r = 4$, $g = 0$)

n	$\alpha = 1$	$\alpha = 2$	$\alpha = \infty$
4	0.501	0.495	0.480
10	0.837	0.836	0.835
20	0.925	0.917	0.922
∞	1.000	1.000	1.000

TABLE VI — EFFICIENCY OF ADJUSTED R_1 RELATIVE TO R_3
($\alpha^* = 2$, $P^* = 0.800$, $g = 0$)

n	$\alpha = 1$	$\alpha = 2$	$\alpha = \infty$
4	0.615	0.575	0.419
10	0.754	0.708	0.528
20	0.818	0.768	0.573
∞	0.873	0.822	0.612

had an effect on the efficiency. To make the procedures more comparable the values for $r = 3$ and $r = 4$ in Table I were averaged with values p and $1 - p$ computed so as to give a probability of *exactly* 0.800 at $\alpha = \alpha^*$. The corresponding values for the average experiment time were then averaged with the same values p and $1 - p$. The nonsequential procedures so altered will be called "adjusted procedures." The efficiency of the adjusted R_1 relative to R_3 is given in Table VI.

In Table VI the last row gives the efficiency of the adjusted procedure R_2 relative to R_3. Thus we can separate out the advantage due to the replacement feature and the advantage due to the sequential feature. Table VII gives these results in terms of percentage reduction of average experiment time.

We note that the reduction due to the replacement feature alone is greatest for small n and essentially constant with α while the reduction

TABLE VII — PER CENT REDUCTION IN AVERAGE EXPERIMENT TIME DUE TO STATISTICAL TECHNIQUES
($\alpha^* = 2$, $P^* = 0.800$, $g = 0$)

α	n	Reduction due to *Replacement* Feature Alone	Reduction due to *Sequential* Feature Alone	Reduction due to both Replacement and Sequential Features
1	4	29.5	12.7	38.5
	10	13.7	12.7	24.6
	20	6.3	12.7	18.2
	∞	0.0	12.7	12.7
2	4	30.1	17.8	42.5
	10	13.9	17.8	29.2
	20	6.6	17.8	23.2
	∞	0.0	17.8	17.8
∞	4	31.5	38.8	58.1
	10	13.6	38.8	47.2
	20	6.3	38.8	42.7
	∞	0.0	38.8	38.8

due to the sequential feature alone is greatest for large α and is independent of n. Hence if the initial sample size per process n is large we can disregard the replacement technique. On the other hand the true value of α is not known and hence the advantage of sequential experimentation should not be disregarded.

The formulas used to compute the accompanying tables are given in Addendum 2.

ACKNOWLEDGEMENT

The author wishes to thank Miss Marilyn J. Huyett for considerable help in computing the tables in this paper. Thanks are also due to J. W. Tukey and other staff members for constructive criticism and numerical errors they have pointed out.

Addendum 1

In this addendum we shall consider the more general problem of selecting the best of k exponential populations treated on a higher mathematical level. For $k = 2$ this reduces to the problem discussed above.

DEFINITIONS AND ASSUMPTIONS

There are given k populations Π_i $(i = 1, 2, \cdots, k)$ such that the lifetimes of units taken from any of these populations are independent chance variables with the exponential density (1) with a common (known or unknown) location parameter $g \geqq 0$. The distributions for the k populations are identical except for the unknown scale parameter $\theta > 0$ which may be different for the k different populations. We shall consider three different cases with regard to g.

Case 1: The parameter g has the value zero $(g = 0)$.

Case 2: The parameter g has a positive, known value $(g > 0)$.

Case 3: The parameter g is unknown $(g \geqq 0)$.

Let the *ordered values* of the k scale parameters be denoted by

$$\theta_1 \geqq \theta_2 \geqq \cdots \geqq \theta_k \tag{4}$$

where equal values may be regarded as ordered in any arbitrary manner. At any time t each population has a certain number of failures associated with it. Let the *ordered values* of these integers be denoted by $r_i = r_i(t)$ so that

$$r_1 \leqq r_2 \leqq \cdots \leqq r_k \tag{5}$$

For each unit the life beyond its guarantee period will be referred to as its Poisson life. Let $L_i(t)$ denote the total amount of Poisson life observed up to time t in the population with r_i failures ($i = 1, 2, \cdots, k$). If two or more of the r_i are equal, say $r_i = r_{i+1} = \cdots = r_{i+j}$, then we shall assign r_i and L_i to the population with the largest Poisson life, r_{i+1} and L_{i+1} to the population with the next largest, $\cdots$, r_{i+j} and L_{i+j} to the population with the smallest Poisson life. If there are two or more *equal pairs* (r_i, L_i) then these should be ordered by a random device giving equal probability to each ordering. Then the subscripts in (5) as well as those in (4) are in one-to-one correspondence with the k given populations. It should be noted that $L_i(t) \geqq 0$ for all i and any time $t \geqq 0$. The complete set of quantities $L_i(t)$ $(i = 1, 2, \cdots, k)$ need not be ordered. Let $\alpha = \theta_1/\theta_2$ so that, since the θ_i are ordered, $\alpha \geqq 1$.

We shall further assume that:

1. The initial number n of units put on test is the same and the starting time is the same for each of the k populations.

2. Each replacement is assumed to be a new unit from the same population as the failure that it replaces.

3. Failures are assumed to be clearly recognizable without any chance of error.

SPECIFICATIONS FOR CASE 1: $g = 0$

Before experimentation starts the experimenter is asked to specify two constants α^* and P^* such that $\alpha^* > 1$ and $\frac{1}{2} < P^* < 1$. The procedure $R_3 = R_3(n)$, which is defined in terms of the specified α^* and P^*, has the property that it will correctly select the population with the largest scale parameter with probability at least P^* whenever $\alpha \geqq \alpha^*$. The initial number n of units put on test may either be fixed by nonstatistical considerations or may be determined by placing some restriction on the average experiment time function.

Rule R_3:

"Continue experimentation with replacement until the inequality

$$\sum_{i=2}^{k} \alpha^{*-(r_i - r_1)} \leqq (1 - P^*)/P^* \tag{6}$$

is satisfied. Then stop and select the population with the smallest number of failures as the one having the largest scale parameter."

Remarks

1. Since $P^* > \frac{1}{2}$ then $(1 - P^*)/P^* < 1$ and hence no two populations can have the same value r_1 at stopping time.
2. For $k = 2$ the inequality (6) reduces to the inequality (3).
3. The procedure R_3 terminates only at a failure time, never between failures, since the left member of (6) depends on t only through the quantities $r_i(t)$.
4. After experimentation is completed one can make, at the $100P$ per cent confidence level, the *confidence statement*

$$\theta_s \leqq \theta_1 \leqq \alpha^* \theta_s \quad (\text{or} \quad \theta_1/\alpha^* \leqq \theta_s \leqq \theta_1) \tag{7}$$

where θ_s is the scale parameter of the selected population.

Numerical Illustrations

Suppose the preassigned constants are $P^* = 0.95$ and $\alpha^* = 19^{1/4} = 2.088$ so that $(1 - P^*)/P^* = \frac{1}{19}$. Then for $k = 2$ the procedure is to stop when $r_2 - r_1 \geqq 4$. For $k = 3$ it is easy to check that the procedure reduces to the simple form: "Stop when $r_2 - r_1 \geqq 5$". For $k > 3$ either calculations can be carried out as experimentation progresses or a table of stopping values can be constructed before experimentation starts. For $k = 4$ and $k = 5$ see Table VIII.

In the above form the proposed rule is to stop when, for at least one

TABLE VIII — SEQUENTIAL RULE FOR $P^* = 0.95$, $\alpha^* = 19^{1/4}$

$k = 4$

$r_2 - r_1$	$r_3 - r_1$	$r_4 - r_1$	
5	5	9	
5	6	6	
6	6	6	*

$k = 5$

$r_2 - r_1$	$r_3 - r_1$	$r_4 - r_1$	$r_5 - r_1$	
5	5	9	10	
5	5	10	10	*
5	6	6	8	
5	6	7	7	
5	7	7	7	*
6	6	6	6	

* Starred rows can be omitted without affecting the test since every integer in these rows is at least as great as the corresponding integer in the previous row. They are shown here to illustrate a systematic method which insures that all the necessary rows are included.

row (say row j) in the table, the observed row vector $(r_2 - r_1, r_3 - r_1, \cdots, r_k - r_1)$ is such that *each component* is at least as large as the corresponding component of row j.

Properties of R_3 for $k = 2$ and $g = 0$

For $k = 2$ and $g = 0$ the procedure R_3 is an example of a Sequential Probability Ratio test as defined by A. Wald in his book.[5] The Average Sample Number (ASN) function and the Operating Characteristics (OC) function for R_3 can be obtained from the general formulae given by Wald. Both of these functions depend on θ_1 and θ_2 only through their ratio α. In our problem there is no excess over the boundary and hence Wald's approximation formulas are *exact*. When our problem is put into the Wald framework, the symmetry of our problem implies equal probabilities of type 1 and type 2 errors. The OC function takes on complementary values for any point $\alpha = \theta_1/\theta_2$ and its reciprocal θ_2/θ_1. We shall therefore compute it only for $\alpha \geqq 1$ and denote it by $P(\alpha)$. For $\alpha > 1$ the quantity $P(\alpha)$ denotes the probability of a correct selection for the true ratio α.

The equation determining Wald's h function[5] is

$$\frac{(\alpha^*)^h}{1 + \alpha} + \frac{\alpha(\alpha^*)^{-h}}{1 + \alpha} = 1 \tag{8}$$

for which the non-zero solution in h is easily computed to be

$$h(\alpha) = \frac{\ln \alpha}{\ln \alpha^*} \tag{9}$$

Hence we obtain from Wald's formula (3:43) in Reference 5

$$P(\alpha) = \frac{\alpha^s}{\alpha^s + 1} \tag{10}$$

where s is the smallest integer greater than or equal to

$$S = \ln [P^*/(1 - P^*)]/\ln \alpha^* \tag{11}$$

In particular, for $\alpha = 1^+$, α^* and ∞ we have

$$P(1^+) = \tfrac{1}{2}, \qquad P(\alpha^*) \geqq P^*, \qquad P(\infty) = 1 \tag{12}$$

We have written $P(1^+)$ above for $\lim P(x)$ as $x \longrightarrow 1$ from the right. The procedure becomes more efficient if we choose P and α^* so that S is an integer. Then $s = S$ and $P(\alpha^*) = P^*$.

Letting F denote the total number of observed failures required to

terminate the experiment we obtain for the ASN function

$$E(F; \alpha) = s\left(\frac{\alpha + 1}{\alpha - 1}\right)\left(\frac{\alpha^s - 1}{\alpha^s + 1}\right) \quad \text{for } \alpha > 1 \quad (13)$$

and, in particular, for $\alpha = 1, \infty$

$$E(F; 1) = s^2 \quad \text{and} \quad E(F; \infty) = s \quad (14)$$

It is interesting to note that for $s = 1$ we obtain

$$E(F; \alpha) = 1 \qquad \textit{for all } \alpha \geqq 1 \quad (15)$$

and that this result is exact since for $s = 1$ the right-hand member S of (3) is at most one and hence the procedure terminates with certainty immediately after the first failure.

As a result of the exponential assumption, the assumption of replacement and the assumption that $g = 0$ it follows that the intervals between failures are independently and identically distributed. For a single population the time interval between failures is an exponential chance variable. Hence, for two populations, the time interval is the minimum of two exponentials which is again exponential. Letting τ denote the (chance) duration of a typical interval and letting T denote the (chance) total time needed to terminate the procedure, we have

$$E(T; \alpha, \theta_2) = E(F; \alpha)E(\tau; \alpha, \theta_2) = E(F; \alpha)\left(\frac{\theta_2}{n}\right)\left(\frac{\alpha}{1 + \alpha}\right) \quad (16)$$

Hence we obtain from (13) and (14)

$$E(T; \alpha, \theta_2) = \frac{\theta_2}{n}\frac{s\alpha}{\alpha - 1}\frac{\alpha^s - 1}{\alpha^s + 1} \qquad \text{for } \alpha > 1 \quad (17)$$

$$E(T; 1, \theta_2) = \frac{\theta_2 s^2}{2n} \quad \text{and} \quad E(T; \infty, \theta_2) = \frac{\theta_2 s}{n} \quad (18)$$

For the numerical illustration treated above with $k = 2$ we have

$$P(\alpha) = \frac{\alpha^4}{1 + \alpha^4} \quad (19)$$

$$P(1^+) = \tfrac{1}{2}; \qquad P(2.088) = 0.95; \qquad P(\infty) = 1 \quad (20)$$

$$E(F; \alpha) = 4\frac{\alpha + 1}{\alpha - 1}\frac{\alpha^4 - 1}{\alpha^4 + 1} = 4\frac{(\alpha + 1)^2(\alpha^2 + 1)}{\alpha^4 + 1} \quad (21)$$

$$E(F; 1) = 16.0; \qquad E(F; 2.088) = 10.2; \qquad E(F; \infty) = 4 \quad (22)$$

$$E(T; 1, \theta_2) = \frac{8\theta_2}{n}; \qquad E(T; 2.088, \theta_2) = \frac{6.9\theta_2}{n}; \qquad E(T; \infty, \theta_2) = \frac{4\theta_2}{n} \tag{23}$$

For $k > 2$ the proposed procedure is an application of a general sequential rule for selecting the best of k populations which is treated in [1]. Proof that the probability specification is met and bounds on the probability of a correct decision can be found there.

CASE 2: COMMON KNOWN $g > 0$

In order to obtain the properties of the sequential procedure R_3 for this case it will be convenient to consider other sequential procedures. Let $\beta = 1/\theta_2 - 1/\theta_1$ so that, since the θ_i are ordered, $\beta \geqq 0$. Let us assume that the experimenter can specify three constants α^*, β^* and P^* such that $\alpha^* > 1$, $\beta^* > 0$ and $\frac{1}{2} < P^* < 1$ and a procedure is desired which will select the population with the largest scale parameter with probability at least P^* whenever we have both

$$\alpha \geqq \alpha^* \quad \text{and} \quad \beta \geqq \beta^*$$

The following procedure meets this specification.

Rule R_3':

"Continue experimentation with replacement until the inequality

$$\sum_{i=2}^{k} \alpha^{*-(r_i - r_1)} e^{-\beta^*(L_1 - L_i)} \leqq (1 - P^*)/P^* \tag{24}$$

is satisfied. Then stop and select the population with the smallest number of failures as the one having the largest scale parameter. If, at stopping time, two or more populations have the same value r_1 then select that particular one of these with the largest Poisson life L_1."

Remarks

1. For $k = 2$ the inequality reduces to

$$(r_2 - r_1) \ln \alpha^* + (L_1 - L_2)\beta^* \geqq \ln [P^*/(1 - P^*)] \tag{25}$$

If $g = 0$ then $L_1 \equiv L_i$ for all t and the procedure R_3' reduces to R_3.

2. The procedure R_3' may terminate not only at failures but also between failures.

3. The same inequality (24) can also be used if experimentation is carried on *without replacement*, one advantage of the latter being that there is less bookkeeping involved. In this case there is a possibility that the units will all fail before the inequality is satisfied so that the procedure is not yet completely defined for this case. One possibility in such a situation is to continue experimentation with new units from each population until the inequality is satisfied. Such a procedure will terminate in a finite time with probability one, i.e., $\text{Prob}\{T > T_0\} \to 0$ as $T_0 \to \infty$, and the probability specification will be satisfied.

4. A procedure R_3' $(n_1, n_2, \cdots, n_k, t_1, t_2, \cdots, t_k)$ using the same inequality (24) but based on different initial sample sizes and/or on different starting times for the initial samples also satisfies the above probability specification. In the case of different starting times it is required that the experimenter wait at least g units of time after the last initial sample is put on test before reaching any decision.

5. One disadvantage of R_3' is that there is some (however remote) possibility of terminating while $r_1 = r_2$. This can be avoided by adding the condition $r_2 > r_1$ to (24) but, of course, the average experiment time is increased. Another way of avoiding this is to use the procedure R_3 which depends only on the number of failures; the effect of using R_3 when $g > 0$ will be considered below.

6. The terms of the sum in (24) represent likelihood ratios. If at any time each term is less than unity then we shall regard the decision to select the population with r_1 failures and L_1 units of Poisson life as optimal. Since $(1 - P^*)/P^* < 1$ then each term must be less than unity at termination.

Properties of Procedure R_3' for $k = 2$

The OC and ASN functions for R_3' will be approximated by comparing R_3' with another procedure R_3'' defined below. We shall assume that P^* is close to unity and that g is small enough (compared to θ_2) so that the probability of obtaining two failures within g units of time is small enough to be negligible. Then we can write approximately at termination

$$L_i \cong nT - r_i g \qquad (i = 1, 2, \cdots, k) \tag{26}$$

and

$$L_1 - L_i \cong (r_i - r_1)g \qquad (i = 2, 3, \cdots, k) \tag{27}$$

Substituting this in (24) and letting

$$\delta^* = \alpha^* e^{\beta^* g} \tag{28}$$

suggests a new rule, say R_3'', which we now define.

Rule R_3''

"Continue experimentation with replacement until the inequality

$$\sum_{i=2}^{k} \delta^{*-(r_i-r_1)} \leqq (1 - P^*)/P^* \tag{29}$$

is satisfied. Then stop and select the population with r_1 failures as the one with the largest scale parameter."

For rule R_3'' the experimenter need only specify P^* and the smallest value δ^* of the *single* parameter

$$\delta = \frac{\theta_1}{\theta_2} e^{g((1/\theta_2)-(1/\theta_1))} = \alpha e^{g\beta} \tag{30}$$

that he desires to detect with probability at least P^*.

We shall approximate the OC and ASN function of R_3'' for $k = 2$ by computing them under the assumption that (27) holds at termination. The results will be considered as an approximation for the OC and ASN functions respectively of R_3' for $k = 2$. The similarity of (29) and (6) immediately suggests that we might replace α^* by δ^* and α by δ in the formulae for (6). To use the resulting expressions for R_3' we would compute δ^* as a function of α^* and β^* by (28) and δ as a function of α and β by (30).

The similarity of (29) and (6) shows that Z_n (defined in Reference 5, page 170) under (27) with $g > 0$ is the same function of δ^* and δ as it is of α^* and α when $g = 0$. To complete the justification of the above result it is sufficient to show that the individual increment z of Z_n is the same function of δ^* and δ under (27) with $g > 0$ as it is of α^* and α when $g = 0$. To keep the increments independent it is necessary to associate each failure with the Poisson life that follows rather than with the Poisson life that precedes the failure. Neglecting the probability that any two failures occur within g units of time we have two values for z, namely

$$z = \log \frac{\frac{n}{\theta_1} e^{-(nt-g)/\theta_1} e^{-nt/\theta_2}}{\frac{n}{\theta_2} e^{-(nt-g)/\theta_2} e^{-nt/\theta_1}} = -\log \delta \tag{31}$$

and, interchanging θ_1 and θ_2, gives $z = \log \delta$. Moreover

$$\text{Prob}\{z = -\log \delta\} = \frac{\int_g^\infty \int_g^\infty \frac{n}{\theta_2} e^{-(nx-g)/\theta_2} e^{-ny/\theta_1}\, dx\, dy}{\frac{\theta_2}{n} e^{-g[\theta_2(n-1)+\theta_1 n]/\theta_1\theta_2} + \frac{\theta_1}{n} e^{-g[\theta_2 n+\theta_1(n-1)]/\theta_1\theta_2}} \tag{32}$$

$$= \frac{\delta}{1+\delta}$$

Thus the OC and ASN functions under (27) with $g > 0$ bear the same relation to δ^* and δ as they do to α^* and α when $g = 0$. Hence, letting w denote the smallest integer greater than or equal to

$$W = \frac{\ln [P^*/(1-P^*)]}{\ln \delta^*} = \frac{\ln [P^*/(1-P^*)]}{g\beta^* + \ln \alpha^*} \tag{33}$$

we can write (omitting P^* in the rule description)

$$P\{\delta;\, R_3'\,(\alpha^*, \beta^*)\} \cong P\{\delta;\, R_3''(\delta^*)\} \cong \frac{\delta^w}{\delta^w + 1} \tag{34}$$

$$E\{F;\, R_3'\,(\alpha^*, \beta^*)\} \cong E\{F;\, R_3''(\delta^*)\}$$

$$\cong \begin{cases} w\left(\dfrac{\delta+1}{\delta-1}\right)\left(\dfrac{\delta^w-1}{\delta^w+1}\right) & \text{for } \delta > 1 \\ w^2 & \text{for } \delta = 1 \end{cases} \tag{35}$$

We can approximate the average time between failures by

$$E\{\tau;\, \theta_1, \theta_2, g\} \cong \frac{(g+\theta_1)(g+\theta_2)}{n(\theta_1+\theta_2+2g)} \leqq g + \frac{\theta_2}{n}\left(\frac{\alpha}{1+\alpha}\right) \tag{36}$$

and the average experiment time by

$$E\{T;\, R_3'(\alpha^*, \beta^*)\} \cong E\{F;\, R_3'(\alpha^*, \beta^*)\}\, \frac{(g+\theta_1)(g+\theta_2)}{n(\theta_1+\theta_2+2g)} \tag{37}$$

Since $\delta \geqq 1$ then $\delta^w/(1+\delta^w)$ is an increasing function of w and by (33) it is a non-increasing function of δ^*. By (28) $\delta^* \geqq \alpha^*$ and hence, if we disregard the approximation (34),

$$P\{\delta;\, R_3''(\alpha^*)\} \cong \frac{[P^*/(1-P^*)]^{\ln \delta/\ln \alpha^*}}{1 + [P^*/(1-P^*)]^{\ln \delta/\ln \alpha^*}} \geqq P\{\delta; R_3''(\delta^*)\} \tag{38}$$

Clearly the rules $R_3(\alpha^*, P^*)$ and $R_3''\,(\alpha^*, P^*)$ are equivalent so that for $g > 0$ we have

$$P\{\delta;\, R_3(\alpha^*)\} \equiv P\{\delta;\, R_3''(\alpha^*)\} \tag{39}$$

and hence, in particular, letting $\delta = \delta^*$ in (38) we have

$$P\{\delta^*; R_3(\alpha^*)\} \geqq P\{\delta^*; R_3''(\delta^*)\} \geqq P^* \tag{40}$$

since the right member of (34) reduces to P^* when W is an integer and $\delta = \delta^*$. The error in the approximations above can be disregarded when g is small compared to θ_2. Thus we have shown that for small values of g/θ_2 the probability specification based on (α^*, β^*, P^*) is satisfied in the sense of (40) if we use the procedure $R_3(\alpha^*, P^*)$, i.e., if we proceed as if $g = 0$.

It would be desirable to show that we can proceed as if $g = 0$ for all values of g and P^*. It can be shown that *for sufficiently large* n the rule $R_3(\alpha^*, P^*)$ meets it specification for all g. One effect of increasing n is to decrease the average time $E(\tau)$ between failures and to approach the corresponding problem *without replacement* since $g/E(\tau)$ becomes large. Hence we need only show that $R_3(\alpha^*, P^*)$ meets its specification for the corresponding problem without replacement. If we disregard the information furnished by Poisson life and rely solely on the counting of failures then the problem reduces to testing in a *single* binomial whether $\theta = \theta_1$ for population Π_1 and $\theta = \theta_2$ for population Π_2 or vice versa. Letting p denote the probability that the next failure arises from Π_1 then we have formally

$$H_0{:}p = \frac{1}{1+\alpha} \qquad \text{versus} \qquad H_1{:}p = \frac{\alpha}{1+\alpha}$$

For preassigned constants $\alpha^* > 1$ and P^* $(\frac{1}{2} < P^* < 1)$ the appropriate sequential likelihood test to meet the specification:

"Probability of a Correct Selection $\geqq P^*$ whenever $\alpha \geqq \alpha^*$" (41)

then turns out to be precisely the procedure $R_3(\alpha^*, P^*)$. Hence we may proceed as if $g = 0$ when n is sufficiently large.

The specifications of the problem may be given in a different form. Suppose $\theta_1^* > \theta_2^*$ are specified and it is desired to have a probability of a correct selection of at least P^* whenever $\theta_1 \geqq \theta_1^* > \theta_2^* \geqq \theta_2$. Then we can form the following sequential likelihood procedure R_3^* which is more efficient than $R_3(\alpha^*, P^*)$.

Rule R_3^*:

"Continue experimentation without replacement until a time t is reached at which the inequality

$$\sum_{i=2}^{k} \left[\frac{e^{t/\theta_2^*} - 1}{e^{t/\theta_1^*} - 1}\right]^{-(r_i - r_1)} \leqq \frac{1 - P^*}{P^*} \tag{42}$$

is satisfied. Then stop and select the population with r_1 failures as the population with $\theta = \theta_1$".

It can be easily shown that the greatest lower bound of the bracketed quantity in (42) is θ_1^*/θ_2^*. Hence for $\theta_1^*/\theta_2^* = \alpha^*$ and $P^* > 1/2$ the time required by $R_3^*(\theta_1^*, \theta_2^*, P^*)$ will always be less than the time required by $R_3(\alpha^*, P^*)$.

Another type of problem is one in which we are given that $\theta = \theta_1^*$ for one population and $\theta = \theta_2^*$ for the $k - 1$ others where $\theta_1^* > \theta_2^*$ are specified. The problem is to select the population with $\theta = \theta_1^*$. Then (42) can again be used. In this case the parameter space is discrete with k points only one of which is correct. If Rule R_3^* is used then the probability of selecting the correct point is at least P^*.

Equilibrium Approach When Failures Are Replaced

Consider first the case in which all items on test are from the same exponential population with parameters (θ, g). Let T_{nj} denote the length of the time interval between the j^{th} and the $j + 1^{\text{st}}$ failures, $(j = 0, 1, \cdots)$, where n is the number of items on test and the 0^{th} failure denotes the starting time. As time increases to infinity the expected number of failures per unit time clearly approaches $n/(\theta + g)$ which is called the equilibrium failure rate. The inverse of this is the expected time between failures at equilibrium, say $E(T_{n\infty})$. The question as to how the quantities $E(T_{nj})$ approach $E(T_{n\infty})$ is of considerable interest in its own right. The following results hold for any fixed integer $n \geqq 1$ unless explicitly stated otherwise. It is easy to see that

$$E(T_{n1}) \leqq E(T_{n\infty}) \leqq E(T_{n0}) \tag{43}$$

since the exact values are respectively

$$\frac{\theta}{n-1}\left(1 - \frac{e^{-(n-1)g/\theta}}{n}\right) \leqq \frac{g+\theta}{n} \leqq g + \frac{\theta}{n} \tag{44}$$

In fact, since all units are new at starting time and since at the time of the first failure all units (except the replacement) have passed their guarantee period with probability one then

$$E(T_{n1}) \leqq E(T_{nj}) \leqq E(T_{n0}) \qquad (j \geqq 0) \tag{45}$$

If we compare the case $g > 0$ with the special case $g = 0$ we obtain

$$E(T_{nj}) \geqq \frac{\theta}{n} \qquad (j = 1, 2, \cdots) \tag{46}$$

and if we compare it with the non-replacement case (g/θ is large) we obtain

$$E(T_{nj}) \leqq \frac{\theta}{n-j} \qquad (j = 1, 2, \cdots, n-1). \quad (47)$$

These comparisons show that the difference in (46) is small when g/θ is small and for $j < n$ the difference in (47) is small when g/θ is large.

It is possible to compute $E(T_{nj})$ exactly for $g \geqq 0$ but the computation is extremely tedious for $j \geqq 2$. The results for $j = 1$ and 0 are given in (44). For $j = 2$

$$E(T_{n2}) = \frac{\theta}{n-2}\left[1 - \frac{(n+2)(n-1)}{n^2} e^{-(n-2)g/\theta} + \frac{n-2}{n-1} e^{-(n-1)g/\theta} - \frac{n-2}{n^2(n-1)} e^{-2(n-1)g/\theta}\right] \qquad (n > 2) \quad (48)$$

and

$$E(T_{22}) = g - \frac{\theta}{4}[1 - 4e^{-g/\theta} + e^{-2g/\theta}] \quad (49)$$

For the case of two populations with a common guarantee period g we can write similar inequalities. We shall use different symbols a, b for the initial sample size from the populations with scale parameters θ_1, θ_2 respectively even though our principal interest is in the case $a = b = n$ say. Let $T_{a,b,j}$ denote the interval between the j^{th} and $j+1^{\text{st}}$ failures in this case and let $\lambda_i = 1/\theta_i$ $(i = 1, 2)$. We then have for all values of a and b

$$[a\lambda_1 + b\lambda_2]^{-1} \leqq E(T_{a,b,j}) \leqq E(T_{a,b,0}) = g + [a\lambda_1 + b\lambda_2]^{-1} \quad (j = 0, 1, 2, \cdots, \infty) \quad (50)$$

$$E(T_{a,b,\infty}) = \frac{(\theta_1 + g)(\theta_2 + g)}{a(\theta_2 + g) + b(\theta_1 + g)} \quad (51)$$

The result for $E(T_{a,b,1})$ corresponding to that in (43) does not hold if the ratio θ_1/θ_2 is too large; in particular it can be shown that

$$E(T_{a,b,1}) = \left(\frac{a\lambda_1}{a\lambda_1 + b\lambda_2}\right)\left(\frac{1}{(a-1)\lambda_1 + b\lambda_2}\right)\left[1 - \frac{\lambda_1 e^{-g[(a-1)\lambda_1 + b\lambda_2]}}{a\lambda_1 + b\lambda_2}\right] + \left(\frac{b\lambda_2}{a\lambda_1 + b\lambda_2}\right)\left(\frac{1}{a\lambda_1 + (b-1)\lambda_2}\right)\left[1 - \frac{\lambda_2 e^{-g[a\lambda_1 + (b-1)\lambda_2]}}{a\lambda_1 + b\lambda_2}\right] \quad (52)$$

is larger than $E(T_{a,b,\infty})$ for $a = b = 1$ when $g/\theta_1 = 0.01$ and $g/\theta_2 = 0.10$

so that $\theta_1/\theta_2 = 10$. The expression (52) reduces to that in (44) if we set $\theta_1 = \theta_2 = \theta$ and replace a and b by $n/2$ in the resulting expression.

Corresponding exact expressions for $E(T_{a,b,j})$ for $j > 1$ are extremely tedious to derive and unwieldy although the integrations involved are elementary. If we let $g \to \infty$ then we obtain expressions for the non-replacement case which are relatively simple. They are best expressed as a recursion formula.

$$E(T_{a,b,j}) = \frac{a\lambda_1}{a\lambda_1 + b\lambda_2} ET_{a-1,b,j-1} + \frac{b\lambda_2}{a\lambda_1 + b\lambda_2} ET_{a,b-1,j-1} \qquad (j \geqq 1) \tag{53}$$

$$E(T_{a,b,1}) = \frac{a\lambda_1}{a\lambda_1 + b\lambda_2} \frac{1}{(a-1)\lambda_1 + b\lambda_2} + \frac{b\lambda_2}{a\lambda_1 + b\lambda_2} \frac{1}{a\lambda_1 + (b-1)\lambda_2} \qquad (a, b \geqq 1) \tag{54}$$

$$E(T_{a,0,j}) \leqq g + \theta_1/a \qquad \text{for } j \geqq a \text{ and } j = 0 \tag{55}$$

$$E(T_{a,0,j}) = \theta_1/(a-j) \qquad \text{for } 1 \leqq j \leqq a-1 \tag{56}$$

Results similar to (55) and (56) hold for the case $a = 0$. The above results for $g = \infty$ provide useful approximations for $E(T_{a,b,j})$ when g is large. Upper bounds are given by

$$E(T_{a,b,j}) \leqq [a\lambda_1 + (b-j)\lambda_2]^{-1} \qquad (j = 1, 2, \cdots, b) \tag{57}$$

$$E(T_{a,b,j+b}) \leqq [(a-j)\lambda_1]^{-1} \qquad (j = 1, 2, \cdots, a-1). \tag{58}$$

Duration of the Experiment

For the sequential rule R_3' with $k = 2$ we can now write down approximations as well as upper and lower bounds to the expected duration $E(T)$ of the experiment. From (50)

$$g + \frac{E(F;\delta)}{n(\lambda_1 + \lambda_2)} \leqq E(T) = \sum_{j=0}^{c-1} E(T_{n,n,j}) + [E(F;\delta) - c]E(T_{n,n,c}) \tag{59}$$

where c is the largest integer less than or equal to $E(F;\delta)$. The right expression of (59) can be approximated by (53) and (54) if g is large. If $c < 2n$ then the upper bounds are given by (57) and (58). A simpler

upper bound, which holds for all values of c is given by

$$E(T) \leqq E(F; \delta)E(T_{n,n,0}) = E(F; \delta)\left(g + \frac{\theta_1}{n}\right) \tag{60}$$

CASE 3: COMMON UNKNOWN LOCATION PARAMETER $g \geqq 0$

In this case the more conservative procedure is to proceed under the assumption that $g = 0$. By the discussion above the probability requirement will in most problems be satisfied for all $g \geqq 0$. The OC and ASN functions, which are now functions of the true value of g, were already obtained above. Of course, we need not consider values of g greater than the smallest observed lifetime of all units tested to failure.

ADDENDUM 2

For completeness it would be appropriate to state explicitly some of the formulas used in computing the tables in the early part of the paper. For the nonsequential, nonreplacement rule R_1 with $k = 2$ the probability of a correct selection is

$$P(\alpha; R_1) = \int_0^\infty \int_0^x f_r(y, \theta_2) f_r(x, \theta_1)\, dy\, dx \tag{61}$$

where

$$f_r(x, \theta) = \frac{r}{\theta} C_r^n (1 - e^{-x/\theta})^{r-1} e^{-x(n-r+1)/\theta}. \qquad (r \leqq n) \tag{62}$$

and C_r^n is the usual combinatorial symbol. This can also be expressed in the form

$$P(\alpha; R_1) = 1 - (rC_r^n)^2 \sum_{j=1}^{r} \frac{(-1)^{j-1}}{n - r + j} C_{j-1}^{r-1}\{B[r, n - r + 1 + \alpha(n - r + j)]\}^{-1} \tag{63}$$

where $B[x, y]$ is the complete Beta function. Equation (66) holds for any $g \geqq 0$.

For the rule R_1 the expected duration of the experiment for $k = 2$ is given by

$$E(T) = \int_0^\infty x\{f_r(x, \theta_1)[1 - F_r(x, \theta_2)] + f_r(x, \theta_2)[1 - F_r(x, \theta_1)]\}\, dx \tag{64}$$

where $f_r(x, \theta)$ is the density in (62) and $F_r(x, \theta)$ is its c.d.f. This can

also be expressed in the form

$$\theta_1 r(C_r^n)^2 \sum_{i=1}^{r} \sum_{j=1}^{r} \frac{(-1)^{i+j} C_{i-1}^{r-1} C_{j-1}^{r-1}}{(n-r+j)[i+n-r+\alpha(j+n-r)]^2} \tag{65}$$

plus another similar expression in which θ_1, α are replaced by θ_2, α^{-1} respectively. For $g > 0$ we need only add g to this result. This result was used to compute $E(T)$ in table 1A for $\alpha = 1$ and $\alpha = 2$. For $\alpha = \infty$ the expression simplifies to

$$E(T) = \theta_2 r C_r^n \sum_{j=1}^{r} C_{j-1}^{r-1} \frac{(-1)^{r-j}}{(n-j+1)^2} \tag{66}$$

which can be shown to be equivalent to

$$E(T) = \theta_2 \sum_{j=1}^{r} \frac{1}{n-j+1} \tag{67}$$

REFERENCES

1. Bechhofer, R. E., Kiefer, J. and Sobel, M., On a Type of Sequential Multiple Decision Procedures for Certain Ranking and Identification Problems with k Populations. To be published.
2. Birnbaum, A., Statistical methods for Poisson processes and exponential populations, J. Am. Stat. Assoc., **49**, pp. 254–266, 1954.
3. Birnbaum, A., Some procedures for comparing Poisson processes or populations, Biometrika, **40**, pp. 447–49, 1953.
4. Girshick, M. A., Contributions to the theory of sequential analysis I, Annals Math. Stat., **17**, pp. 123–43, 1946.
5. Wald, A., Sequential Analysis, John Wiley and Sons, New York, 1947.

A Class of Binary Signaling Alphabets

By DAVID SLEPIAN

(Manuscript received September 27, 1955)

A class of binary signaling alphabets called "group alphabets" is described. The alphabets are generalizations of Hamming's error correcting codes and possess the following special features: (1) all letters are treated alike in transmission; (2) the encoding is simple to instrument; (3) maximum likelihood detection is relatively simple to instrument; and (4) in certain practical cases there exist no better alphabets. A compilation is given of group alphabets of length equal to or less than 10 binary digits.

INTRODUCTION

This paper is concerned with a class of signaling alphabets, called "group alphabets," for use on the symmetric binary channel. The class in question is sufficiently broad to include the error correcting codes of Hamming,[1] the Reed-Muller codes,[2] and all "systematic codes".[3] On the other hand, because they constitute a rather small subclass of the class of all binary alphabets, group alphabets possess many important special features of practical interest.

In particular, (1) all letters of the alphabets are treated alike under transmission; (2) the encoding scheme is particularly simple to instrument; (3) the decoder — a maximum likelihood detector — is the best possible theoretically and is relatively easy to instrument; and (4) in certain cases of practical interest the alphabets are the best possible theoretically.

It has very recently been proved by Peter Elias[4] that there exist group alphabets which signal at a rate arbitarily close to the capacity, C, of the symmetric binary channel with an arbitrarily small probability of error. Elias' demonstration is an existence proof in that it does not show *explicitly* how to construct a group alphabet signaling at a rate greater than $C - \varepsilon$ with a probability of error less than δ for arbitrary positive δ and ε. Unfortunately, in this respect and in many others, our understanding of group alphabets is still fragmentary.

In Part I, group alphabets are defined along with some related con-

cepts necessary for their understanding. The main results obtained up to the present time are stated without proof. Examples of these concepts are given and a compilation of the best group alphabets of small size is presented and explained. This section is intended for the casual reader.

In Part II, proofs of the statements of Part I are given along with such theory as is needed for these proofs.

The reader is assumed to be familiar with the paper of Hamming,[1] the basic papers of Shannon[5] and the most elementary notions of the theory of finite groups.[6]

Part I — Group Alphabets and Their Properties

1.1 Introduction

We shall be concerned in all that follows with communication over the symmetric binary channel shown on Fig. 1. The channel can accept either of the two symbols 0 or 1. A transmitted 0 is received as a 0 with probability q and is received as a 1 with probability $p = 1 - q$: a transmitted 1 is received as a 1 with probability q and is received as a 0 with probability p. We assume $0 \leqq p \leqq \frac{1}{2}$. The "noise" on the channel operates independently on each symbol presented for transmission. The capacity of this channel is

$$C = 1 + p \log_2 p + q \log_2 q \text{ bits/symbol} \tag{1}$$

By a *K-letter, n-place binary signaling alphabet* we shall mean a collection of K distinct sequences of n binary digits. An individual sequence of the collection will be referred to as a *letter* of the alphabet. The integer K is called the size of the alphabet. A letter is transmitted over the channel by presenting in order to the channel input the sequence of n zeros and ones that comprise the letter. A *detection scheme* or *detector* for

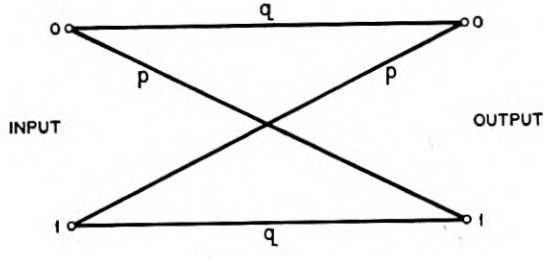

Fig. 1 — The symmetric binary channel.

a given K-letter, n-place alphabet is a procedure for producing a sequence of letters of the alphabet from the channel output.

Throughout this paper we shall assume that signaling is accomplished with a given K-letter, *n-place* alphabet by choosing the letters of the alphabet for transmission independently with equal probability $1/K$.

Shannon[5] has shown that for sufficiently large n, there exist K-letter, n-place alphabets and detection schemes that signal over the symmetric binary channel at a rate $R > C - \varepsilon$ for arbitrary $\varepsilon > 0$ and such that the probability of error in the letters of the detector output is less than any $\delta > 0$. Here C is given by (1) and is shown as a function of p in Fig. 2. No algorithm is known (other than exhaustvie procedures) for the construction of K-letter, n-place alphabets satisfying the above inequalities for arbitrary positive δ and ε except in the trivial cases $C = 0$ and $C = 1$.

1.2 THE GROUP B_n

There are a totality of 2^n different n-place binary sequences. It is frequently convenient to consider these sequences as the vertices of a cube of unit edge in a Euclidean space of n-dimensions. For example the 5-place sequence 0, 1, 0, 0, 1 is associated with the point in 5-space whose

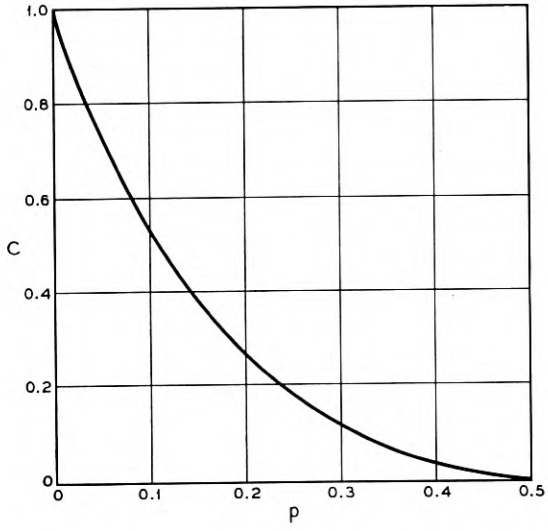

Fig. 2 — The capacity of the symmetric binary channel.

$$C = 1 + p \log_2 p + (1 - p) \log_2 (1 - p)$$

coordinates are (0, 1, 0, 0, 1). For convenience of notation we shall generally omit commas in writing a sequence. The above 5-place sequence will be written, for example, 01001.

We define the *product of two n-place binary sequences*, $a_1a_2 \cdots a_n$ and $b_1b_2 \cdots b_n$ as the n-place binary sequence

$$a_1 \dotplus b_1 , \qquad a_2 \dotplus b_2 , \cdots , a_n \dotplus b_n$$

Here the a's and b's are zero or one and the $\dotplus$ sign means addition modulo 2. (That is $0 \dotplus 0 = 1 \dotplus 1 = 0, \quad 0 \dotplus 1 = 1 \dotplus 0 = 1$) For example, (01101) (00111) = 01010. With this rule of multiplication the 2^n n-place binary sequences form an Abelian group of order 2^n. The elements of the group, denoted by $T_1 , T_2 , \cdots , T_{2^n}$, say, are the n-place binary sequences; the identity element I is the sequence $000 \cdots 0$ and

$$IT_i = T_iI = T_i ; \qquad T_iT_j = T_jT_i ; \qquad T_i(T_jT_k) = (T_iT_j)T_k ;$$

the product of any number of elements is again an element; every element is its own reciprocal, $T_i = T_i^{-1}$, $T_i^2 = I$. We denote this group by B_n.

All subgroups of B_n are of order 2^k where k is an integer from the set $0, 1, 2, \cdots , n$. There are exactly

$$N(n, k) = \frac{(2^n - 2^0)(2^n - 2^1)(2^n - 2^2) \cdots (2^n - 2^{k-1})}{(2^k - 2^0)(2^k - 2^1)(2^k - 2^2) \cdots (2^k - 2^{k-1})} \qquad (2)$$

$$= N(n, n - k)$$

distinct subgroups of B_n of order 2^k. Some values of $N(n, k)$ are given in Table I.

TABLE I — SOME VALUES OF N(n, k), THE NUMBER OF SUBGROUPS OF B_n OF ORDER 2^k. $N(n, k) = N(n, n - k)$

$n\backslash k$	0	1	2	3	4	5
2	1	3	1			
3	1	7	7	1		
4	1	15	35	15	1	
5	1	31	155	155	31	1
6	1	63	651	1395	651	63
7	1	127	2667	11811	11811	2667
8	1	255	10795	97155	200787	97155
9	1	511	43435	788035	3309747	3309747
10	1	1023	174251	6347715	53743987	109221651

1.3 GROUP ALPHABETS

An n-place *group alphabet* is a K-letter, n-place binary signaling alphabet whose letters form a subgroup of B_n. Of necessity the size of an n-place group alphabet is $K = 2^k$ where k is an integer satisfying $0 \leqq k \leqq n$. By an (n, k)-*alphabet* we shall mean an n-place group alphabet of size 2^k. Example: the $N(3, 2) = 7$ distinct (3, 2)-alphabets are given by the seven columns

(i)	(ii)	(iii)	(iv)	(v)	(vi)	(vii)
000	000	000	000	000	000	000
100	100	100	010	010	001	110
010	001	011	001	101	110	011
110	101	111	011	111	111	101

(3)

1.4 STANDARD ARRAYS

Let the letters of a specific (n, k)-alphabet be $A_1 = I = 00 \cdots 0$, $A_2, A_3, \cdots, A_\mu$, where $\mu = 2^k$. The group B_n can be developed according to this subgroup and its cosets:

$$B_n = \begin{array}{llll} I, & A_2, & A_3, & \cdots, A_\mu \\ S_2, & S_2A_2, & S_2A_3, & \cdots, S_2A_\mu \\ S_3, & S_3A_2, & S_3A_3, & \cdots, S_3A_\mu \\ \cdot & & & \\ \cdot & & & \\ \cdot & & & \\ S_\nu, & S_\nu A_2, & S_\nu A_3, & \cdots, S_\nu A_\mu \end{array} \qquad (4)$$

$$\mu = 2^k, \qquad \nu = 2^{n-k}.$$

In this array every element of B_n appears once and only once. The collection of elements in any row of this array is called a *coset* of the (n, k)-alphabet. Here S_2 is any element of B_n not in the first row of the array, S_3 is any element of B_n not in the first two rows of the array, etc. The elements $S_2, S_3, \cdots, S_\nu$ appearing under I in such an array will be called the *coset leaders*.

If a coset leader is replaced by any element in the coset, the same coset will result. That is to say the two collections of elements

$$S_i, \qquad S_iA_2, \qquad S_iS_3, \cdots, S_iA_\mu$$

and

$$S_iA_k, \qquad (S_iA_k)A_2, \qquad (S_iA_k)A_3, \cdots (S_iA_k)A_\mu$$

are the same.

We define the *weight* $w_i = w(T_i)$ of an element, T_i, of B_n to be the number of ones in the n-place binary sequence T_i.

Henceforth, unless otherwise stated, we agree in dealing with an array such as (4) to adopt the following convention:

the leader of each coset shall be taken to be an element of minimal weight in that coset. (5)

Such a table will be called a *standard array*.

Example: B_4 can be developed according to the (4, 2)-alphabet 0000, 1100, 0011, 1111 as follows

0000	1100	0011	1111
1010	0110	1001	0101
1110	0010	1101	0001
1000	0100	1011	0111

(6)

According to (5), however, we should write, for example

0000	1100	0011	1111
1010	0110	1001	0101
0010	1110	0001	1101
1000	0100	1011	0111

(7)

The coset leader of the second coset of (6) can be taken as any element of that row since all are of weight 2. The leader of the third coset, however, should be either 0010 or 0001 since these are of weight one. The leader of the fourth coset should be either 1000 or 0100.

1.5 THE DETECTION SCHEME

Consider now communicating with an (n, k)-alphabet over the symmetric binary channel. When any letter, say A_j, of the alphabet is transmitted, the received sequence can be of any element of B_n. We agree to use the following detector:

if the received element of B_n lies in column i of the array (4), *the detector prints the letter A_i, $i = 1, 2, \cdots, \mu$. The array* (4) *is to be constructed according to the convention* (5). (8)

The following propositions and theorems can be proved concerning signaling with an (n, k)-alphabet and the detection scheme given by (8).

1.6 BEST DETECTOR AND SYMMETRIC SIGNALING

Define the *probability* $\ell_i = \ell(T_i)$ of an element T_i of B_n to be $\ell_i = p^{w_i}q^{n-w_i}$ where p and q are as in (1) and w_i is the weight of T_i. Let

Q_i, $i = 1, 2, \cdots, \mu$ be the sum of the probabilities of the elements in the ith column of the standard array (4).

Proposition 1. The probability that any transmitted letter of the (n, k)-alphabet be produced correctly by the detector is Q_1.

Proposition 2. The equivocation[5] per symbol is

$$H_y(x) = -\frac{1}{n}\sum_{i=1}^{\mu} Q_i \log_2 Q_i$$

Theorem 1. The detector (8) is a maximum likelihood detector. That is, for the given alphabet no other detection scheme has a greater average probability that a transmitted letter be produced correctly by the detector.

Let us return to the geometrical picture of n-place binary sequences as vertices of a unit cube in n-space. The choice of a K-letter, n-place alphabet corresponds to designating K particular vertices as letters. Since the binary sequence corresponding to any vertex can be produced by the channel output, any detector must consist of a set of rules that associates various vertices of the cube with the vertices designated as letters of the alphabet. We assume that every vertex is associated with some letter. The vertices of the cube are divided then into disjoint sets, $W_1, W_2, \cdots, W_K$ where W_i is the set of vertices associated with ith letter of the signaling alphabet. A maximum likelihood detector is characterized by the fact that every vertex in W_i is as close to or closer to the ith letter than to any other letter, $i = 1, 2, \cdots, K$. For group alphabets and the detector (8), this means that no element in the ith column of array (4) is closer to any other A than it is to A_i, $i = 1, 2, \cdots, \mu$.

Theorem 2. Associated with each (n, k)-alphabet considered as a point configuration in Euclidean n-space, there is a group of $n \times n$ orthogonal matrices which is transitive on the letters of the alphabet and which leaves the unit cube invariant. The maximum likelihood sets W_1, $W_2, \cdots W_\mu$ are all geometrically similar.

Stated in loose terms, this theorem asserts that in an (n, k)-alphabet every letter is treated the same. Every two letters have the same number of nearest neighbors associated with them, the same number of next nearest neighbors, etc. The disposition of points in any two W regions is the same.

1.7 GROUP ALPHABETS AND PARITY CHECKS

Theorem 3. Every group alphabet is a systematic[3] code: every systematic code is a group alphabet.[7]

We prefer to use the word "alphabet" in place of "code" since the latter has many meanings. In a *systematic alphabet*, the places in any letter can be divided into two classes: the information places — k in number for an (n, k)-alphabet — and the check positions. All letters have the same information places and the same check places. If there are k information places, these may be occupied by any of the 2^k k-place binary sequences. The entries in the $n - k$ check positions are fixed linear (mod 2) combinations of the entries in the information positions. The rules by which the entries in the check places are determined are called *parity checks*. Examples: for the (4, 2)-alphabet of (6), namely 0000, 1100, 0011, 1111, positions 2 and 3 can be regarded as the information positions. If a letter of the alphabet is the sequence $a_1a_2a_3a_4$, then $a_1 = a_2$, $a_4 = a_3$ are the parity checks determining the check places 1 and 4. For the (5, 3)-alphabet 00000, 10001, 01011, 00111, 11010, 10110, 01100, 11101 places 1, 2, and 3 (numbered from the left) can be taken as the information places. If a general letter of the alphabet is $a_1a_2a_3a_4a_5$, then $a_4 = a_2 + a_3$, $a_5 = a_1 + a_2 + a_3$.

Two group alphabets are called *equivalent* if one can be obtained from the other by a permutation of places. Example: the 7 distinct (3, 2)-alphabets given in (3) separate into three equivalence classes. Alphabets (i), (ii), and (iv) are equivalent; alphabets (iii), (v), (vi), are equivalent; (vii) is in a class by itself.

Proposition 3. Equivalent (n, k)-alphabets have the same probability Q_1 of correct transmission for each letter.

Proposition 4. Every (n, k)-alphabet is equivalent to an (n, k)-alphabet whose first k places are information places and whose last $n - k$ places are determined by parity checks over the first k places.

Henceforth we shall be concerned only with (n, k)-alphabets whose first k places are information places. The parity check rules can then be written

$$a_i = \sum_{j=1}^{k} \gamma_{ij} a_j, \qquad i = k + 1, \cdots, n \tag{9}$$

where the sums are of course mod 2. Here, as before, a typical letter of the alphabet is the sequence $a_1a_2 \cdots a_n$. The γ_{ij} are $k(n - k)$ quantities, zero or one, that serve to define the particular (n, k)-alphabet in question.

1.8 MAXIMUM LIKELIHOOD DETECTION BY PARITY CHECKS

For any element, T, of B_n we can form the sum given on the right of (9). This sum may or may not agree with the symbol in the ith place of

T. If it does, we say T satisfies the ith-place parity check; otherwise T fails the ith-place parity check. When a set of parity check rules (9) is given, we can associate an $(n - k)$-place binary sequence, $R(T)$, with each element T of B_n. We examine each check place of T in order starting with the $(k + 1)$-st place of T. We write a zero if a place of T satisfies the parity check; we write a one if a place fails the parity check. The resultant sequence of zeros and ones, written from left to right is $R(T)$. We call $R(T)$ the *parity check sequence* of T. Example: with the parity rules $a_4 = a_2 + a_3$, $a_5 = a_1 + a_2 + a_3$ used to define the (5, 3)-alphabet in the examples of Theorem 3, we find $R(11000) = 10$ since the sum of the entries in the second and third places of 11001 is not the entry of the fourth place and since the sum of $a_1 = 1$, $a_2 = 1$, and $a_3 = 0$ is $0 = a_5$.

Theorem 4. Let $I, A_2, \cdots A_\mu$ be an (n, k)-alphabet. Let $R(T)$ be the parity check sequence of an element T of B_n formed in accordance with the parity check rules of the (n, k)-alphabet. Then $R(T_1) = R(T_2)$ if and only if T_1 and T_2 lie in the same row of array (4). The coset leaders can be ordered so that $R(S_i)$ is the binary symbol for the integer $i - 1$.

As an example of Theorem 4 consider the (4, 2)-alphabet shown with its cosets below

0000	1011	0101	1110
0100	1111	0001	1010
0010	1001	0111	1100
1000	0011	1101	0110

The parity check rules for this alphabet are $a_3 = a_1$, $a_4 = a_1 + a_2$. Every element of the second row of this array satisfies the parity check in the third place and fails the parity check in the 4th place. The parity check sequence for the second row is 01. The parity check for the third row is 10, and for the fourth row 11. Since every letter of the alphabet satisfies the parity checks, the parity check sequence for the first row is 00. We therefore make the following association between parity check sequences and coset leaders

$$\begin{aligned} 00 &\rightarrow 0000 = S_1 \\ 01 &\rightarrow 0100 = S_2 \\ 10 &\rightarrow 0010 = S_3 \\ 11 &\rightarrow 1000 = S_4 \end{aligned}$$

1.9 INSTRUMENTING A GROUP ALPHABET

Proposition 4 attests to the ease of the encoding operation involved

with the use of an (n, k)-alphabet. If the original message is presented as a long sequence of zeros and ones, the sequence is broken into blocks of length k places. Each block is used as the first k places of a letter of the signaling alphabet. The last n-k places of the letter are determined by fixed parity checks over the first k places.

Theorem 4 demonstrates the relative ease of instrumenting the maximum likelihood detector (8) for use with an (n, k)-alphabet. When an element T of B_n is received at the channel output, it is subjected to the n-k parity checks of the alphabet being used. This results in a parity check sequence $R(T)$. $R(T)$ serves to identify a unique coset leader, say S_i. The product S_iT is then formed and produced as the detector output. The probability that this be the correct letter of the alphabet is Q_1.

1.10 BEST GROUP ALPHABETS

Two important questions regarding (n, k)-alphabets naturally arise. What is the maximum value of Q_1 possible for a given n and k and which of the $N(n, k)$ different subgroups give rise to this maximum Q_1? The answers to these questions for general n and k are not known. For many special values of n and k the answers are known. They are presented in Tables II, III and IV, which are explained below.

The probability Q_1 that a transmitted letter be produced correctly by the detector is the sum, $Q_1 = \sum_1^\nu \ell(S_i)$ of the probabilities of the coset leaders. This sum can be rewritten as $Q_1 = \sum_{i=0}^{n} \alpha_i\, p^i q^{n-i}$ where α_i is the number of coset leaders of weight i. One has, of course, $\sum \alpha_i = \nu = 2^{n-k}$ for an (n, k)-alphabet. Also $\alpha_i \leqq \binom{n}{i} = \dfrac{n!}{i!(n-i)!}$ since this is the number of elements of B_n of weight i.

The α_i have a special physical significance. Due to the noise on the channel, a transmitted letter, A_i, of an (n, k)-alphabet will in general be received at the channel output as some element T of B_n different from A_i. If T differs from A_i in s places, i.e., if $w(A_iT) = s$, we say that an s-tuple error has occurred. For a given (n, k)-alphabet, α_i is the number of i-tuple errors which can be corrected by the alphabet in question, $i = 0, 1, 2, \cdots, n$.

Table II gives the α_i corresponding to the largest possible value of Q_1 for a given k and n for $k = 2, 3, \cdots n-1$, $n = 4 \cdots, 10$ along with a few other scattered values of n and k. For reference the binomial coefficients $\binom{n}{i}$ are also listed. For example, we find from Table II that the best group alphabet with $2^4 = 16$ letters that uses $n = 10$ places has a

probability of correct transmission $Q_1 = q^{10} + 10q^9p + 39q^8p^2 + 14q^7p^3$. The alphabet corrects all 10 possible single errors. It corrects 39 of the possible $\binom{10}{2} = 45$ double errors (second column of Table II) and in addition corrects 14 of the 120 possible triple errors. By adding an additional place to the alphabet one obtains with the best (11, 4)-alphabet an alphabet with 16 letters that corrects all 11 possible single errors and all 55 possible double errors as well as 61 triple errors. Such an alphabet might be useful in a computer representing decimal numbers in binary form.

For each set of α's listed in Table II, there is in Table III a set of parity check rules which determines an (n, k)-alphabet having the given α's. The notation used in Table III is best explained by an example. A (10, 4)-alphabet which realizes the α's discussed in the preceding paragraph can be obtained as follows. Places 1, 2, 3, 4 carry the information. Place 5 is determined to make the mod 2 sum of the entries in places 3, 4, and 5 equal to zero. Place 6 is determined by a similar parity check on places 1, 2, 3, and 6; place 7 by a check on places 1, 2, 4, and 7, etc.

It is a surprising fact that for all cases investigated thus far an (n, k)-alphabet best for a given value of p is uniformly best for all values of p, $0 \leqq p \leqq \frac{1}{2}$. It is of course conjectured that this is true for all n and k.

It is a further (perhaps) surprising fact that the best (n, k)-alphabets are not necessarily those with greatest nearest neighbor distance between letters when the alphabets are regarded as point configurations on the n-cube. For example, in the best (7, 3)-alphabet as listed in Table III, each letter has two nearest neighbors distant 3 edges away. On the other hand, in the (7, 3)-alphabet given by the parity check rules 413, 512, 623, 7123 each letter has its nearest neighbors 4 edges away. This latter alphabet does not have as large a value of Q_1, however, as does the (7, 3)-alphabet listed on Table III.

The cases $k = 0, 1, n - 1, n$ have not been listed in Tables II and III. The cases $k = 0$ and $k = n$ are completely trivial. For $k = 1$, all $n > 1$ the best alphabet is obtained using the parity rule $a_2 = a_3 = \cdots = a_n = a_1$. If $n = 2j$,

$$Q_1 = \sum_0^{j-1} \binom{n}{i} p^i q^{n-i} + \frac{1}{2}\binom{n}{j} p^j q^j. \text{ If } n = 2j + 1, Q_1 = \sum_0^{j} \binom{n}{i} p^i q^{n-i}.$$

For $k = n - 1$, $n > 1$, the maximum Q_1 is $Q_1 = q^{n-1}$ and a parity rule for an alphabet realizing this Q_1 is $a_n = a_1$.

If the α's of an (n, k)-alphabet are of the form $\alpha_i = \binom{n}{i}$, $i = 0, 1,$

TABLE II — PROBABILITY OF NO ERROR WITH BEST ALPHABETS, $Q_1 = \sum \alpha_i p^i q^{n-i}$

	i	$\binom{n}{i}$	$k=2$ a_i	$k=3$ a_i	$k=4$ a_i	$k=5$ a_i	$k=6$ a_i	$k=7$ a_i	$k=8$ a_i	$k=9$ a_i	$k=10$ a_i
$n=4$	0	1	1								
	1	4	3								
$n=5$	0	1	1	1							
	1	5	5	3							
	2	10	2								
$n=6$	0	1	1	1	1						
	1	6	6	6	3						
	2	15	9	1							
$n=7$	0	1	1	1	1	1					
	1	7	7	7	7	3					
	2	21	18	8							
	3	25	6								
$n=8$	0	1	1	1	1	1	1				
	1	8	8	8	8	7	3				
	2	28	28	20	7						
	3	56	27	3							
$n=9$	0	1	1	1	1	1	1	1			
	1	9	9	9	9	9	7	3			
	2	36	36	33	22	6					
	3	84	64	21							
	4	126	18								
$n=10$	0	1	1	1	1	1	1	1	1		
	1	10	10	10	10	10	10	7	3		
	2	45	45	45	39	21	5				
	3	120	110	64	14						
	4	210	90	8							
$n=11$	0	1	1	1	1		1	1	1	1	
	1	11	11	11	11		11	11	7	3	
	2	55	55	55	55		20	4			
	3	165	165	126	61						
	4	330	226	63							
	5	462	54								
$n=12$	0	1	1	1				1	1	1	1
	1	12	12	12				12	12	7	3
	2	66	66	66				19	3		
	3	220	220	200							
	4	495	425	233							
	5	792	300								

$2, \cdots, j$, $\alpha_{j+1} = r$ some integer, $\alpha_{j+2} = \alpha_{j+3} = \cdots = \alpha_n = 0$, then there does not exist a 2^k-letter, n-place alphabet of any sort better than the given (n, k)-alphabet. It will be observed that many of the α's of Table II are of this form. It can be shown that

Proposition 5 if $n + \binom{n-k}{2} + \binom{n-k}{3} \geqq 2^{n-k} - 1$ there exists no 2^k-letter, n-place alphabet better than the best (n, k)-alphabet.

When the inequality of proposition 5 holds the α's are either $\alpha_0 = 1$, $\alpha_1 = 2^{n-k} - 1$, all other $\alpha = 0$; or $\alpha_0 = 1$, $\alpha_1 = \binom{n}{1}$, $\alpha_2 = 2^{n-k} - 1 - \binom{n}{1}$ all other $\alpha = 0$; or the trivial $\alpha_0 = 1$ all other $\alpha = 0$ which holds when $k = n$. The region of the $n - k$ plane for which it is known that (n, k)-alphabets cannot be excelled by any other is shown in Table IV.

1.11 A DETAILED EXAMPLE

As an example of the use of (n, k)-alphabets consider the not unrealistic case of a channel with $p = 0.001$, i.e., on the average one binary digit per thousand is received incorrectly. Suppose we wish to transmit messages using 32 different letters. If we encode the letters into the 32 5-place binary sequences and transmit these sequences without further encoding, the probability that a received letter be in error is $1 - (1 - p)^5 = 0.00449$. If the best (10, 5)-alphabet as shown in Tables II and III is used, the probability that a letter be wrong is $1 - Q_1 = 1 - q^{10} - 10q^9p - 21q^8p^2 = 24p^2 - 72p^3 + \cdots = 0.000024$. Thus by reducing the signaling rate by $\frac{1}{2}$, a more than *one hundredfold* reduction in probability of error is accomplished.

A (10, 5)-alphabet to achieve these results is given in Table III. Let a typical letter of the alphabet be the 10-place sequence of binary digits $a_1a_2 \cdots a_9a_{10}$. The symbols $a_1a_2a_3a_4a_5$ carry the information and can be any of 32 different arrangements of zeros and ones. The remaining places are determined by

$$
\begin{aligned}
a_6 &= a_1 \dot{+} a_3 \dot{+} a_4 \dot{+} a_5 \\
a_7 &= a_1 \dot{+} a_2 \dot{+} a_4 \dot{+} a_5 \\
a_8 &= a_1 \dot{+} a_2 \dot{+} a_3 \dot{+} a_5 \\
a_9 &= a_1 \dot{+} a_2 \dot{+} a_3 \dot{+} a_4 \\
a_{10} &= a_1 \dot{+} a_2 \dot{+} a_3 \dot{+} a_4 \dot{+} a_5
\end{aligned}
$$

To design the detector for this alphabet, it is first necessary to determine the coset leaders for a standard array (4) formed for this alphabet.

Table III — Parity Check Rules for Best Alphabets

	$k = 2$	$k = 3$	$k = 4$	$k = 5$	$k = 6$	$k = 7$	$k = 8$	$k = 9$	$k = 10$
$n = 4$	3 2 4 1 2								
$n = 5$	3 1 2 4 2 5 1	4 1 2 5 1 3							
$n = 6$	3 2 4 1 2 5 1 6 1	4 1 2 5 1 3 6 2 3	5 1 2 3 6 1 2 4						
$n = 7$	3 1 4 1 5 1 6 1 2 7 2	4 1 3 5 1 2 6 1 2 3 7 1 2 3	5 1 3 4 6 1 2 4 7 1 2 3	6 1 7 1					
$n = 8$	3 1 4 1 5 2 6 2 7 1 2 8 1 2	4 1 5 1 2 6 1 3 7 2 3 8 1 2 3	5 1 3 4 6 1 2 4 7 1 2 3 8 1 2 3 4	6 1 3 4 7 1 2 4 8 1 2 3	7 1 8 1				
$n = 9$	3 1 4 1 5 1 6 2 7 2 8 1 2 9 1 2	4 1 5 2 6 1 2 7 1 3 8 2 3 9 1 2 3	5 1 3 4 6 1 2 4 7 1 2 3 8 1 2 3 9 1 2 3	6 1 3 4 5 7 1 2 4 5 8 1 2 3 5 9 1 2 3 4	7 1 3 4 8 1 2 4 9 1 2 3	8 1 9 1			

$n = 10$	3 1 4 1 5 1 6 2 7 2 8 1 2 9 1 2 10 1 2	4 1 5 2 6 3 7 1 2 8 1 3 9 2 3 10 1 2 3	5 3 4 6 1 2 3 7 1 2 4 8 1 3 4 9 2 3 4 10 1 2 3 4	6 1 3 4 5 7 1 2 4 5 8 1 2 3 5 9 1 2 3 4 10 1 2 3 4 5	7 1 3 4 5 8 1 2 4 5 9 1 2 3 5 6 10 1 2 3 4 6	8 1 3 4 9 1 2 4 10 1 2 3	9 1 10 1		
$n = 11$	3 1 4 1 5 1 6 2 7 2 8 2 9 1 2 10 1 2 11 1 2	4 3 5 3 6 2 7 1 3 8 1 3 9 1 2 10 1 2 3 11 1 2 3	5 1 3 6 2 4 7 1 4 8 2 3 9 1 3 4 10 2 3 4 11 1 2 3 4		7 1 3 4 5 6 8 1 2 4 5 6 9 1 2 3 5 6 10 1 2 3 4 6 11 1 2 3 4 5	8 1 3 4 5 9 1 2 4 5 7 10 1 2 3 5 6 11 1 2 3 4 6 7	9 1 3 4 10 1 2 4 11 1 2 3	10 1 11 1	
$n = 12$	3 1 4 1 5 1 6 1 7 2 8 2 9 2 10 2 11 1 2 12 1 2	4 1 5 2 6 3 7 1 2 8 1 2 9 1 3 10 2 3 11 1 2 3 12 1 2 3				8 1 3 4 5 6 9 1 2 4 5 6 10 1 2 3 5 6 7 11 1 2 3 4 6 7 12 1 2 3 4 5 7	9 1 2 3 5 6 7 8 10 1 2 3 4 6 11 1 2 4 5 7 12 1 3 4 5 8	10 1 2 3 11 1 2 4 12 1 3 4	11 1 12 1

TABLE IV — REGION OF THE n-k PLANE FOR WHICH IT IS KNOWN THAT (n, k)-ALPHABETS CANNOT BE EXCELLED

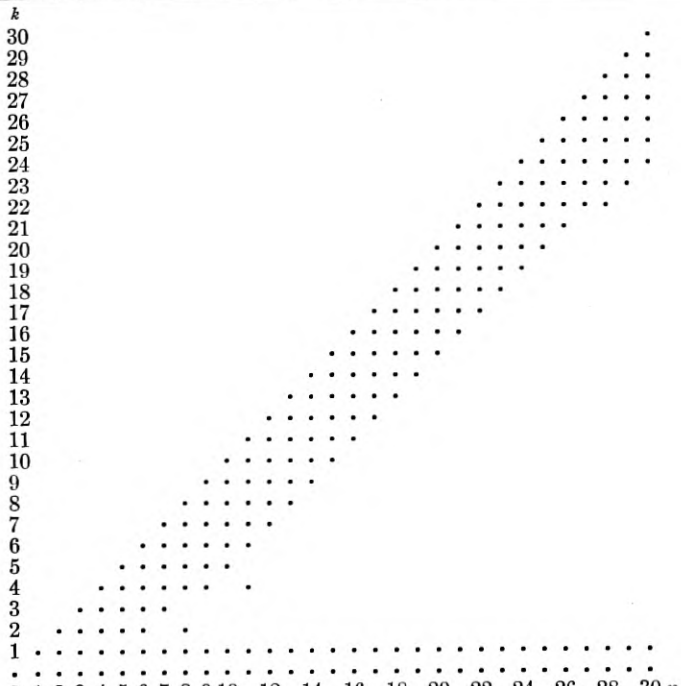

This can be done by a variety of special methods which considerably reduce the obvious labor of making such an array. A set of best S's along with their parity check symbols is given in Table V.

A maximum likelihood detector for the (10, 5)-alphabet in question forms from each received sequence $b_1b_2 \cdots b_{10}$ the parity check symbol $c_1c_2c_3c_4c_5$ where

$$
\begin{aligned}
c_1 &= b_6 + b_1 + b_3 + b_4 + b_5 \\
c_2 &= b_7 + b_1 + b_2 + b_4 + b_5 \\
c_3 &= b_8 + b_1 + b_2 + b_3 + b_5 \\
c_4 &= b_9 + b_1 + b_2 + b_3 + b_4 \\
c_5 &= b_{10} + b_1 + b_2 + b_3 + b_4 + b_5
\end{aligned}
$$

According to Table V, if $c_1c_2c_3c_4c_5$ contains less than three ones, the detector should brint $b_1b_2b_3b_4b_5$. The detector should print $(b_1 + 1)b_2b_3b_4b_5$ if the parity check sequence $c_1c_2c_3c_4c_5$ is either 11111 or 11110; the de-

TABLE V — COSET LEADERS AND PARITY CHECK SEQUENCES FOR (10,5)-ALPHABET

$c_1c_2c_3c_4c_5$	$\leftrightarrow$	S	$c_1c_2c_3c_4c_5$	$\leftrightarrow$	S
00000		0000000000	11100		0000100001
10000		0000010000	11010		0001000001
01000		0000001000	11001		0001000010
00100		0000000100	10110		0010000001
00010		0000000010	10101		0010000010
00001		0000000001	10011		0010000100
11000		0000011000	01110		0100000001
10100		0000010100	01101		0100000010
10010		0000010010	01011		0100000100
10001		0000010001	00111		0100001000
01100		0000001100	11110		1000000001
01010		0000001010	11101		0000100000
01001		0000001001	11011		0001000000
00110		0000000110	10111		0010000000
00101		0000000101	01111		0100000000
00011		0000000011	11111		1000000000

tector should print $b_1(b_2 \dotplus 1)b_3b_4b_5$ if the parity check sequence is 01111, 00111, 01011, 01101, or 01110; the detector should print $b_1b_2(b_3 \dotplus 1)b_4b_5$ if the parity check sequence is 10111, 10011, 10101, or 10110; the detector should print $b_1b_2b_3(b_4 \dotplus 1)b_5$ if the parity check sequence is 11011, 11001, 11010; and finally the detector should print $b_1b_2b_3b_4(b_5 \dotplus 1)$ if the parity check sequence is 11101 or 11100.

Simpler rules of operation for the detector may possibly be obtained by choice of a different set of S's in Table V. These quantities in general are not unique. Also there may exist non-equivalent alphabets with simpler detector rules that achieve the same probability of error as the alphabet in question.

PART II — ADDITIONAL THEORY AND PROOFS OF THEOREMS OF PART I

2.1 THE ABSTRACT GROUP C_n

It will be helpful here to say a few more words about B_n, the group of n-place binary sequences under the operation of addition mod 2. This group is simply isomorphic with the abstract group C_n generated by n commuting elements of order two, say $a_1, a_2, \cdots, a_n$. Here $a_ia_j = a_ja_i$ and $a_i^2 = I$, $i, j = 1, 2, \cdots, n$, where I is the identity for the group. The eight distinct elements of C_3 are, for example, I, a_1, a_2, a_3, a_1a_2, a_1a_3, a_2a_3, $a_1a_2a_3$. The group C_n is easily seen to be isomorphic with the n-fold direct product of the group C_1 with itself.

It is a considerable saving in notation in dealing with C_n to omit the symbol "a" and write only the subscripts. In this notation for example, the elements of C_4 are I, 1, 2, 3, 4, 12, 13, 14, 23, 24, 34, 123, 124, 134, 234, 1234. The product of two or more elements of C_n can readily be written down. Its symbol consists of those numerals that occur an odd number of times in the collection of numerals that comprise the symbols of the factors. Thus, (12)(234)(123) = 24.

The isomorphism between C_n and B_n can be established in many ways. The most convenient way, perhaps, is to associate with the element $i_1 i_2 i_3 \cdots i_k$ of C_n the element of B_n that has ones in places $i_1, i_2, \cdots, i_k$ and zeros in the remaining $n - k$ places. For example, one can associate 124 of C_4 with 1101 of B_4; 14 with 1001, etc. In fact, the numeral notation afforded by this isomorphism is a much neater notation for B_n than is afforded by the awkward strings of zeros and ones. There are, of course, other ways in which elements of C_n can be paired with elements of B_n so that group multiplication is preserved. The collection of all such "pairings" makes up the group of automorphisms of C_n. This group of automorphisms of C_n is isomorphic with the group of non-singular linear homogenous transformations in a field of characteristic 2.

An element T of C_n is said to be *dependent* upon the set of elements $T_1, T_2, \cdots, T_j$ of C_n if T can be expressed as a product of some elements of the set $T_1, T_2, \cdots, T_j$; otherwise, T is said to be *independent* of the set. A set of elements is said to be independent if no member can be expressed solely in terms of the other members of the set. For example, in C_8, 1, 2, 3, 4 form a set of independent elements as do likewise 2357, 12357, 14. However, 135 depends upon 145, 3457, 57 since 135 = (145)(3457)(57). Clearly any set of n independent elements of C_n can be taken as generators for the group. For example, all possible products formed of 12, 123, and 23 yield the elements of C_3.

Any k independent elements of C_n serve as generators for a subgroup of order 2^k. The subgroup so generated is clearly isomorphic with C_k. All subgroups of C_n of order 2^k can be obtained in this way.

The number of ways in which k independent elements can be chosen from the 2^n elements of C_n is

$$F(n, k) = (2^n - 2^0)(2^n - 2^1)(2^n - 2^2) \cdots (2^n - 2^{k-1})$$

For, the first element can be chosen in $2^n - 1$ ways (the identity cannot be included in a non-trivial set of independent elements) and the second element can be chosen in $2^n - 2$ ways. These two elements determine a subgroup of order 2^2. The third element can be chosen as any element of the remaining $2^n - 2^2$ elements. The 3 elements chosen determine a

subgroup of order 2^3. A fourth independent element can be chosen as any of the remaining $2^n - 2^3$ elements, etc.

Each set of k independent elements serves to generate a subgroup of order 2^k. The quantity $F(n, k)$ is not, however, the number of distinct subgroups of C_n of this order, for, a given subgroup can be obtained from many different sets of generators. Indeed, the number of different sets of generators that can generate a given subgroup of order 2^k of C_n is just $F(k, k)$ since any such subgroup is isomorphic with C_k. Therefore the number of subgroups of C_n of order 2^k is $N(n, k) = F(n, k)/F(k, k)$ which is (2). A simple calculation gives $N(n, k) = N(n, n - k)$.

2.2 PROOF OF PROPOSITIONS 1 AND 2

After an element A of B_n has been presented for transmission over a noisy binary channel, an element T of B_n is produced at the channel output. The element $U = AT$ of B_n serves as a record of the noise during the transmission. U is an n-place binary sequence with a one at each place altered in A by the noise. The channel output, T, is obtained from the input A by multiplication by U: $T = UA$. For channels of the sort under consideration here, the probability that U be any particular element of B_n of weight w is $p^w q^{n-w}$.

Consider now signaling with a particular (n, k)-alphabet and consider the standard array (4) of the alphabet. If the detection scheme (8) is used, a transmitted letter A_i will be produced without error if and only if the received symbol is of the form $S_j A_i$. That is, there will be no error only if the noise in the channel during the transmission of A_i is represented by one of the coset leaders. (This applies for $i = 1, 2, \cdots, \mu = 2^k$). The probability of this event is Q_1 (Proposition 1, Section 1.6). The convention (5) makes Q_1 as large as is possible for the given alphabet.

Let X refer to transmitted letters and let Y refer to letters produced by the detector. We use a vertical bar to denote conditions when writing probabilities. The quantity to the right of the bar is the condition. We suppose the letters of the alphabet to be chosen independently with equal probability 2^{-k}.

The equivocation $h(X \mid Y)$ obtained when using an (n, k)-alphabet with the detector (8) can most easily be computed from the formula

$$h(X \mid Y) = h(X) - h(Y) + h(Y \mid X) \tag{10}$$

The entropy of the source is $h(X) = k/n$ bits per symbol. The probability that the detector produce A_j when A_i was sent is the probability that the noise be represented by $A_i A_j S_\ell$, $\ell = 1, 2, \cdots, \nu$. In symbols,

$$Pr(Y \rightarrow A_j \mid X \rightarrow A_i) = \sum_t Pr(N \rightarrow A_i A_j S_t) = Q(A_i A_j)$$

where $Q(A_i)$ is the sum of the probabilities of the elements that are in the same column as A_i in the standard array. Therefore

$$Pr(Y \rightarrow A_j) = \sum_i Pr(Y \rightarrow A_j \mid X \rightarrow A_i) Pr(X \rightarrow A_i) = \frac{1}{2^k} \sum_i Q(A_i A_j)$$

$$= \frac{1}{2^k}, \qquad \text{since } \sum_i Q(A_i A_j) = \sum_i Q(A_i) = 1.$$

This last follows from the group property of the alphabet. Therefore

$$h(Y) = -\frac{1}{n} \sum Pr(Y \rightarrow A_j) \log Pr(Y \rightarrow A_j) = \frac{k}{n} \text{ bits/symbol.}$$

It follows then from (10) that

$$h(X \mid Y) = h(Y \mid X)$$

The computation of $h(Y \mid X)$ follows readily from its definition

$$h(Y \mid X) = \sum_i Pr(X \rightarrow A_i) h(Y \mid X \rightarrow A_i)$$

$$= -\sum_{ij} Pr(X \rightarrow A_i) Pr(Y \rightarrow A_j \mid X \rightarrow A_i)$$

$$\log Pr(Y \rightarrow A_j \mid X \rightarrow A_i)$$

$$= -\frac{1}{2^k} \sum_{ij} \sum_t Pr(N \rightarrow A_i S_t A_j) \log \sum_m Pr(N \rightarrow A_i S_m A_j)$$

$$= -\frac{1}{2^k} \sum_{ij} Q(A_i A_j) \log Q(A_i A_j)$$

$$= -\sum_i Q(A_i) \log Q(A_i)$$

Each letter is n binary places. Proposition 2, then follows.

2.3 DISTANCE AND THE PROOF OF THEOREM 1

Let A and B be two elements of B_n. We define the *distance*, $d(A, B)$, between A and B to be the weight of their product,

$$d(A, B) = w(AB) \tag{11}$$

The distance between A and B is the number of places in which A and B differ and is just the "Hamming distance." [1] In terms of the n-cube, $d(A, B)$ is the minimum number of edges that must be traversed to go

from vertex A to vertex B. The distance so defined is a monotone function of the Euclidean distance between vertices.

It follows from (11) that if C is any element of B_n then

$$d(A, B) = d(AC, BC) \tag{12}$$

This fact shows the detection scheme (8) to be a maximum likelihood detector. By definition of a standard array, one has

$$d(S_i, I) \leqq d(S_iA_j, I) \qquad \text{for all } i \text{ and } j$$

The coset leaders were chosen to make this true. From (12),

$$\begin{aligned} d(S_i, I) &= d(S_iA_mS_i, I\,A_mS_i) = d(S_iA_m, A_m) \\ d(S_iA_j, I) &= d(S_iA_jS_iA_m, I\,S_iA_m) = d(A_jA_m, S_iA_m) \\ &= d(S_iA_m, A_\ell) \end{aligned}$$

where $A_\ell = A_jA_m$. Substituting these expressions in the inequality above yields

$$d(S_iA_m, A_m) \leqq d(S_iA_m, A_\ell) \qquad \text{for all } i, m, \ell$$

This equation says that an arbitrary element in the array (4) is at least as close to the element at the top of its column as it is to any other letter of the alphabet. This is the maximum likelihood property.

2.4 PROOF OF THEOREM 2

Again consider an (n, k)-alphabet as a set of vertices of the unit n-cube. Consider also n mutually perpendicular hyperplanes through the centroid of the cube parallel to the coordinate planes. We call these planes "symmetry planes of the cube" and suppose the planes numbered in accordance with the corresponding parallel coordinate planes.

The reflection of the vertex with coordinates $(a_1, a_2, \cdots, a_i, \cdots, a_n)$ in symmetry plane i yields the vertex of the cube whose coordinates are $(a_1, a_2, \cdots, a_i \dotplus 1, \cdots, a_n)$. More generally, reflecting a given vertex successively in symmetry planes $i, j, k, \cdots$ yields a new vertex whose coordinates differ from the original vertex precisely in places $i, j, k \cdots$. Successive reflections in hyperplanes constitute a transformation that leaves distances between points unaltered and is therefore a "rotation." The rotation obtained by reflecting successively in symmetry planes i, j, k, etc. can be represented by an n-place symbol having a one in places i, j, k, etc. and a zero elsewhere.

We now regard a given (n, k)-alphabet as generated by operating on the vertex $(0, 0, \cdots, 0)$ of the cube with a certain collection of 2^k ro-

tation operators. The symbols for these operators are identical with the sequences of zeros and ones that form the coordinates of the 2^k points. It is readily seen that these rotation operators form a group which is transitive on the letters of the alphabet and which leave the unit cube invariant. Theorem 2 then follows.

Theorem 2 also follows readily from consideration of the array (4). For example, the maximum likelihood region associated with I is the set of points I, S_2, S_3, $\cdots$, S_ν. The maximum likelihood region associated with A_i is the set of points A_i, A_iS_2, A_iS_3, $\cdots$, A_iS_ν. The rotation (successive reflections in symmetry planes of the cube) whose symbol is the same as the coordinate sequence of A_i sends the maximum likelihood region of I into the maximum likelihood region of A_i, $i = 1, 2, \cdots, \mu$.

2.5 PROOF OF THEOREM 3

That every systematic alphabet is a group alphabet follows trivially from the fact that the sum mod 2 of two letters satisfying parity checks is again a letter satisfying the parity checks. The totality of letters satisfying given parity checks thus constitutes a finite group.

To prove that every group alphabet is a systematic code, consider the letters of a given (n, k)-alphabet listed in a column. One obtains in this way a matrix with 2^k rows and n columns whose entries are zeros and ones. Because the rows are distinct and form a group isomorphic to C_k, there are k linearly independent rows (mod 2) and no set of more than k independent rows. The rank of the matrix is therefore k. The matrix therefore possesses k linearly independent (mod 2) columns and the remaining $n - k$ columns are linear combinations of these k. Maintaining only these k linearly independent columns, we obtain a matrix of k columns and 2^k rows with rank k. This matrix must, therefore, have k linearly independent rows. The rows, however, form a group under mod 2 addition and hence, since k are linearly independent, all 2^k rows must be distinct. The matrix contains only zeros and ones as entries; it has 2^k distinct rows of k entries each. The matrix must be a listing of the numbers from 0 to $2^k - 1$ in binary notation. The other $n - k$ columns of the original matrix considered are linear combinations of the columns of this matrix. This completes the proof of Theorem 3 and Proposition 4.

2.6 PROOF OF THEOREM 4

To prove Theorem 4 we first note that the parity check sequence of the product of two elements of B_n is the mod 2 sum of their separate

parity check sequences. It follows then that all elements in a given coset have the same parity check sequence. For, let the coset be S_i, S_iA_2, S_iA_3, $\cdots$ S_iA_μ. Since the elements $I, A_2, A_3, \cdots, A_\mu$ all have parity check sequence $00 \cdots 0$, all elements of the coset have parity check $R(S_i)$.

In the array (4) there are 2^{n-k} cosets. We observe that there are 2^{n-k} elements of B_n that have zeros in their first k places. These elements have parity check symbols identical with the last $n - k$ places of their symbols. These elements therefore give rise to 2^{n-k} different parity check symbols. The elements must be distributed one per coset. This proves Theorem 4.

2.7 PROOF OF PROPOSITION 5

If

$$n \geqq 2^{n-k} - \binom{n-k}{2} - \binom{n-k}{3} - 1$$

we can explicity exhibit group alphabets having the property mentioned in the paragraph preceding Proposition 5. The notation of the demonstration is cumbersome, but the idea is relatively simple.

We shall use the notation of paragraph 2.1 for elements of B_n, i.e., an element of B_n will be given by a list of integers that specify what places of the sequence for the element contain ones. It will be convenient furthermore to designate the first k places of a sequence by the integers $1, 2, 3, \cdots, k$ and the remaining $n - k$ places by the "integers" $1', 2', 3', \cdots, \ell'$, where $\ell = n - k$. For example, if $n = 8$, $k = 5$, we have

$$10111010 \leftrightarrow 13452'$$
$$10000100 \leftrightarrow 11'$$
$$00000101 \leftrightarrow 1'3'$$

Consider the group generated by the elements $1', 2', 3', \cdots, \ell'$, i.e. the 2^ℓ elements $I, 1', 2', \cdots, \ell', 1'2', 1'3', \cdots, 1'2'3' \cdots \ell'$. Suppose these elements listed according to decreasing weight (say in decreasing order when regarded as numbers in the decimal system) and numbered consecutively. Let B_i be the ith element in the list. Example: if $\ell = 3$, $B_1 = 1'2'3'$, $B_2 = 2'3'$, $B_3 = 1'3'$, $B_4 = 1'2'$, $B_5 = 3'$, $B_6 = 2'$, $B_7 = 1'$.

Consider now the (n, k)-alphabet whose generators are

$$1B_1, 2B_2, 3B_3, \cdots, kB_k$$

We assert that if

$$n \geqq 2^{n-k} - \binom{n-k}{2} - \binom{n-k}{3} - 1$$

this alphabet is as good as any other alphabet of 2^k letters and n places.

In the first place, we observe that every letter of this (n, k)-alphabet (except I) has unprimed numbers in its symbols. It follows that each of the 2^ℓ letters $I, 1', 2', \cdots, \ell', 1'2', \cdots, 1'2' \cdots \ell'$ occurs in a different coset of the given (n, k)-alphabet. For, if two of these letters appeared in the same coset, their product (which contains only primed numbers) would have to be a letter of the (n, k) alphabet. This is impossible since every letter of the (n, k) alphabet has unprimed numbers in its symbol. Since there are precisely 2^ℓ cosets we can designate a coset by the single element of the list $B_1, B_2, \cdots, B_{2^\ell} = I$ which appears in the coset.

We next observe that the condition

$$n \geqq 2^{n-k} - \binom{n-k}{2} - \binom{n-k}{3} - 1$$

guarantees that B_{k+1} is of weight 3 or less. For, the given condition is equivalent to

$$k \geqq 2^\ell - \binom{\ell}{0} - \binom{\ell}{1} - \binom{\ell}{2} - \binom{\ell}{3}$$

We treat several cases depending on the weight of B_{k+1}.

If B_{k+1} is of weight 3, we note that for $i = 1, 2, \cdots, k$, the coset containing B_i also contains an element of weight one, namely the element i obtained as the product of B_i with the letter iB_i of the given (n, k)-alphabet. Of the remaining $(2^\ell - k)$ B's, one is of weight zero, ℓ are of weight one, $\binom{\ell}{2}$ are of weight 2 and the remaining are of weight 3. We have, then $\alpha_0 = 1$, $\alpha_1 = \ell + k = n$. Now every B of weight 4 occurs in the list of generators $1B_1, 2B_2, \cdots, kB_k$. It follows that on multiplying this list of generators by any B of weight 3, at least one element of weight two will result. (E.g., $(1'2'3')(j1'2'3'4') = j4'$) Thus every coset with a B of weight 2 or 3 contains an element of weight 2 and $\alpha_2 = 2^\ell - \alpha_0 - \alpha_1$.

The argument in case B_{k+1} is of weight two or one is similar.

2.8 MODULAR REPRESENTATIONS OF C_n

In order to explain one of the methods used to obtain the best (n, k)-alphabets listed in Tables II and III, it is necessary to digress here to present additional theory.

It has been remarked that every (n, k)-alphabet is isomorphic with C_k. Let us suppose the elements of C_k listed in a column starting with I and proceeding in order I, 1, 2, 3, $\cdots$, k, 12, 13, $\cdots$, $(k-1)k$, 123, $\cdots \cdots$, 123 $\cdots$ k. The elements of a given (n, k)-alphabet can be paired off with these abstract elements so as to preserve group multiplication. This can be done in many different ways. The result is a matrix with elements zero and one with n columns and 2^k rows, these latter being labelled by the symbols I, 1, 2, $\cdots$ etc. What can be said about the columns of this matrix? How many different columns are possible when all (n, k)-alphabets and all methods of establishing isomorphism with C_k are considered?

In a given column, once the entries in rows 1, 2, $\cdots$, k are known, the entire column is determined by the group property. There are therefore only 2^k possible different columns for such a matrix. A table showing these 2^k possible columns of zeros and ones will be called a *modular representation* table for C_k. An example of such a table is shown for $k = 4$ in Table VI.

It is clear that the columns of a modular representation table can also be labelled by the elements of C_k, and that group multiplication of these column labels is isomorphic with mod 2 addition of the columns. The table is a symmetric matrix. The element with row label A and column label B is one if the symbols A and B have an odd number of different numerals in common and is zero otherwise.

Every (n, k)-alphabet can be made from a modular representation table by choosing n columns of the table (with possible repetitions) at least k of which form an independent set.

TABLE VI — MODULAR REPRESENTATION TABLE FOR GROUP C_4

	I	1	2	3	4	12	13	14	23	24	34	123	124	134	234	1234
I	0	0	0	0	0	0	0	0	0	0	0	0	0	0	0	0
1	0	1	0	0	0	1	1	1	0	0	0	1	1	1	0	1
2	0	0	1	0	0	1	0	0	1	1	0	1	1	0	1	1
3	0	0	0	1	0	0	1	0	1	0	1	1	0	1	1	1
4	0	0	0	0	1	0	0	1	0	1	1	0	1	1	1	1
12	0	1	1	0	0	0	1	1	1	1	0	0	0	1	1	0
13	0	1	0	1	0	1	0	1	1	0	1	0	1	0	1	0
14	0	1	0	0	1	1	1	0	0	1	1	1	0	0	1	0
23	0	0	1	1	0	1	1	0	0	1	1	0	1	1	0	0
24	0	0	1	0	1	1	0	1	1	0	1	1	0	1	0	0
34	0	0	0	1	1	0	1	1	1	1	0	1	1	0	0	0
123	0	1	1	1	0	0	0	1	0	1	1	1	0	0	0	1
124	0	1	1	0	1	0	1	0	1	0	1	0	1	0	0	1
134	0	1	0	1	1	1	0	0	1	1	0	0	0	1	0	1
234	0	0	1	1	1	1	1	1	0	0	0	0	0	0	1	1
1234	0	1	1	1	1	0	0	0	0	0	0	1	1	1	1	0

We henceforth exclude consideration of the column I of a modular representation table. Its inclusion in an (n, k)-alphabet is clearly a waste of 1 binary digit.

It is easy to show that every column of a modular representation table for C_k contains exactly 2^{k-1} ones. Since an (n, k)-alphabet is made from n such columns the alphabet contains a total of $n2^{k-1}$ ones and we have

Proposition 6. The weights of an (n, k)-alphabet form a partition of $n2^{k-1}$ into $2^k - 1$ non-zero parts, each part being an integer from the set $1, 2, \cdots, n$.

The identity element always has weight zero, of course.

It is readily established that the product of two elements of even weight is again an element of even weight as is the product of two elements of odd weight. The product of an element of even weight with an element of odd weight yields an element of odd weight.

The elements of even weight of an (n, k)-alphabet form a subgroup and the preceding argument shows that this subgroup must be of order 2^k or 2^{k-1}. If the group of even elements is of order 2^{k-1}, then the collection of even elements is a possible $(n, k-1)$-alphabet. This $(n, k-1)$ alphabet may, however, contain the column I of the modular representation table of C_{k-1}. We therefore have

Proposition 7. The partition of Proposition 6 must be either into $2^k - 1$ even parts or else into 2^{k-1} odd parts and $2^{k-1} - 1$ even parts. In the latter case, the even parts form a partition of $\alpha 2^{k-2}$ where α is some integer of the set $k - 1, k, \cdots, n$ and each of the parts is an integer from the set $1, 2, \cdots, n$.

2.9 THE CHARACTERS OF C_k

Let us replace the elements of B_n (each of which is a sequence of zeros and ones) by sequences of $+1$'s and -1's by means of the following substitution

$$\begin{aligned} 0 &\leftrightarrow 1 \\ 1 &\leftrightarrow -1. \end{aligned} \tag{13}$$

The multiplicative properties of elements of B_n can be preserved in this new notation if we define the product of two $+1$, -1 symbols to be the symbol whose ith component is the ordinary product of the ith components of the two factors. For example, 1011 and 0110 become respectively $-11\ -1\ -1$ and $1\ -1\ -11$. We have

$$(-11\ -1\ -1)(1\ -1\ -11) = (-1\ -11\ -1)$$

corresponding to the fact that

$$(1011)\ (0110) = (1101)$$

If the $+1$, -1 symbols are regarded as shorthand for diagonal matrices, so that for example

$$-11\ -1\ -1 \leftrightarrow \begin{vmatrix} -1 & 0 & 0 & 0 \\ 0 & 1 & 0 & 0 \\ 0 & 0 & -1 & 0 \\ 0 & 0 & 0 & -1 \end{vmatrix}$$

then group multiplication corresponds to matrix multiplication.

(While much of what follows here can be established in an elementary way for the simple group at hand, it is convenient to fall back upon the established general theory of group representations[8] for several propositions.

The substitution (13) converts a modular representation table (column I included) into a square array of $+1$'s and -1's. Each column (or row) of this array is clearly an irreducible representation of C_k. Since C_k is Abelian it has precisely 2^k irreducible representations each of degree one. These are furnished by the converted modular table. This table also furnishes then the characters of the irreducible representations of C_k and we refer to it henceforth as a *character table.*

Let $\chi^\alpha(A)$ be the entry of the character table in the row labelled A and column labelled α. The orthogonality relationship for characters gives

$$\sum_{A \subset C_k} \chi^\alpha(A)\chi^\beta(A) = 2^k\delta_{\alpha\beta}$$

$$\sum_{\alpha \subset C_k} \chi^\alpha(A)\chi^\alpha(B) = 2^k\delta_{AB}$$

where δ is the usual Kronecker symbol. In particular

$$\sum_{A \subset C_k} \chi^I(A)\chi^\beta(A) = \sum_{A \subset C_k} \chi^\beta(A) = 0, \qquad \beta \neq I$$

Since each $\chi^\beta(A)$ is $+1$ or -1, these must occur in equal numbers in any column $\beta \neq I$. This implies that each column except I of the modular representation table contains 2^{k-1} ones, a fact used earlier.

Every matrix representation of C_k can be reduced to its irreducible components. If the trace of the matrix representing the element A in an arbitrary matrix representation of C_k is $\chi(A)$, then this representation contains the irreducible representation having label β in the character table d_β times where

$$d_\beta = \frac{1}{2^k} \sum_{A \subset C_k} \chi(A)\chi^\beta(A) \tag{14}$$

Every (n, k)-alphabet furnishes us with a matrix representation of C_k by means of (13) and the procedure outlined below (13). The trace $\chi(A)$ of the matrix representing the element A of C_k is related to the weight of the letter by

$$\chi(A) = n - 2w(A) \tag{15}$$

Equations (14) and (15) permit us to compute from the weights of an (n, k)-alphabet what irreducible representations are present in the alphabet and how many times each is contained. It is assumed here that the given alphabet has been made isomorphic to C_k and that the weights are labelled by elements of C_k.

Consider the converse problem. Given a set of numbers $w_1, w_2, \cdots, w_{2^k}$ that satisfy Propositions 6 and 7. From these we can compute quantities $\chi_i = n - 2w_i$ as in (15). It is clear that the given w's will constitute the weights of an (n, k)-alphabet if and only if the 2^k χ_i can be labelled with elements of C_k so that the 2^k sums (14) (β ranges over all elements of C_k) are non-negative integers. The integers d_β tell what representations to choose to construct an (n, k)-alphabet with the given weights w_1.

2.10 CONSTRUCTION OF BEST ALPHABETS

A great many different techniques were used to construct the group alphabets listed in Tables II and III and to show that for each n and k there are no group alphabets with smaller probability of error. Space prohibits the exhibition of proofs for all the alphabets listed. We content ourselves here with a sample argument and treat the case $n = 10$, $k = 4$ in detail.

According to (2) there are $N(10, 4) = 53{,}743{,}987$ different (10, 4)-alphabets. We now show that none is better than the one given in Table III. The letters of this alphabet and weights of the letters are

I	0
1 6 7 8 10	5
2 6 7 9 10	5
3 5 6 8 9 10	6
4 5 7 8 9 10	6
1 2 8 9	4
1 3 5 7 9	5

1 4 5 6 9	5
2 3 5 7 8	5
2 4 5 6 8	5
3 4 6 7	4
1 2 3 5 7 9	6
1 2 4 5 7 10	6
1 3 4 8 10	5
2 3 4 9 10	5
1 2 3 4 6 7 8 9	8

The notation is that of Section 2.1. By actually forming the standard array of this alphabet, it is verified that

$$\alpha_0 = 1, \qquad \alpha_1 = 10, \qquad \alpha_2 = 39, \qquad \alpha_3 = 14.$$

Table II shows $\binom{10}{2} = 45$, whereas $\alpha_2 = 39$, so the given alphabet does not correct all possible double errors. In the standard array for the alphabet, 39 coset leaders are of weight 2. Of these 39 cosets, 33 have only one element of weight 2; the remaining 6 cosets each contain two elements of weight 2. This is due to the two elements of weight 4 in the given group, namely 1289 and 3467. A portion of the standard array that demonstrates these points is

I	1289	3467
.	.	.
.	.	.
12	89	.
18	29	.
19	28	.
34	.	67
36	.	47
37	.	46
.	.	.
.	.	.

In order to have a smaller probability of error than the exhibited alphabet, it is necessary that a (10, 4)-alphabet have an $\alpha_2 > 39$. We proceed to show that this is impossible by consideration of the weights of the letters of possible (10, 4)-alphabets.

We first show that every (10, 4)-alphabet must have at least one element (other than the identity, I) of weight less than 5. By Propositions 6 and 7, Section 2.8, the weights must form a partition of $10 \cdot 8 = 80$ into 15 positive parts. If the weights are all even, at least two must be less than 6 since $14 \cdot 6 = 84 > 80$. If eight of the weights are odd, we see from $8 \cdot 5 + 7 \cdot 6 = 82 > 80$ that at least one weight must be less than 5.

An alphabet with one or more elements of weight 1 must have an $\alpha_2 \leqq 36$, for there are nine elements of weight 2 which cannot possibly be coset leaders. To see this, suppose (without loss of generality) that the alphabet contains the letter 1. The elements 12, 13, 14, $\cdots$ 1 10 cannot possibly be coset leaders since the product of any one of them with the letter 1 yields an element of weight 1.

An alphabet with one or more elements of weight 2 must have an $\alpha_2 \leqq 37$. Suppose for example, the alphabet contained the letter 12. Then 13 and 23 must be in the same coset, 14 and 24 must be in the same coset, $\cdots$, 1 10 and 2 10 must be in the same coset. There are at least eight elements of weight two which are not coset leaders.

Each element of weight 3 in the alphabet prevents three elements of weight 2 from being coset leaders. For example, if the alphabet contains 123, then 12, 13, and 23 cannot be coset leaders. We say that the three elements of weight 2 are "blocked" by the letter of weight 3. Suppose an alphabet contains at least three letters of weight three. There are several cases: (A) if three letters have no numerals in common, e.g., 123, 456, 789, then nine distinct elements of weight 2 are blocked and $\alpha_2 \leqq 36$; (B) if no two of the letters have more than a single numeral in common, e.g., 123, 345, 789, then again nine elements of weight 2 are blocked and $\alpha_2 \leqq 36$; and (C) if two of the letters of weight 3 have two numerals in common, e.g., 123, 234, then their product is a letter of weight 2 and by the preceding paragraph $\alpha_2 \leqq 37$. If an alphabet contains exactly two elements of weight 3 and no elements of weight 2, the elements of weight 3 block six elements of weight 2 and $\alpha_2 \leqq 39$.

The preceding argument shows that to be better than the exhibited alphabet a (10, 4)-alphabet with letters of weight 3 must have just one such letter. A similar argument (omitted here) shows that to be better than the exhibited alphabet, a (10, 4)-alphabet cannot contain more than one element of weight 4. Furthermore, it is easily seen that an alphabet containing one element of weight 3 and one element of weight 4 must have an $\alpha_2 \leqq 39$.

The only new contenders for best (10, 4)-alphabet are, therefore, alphabets with a single letter other than I of weight less than 5, and this letter must have weight 3 or 4. Application of Propositions 6 and 7 show that the only possible weights for alphabets of this sort are: 35^76^7 and 5^846^6 where 5^7 means seven letters of weight 5, etc. We next show that there do not exist (10, 4)-alphabets having these weights.

Consider first the suggested alphabet with weights 35^76^7. As explained in Section 2.9, from such an alphabet we can construct a matrix representation of C_4 having the character $\chi(I) = 10$, one matrix of trace 4,

seven of trace 0 and seven of trace -2. The latter seven matrices correspond to elements of even weight and together with I must represent a subgroup of order 8. We associate them with the subgroup generated by the elements 2, 3, and 4. We have therefore

$$\chi(I) = 10, \qquad \chi(2) = \chi(3) = \chi(4) = \chi(23) = \chi(24) = \chi(34) = \chi(234) = -2.$$

Examination of the symmetries involved shows that it doesn't matter how the remaining χ_i are associated with the remaining group elements. We take, for example

$$\chi(1) = 4, \qquad \chi(12) = \chi(13) = \chi(14) = \chi(123) = \chi(124) = \chi(134) = \chi(1234) = 0.$$

Now form the sum shown in equation (14) with $\beta = 1234$ (i.e., with the character χ^{1234} obtained from column 1234 of the Table VI by means of substitution (13). There results $d_{1234} = \frac{1}{2}$ which is impossible. Therefore there does not exist a (10, 4)-alphabet with weights $35^{7}6^{7}$.

The weights $5^{8}46^{6}$ correspond to a representation of C_4 with character $\chi(I) = 10, 0^{8}, 2, (-2)^{6}$. We take the subgroup of elements of even weight to be generated by 2, 3, and 4. Except for the identity, it is clearly immaterial to which of these elements we assign the character 2. We make the following assignment: $\chi(I) = 10, \chi(2) = 2, \chi(3) = \chi(4) = \chi(23) = \chi(24) = \chi(34) = \chi(234) = -2, \quad \chi(1) = \chi(12) = \chi(13) = \chi(14) = \chi(123) = \chi(124) = \chi(134) = \chi(1234) = 0$. The use of equation (14) shows that $d_2 = \frac{1}{2}$ which is impossible.

It follows that of the 53,743,987 (10, 4)-alphabets, none is better than the one listed on Table III.

Not all the entries of Table III were established in the manner just demonstrated for the (10, 4)-alphabet. In many cases the search for a best alphabet was narrowed down to a few alphabets by simple arguments. The standard arrays for the alphabets were constructed and the best alphabet chosen. For large n the labor in making such a table can be considerable and the operations involved are highly liable to error when performed by hand.

I am deeply indebted to V. M. Wolontis who programmed the IBM CPC computer to determine the α's of a given alphabet and who patiently ran off many such alphabets in course of the construction of Tables II and III. I am also indebted to Mrs. D. R. Fursdon who evaluated many of the smaller alphabets by hand.

REFERENCES

1. R. W. Hamming, B.S.T.J., **29,** pp. 147–160, 1950.
2. I. S. Reed, Transactions of the Professional Group on Information Theory, PGIT-4, pp. 38–49, 1954.
3. See section 7 of R. W. Hamming's paper, loc. cit.
4. I.R.E. Convention Record, Part 4, pp. 37–45, 1955 National Convention, March, 1955.
5. C. E. Shannon, B.S.T.J., **27,** pp. 379–423 and pp. 623–656, 1948.
6. Birkhoff and MacLane, A Survey of Modern Algebra, Macmillan Co., New York, 1941. Van der Waerden, Modern Algebra, Ungar Co., New York, 1953. Miller, Blichfeldt, and Dickson, Finite Groups, Stechert, New York, 1938.
7. This theorem has been previously noted in the literature by Kiyasu-Zen'iti, Research and Development Data No. 4, Ele. Comm. Lab., Nippon Tele. Corp. Tokyo, Aug., 1953.
8. F. D. Murnaghan, Theory of Group Representations, Johns Hopkins Press, Baltimore, 1938. E. Wigner, Gruppentheorie, Edwards Brothers, Ann Arbor, Michigan, 1944.

Bell System Technical Papers Not Published in This Journal

ALLEN, L. J., see Fewer, D. R.

ALLISON, H. W., see Moore, G. E.

BAKER, W. O., see Winslow, F. H.

BARSTOW, J. M.[1]
Color TV — How it Works, I.R.E. Student Quarterly, **2,** pp. 11–16, Sept., 1955.

BASSECHES, H.[1] and MCLEAN, D. A.[1]
Gassing of Liquid Dielectrics Under Electrical Stress, Ind. & Engg. Chem., **47,** pp. 1782–1794, Sept., 1955.

BECK, A. C.[1]
Measurement Techniques for Multimode Waveguides, Proc. I.R.E., MRI, **4,** pp. 325–6, Oct. 1, 1955.

BECKER, J. A.[1]
The Life History of Adsorbed Atoms, Ions, and Molecules, N. Y. Acad. Sci. Ann., **58,** pp. 723–740, Sept. 15, 1955.

BLACKWELL, J. H., see Fewer, D. R.

BOORSE, H. A., see Smith, B.

BOZORTH, R. M.,[1] GETLIN, B. B.,[1] GALT, J. K.,[1] MERRITT, F. R.,[1] and YAGER, W. A.[1]
Frequency Dependence of Magnetocrystalline Anisotropy, Letter to the Editor, Phys. Rev., **99,** p. 1898, Sept. 15, 1955.

1. Bell Telephone Laboratories, Inc.

BOZORTH, R. M.[1], TILDEN, E. F.,[1] and WILLIAMS, A. J.[1]
Anisotropy and Magnetostriction of Some Ferrites, Phys. Rev., **99,** pp. 1788–1798, Sept. 15, 1955.

BRIDGERS, H. E.,[1] and KOLB, E. D.[1]
Rate-Grown Germanium Crystals for High-Frequency Transistors, Letter to the Editor, J. Appl. Phys., **26,** pp. 1188–1189, Sept., 1955.

BULLINGTON, K.[1]
Characteristics of Beyond-the-Horizon Radio Transmission, Proc. I.R.E., **43,** pp. 1175–1180, Oct., 1955.

BULLINGTON, K.[1] INKSTER, W. J.,[5] and DURKEE, A. L.[1]
Results of Propagation Tests at 505 Mc and 4,090 Mc on Beyond-Horizon Paths, Proc. I.R.E., **43,** pp. 1306–1316, Oct., 1955.

CALBICK, C. J.[1]
Surface Studies with the Electron Microscope, N. Y. Acad. Sci. Ann., **58,** pp. 873–892, Sept. 15, 1955.

CASS, R. S., see Fewer, D. R.

DURKEE, A. L., see Bullington, K.

FEWER, D. R.,[1] BLACKWELL, J. H.,[4] ALLEN, L. J.,[4] and CASS, R. S.[4]
Audio-Frequency Circuit Model of the 1-Dimensional Schroedinger Equation and Its Sources of Error, Canadian J. of Phys., **33,** pp. 483–491, Aug., 1955.

FRANCOIS, E. E., see Law, J. T.

DAVIS, J. L., see Suhl, H.

GALT, J. K., see Bozorth, R. M., and Yager, W. A.

GARN, P. D.,[1] and HALLINE, MRS. E. W.[1]
Polarographic Determination of Phthalic and Anhydride Alkyd Resins, Anal Chem., **27,** pp. 1563–1565, Oct., 1955.

1. Bell Telephone Laboratories, Inc.
4. University of Western Ontario, London, Canada
5. Bell Telephone Company of Canada, Montreal

GETLIN, B. B., see Bozorth, R. M.

GIANOLA, U. F.[1]
Application of the Wiedemann Effect to the Magnetostrictive Coupling of Crossed Coils, J. Appl. Phys., **26,** pp. 1152–1157, Sept., 1955.

GOSS, A. J., see Hassion, F. X.

GREEN, E. I.[1]
The Story of Q, American Scientist, **43:** pp. 584–594, Oct., 1955.

HALLINE, MRS. E. W., see Garn, P. D.

HARROWER, G. A.[1]
Measurement of Electron Energies by Deflection in a Uniform Electric Field, Rev. Sci. Instr., **26,** pp. 850–854, Sept., 1955.

HASSION, F. X.,[1] GOSS, A. J.,[1] and TRUMBORE, F. A.[1]
The Germanium-Silicon Phase Diagram, J. Phys. Chem., **59,** p. 1118, Oct., 1955.

HASSION, F. X.,[1] THURMOND, C. D.,[1] and TRUMBORE, F. A.[1]
On the Melting Point of Germanium, J. Phys. Chem., **59,** p. 1076, Oct., 1955.

HINES, M. E.,[1] HOFFMAN, G. W.,[1] and SALOOM, J. A.[1]
Positive-Ion Drainage in Magnetically Focused Electron Beams, J. Appl. Phys., **26,** pp. 1157–1162, Sept., 1955.

HOFFMAN, G. W., see Hines, M. E.

INKSTER, W. J., see Bullington, K.

KELLY, M. J.[1]
Training Programs of Industry for Graduate Engineers, Elec. Engg., **74,** pp. 866–869, Oct., 1955.

KOLB, E. D., see Bridgers, H. E.

1. Bell Telephone Laboratories, Inc.

LAW, J. T.,[1] and FRANCOIS, E. E.[1]
Adsorption of Gasses and Vapors on Germanium, N. Y. Acad. Sci. Ann., **58,** pp. 925–936, Sept. 15, 1955.

LOVELL, MISS L. C., see Pfann, W. G.

MATREYEK, W., see Winslow, F. H.

MCLEAN, D. A., see Basseches, H.

MERRITT, F. R., see Bozorth, R. M., and Yager, W. A.

MEYER, F. T.[1]
An Improved Detached-Contact Type of Schematic Circuit Drawing, A.I.E.E. Commun. & Electronics, **20,** pp. 505–513, Sept., 1955.

MILLER, B. T.[2]
Telephone Merchandising, Telephony, **149,** pp. 116–117, Oct. 22, 1955.

MILLER, S. L.[1]
Avalanche Breakdown in Germanium, Phys. Rev., **99,** pp. 1234–1241, Aug. 15, 1955.

MOORE, G. E.,[1] and ALLISON, H. W.[1]
Adsorption of Strontium and of Barium on Tungsten, J. Chem. Phys., **23,** pp. 1609–1621, Sept., 1955.

NEISSER, W. R.,[1]
Liquid Nitrogen Coal Traps, Rev. Sci. Instr., **26,** p. 305, Mar., 1955.

OSTERGREN, C. N.[2]
Some Observations on Liberalized Tax Depreciation, Telephony, **149,** pp. 16-23-37, Oct. 1, 1955.

OSTERGREN, C. N.[2]
Depreciation and the New Law, Telephony, **149,** pp. 96-100-104-108, Oct. 22, 1955.

PAPE, N. R., see Winslow, F. H.

1. Bell Telephone Laboratories, Inc.
2. American Telephone and Telegraph Co.

PEDERSEN, L.[1]
Aluminum Die Castings for Carrier Telephone Systems, A.I.E.E. Commun. & Electronics, **20,** pp. 434–439, Sept., 1955.

PETERS, H.[1]
Hard Rubber, Ind. and Engg. Chem., Part II, pp. 2220–2222, Sept. 20, 1955.

PFANN, W. G.[1]
Temperature-Gradient Zone-Melting, J. Metals, **7,** p. 961, Sept., 1955.

PFANN, W. G.,[1] and LOVELL, MISS L. C.[1]
Dislocation Densities in Intersecting Lineage Boundaries in Germanium, Letter to the Editor, Acta. Met., **3,** pp. 512–513, Sept., 1955.

PIERCE, J. R.[1]
Orbital Radio Relays, Jet Propulsion, **25,** pp. 153–157, Apr., 1955.

POOLE, K. M.[1]
Emission from Hollow Cathodes, J. Appl. Phys., **26,** pp. 1176–1179, Sept., 1955.

SALOOM, J. A., see Hines, M. E.

SLICHTER, W. P.[1]
Proton Magnetic Resonance in Polyamides, J. Appl. Phys., **26,** pp., 1099–1103, Sept., 1955.

SMITH, B.,[1] and BOORSE, H. A.[6]
Helium II Film Transport. II. The Role of Surface Finish, Phys. Rev. **99,** pp. 346–357, July 15, 1955.

SMITH, B.,[1] and BOORSE, H. A.[6]
Helium II Film Transport. IV. The Role of Temperature, Phys. Rev., **99,** pp. 367–370, July 15, 1955.

SUHL, H.,[1] VAN UITERT, L. G.,[1] and DAVIS, J. L.[1]
Ferromagnetic Resonance in Magnesium-Manganese Aluminum Ferrite Between 160 and 1900 Mc., Letter to the Editor, J. Appl. Phys., **26,** pp. 1181–1182, Sept., 1955.

1. Bell Telephone Laboratories, Inc.
6. Columbia University, New York City

THURMOND, C. D., see Hassion, F. X.

TIDD, W. H.[1]
Demonstration of Bandwidth Capabilities of Beyond-Horizon Tropospheric Radio Propagation, Proc. I.R.E., **43,** pp. 1297–1299, Oct., 1955.

TIEN, P. K.,[1] and WALKER, L. R.[1]
Large Signal Theory of Traveling-Wave Amplifiers, Proc. I.R.E., **43,** p. 1007, Aug., 1955.

TILDEN, E. F., see Bozorth, R. M.

TRUMBORE, F. A., see Hassion, F. X.

UHLIR, A., JR.[1]
Micromachining with Virtual Electrodes, Rev. Sci., Instr., **26,** pp. 965–968, Oct., 1955.

ULRICH, W., see Yokelson, B. J.

VAN UITERT, L. G., see Suhl, H.

WALKER, L. R., see Tien, P. K.

WEIBEL, E. S.[1]
Vowel Synthesis by Means of Resonant Circuits, J. Acous. Soc., **27,** pp. 858–865, Sept., 1955.

WILLIAMS, A. J., see Bozorth, R. M.

WINSLOW, F. H.,[1] BAKER, W. O.,[1] and YAGER, W. A.[1]
Odd Electrons in Polymer Molecules, Am. Chem. Soc., **77,** pp. 4751–4756, Sept. 20, 1955.

WINSLOW, F. H.,[1] BAKER, W. O.,[1] PAPE, N. R.[1] and MATREYEK, W.[1]
Formation and Properties of Polymer Carbon, J. Polymer Science, **16,** p. 101, Apr., 1955.

YAGER, W. A., see Bozorth, R. M.

1. Bell Telephone Laboratories, Inc.

YAGER, W. A.,[1] GALT, J. K.[1] and MERRITT, F. R.[1]
Ferromagnetic Resonance in Two-Nickel-Iron Ferrites, Phys. Rev., **99,** pp. 1203–1209, Aug. 15, 1955.

YOKELSON, B. J.,[1] and ULRICH, W.[1]
Engineering Multistage Diode Logic Circuits, A.I.E.E. Commun. & Electronics, **20,** pp. 466–475, Sept., 1955.

1. Bell Telephone Laboratories, Inc.

Recent Monographs of Bell System Technical Papers Not Published in This Journal*

ARNOLD, W. O., and HOEFLE, R. R.
A System Plan for Air Traffic Control, Monograph 2483.

BECK, A. C.
Measurement Techniques for Multimode Waveguides, Monograph 2421.

BECKER, J. A., and BRANDES, R. G.
Adsorption of Oxygen on Tungsten as Revealed in Field Emission Microscope, Monograph 2493.

BOYLE, W. S., see Germer, L. H.

BRANDES, R. G., see Becker, J. A.

BRATTAIN, W. H., see Garrett, C. G. B.

GARRETT, C. G. B., and BRATTAIN, W. H.
Physical Theory of Semiconductor Surfaces, Monograph 2453.

GERNER, L. H., BOYLE, W. S., and KISLIUK, P.
Discharges at Electrical Contacts — II, Monograph 2499.

HOEFLE, R. R., see Arnold, W. O.

KISLIUK, P., see Germer, L. H.

LINVILL, J. G.
Nonsaturating Pulse Circuits Using Two Junction Transistors, Monograph 2475.

* Copies of these monographs may be obtained on request to the Publication Department, Bell Telephone Laboratories, Inc., 463 West Street, New York 14, N. Y. The numbers of the monographs should be given in all requests.

MASON, W. P.
Relaxations in the Attenuation of Single Crystal Lead, Monograph 2454.

MEYER, F. T.
An Improved Detached-Contact-Type of Schematic Circuit Drawing, Monograph 2456.

VOGEL, F. L., JR.
Dislocations in Low-Angle Boundaries in Germanium, Monograph 2455.

WALKER, L. R.
Generalizations of Brillouin Flow, Monograph 2432.

WARNER, A. W.
Frequency Aging of High-Frequency Plated Crystal Units, Monograph 2474.

WEIBEL, E. S.
On Webster's Horn Equation, Monograph 2450.

Contributors to This Issue

A. C. Beck, E.E., Rensselaer Polytechnic Institute, 1927; Instructor, Rensselaer Polytechnic Institute, 1927–1928; Bell Telephone Laboratories, 1928 –. With the Radio Research Department he was engaged in the development and design of short-wave and microwave antennas. During World War II he was chiefly concerned with radar antennas and associated waveguide structures and components. For several years after the war he worked on development of microwave radio repeater systems. Later he worked on microwave transmission developments for broadband communication. Recently he has concentrated on further developments in the field of broadband communication using circular waveguides and associated test equipment.

J. S. Cook, B.E.E., and M.S., Ohio State University, 1952; Bell Telephone Laboratories, 1952 –. Mr. Cook is a member of the Research in High-Frequency and Electronics Department at Murray Hill and has been engaged principally in research on the traveling-wave tube. Mr. Cook is a member of the Institute of Radio Engineers and belongs to the Professional Group on Electron Devices.

O. E. DeLange, B.S. University of Utah, 1930; M.A. Columbia University, 1937; Bell Telephone Laboratories, 1930 –. His early work was principally on the development of high-frequency transmitters and receivers. Later he worked on frequency modulation and during World War II was concerned with the development of radar. Since that time he has been involved in research using broadband systems including microwave and baseband. Mr. DeLange is a member of the Institute of Radio Engineers.

R. Kompfner, Engineering Degree, Technische Hochschule, Vienna, 1933; Ph.D., Oxford, 1951; Bell Telephone Laboratories, 1951 –. Between 1941–1950 he did work for the British Admiralty at Birmingham University and Oxford University in the Royal Naval Scientific Service. He invented the traveling-wave tube and for this achievement Dr. Kompfner received the 1955 Duddell Medal, bestowed by the Physical Society of England. In the Laboratories' Research in High Frequency

and Electronics Department, he has continued his research on vacuum tubes, particularly those used in the microwave region. He is a Fellow of the Institute of Radio Engineers and of the Physical Society in London.

CHARLES A. LEE, B.E.E., Rensselaer Polytechnic Institute, 1943; Ph.D., Columbia University, 1953; Bell Telephone Laboratories, 1953–. When Mr. Lee joined the Laboratories he became engaged in research concerning solid state devices. In particular he has been developing techniques to extend the frequency of operation of transistors into the microwave range, including work on the diffused base transistor. During World War II, as a member of the United States Signal Corps, he was concerned with the determination and detection of enemy countermeasures in connection with the use of proximity fuses by the Allies. He is a member of the American Physical Society and the American Institute of Physics. He is also a member of Sigma Xi, Tau Beta Pi and Eta Kappa Nu.

JOHN R. PIERCE, B.S., M.S. and Ph.D., California Institute of Technology 1933, 1934 and 1936; Bell Telephone Laboratories, 1936–. Appointed Director of Research — Electrical Communications in August, 1955. Dr. Pierce has specialized in Development of Electron Tubes and Microwave Research since joining the Laboratories. During World War II he concentrated on the development of electronic devices for the Armed Forces. Since the war he has done research leading to the development of the beam traveling-wave tube for which he was awarded the 1947 Morris Liebmann Memorial Prize of the Institute of Radio Engineers. Dr. Pierce is author of two books: *Theory and Design of Electron Beams*, published in second edition last year, and *Traveling Wave Tubes* (1950). He was voted the "Outstanding Young Electrical Engineer of 1942" by Eta Kappa Nu. Fellow of the American Physical Society and the I.R.E. Member of the National Academy of Sciences, the A.I.E.E., Tau Beta Pi, Sigma Xi, Eta Kappa Nu, the British Interplanetary Society, and the Newcomen Society of North America.

C. F. QUATE, B.S., University of Utah 1944; Ph.D., Stanford University 1950; Bell Laboratories 1950–. Dr. Quate has been engaged in research on electron dynamics — the study of vacuum tubes in the microwave frequency range. He is a member of I.R.E.

DAVID SLEPIAN, University of Michigan, 1941–1943; M.A. and Ph.D., Harvard University, 1946–1949; Bell Telephone Laboratories, 1950–. Dr.

Slepian has been engaged in mathematical research in communication theory, switching theory and theory of noise. Parker Fellow in physics, Harvard University 1949–50. Member of I.R.E., American Mathematical Society, the American Association for the Advancement of Science and Sigma Xi.

Milton Sobel, B.S., City College of New York, 1940; M.A., 1946 and Ph.D., 1951, Columbia University; U. S. Census Bureau, Statistician, 1940–41; U. S. Army War College, Statistician, 1942–44; Columbia University, Department of Mathematics, Assistant, 1946–48 and Research Associate 1948–50; Wayne University, Assistant Professor of Mathematics, 1950–52; Columbia University, Department of Mathematical Statistics, Visiting Lecturer, 1952; Cornell University, fundamental research in mathematical statistics, 1952–54; Bell Telephone Laboratories, 1954–. Dr. Sobel is engaged in fundamental research on life testing reliability problems with special application to transistors and is a consultant on many Laboratories projects. Member of Institute of Mathematical Statistics, American Statistical Association and Sigma Xi.

Morris Tanenbaum, A.B., Johns Hopkins University, 1949; M.A., Princeton University, 1950; Ph.D. Princeton University, 1952; Bell Telephone Laboratories, 1952–. Dr. Tanenbaum has been concerned with the chemistry and semiconducting properties of intermetallic compounds. At present he is exploring the semiconducting properties of silicon and the feasibility of silicon semiconductor devices. Dr. Tanenbaum is a member of the American Chemical Society and American Physical Society. He is also a member of Phi Lambda Upsilon, Phi Beta Kappa and Sigma Xi.

Donald E. Thomas, B.S. in E.E., Pennsylvania State College, 1929; M.A., Columbia University, 1932; Bell Telephone Laboratories, 1929–1942, 1946–. His first assignment at the Laboratories was in submarine cable development. Just prior to World War II he became engaged in the development of sea and airborne radar and continued in this work until he left for military duty in 1942. During World War II he was made a member of the Joint and Combined Chiefs of Staff Committees on Radio Countermeasures. Later he was a civilian member of the Department of Defense's Research and Development Board Panel on Electronic Countermeasures. Upon rejoining the Laboratories in 1946, Mr. Thomas was active in the development and installation of the first deep sea repeatered submarine telephone cable, between Key West and Havana,

which went into service in 1950. Later he was engaged in the development of transistor devices and circuits for special applications. At the present time he is working on the evaluation and feasibility studies of new types of semiconductors devices. He is a senior member of the I.R.E. and a member of Tau Beta Pi and Phi Kappa Phi.

LAURENCE R. WALKER, B.Sc. and Ph.D., McGill University, 1935 and 1939; University of California 1939–41; Radiation Laboratory, Massachusetts Institute of Technology, 1941–45; Bell Telephone Laboratories, 1945–. Dr. Walker has been primarily engaged in the development of microwave oscillators and amplifiers. At present he is a member of a physical research group concerned with the applied physics of solids. Fellow of the American Physical Society.